Cell Nonautonomous Regulation of Longevity and Behavior

by

Elizabeth S. Kitto

A dissertation submitted in partial fulfillment
of the requirements for the degree of
Doctor of Philosophy
(Molecular and Integrative Physiology)
in the University of Michigan
2025

Doctoral Committee:

Associate Professor Scott F. Leiser, Chair
Assistant Professor Eleni Gourgou, Wayne State University
Professor Catherine Kaczorowski
Professor Scott D. Pletcher
Assistant Professor Matthias Truttmann

Elizabeth S. Kitto

esdean@umich.edu

ORCID iD: 0000-0003-3414-1509

© Elizabeth S. Kitto 2025

Acknowledgements

I would like to express my thanks and appreciation to everyone who has supported me on my way to graduate school and during my degree. First and foremost, I am grateful to my parents, John and Leah, for encouraging a deep curiosity about the world from a young age and for always prioritizing my education. I would also like to thank my husband, David, for moving to Michigan to pursue our degrees together, for his endless support throughout the ups and downs of graduate school, and for spending countless hours of his life listening to me talk about worms. This experience has been so much better by having someone who shares and understands my dedication to research while simultaneously keeping me grounded and reminding me to focus on the non-science parts of life too.

I am also incredibly grateful to my supervisor, Dr. Scott Leiser, for his unwavering support. I especially appreciate that Scott encouraged me to follow my own research interests and let me play around with almost anything I wanted to test in the lab. I also would like to thank Scott for fostering an inclusive environment that encourages collaboration and makes the lab a fun place to be. Within the Leiser Lab, I appreciate the unique contributions of every previous and current lab member. Specifically, I would like to give a huge thanks to Dr. Hillary Miller and Dr. Shijiao Huang for teaching me everything when I first joined the lab and for providing the groundwork for many of the projects I worked on. I would also like to thank Dr. Marshall Howington and Dr. Hyo Sub-Choi for paving the way along with Hillary as the lab's first graduate students, and establishing a positive, supportive, and fun environment.

Of course, I also need to thank current members of the Leiser Lab, starting with the wonderful post-docs and research investigators. First, thank you to Dr. Safa Beydoun for her willingness to collaborate on pretty much anything, her general guidance on navigating graduate school and life, for advocating for me when I hesitated to ask for something myself, and for going to all the best conferences together. Dr. Rebecca Cox also gave invaluable advice on the Ph.D. process, had an answer for any and every scientific question, and brought a lot of joy, cat photos, and baby photos to Bay 2. Dr. Ajay Bhat provided inspiration on how to creatively ask and answer interesting questions, was eager to have deep conversations about my science, and was always ready to joke around (I think, I'm still not completely sure whether he was being serious or sassy this whole time).

I would also like to extend my heartfelt thanks to the incredible graduate students who have been a constant source of support and camaraderie throughout this journey. Meg, Angela, Faith, Madeline, and Sarah, your friendship, generosity, and willingness to collaborate have made all the difference in both my research and my day-to-day life in the lab. I truly appreciate the thoughtful discussions, the moments of encouragement, and all of the crazy conversations we have on Fridays. A special thanks to Meg for being our cat dealer, to Angela for a wonderful trip to Spain together, and to Sarah for her patience as I continue to learn how to be a better mentor. I am also grateful to the undergraduate students Mira, Dani, and Ella, whose enthusiasm, hard work, and dedication to assisting with my research have been invaluable. Your contributions have not only advanced this work but have also reminded me of the excitement and curiosity that initially drew me to science.

Finally, I would like to express my sincere appreciation to the administrative staff members Lori Meggitt, Jason Yunk, Michele Boggs, and Jeannie Worrall who have made all the

paperwork and milestones of the degree progress go as smoothly as possible. Their excellent communication and attention to detail have been invaluable. I am also deeply grateful to my committee members—Dr. Scott Pletcher, Dr. Matthias Truttmann, Dr. Eleni Gourgou, and Dr. Catherine Kaczorowski—for their insightful guidance, constructive feedback, and expertise. Their thoughtful critiques and encouragement have significantly shaped the development of this dissertation, and I am honored to have had the opportunity to learn from each of them.

To conclude, I want to express my deep appreciation to everyone who has supported me throughout this process, whether through direct contributions, advice, or just being there when I needed it. This work is as much a reflection of the community around me as it is of my own efforts, and I'm genuinely grateful for all who have helped me get to this point.

Table of Contents

Acknowledgements ii

List of Tables xi

List of Figures xii

List of Appendices xvi

Abstract xvii

Chapter 1 Introduction 1

1.1 Motivation for and the Current State of Understanding the Biology of Aging 1

1.1.1 People around the world are living longer, but not healthier lives. 1

1.1.2 Activation of stress-response pathways can extend lifespan. 3

1.1.3 Stress response pathways can be activated via environmental, genetic and pharmaceutical interventions. 4

1.2 Cell Nonautonomous Signaling and Hormesis in Health and Longevity 5

1.2.1 Cell nonautonomous signaling plays a critical role in activating hormetic stress-response pathways. 5

1.2.2 Caenorhabditis elegans 7

1.2.3 Drosophila melanogaster 21

1.2.4 Mammals 31

1.2.5 Emerging Concepts in Cell Nonautonomous Signaling and Longevity 40

1.3 Potential Obstacles to Anti-Aging Treatments 44

1.3.1 Challenges facing environmental longevity interventions 44

1.3.2 Challenges facing pharmaceutical longevity interventions 48

1.3.3 The complex interplay between longevity interventions, reproduction, stress resistance, and behavior 52

1.4 Goals of this Dissertation 56

Chapter 2 Touch Limits Lifespan through Neural to Intestinal Signaling 59

2.1 Foreword 59

2.2 Abstract 60

2.3 Introduction 60

2.4 Mechanosensation attenuates DR-mediated longevity in an *fmo-2* dependent manner. 62

2.5 Signaling from dopamine and tyramine is required for touch to regulate longevity. 73

2.6 Insulin and GnRH neuropeptides convey touch signaling to mediate *fmo-2* induction and longevity 80

2.7 Discussion 89

2.8 Materials and Methods 91

2.8.1 Strains and Growth Conditions 91

2.8.2 tdc-1 Rescue Constructs 101

2.8.3 Fake Lawn Preparation 101

2.8.4 RNAi Knockdown 102

2.8.5 Drug Treatments 102

2.8.6 Lifespan Measurements 103

2.8.7 RNAi Lifespans 104

2.8.8 Slide Microscopy 104

2.8.9 Lawn Occupancy Measurements 105

2.8.10 Chemotaxis Assays 106

2.8.11 Heat Stress Assays 106

2.8.12 Statistical Analysis 107

Chapter 3 The Hypoxic Response Extends Lifespan through a Bioaminergic and Peptidergic Neural Circuit 108

3.1 Foreword 108

3.2 Abstract 109

3.3 Introduction 110

3.4 Results 112

3.4.1 Serotonin signaling through the ADF neuron and the SER-7 receptor are necessary and sufficient for the hypoxic response to extend lifespan. 112

3.4.2 Tyraminergic signaling from the RIM neuron and the tyramine receptor TYRA-3 are required for vhl-1 knockdown to extend lifespan. 120

3.4.3 Oxygen and carbon dioxide sensing neurons act downstream of serotonin signaling. 125

3.4.4 The neuropeptide NLP-17 and its receptors contribute to vhl-1-mediated longevity. 127

3.5 Discussion 131

3.6 Methods 135

3.6.1 Strains and Growth Conditions 135

3.6.2 Generating transgenic strains 135

3.6.3 RNAi Knockdown 137

3.6.4 Quantitative PCR 138

3.6.5 Lifespan Measurements 138

3.6.6 RNAi Lifespans 139

3.6.7 Fluorescent Slide Microscopy 139

3.6.8 Statistical Analysis 140

3.7 Acknowledgements and Funding 140

3.8 Supplementary Tables 141

Chapter 4 Metabolic Regulation of Behavior by the Intestinal Enzyme *fmo-2*. 145

4.1 Foreword 145

4.2 Abstract 146

4.3 Introduction 147

4.4 Results 150

4.4.1 fmo-2 expression alters *C. elegans* sensory perception, foraging, and reproductive behavior 150

4.4.2 fmo-2 expression interacts with tryptophan metabolism to alter exploratory behavior 157

4.4.3 Knocking out fmo-2 suppresses exploratory behavior by modifying serotonin signaling. 160

4.4.4 Increased quinolinic acid lowers exploratory behavior in the fmo-2 overexpressor. 165

4.4.5 The mechanisms through which fmo-2 expression effects exploratory behavior, other behaviors, and longevity are partially but not completely overlapping. 170

4.5 Discussion 176

4.6 Methods 179

4.6.1 Strains and Growth Conditions 179

4.6.2 Pumping Assays 179

4.6.3 Thrashing Assays 179

4.6.4 30-minute Video Recordings for Speed and Movement Patterns 179

4.6.5 Gentle Touch Response Assay 180

4.6.6 Harsh Touch Response Assay 181

4.6.7 Chemotaxis Assay 181

4.6.8 Pathogen Fleeing Assay 182

4.6.9 Basal and Enhanced Slowing Response Assay 183

4.6.10 Brood Size Assay 183

4.6.11 Exploration Assays 183

4.6.12 Exploration Assays with Metabolite/Compound Supplementation 184

4.6.13 Behavioral State Assays 184

4.6.14 Generating tissue-specific fmo-2 overexpressors 185

4.6.15 RNAi Knockdown 185
4.6.16 Quantitative PCR for RNAi validation 185
4.6.17 Enzymatic Activity Assay 186
4.6.18 Serotonin Immobilization Assay 186
4.6.19 Lifespan Measurements 187
4.6.20 RNAi Lifespans 187
4.6.21 Fluorescent Slide Microscopy 188
4.6.22 Statistical Analysis 188
Chapter 5 Methods for Metabolic Inactivation of *E. coli* and for Automated Image Quantification in *C. elegans* Research. 192
5.1 Foreword 192
5.2 Method to metabolically inactivate bacteria for *Caenorhabditis elegans* research 193
5.2.1 Abstract 193
5.2.2 Introduction 194
5.2.3 Protocol 197
5.2.4 Representative Results 202
5.2.5 Discussion 206
5.2.6 Acknowledgements: 210
5.3 findWormz is a user-friendly automated fluorescence quantification method for *C. elegans* research. 210
5.3.1 Abstract 210
5.3.2 Description 211
5.3.3 Methods 217
5.3.4 findWormz Detailed Protocol 218
Chapter 6 Conclusions and Future Directions 225
6.1 Summary of Conclusions 225

6.2 Recommendations for Future Work..... 229

6.2.1 How do multiple forms of food perception interact to modify lifespan? 229

6.2.2 Can we use our knowledge of these neural circuits to identify a central regulator of aging, and/or new longevity interventions?..... 239

6.2.3 Do other genetic and pharmaceutical longevity interventions affect behavior and could altered behavior be used as a screening tool for pro-longevity genes?..... 245

6.2.4 Can we identify commonalities between extensively mapped behavioral circuits and newly discovered cell nonautonomous longevity pathways? 248

6.2.5 Are the effects of Fmos on longevity and behavior conserved from worms to mammals? 250

6.2.6 Methods..... 252

Appendices.....256

Bibliography 272

List of Tables

Table 2.1 RNAi used in this work. 99

Table 2.2 Strains used in this work. 101

Table 3.1 RNAi used in this work. 141

Table 3.2 Strains used in this work. 144

Table 4.1 RNAi used in this work. 190

Table 4.2 *C. elegans* strains used in this work. 191

Table 5.1 Comparisons of methods to kill OP50. 197

Table 5.2 Example input for the conditions_map file 222

Table 6.1 Water-soluble taste compounds screened for effects on *fmo-2* induction under fed and DR conditions 233

Table 6.2 Tyramine signaling contributes to multiple cell nonautonomous longevity circuits. . 241

Table 6.3 RIS signaling may contribute to multiple cell nonautonomous longevity circuits. 245

List of Figures

Figure 1.1 Geroscience aims to improve healthspan in an aging population. 2

Figure 1.2 Mild stress exposure that produces a beneficial effect is known as hormesis..... 4

Figure 1.3 Summary of the role energy balance and insulin signaling on cell nonautonomous modulation of longevity in *C. elegans.* 11

Figure 1.4 Summary of the role of proteostasis in cell nonautonomous modulation of longevity in *C. elegans.*..... 15

Figure 1.5 Summary of the role of perception on cell nonautonomous modulation of longevity in *C. elegans.*..... 21

Figure 1.6 Summary of the role energy balance and insulin signaling on cell nonautonomous modulation of longevity in *D. melanogaster.* 25

Figure 1.7 Summary of the role of proteostasis in cell nonautonomous modulation of longevity in *D. melanogaster.*..... 28

Figure 1.8 Summary of the role of perception on cell nonautonomous modulation of longevity in *D. melanogaster.*..... 31

Figure 1.9 The intersection of cell nonautonomous signaling and aging in mammals..... 40

Figure 1.10 Summary model..... 43

Figure 1.11 A summary of the challenges facing environmental, genetic, and pharmaceutical longevity treatments..... 44

Figure 2.1 Touch blunts DR-mediated longevity through suppression of *fmo-2*. 63

Supplemental Figure 2.1 The fake lawn is not edible and does not blunt DR-mediated *fmo-2* induction via chemosensation. 66

Figure 2.2 Multiple putative mechanoreceptor proteins affect the ability of the fake lawn to blunt DR-mediated longevity..... 69

Supplemental Figure 2.2 250 μM amiloride has the greatest blocking effect on DR + touch..... 70

Supplemental Figure 2.3 Knocking down many mechanoreceptors alters baseline fed and DR *fmo-2* induction and longevity with and without touch. 72

Figure 2.3 The bioamines dopamine and tyramine modulate DR-mediated longevity downstream of touch. 75

Supplemental Figure 2.4 Dopamine and tyramine signaling, but not serotonin, GABA, glutamate, or acetylcholine signaling are required for touch to attenuate DR. 77

Figure 2.4 Dopamine production from any dopaminergic neuron class and tyramine production from the uv1 neuroendocrine cells is sufficient for touch to blunt DR. 79

Figure 2.5 Insulin-, GnRH-, and NLP-family neuroendocrine signals are required for touch to blunt DR. 82

Supplemental Figure 2.5 Many neuroendocrine genes regulate DR-mediated fmo-2 induction and longevity within and independently of the touch pathway.. 84

Supplemental Figure 2.6 Some signals involved in touch attenuation of DR-mediated longevity also modify lawn occupancy behavior. 88

Figure 3.1 ADF serotonergic neurons are necessary and sufficient to extend lifespan downstream of the hypoxic response. 114

Supplemental Figure 3.1 *tph-1* is required for *vhl-1* mediated longevity. 116

Figure 3.2 *ser-7* expression in the GABAergic RIS neuron is required for hypoxia to extend lifespan. 118

Supplemental Figure 3.2 *ser-7* expression in each *ser-7* expressing neuron is rescued by at least one construct, and *ser-7* is required for *vhl-1*-mediated longevity. 119

Figure 3.3 GABA and tyramine synthesis are required for the hypoxic response to extend lifespan. 121

Supplemental Figure 3.3 Acetylcholine, glutamate, and dopamine synthesis are not fully required for *vhl-1* RNAi to extend lifespan. 122

Figure 3.4 The RIM neuron and the tyramine receptor *tyra-3* act in the hypoxic response-mediated longevity pathway. 123

Supplemental Figure 3.4 *tyra-2* and *ser-2* are not necessary for *vhl-1*-mediated longevity, while *lgc-55* is partially required. 125

Figure 3.5 High- and low-oxygen sensing neurons are important for hypoxic response-mediated longevity. 127

Figure 3.6 The neuropeptide *nlp-17* and its receptors *npr-37* and *npr-43* are required for hypoxic response-mediated longevity 129

Supplemental Figure 3.5 qPCR validation of RNAi hits from Figure 5, and neuropeptide screen hits that did not validate. 130

Figure 3.7 Working model of the hypoxia-mediated longevity pathway. 131

Supplemental Figure 4.1 *fmo-2* knockout and overexpressing animals have normal movement capacity during young adulthood. 151

Figure 4.1 *fmo-2* expression alters *C. elegans* sensory perception, foraging, and reproductive behavior 152

Supplemental Figure 4.2 The effects of *fmo-2* expression on exploratory behavior persist through mid-adulthood and both neural and intestinal *fmo-2* expression contribute to changes in exploratory behavior. 156

Figure 4.2 *fmo-2* expression interacts with tryptophan metabolism to alter exploratory behavior 158

Supplemental Figure 4.3 Supplementation with glutathione, methimazole, and pyruvate do not modify exploration, knocking down *aat-2* and *aat-3* blocks tryptophan-mediated decreases in exploration, and *sams-1* does not interact with *fmo-2* to modify exploration. 159

Figure 4.3 Knocking out *fmo-2* suppresses exploratory behavior by modifying serotonin signaling. 162

Supplemental Figure 4.4 Knocking out f*mo-2* increases *tph-1p::GFP* fluorescence in the NSM neurons and knocking down *tph-1* or *pah-1* partially rescues the exploration of the *fmo-2* knockout. 163

Figure 4.4 The kynurenine metabolites quinolinic and kynurenic acid contribute to exploratory behavior changes in the *fmo-2* overexpressor. 166

Supplemental Figure 4.5 Additional data from the tryptophan metabolism RNAi knockdown and knockout screen. 168

Figure 4.5 The mechanisms through which *fmo-2* expression affects exploratory behavior, other behaviors, and longevity are partially but not completely overlapping. 172

Supplemental Figure 4.6 *vhl-1* RNAi extends lifespan in WT and *pah-1; tph-1* but this effect is partially blocked by *fmo-2* knockout. 174

Figure 5.1 Workflow for paraformaldehyde treatment. 203

Figure 5.2 Treatment of bacteria with PFA inhibits proliferation and metabolism. 204

Figure 5.3 Worms attracted to PFA-treated OP50. 205

Figure 5.4 Worms grow and develop on PFA-treated OP50. 207

Figure 5.5 The findWormz method automatically identifies and quantifies the fluorescence intensity of individual *C. elegans*.. 214

Figure 5.6 Example brightfield input image for findWormz quantification. 221

Figure 5.7 Example output image from findWormz quantification. 224

Figure 6.1 Olfaction, mechanosensation, gustation, and enteric perception contribute to food sensing across taxa. 232

Figure 6.2 *del-3; del-7* knockout extends lifespan non-additively with dietary restriction. 233

Figure 6.3 Many water-soluble taste compounds affect *fmo-2* induction under fed and DR conditions in *C. elegans*. 237

Figure 6.4 Ammonium acetate and glycerol can modify lifespan under fed and dietary restriction conditions. 238

Figure 6.5 Food-like smell and touch additively suppress DR-mediated *fmo-2* induction but not lifespan. 240

Figure 6.6 NLP-2/GnRH is required for DR-mediated *fmo-2* induction and longevity in *C. elegans.* 243

Figure 6.7 Restoring tyramine synthesis in the uv1 and the RIML neurons extends lifespan in *C. elegans.* 244

Figure 6.8 Multiple longevity interventions alter exploratory behavior in *C. elegans.* 247

List of Appendices

Appendix A: Annotated worm_batch.R Code 256

Appendix B: Annotated findWormz.R Code 258

Appendix C: Annotated findWormz.R Code 265

Abstract

Aging is a complex biological process influenced by environmental, genetic, and physiological factors. Recent progress in aging research indicates that diverse environmental stressors, including changes in nutrient supply, oxygen levels, and temperature, can significantly improve health and extend lifespan across species. The beneficial effects of these environmental stressors are frequently mediated by cell nonautonomous signaling, where sensory cells relay critical information to peripheral tissues to initiate a protective stress response. Intriguingly, activating these neural pathways can enhance health and longevity even when external stressors are not present. Understanding the pathways that regulate aging, particularly those involving cell nonautonomous signaling, is crucial for developing effective treatments that promote healthspan and lifespan. This dissertation explores how sensory perception and neural circuits influence longevity, health, and behavior using *Caenorhabditis elegans* as a model organism.

This work first examines the interaction between sensory perception and dietary restriction (DR), a well-established longevity intervention. I demonstrate that tactile cues resembling bacterial food disrupt the lifespan extension provided by DR. This effect relies on primary mechanoreceptors and downstream neurotransmitters, including dopamine and tyramine, as well as neuropeptides like insulin and GnRH. These findings reveal a novel sensory pathway linking touch to systemic longevity regulation, emphasizing the role of neural sensory perception in aging. My collaborators and I then investigate the response to low oxygen, or hypoxia, another environmental longevity intervention. Hypoxia-induced longevity requires serotonin signaling

through ADF serotonergic neurons and SER-7 receptor activity in RIS interneurons. This pathway also engages additional neuromodulators, such as tyramine, GABA, and NLP-17. By dissecting these molecular mechanisms, we identify potential therapeutic targets for neural aging interventions, such as modulating hypoxic signaling components in specific neuronal subsets to minimize adverse effects.

In addition to signaling from the nervous system to peripheral tissues in longevity pathways, I also explore cell nonautonomous signals originating from peripheral tissues and modifying the nervous system. This retrograde signaling is explored in the context of *fmo-2*, a gene involved in longevity and metabolism. My collaborators and I find that altering *fmo-2* expression affects exploratory behavior through modifying tryptophan metabolism, linking broad metabolic changes to altered neural signaling. Normal exploratory behavior can be restored in *fmo-2* mutants through modifying serotonin and quinolinic acid synthesis, highlighting the interconnectedness of metabolism, behavior, and longevity, while also illustrating the challenges posed by pleiotropic effects in longevity interventions.

Finally, this dissertation addresses methodological challenges in *C. elegans* research. By developing a metabolically inactive bacterial food source and automated fluorescent image quantification techniques, I improve our capacity to study neural signaling and metabolic pathways with greater throughput and precision. Collectively, this work explores the intricate interplay between sensory perception, neural signaling, and peripheral longevity pathways. Ultimately, these findings could contribute to the broader goal of identifying conserved mechanisms that promote health and longevity in humans.

Chapter 1 Introduction

1.1 Motivation for and the Current State of Understanding the Biology of Aging

1.1.1 People around the world are living longer, but not healthier lives.

Between 2020 and 2050, the proportion of the global population over the age of 65 is expected to double and the number of people aged 80 years and older will triple[1] (**Figure 1.1A**). While these numbers reflect great improvements in child mortality and treating infectious disease[2,3], they do not reflect a compression of morbidity: there has been little change in the age of onset of chronic health conditions despite increasing lifespan[2]. As a result, the prevalence of age-associated chronic diseases such as cancer, dementia, diabetes, and heart disease has risen markedly[2,4]. As of 2017, age-associated chronic diseases affected nearly two thirds of adults in the United States[5]. This increasing prevalence of age-associated disease not only has consequences for aging individuals and caretakers, but also results in a strained healthcare system lacking in capacity and financial resources[2].

Traditionally, biomedical research aims to understand the molecular mechanisms of a specific disease to develop a targeted pharmaceutical treatment. This approach prioritizes the discovery of different individual treatments or cures for many chronic conditions like cancer, diabetes, heart disease, and dementia. However, curing a patient of one chronic condition does relatively little to extend healthspan, as they are still at high risk for other age-associated diseases. For example, curing all forms of cancer would only extend average lifespan in the United States by about two years[6]. This high likelihood of chronic disease comorbidity can also

be observed in **Figure 1.1B**, where data from a representative population of ~750,000 people in Scotland shows the average number of comorbid chronic conditions rising with age[7]. Rather than attempting to cure each chronic disease, an alternative approach to improving human health is to instead target the primary driver of all these conditions—the aging process itself (**Figure 1.1C**). If this strategy is followed, it is predicted that each year average healthspan is extended in the United States will reduce medical spending by approximately 3.5 trillion dollars over the next 50 years[6]. Consequently, understanding the biology of aging has great potential to dramatically extend human healthspan and, in the process, reduce the financial and emotional burden of age-associated disease.

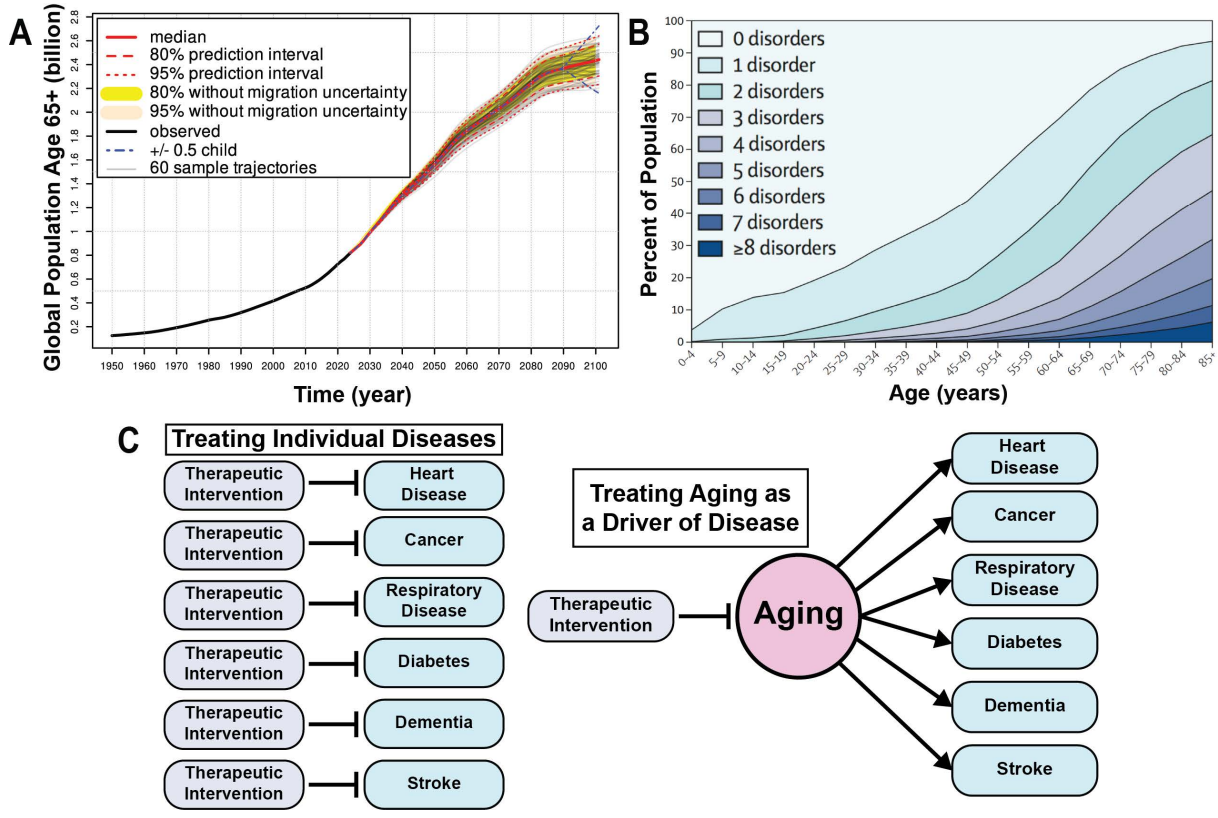


Figure 1.1 Geroscience aims to improve healthspan in an aging population. A) Measured and projected population aged 65 and up from 1950 to 2100. Data from the United Nations Department of Economic and Social Affairs[1]. **B)** Percent of the population diagnosed with one or more chronic disease by age. Data from Barnett *et al,* 2012[7]. **C)** Diagram of two approaches to treating chronic age-associated disease.

1.1.2 Activation of stress-response pathways can extend lifespan.

The first clear evidence that aging rate is modifiable came in 1935, when McCay and colleagues reported that dietary restriction extended mean lifespan in rats[8]. This finding has been replicated by many research groups across taxa[9-12], and caloric restriction shows promise in improving health markers in healthy human populations[13-15]. Initially, after the discovery that environmental factors could influence the rate of aging, the prevailing scientific view was that aging was governed by highly complex genetic interactions and identifying single genes that could alter lifespan seemed unlikely, if not impossible[16]. This assumption was challenged in 1983, when Klass *et al* identified the first genetic mutants with extended lifespans, demonstrating that it is possible for single gene modifications to impact longevity[17,18]. Subsequent work from the Johnson, Kenyon, and Ruvkun laboratories further supported these findings by demonstrating the role of insulin signaling and the FOXO transcription factor DAF-16 in regulating *C. elegans* lifespan[19-21].

In the following decades, many additional physiological pathways that influence the aging process have been discovered in various model organisms. These interventions, such as dietary restriction (DR)[22], temperature stress[23,24], insulin signaling[21,25,26], and hypoxia[27,28], share a common theme in that they activate stress response pathways that benefit the organism when applied at an appropriate dose. This phenomenon, where a mild dose of a stressor stimulates beneficial activation of stress response pathways, is referred to as hormesis[29,30] (**Figure 1.2**). Hormetic stressors are often first perceived by sensory cells in the nervous system that activate pro-longevity pathways in peripheral tissues to extend lifespan via cell nonautonomous signaling[31]. However, the ability of a stressor to induce a beneficial hormetic effect depends on

the baseline health of the organism, the specific dose of the stressor, and levels of other, co-occurring environmental stressors[32].

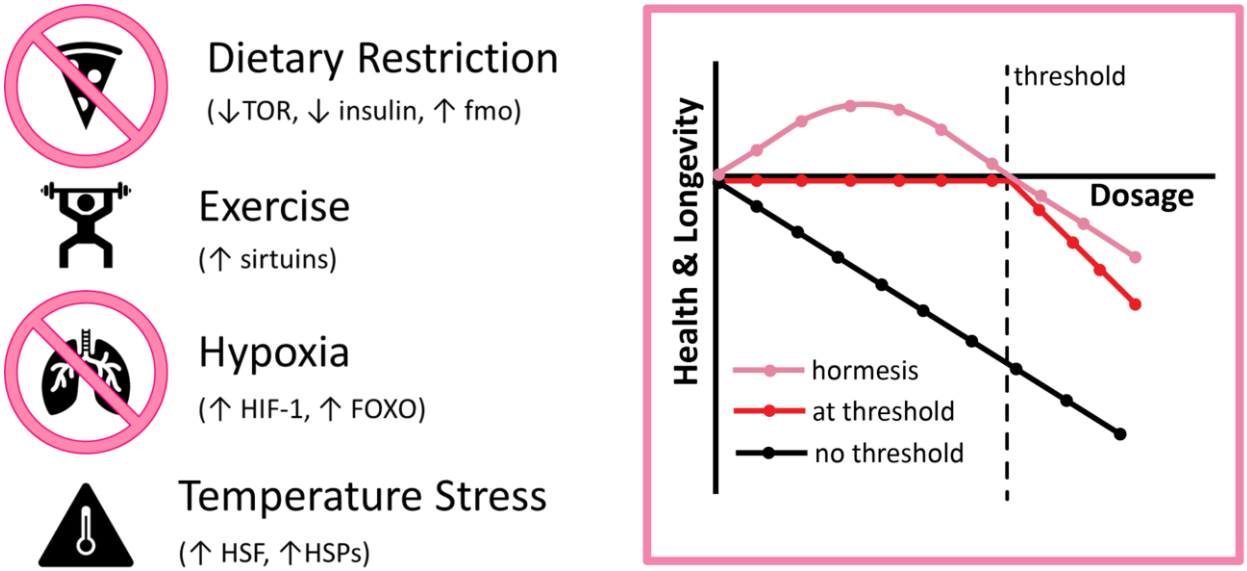


Figure 1.2 Mild stress exposure that produces a beneficial effect is known as hormesis. Examples of environmental stressors that promote a hormetic effect on lifespan through distinct molecular mechanisms (left) and a diagram of the concept of hormesis (right). Plot on right is adapted from Calabrese *et al.*, 2015[29].

1.1.3 Stress response pathways can be activated via environmental, genetic and pharmaceutical interventions.

Within the field of biogerontology, three primary strategies have emerged to induce a hormetic response and improve organismal health: environmental interventions, genetic interventions, and pharmaceutical interventions. Environmental interventions show promise in that exposing animals to actual stressors robustly extends lifespan across taxa and does not require development of and access to pharmaceuticals. However, these types of lifestyle interventions like calorie restriction are often not practical for improving healthspan on a large scale due to low adherence, difficulty in achieving the correct dose, and broad physiological effects that extend beyond aging[33-36]. One potential solution to these issues is to activate stress-response pathways through genetic or pharmaceutical means. For instance, dietary restriction

promotes lifespan across species through several mechanisms, including reduced insulin and mTOR signaling[37]. Genetic modifications that decrease insulin and growth hormone signaling can also mimic the effects of DR[38-40]. Similarly, pharmaceutical agents like rapamycin can mimic DR by inhibiting mTOR signaling, thereby improving health[41]. Currently, much work is focused on identifying pro-longevity circuits downstream of environmental interventions, with the goal of finding targeted pharmaceutical strategies that are more feasible than administrating stressors like DR in human populations[42].

In the remainder of this chapter, we will explore what is currently known about cell nonautonomous signaling and hormesis in health and longevity. We will then explore potential obstacles to implementing environmental, genetic, and pharmaceutical anti-aging interventions in humans. Finally, we will synthesize these concepts to highlight how the work presented in this thesis contributes to three key challenges facing anti-aging treatments.

1.2 Cell Nonautonomous Signaling and Hormesis in Health and Longevity[1]

1.2.1 Cell nonautonomous signaling plays a critical role in activating hormetic stress-response pathways.

Deciphering how cells relay information to one another remains a foundational discovery in biology. It was first posited by John Langley that cells express receptor proteins on the extracellular side of the cell membrane and, when bound by a signaling molecule, initiate a downstream physiological response[43]. This was validated by a series of discoveries, starting with Rita Levi-Montalcini's identification of nerve growth factor in the 1950s, followed by the discovery of additional growth factors[44], and ultimately leading to the identification of the

[1] This section is revised and updated from the publication "Cell Nonautonomous Regulation of Health and Longevity**"** in *Elife* (2020 Dec 10;9:e62659) with authors listed as Miller, H.A., **Dean, E.S**., Pletcher, S.D., and Leiser, S.F.

receptors themselves[45]. These discoveries were pivotal in furthering our understanding of cellular patterning during development[46] and how organisms adapt to external stimuli. This principle that cells can relay critical information to other cells in response to an initial signaling cue has profound implications: genes expressed in one cell or tissue can influence the physiology of distant cells and tissues. This ability of gene expression in one cell to affect processes in other cells and tissues is known as cell nonautonomous action or signaling.

More recently, high-profile studies from multiple laboratories have demonstrated that many signaling pathways known to improve longevity—such as mitochondrial stress, insulin-like signaling, heat shock, and the hypoxic response—operate through cell nonautonomous signaling mechanisms[47-52]. These pathways typically originate in sensory cells, often neurons, that signal to peripheral tissues to promote survival in stressful environments. Importantly, activating these stress response pathways, either through genetic modification or exposure to environmental stress, is often sufficient to improve health and longevity. Additionally, careful genetic modification of these pathways has the potential to target the aging process while sparing growth, developmental, and reproductive consequences of environmental stress. The growing understanding of cell nonautonomous signaling in aging is a relatively recent concept in geroscience that presents promising opportunities to identify pharmaceutical interventions that modulate signaling to enhance healthspan and longevity.

In this review, we summarize the recent wave of studies investigating the effects of cell nonautonomous signaling on canonical aging pathways across taxa. We also highlight where the field has excelled and draw insights from other research areas that have successfully mapped the neuronal circuitry underlying behavioral phenotypes.

1.2.2 Caenorhabditis elegans

Utilization of the model organism *C. elegans* has played an integral role in advancing the biology of aging. The discovery that mutations in the sole insulin-like growth factor receptor (IGFR), *daf-2*, can double the lifespan of a multicellular organism helped launch the field[19,21,38]. With their discrete, well-defined somatic cell fates, *C. elegans* provide an ideal model system for studying how cell nonautonomous signaling influences complex phenotypes like aging. We begin by discussing the extensive work on different *C. elegans* pathways that protect against stress and modify aging through cell nonautonomous mechanisms.

1.2.2.1 Energy balance and insulin signaling

After discovering that reduced insulin signaling extends lifespan, the aging field explored the tissue specificity of insulin signaling in longevity. The Kenyon lab used mosaic expression of *daf-2* to identify specific cell lineages where mutations are necessary for lifespan extension, marking the first clear demonstration of cell nonautonomous signaling in aging[53]. Subsequent epistasis experiments revealed that the longevity benefits of *daf-2* mutations depend on the class O forkhead transcription factor *daf-16*, whose nuclear localization drives pro-longevity effects[54]. From these initial studies on tissue specific activity of insulin signaling, cell nonautonomous signaling and the nervous system soon emerged as key players in regulating longevity (**Figure 1.3**).

While most of *daf-16*'s pro-longevity effects are thought to be tied to cell autonomous transcription of target genes in the intestine[55], intestinal expression of *daf-16* also induces target genes in other peripheral tissues including the nervous system. This cell nonautonomous signaling between the nervous system and peripheral DAF-16 is bidirectional: DAF-16 activity can be induced by neurons *and* neuron-specific genes are targets of DAF-16. For example, a

study analyzing RNA in isolated neurons of *daf-16* and *daf-16; daf-2* mutants found that *daf-16* targets genes exclusively expressed in mechanosensory neurons[56]. This led to the identification of a novel gene, *fkh-9*/FOXL1, that, when knocked out, entirely abrogates *daf-2* lifespan. However, cell nonautonomous signals from the nervous system to *daf-16* in peripheral tissues can also modify aging. Specifically, another transcriptional microarray analysis identified a set of neuronally expressed genes downregulated in animals on *daf-2* RNAi and upregulated in animals on *daf-16* RNAi[57]. One of these hits, the insulin-like peptide *ins-7*, is required for *daf-2* RNAi-mediated lifespan extension, suggesting *ins-7* may act as a cell nonautonomous signal from the nervous system to the intestine. These data are compelling as *C. elegans* are predicted to have 40 insulin-like peptides that both agonize and antagonize *daf-2,* some of which modify the lifespan of wild-type animals when neuronally overexpressed[58]. In addition to neuronal signaling molecules, individual neurons can also modify lifespan through cell nonautonomous activation of *daf-16*. When the projections of sensory amphid neurons are genetically knocked out or laser ablated, the animals live longer, often with the requirement of *daf-16* activity[59,60].

Insulin signaling also regulates longevity through cell nonautonomous communication between non-neuronal tissues. For example, recent studies show that some DAF-16 target genes, like *dod-8*, *dod-11*, and *hsp-12.6*, influence muscle aging non-autonomously[61], supporting the idea that metabolism and aging are interrelated, with bidirectional signaling between tissues. Foundational work from the Kenyon lab also discovered that ablating the germline inactivates *daf-16* and extends lifespan[62] through activation of a *daf-12*-dependent sterol signaling pathway in somatic reproductive tissues[63]. Modification of these reproductive tissues then induces the expression of *lips-17/fard-1* and produces an unknown lipophilic signal to increase *sod-3/dod-8*

in other somatic tissues[61]. This signaling pathway illustrates how cells signaling across tissues that "times are good/bad" can influence the aging process.

Intriguing work from the Ruvkun lab has also found that germline modification of insulin signaling interacts with the nervous system through microRNAs (miRNAs). miRNAs were discovered in *C. elegans*[64], and their small size, abundance across the genome, and evolutionary conservation, makes them an intriguing cell nonautonomous signaling molecule. One miRNA, *mir-71* is necessary for lifespan extension in *glp-1* germline mutants, and *mir-71* overexpression in a *glp-1* background extends lifespan beyond that of germline mutations alone[65]. Rescuing *mir-71* only in neurons is sufficient to rescue the germline mutant longevity phenotype, and intestinal *daf-16* expression is necessary for *mir-71* overexpression to extend lifespan in germline mutants. While this study presents an incomplete picture, it provides sound evidence for future studies to consider miRNAs as a target for inter-tissue signaling during the aging process.

In addition to modification of insulin signaling, germline ablation-mediated longevity also requires other types of cell nonautonomous signaling. For example, the absence of gonadal stem cell signaling leads to activation of intestinal transcription factors like *skn-1*/Nrf2 that help to globally remodel the organism's metabolism[66]. A lack of gonadal stem cells also increases circulating fatty acids (FAs) that are normally deposited in this tissue. This increase in circulating lipids may induce *skn-1*/Nrf2 nuclear localization that, in turn, enhances lipid metabolism and increases lifespan. *nhr-49*/HNF4α, a nuclear hormone receptor widely expressed throughout somatic tissues, also regulates both *glp-1*-mediated longevity and lipid metabolism[67]. Furthermore, *nhr-49* overexpression extends lifespan in a *daf-16*- and *glp-1*-dependent manner. While this work cannot be directly translated to human health, these data provide initial evidence

for critical signaling events between stem cells and nearby somatic tissues that influence longevity.

Multiple nutrient sensing pathways that interact with insulin signaling are conserved from worms to mammals including the target of rapamycin (TOR) and AMP-activated protein kinase (AMPK) pathways. The latter nematode ortholog, *aak-2*, has increased activity under low energy conditions and is sufficient to promote longevity when overexpressed[68]. Follow-up studies show that *aak-2* activity suppresses cAMP-response element binding protein (CREB)/CREB-regulated transcription coactivator 1 (CRTC-1) transcriptional regulation and this ultimately extends lifespan[69]. *crtc-1* neuron-specific knockout extends lifespan without the undesirable pleiotropic effects that accompany AMPK activation, like decreased growth and fecundity[70]. Interestingly, *nhr-49/*HNF4α is activated by AAK-2[71], and its neuronal expression is required for the lifespan extension in AAK-2 overexpressing animals. Furthermore, neuronal CRTC-1 is sufficient to block AMPK-mediated longevity. Neuronal *crtc-1* levels modify intestinal *aak-2* activity through the neurotransmitter octopamine as a mechanism for the nervous system to convey "times are good".

TOR and AMPK play antagonistic roles in modulating lifespan and metabolism. Downregulation of TORC1 complex proteins, like *raga-1*, increases lifespan[72] but requires neuronal *aak-2* activity[49]. Moreover, neuronal TORC1 expression is sufficient to shorten lifespan, consistent with a central "times are good" signal modulating longevity. RNA-seq comparisons of wild-type to *raga-1* knockout and neuronal overexpression identified *unc-64/*syntaxin as epistatic to neuronal *raga-1* activity. This work supports neural signaling as a driver of metabolic rearrangements, like increased mitochondrial fragmentation, that occur in peripheral tissues.

Although many of these studies identify the existence of neurosignaling pathways that drive metabolic changes in peripheral tissues, few have identified the signal(s) through which the nervous system transmits information to these tissues. Probing the precise mechanisms of nervous system to intestinal signaling is an essential next step in furthering our understanding of how cell nonautonomous signaling influences aging.

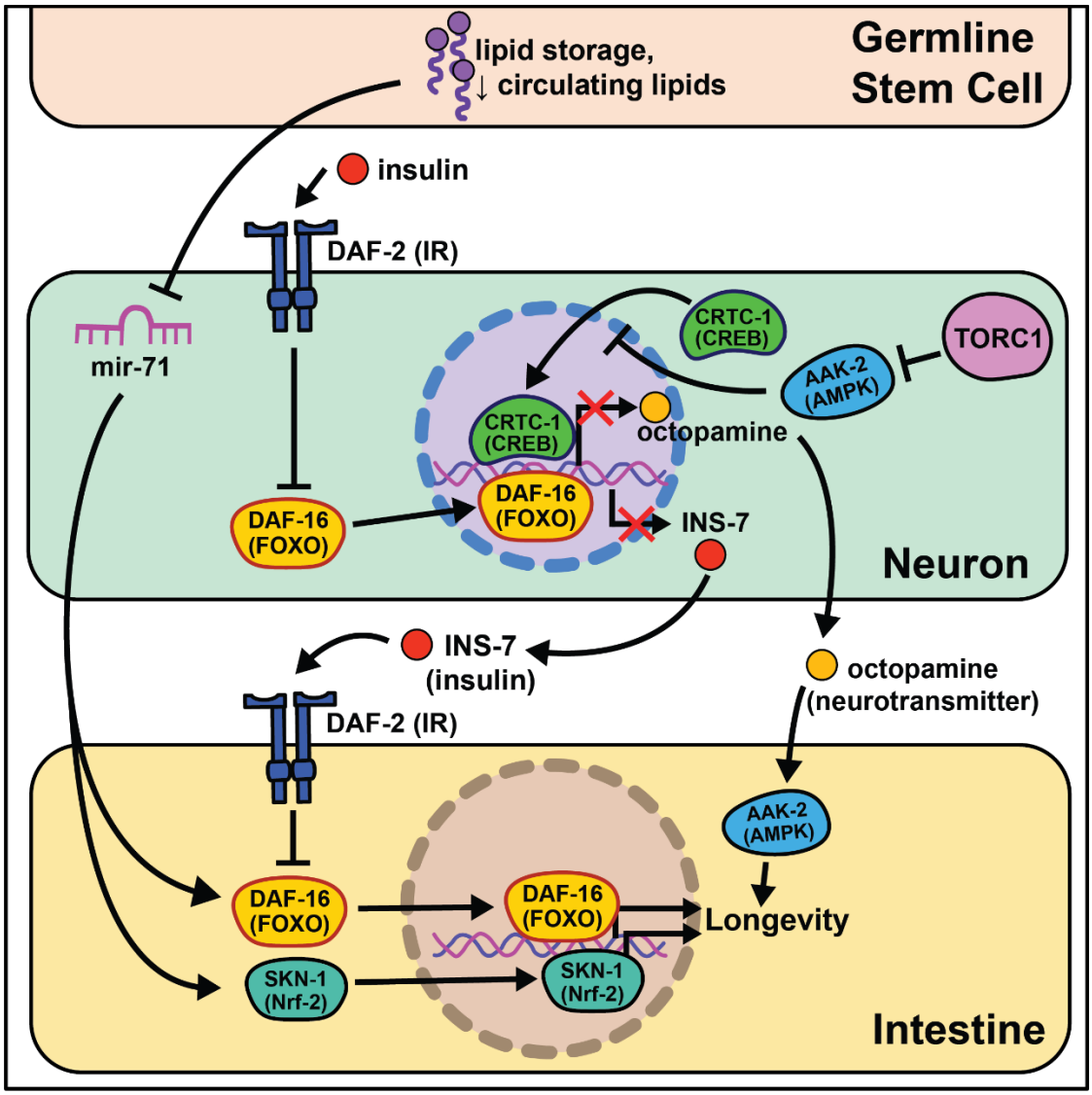


Figure 1.3 Summary of the role energy balance and insulin signaling on cell nonautonomous modulation of longevity in *C. elegans*. Mammalian orthologs are listed in parentheses. If there are no parentheses, the name is shared across taxa.

1.2.2.2 Proteostasis signaling pathways

A significant body of literature links increased stress resistance with longevity, leading to the hypothesis that acute moderate stress can trigger hormetic effects that extend lifespan[29]. Eukaryotic cells have evolved several organelle-specific stress responses that, when induced, extend nematode lifespan. One of these longevity-promoting stress responses is the unfolded protein response (UPR), a cellular signaling mechanism that helps maintain the balance of protein folding when stressful events cause the accumulation of unfolded proteins. This response can occur in either the mitochondria (mt-UPR) or the endoplasmic reticulum (ER-UPR).

Much like stress responses resulting from energy imbalance, these stress-response pathways that maintain proteostasis can also promote longevity. One example of mt-UPR mediated longevity is that knockdown of complex IV of the electron transport chain (ETC) with *cco-1* RNAi leads to delayed growth, slowed movement, reduced body length, and increased lifespan. Notably, *cco-1* knockdown exclusively in neurons increases lifespan without pleiotropic phenotypes by altering mitochondrial homeostasis in peripheral tissues[73]. Interestingly, this lifespan extension requires the mitochondrial unfolded protein response (mt-UPR), but not *daf-16*/insulin signaling. A follow up study using the heat shock protein-6 (*hsp-6*p::GFP) transcriptional reporter identified *vps-35* as lacking peripheral mt-UPR[74]. VPS-35 is a highly conserved protein in the retromer complex, involved in recycling Wnt and the Wnt secretion factor MG-4[75]. In agreement with this, the Wnt receptor *egl-20* is necessary and sufficient for cell nonautonomous mt-UPR induction and longevity. Neuronal serotonin production is also necessary for cell nonautonomous mt-UPR even though the loss of each of the four known serotonin receptors (*ser-1, ser-4, ser-7*, and *mod-1*) has no effect[74]. These results clearly define that mitochondrial stress, through reduction of ETC activity or separate activation of the mt-UPR, can be transmitted by neurons cell nonautonomously to modify aging. As with many of

these neuronal based networks, however, the central signaling pathways that activate the mt-UPR are not fully characterized.

In addition to the mt-UPR, multiple labs find that neuronal activation of the ER-UPR is sufficient to enhance stress resistance and extend lifespan[76-80]. This crucial discovery stems from identifying that the constitutively active spliceoform of X-box binding protein *1* (*xbp-1s)*, a transcription factor activated by the ER-UPR, rescues older animal survival on the oxidative stressor paraquat[76]. Expression of *xbp-1s* in the nervous system or intestine extends lifespan, and exclusive *xbp-1s* expression in the neurons is sufficient to increase paraquat stress resistance in young and older animals. It is likely that neuronal ER-UPR releases an activation signal conferring *xbp-1s* upregulation in the intestines that rescues motility in models of proteotoxicity like Aβ, polyglutamine aggregates (Q40), and dynamin[77].

More recent studies have begun to parse out where *xbp-1s* is required in the nervous system to extend lifespan. Work by the Taylor lab discovered that proteotoxic stress induced *xbp-1s* in the RIM and RIC neurons, and that *xbp-1* expression in just these neurons is sufficient to activate the intestinal ER-UPR. RIM is the primary tyramine producing neuron in *C. elegans*, and tyramine signaling was also required for neuronal *xbp-1s* to induce the intestinal ER-UPR[81]. While this study suggests the neurotransmitter tyramine may act as a cell nonautonomous signal in ER-UPR mediated longevity, work by the Dillin lab proposes a different cell nonautonomous signal. Specifically, Frakes *et al.* identified that expression of *xbp-1s* in glial cells is sufficient to extend lifespan and activate the ER-UPR in peripheral tissues[78]. This *xbp-1s*-mediated signal requires neuropeptide signaling but not neurotransmission for intestinal induction of *hsp-4,* suggesting a neuropeptide is the intermediate signal from the glia cells to the intestine[78]. While it is useful to identify neuropeptides as the causative signaling molecules, there remain hundreds of

potential coding regions annotated as "neuropeptides" in *C. elegans*[82,83]. Additional work in this area should examine whether neuronal and glial *xbp-1s* communicate to the intestine through distinct or partially overlapping mechanisms to better understand how tyramine and neuropeptide signaling may interact to induce the intestinal ER-UPR.

Another open question surrounds whether other transcription factors that respond to the ER-UPR can recapitulate the effects of *xbp-1* activation. Preliminary findings point to *xbp-1* activity, not *pek-1* or *atf-6,* a kinase and a transcription factor also activated by the ER-UPR[78]*,* as key to modifying lifespan. This implies that uncovering the pro-longevity targets of XBP-1 will be of high interest to understand and translate these results. Neuronal activation of *xbp-1s* results in changes in fat metabolism, a build-up in oleic acid (OA), and leaner animals[80]. It is possible that the pro-longevity phenotypes associated with *xbp-1s* are due to increased expression of lysosomal genes, like *asp-13* and *vha-18*, that enhance acidity and, therefore, protease activity. Furthermore, the lifespan phenotype and expansion of the ER in *xbp-1s* animals requires lipid depletion[79]. Initial results show enhanced intestinal lipid depletion through *ehbp-1* overexpression modestly extends lifespan and partially recapitulates the effects of *xbp-1s*. Taken together, these data emphasize the significant role metabolically active tissues, like the intestine, play in properly responding to cues from the nervous system (summarized in **Figure 1.4**). While the ER-UPR field is beginning to narrow in on specific neuronal cells and signaling molecules, much is left to delineate in the neuronal circuitry. Understanding how, when and where neuromodulators affect normal and pro-longevity conditions is paramount in translating these results to higher organisms and discovering therapeutic treatments to mimic these phenomena.

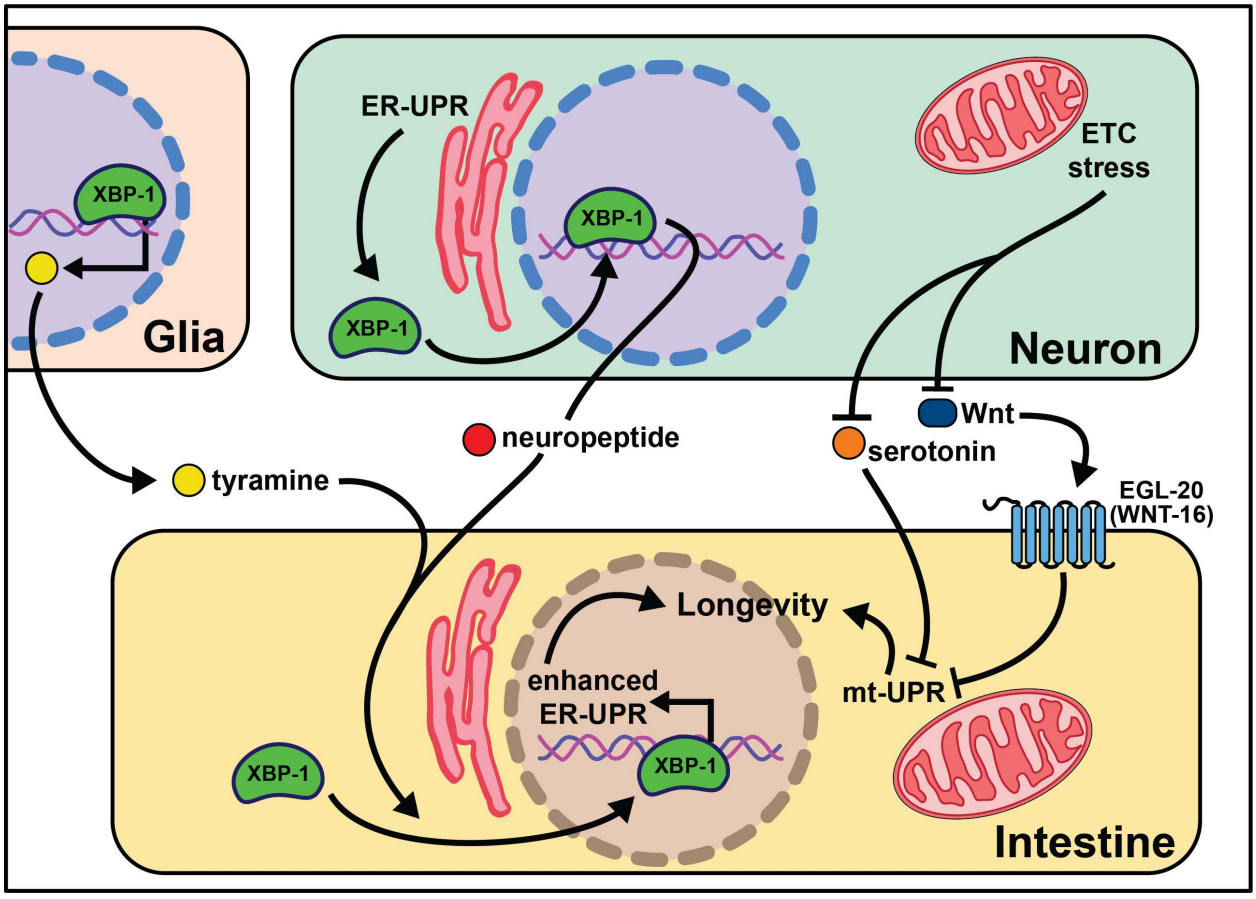


Figure 1.4 Summary of the role of proteostasis in cell nonautonomous modulation of longevity in *C. elegans*. Mammalian orthologs are listed in parentheses. If there are no parentheses, the name is shared across taxa.

1.2.2.3 Perception of external stimuli

An organism's ability to respond to changes in the environment, such as temperature, oxygen levels, and smells, is vital to their survival. In this section, we chronicle research findings linking perception of environmental cues to hormetic activation of longevity circuits (**Figure 1.5**). Some of these pathways converge on downstream components of the energy balance and proteostasis responses previously discussed, while others are thought to benefit lifespan through distinct mechanisms.

As poikilotherms, *C. elegans* are responsive to heat- and cold-shock. Generally, longevity varies inversely with temperature, where animals housed at lower temperatures (15 °C) live

longer than those at higher temperatures (25 ℃)[84]. Based on our understanding of thermodynamics this observation seems intuitive, but several papers have challenged this theory and shown that changes in lifespan across temperature are genetically modulated. In fact, many pro-longevity genetic mutations have a distinct relationship with temperature, promoting longevity at either cold or warm temperatures but rarely both[85]. These data are consistent with many genes playing an active role in the physiological response to changes in temperature. Whether by modifying the perception of or response to temperature, this interplay suggests that genes actively influence lifespan at various temperatures, refuting thermodynamics as the sole influence on temperature-mediated lifespan changes.

A robust body of research surrounds the connection between activating the heat shock response (HSR) and longevity. In *C. elegans*, post-reproductive adulthood is accompanied by an abrupt decline in protein quality control[86-88]. Thus, maintaining the ability to effectively respond to heat stress remains a hallmark of long-lived animals. It is important to note that heat shock, described in the literature as >30 ℃, likely uses partially distinct genetic mechanisms from warmer conditions (22 ℃-25 ℃) that will be addressed separately.

Early studies implicate the nervous system in regulating proteostasis through the HSR. Key signaling components of amphid neurons, *gcy-3* and *ttx-3*, are necessary for proper induction of global HSR during heat shock[89]. These early studies also implicate an unknown neurotransmitter in signaling from the nervous system to promote survival during heat shock. Optogenetic stimulation of the AFD thermosensory neurons triggers serotonin release from the ADF neurons that activates heat shock factor 1 (HSF-1) in the germline in the absence of heat shock[90]. In the absence of *ser-1*, a 5-HT2B serotonin receptor ortholog, HSF-1 is not re-localized to the nucleus upon AFD optogenetic excitation or heat shock. This result suggests that *ser-1* is

necessary for proper signaling during HSR. It is worth noting there is no predicted synapse or gap junction between AFD and ADF neurons, meaning there are likely intermediate signaling molecule(s) and/or cells yet to be discovered.

While HSR proteins are necessary for animals to survive warmer temperatures[91], it is significant that overexpression of *hsf-1* in neurons is also sufficient to increase stress resistance and longevity at standard temperatures (20 °C)[92]. Linking back to earlier work, intact signaling from the AFD/AIY neurons is required for heat stress resistance in worms overexpressing *hsf-1*[89]. This may be through *pat-4/* integrin-linked kinase (ILK) activity in the AFD/AIY[93]. Interestingly, intestinal *daf-16* activity is required for *hsf-1* overexpression to extend lifespan but is not required for heat stress resistance[92], suggesting these phenotypes have distinct signaling events despite their positive correlation.

Less is known about the mechanisms of cold- and warm-sensory signaling and metabolic remodeling that promotes longevity. As with the HSR, the AFD neurons are thought to play a role in appropriately responding to warmer temperatures as laser ablation and genetic disruption exclusively shortens lifespan at 25 °C[91]. Mutants lacking functional CNG calcium channels, a *tax-2/tax-4* heterodimer, are also short-lived at 25 °C and thought to be necessary for AFD neuronal activity when exposed to warm temperatures. These results are corroborated in a recent study showing the ASJ sensory neurons also require functional *tax-2/tax-4* channels to sense warm temperatures and activate intestinal *daf-16* to extend lifespan[94,95]. Experimental evidence suggests once these thermosensory neurons are activated they deploy *daf-9*, a cytochrome P450 ortholog, which inhibits *daf-12*, a nuclear hormone receptor, allowing worms to live longer at 25 °C[91]. An important distinction remains between AFD activation during warm- and heat-shock as many heat shock proteins, like *hsp-60* and *hsp-70*, are not upregulated at 25 °C[91]. These data

suggest that perception and response to temperature through thermosensory neurons are sufficient to modulate aging across temperatures. They also refute thermodynamics as the sole mechanism for how poikilotherms live shorter at higher temperatures.

In agreement with neural modulation of aging in warmer temperatures, a transient receptor potential (TRP) channel, TRPA-1, detects cold temperatures in chemosensory neurons. TRPA-1 signals through a protein kinase C (PKC) ortholog, PKC-2, to increase intestinal DAF-16 activity and therefore lifespan[96]. Loss of *trpa-1* channels in the nervous system prevents the lifespan increase observed in Wild-Type (WT) worms at cooler temperatures (15-20 °C) but does not change longevity at warmer temperatures (25 °C). Interestingly, human transgenic TRPA-1 recapitulates many of these findings, suggesting a conservation in function. An unbiased screen of all sensory neurons showed *trpa-1* expression in the head neuron IL1 is necessary and sufficient to rescue *trpa-1* knockout. Further, genetically knocking out glutamate secretion and uptake prevents IL1 from modifying lifespan[94]. MGL-1, the glutamate receptor implicated in this study, is only expressed in neurons, indicating there must be another neuron involved in this pathway. Knocking out serotonin signaling blocks the effects of IL1 on lifespan, and transgenic serotonin expression in the NSM enteric neuron rescues the phenotype. The intestinal GPCR *ser-7* is the likely downstream receptor responding to serotonin release[94]. This study offers a more complete model than is often presented in the field, and suggests it is feasible for other cell nonautonomous signaling pathways to be more explicitly characterized in future studies.

In addition to responding to temperature change, the *C. elegans* nervous system plays a crucial role in determining nutrient quality and safety as they forage for food. Interestingly, the lack of any perceived food signal (i.e. dietary restriction (DR)), can also act as a signal on its own. DR, first reported to increase lifespan in rats in 1935[97], is an intervention that significantly

limits food intake without causing malnutrition, and has been the most consistent intervention to increase longevity across species[37]. However, since implementation of any dietary intervention for humans at a whole population level is challenging, mapping out the molecular and signaling mechanisms downstream of food perception, where they can be targeted directly, circumvents the challenges of adopting population level-DR protocols.

The first report of DR acting through a sensory, cell nonautonomous signaling mechanism in worms was in 2007. Bishop and Guarente identified the antioxidant response transcription factor skinhead 1 (SKN-1) in ASI sensory neurons leads to increased whole-body respiration and extended lifespan[98]. This report remains foundational in establishing food perception, or lack thereof, as a major driver of the health benefits of DR. More recent studies corroborate the significance of sensory neurons in lifespan when nematodes are subjected to long- and short-term starvation. A subset of sensory neurons, the ASI and ASJ, shorten lifespan through the expression of insulin-like peptide (ILP) *ins-6* during food perception[95]. More specifically, *ins-6* is released upon feeding, and *ins-6* overexpression exclusively in the ASI or ASJ neurons blocks the longevity effects of *tax-2; tax-4* mutant worms when fasted. This suggests that an unknown inverse signal may suppress *ins-6* expression during fasting.

Sensory cues from food perceived by the nervous system trigger a host of behavioral and metabolic rearrangements that accompany changes in lifespan. Particularly, in the absence of food, nematodes tend to increase their movement when foraging and stop pharyngeal pumping[99-101]. Once an attractive odorant is perceived, serotonin is released triggering triglyceride fat catabolism by a predicted acyl-CoA oxidase, *acox-1*[102]. Surprisingly, this fat catabolism is necessary and sufficient to modulate changes in behavior. *acox-1* mutants do not respond with the canonical behavioral changes observed when animals are exposed to exogenous serotonin[103].

Additionally, rescuing *acox-1* expression in the intestine alone abrogates the fat accumulation and pumping response to serotonin exposure. *egl-2*, an ether-à-go-go (EAG) potassium channel expressed in the sensory neurons, likely functions as an intermediary neuron signaling back to serotonin neurons communicating satiety from peripheral tissues. Intriguingly, antagonizing serotonin signaling through an atypical antidepressant mianserin extends lifespan and is non-additive with DR[104,105].The role of neuronal serotonin signaling in food perception and DR-mediated longevity is also supported by the finding that the smell of food attenuates DR lifespan extension in a serotonin- and dopamine-dependent manner[105]. Based on these findings, it is worth exploring whether the changes in metabolism and lifespan when serotonin signaling is antagonized are acting within the same pathway. Together, these results also corroborate the hypothesis that a feed-forward signal is released from the intestine back to the nervous system during food perception.

Finally, recognition of low-oxygen conditions or genetic stabilization of the conserved hypoxia-inducible factor-1 (HIF-1) extends nematode longevity[106,107]. A single protein, flavin-containing monooxygenase-2 (FMO-2), is both necessary and sufficient to provide many of the benefits of HIF-1 activation[48]. This hypoxia-FMO-2 longevity pathway also relies on cell nonautonomous signaling between neurons and the intestine: neuronal stabilization of HIF-1 is sufficient to induce intestinal *fmo-2* and improve health and longevity. Serotonergic signaling is required for HIF-1-mediated longevity and *fmo-2* induction, while FMO-2 overexpression in the intestine is sufficient to increase lifespan. Interestingly, other researchers have found FMO induction in multiple mammalian models with increased lifespan, including DR, consistent with FMOs playing a conserved role in promoting long-term health and increasing the likelihood these results will be translatable to human longevity[108-110].

Together, perception of many environmental signals influence lifespan in *C. elegans*. While the mode of sensory detection varies between these environmental signals, perception of temperature, oxygen, food availability, and chemosensory cues all activate sensory neuron-initiated signaling pathways. This external perception interacts with internal cues (e.g. germline signals, proteostasis, and metabolism) to appropriately respond and modify physiology. While we have begun to identify the cells and signals involved in these sensory-driven longevity pathways, many questions remain regarding how information is transmitted and interpreted both within and between tissues.

A

Intervention	Neuron A	Neuron B	Neuron C
Heat Stress	AFD	ADF	NA
Cold Stress	IL1	NSM	unknown
Dietary Restriciton	NA	ASI/ASJ	NA
Hypoxia	NA	RIM	NA

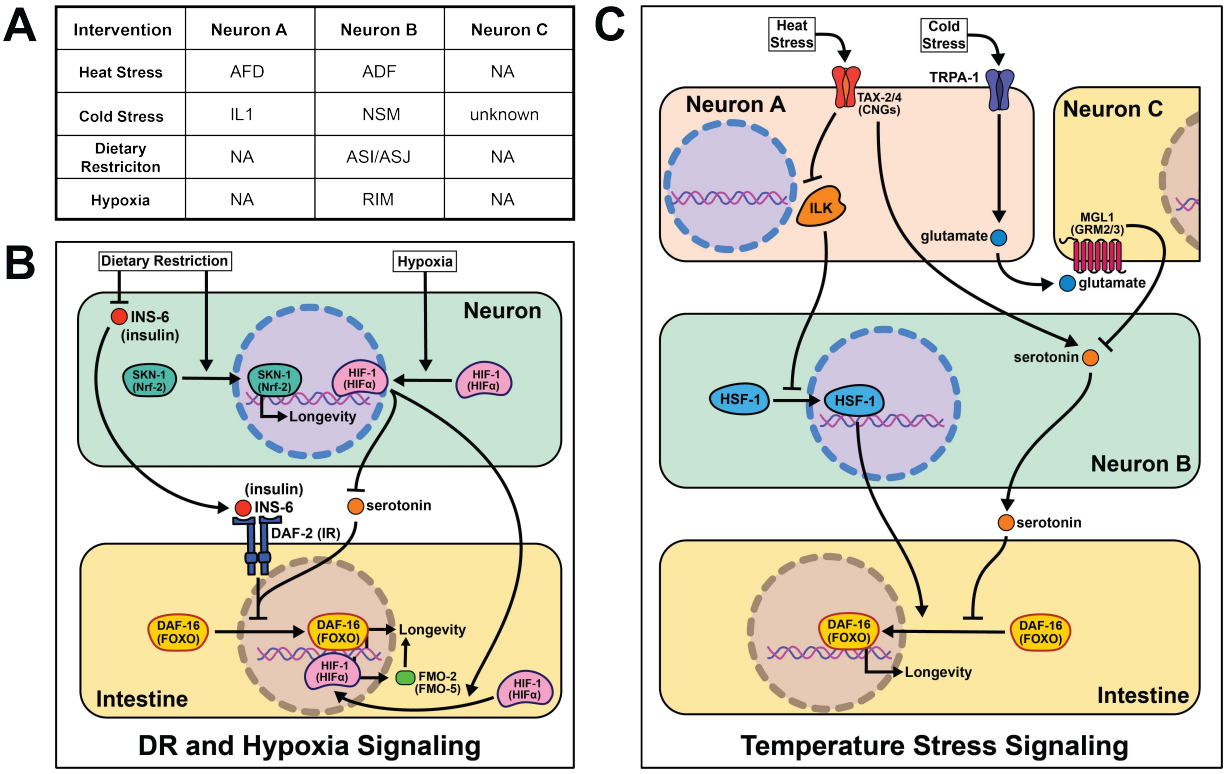


Figure 1.5 Summary of the role of perception on cell nonautonomous modulation of longevity in *C. elegans*. Mammalian orthologs are listed in parentheses. If there are no parentheses, the name is shared across taxa.

1.2.3 Drosophila melanogaster

While *C. elegans,* with its simplicity and constant number of somatic cells, is perhaps the most powerful system for identifying genetic mechanisms of aging, this model does pose some

limitations: the nematode nervous system is rudimentary, precise manipulation of diet and other environmental factors is difficult, and the limited behavioral repertoire of the worm is restrictive. Conversely, studies of cell nonautonomous modulation of aging in vertebrate animals are impeded by multiple factors, including but not limited to 1) the time required for measuring a longer lifespan, 2) challenges in using large-scale genetic modification for pathway discovery, and 3) the difficulty of identifying small subsets of key cells within substantially larger and more complex tissues.

Given the remarkable advances in neuroscience, together with its long-standing success as a model for both behavioral neuroscience and aging biology, the vinegar fly, *Drosophila melanogaster*, provides unique strengths to investigate these questions. Conservation of mechanisms of aging, including insulin/FOXO-related signaling and sensory-derived control of longevity, in worms, flies, and mammals suggests that signaling mechanisms likely become more complex in higher organisms but produce similar pro-longevity outcomes. Although the phylogenetic relationship between nematodes, arthropods, and vertebrates is debated, 18S rRNA and mitochondrial rDNA sequencing suggests a greater evolutionary distance between *D. melanogaster* and *C. elegans* than between *D. melanogaster* and *M. musculus*[111]. Consequently, mechanisms of aging conserved between worms and flies are also likely to span the smaller evolutionary gap between flies and mammals. In the following sections we provide an overview of key cell nonautonomous modulators of fly health and aging[25,112].

1.2.3.1 Energy Balance and insulin signaling

Soon after the foundational discovery that reduced insulin signaling increases nematode lifespan, experiments in *Drosophila* revealed that such results were not worm-specific and that this pathway may be involved in modulating aging across taxa[113]. Mutations disrupting

molecules in this pathway such as the single insulin receptor, *dInR*, or the *fly* homolog of the insulin receptor substrate, *chico*, exert cell nonautonomous effects on aging, where reduced insulin/IGF-1 signaling (IIS) is associated with extended lifespan[39,114]. Genetic manipulations that mimic reduced IIS, such as overexpression of *dFOXO* in the abdominal or pericerebral fat body or overexpression of phosphatase, *dPTEN*, in the pericerebral fat body also extend fly lifespan[115,116]. These data indicate that insulin signaling acts cell nonautonomously to control aging and promotes bi-directional signaling between peripheral tissues and neurons similarly to what is seen in *C. elegans*.

The *Drosophila melanogaster* genome encodes several insulin-like peptide genes (*dilps*), which are produced in a handful of neurosecretory cells in the *pars intercerebralis* region of the fly brain. These insulin producing cells, called IPCs, release the signaling molecules into the hemolymph to signal to the rest of the body through a single insulin-like receptor (*InR*)[117-119]. Among their range of biological functions in development and physiology, *dilps* modulate aging, and in this context the most well-studied are *dilp2*, *dilp3*, *dilp5,* and *dilp6*[119-121] . Partial ablation of IPCs—the production site of DILPs 2, 3, and 5—reduces IIS and increases lifespan[122,123]. Knocking down GABA-B receptors in IPCs decreases DILP secretion in fed and fasted conditions, yielding a small but significant decrease in stress resistance and lifespan under starvation[124]. Mutation of *dilp2*, *dilp3*, and *dilp5* together increases lifespan as does loss of *dilp2* alone, although loss of other individual *dilps* does not[119]. Induction of *dilp6* in fat body tissue also promotes longevity. However, it is unclear whether this is a direct effect of DILP6 or is due to a decrease in the secretion of DILP2 from the IPCs[120]. Similarly, the extended lifespan observed following increased *dFOXO* expression in pericerebral fat body may also result from a decrease in *dilp2* expression in the IPCs[125]. More recent work has revealed a role for *dilp1* in

promoting lifespan[126], potentially through induction of adipokinetic hormone (AKH), which is a functional homolog of mammalian glucagon[127] and which increases fly lifespan, fat metabolism, and free fatty acid catabolism[128,129].

The link between lifespan extension from manipulation of neuronal *dilps* and the insulin-responsive transcription factor FOXO in peripheral tissues are less clear in *Drosophila* compared to in *C. elegans*, suggesting that IIS extends lifespan, at least partly, through FOXO-independent pathways. Loss of *dilp2* does not influence the expression of known FOXO target genes and interactions with *dilp1* do not modify this result[126]. Flies lacking IPCs or with loss of *dilps 2, 3,* and *5* exhibit an abnormal response to diet manipulation[119,121], although *dFOXO* mutation leaves the response largely intact[130]. Furthermore, loss of *dFOXO* only partially rescues longevity benefits of *chico* mutants[131].

Another nutrient-sensing pathway that acts cell nonautonomously in flies, like worms, is AMPK. Neuronal or intestinal activation of AMPK or Atg1 induces autophagy in both the brain and gut to slow organismal aging and improves numerous healthspan measures[132]. Downstream of this activation, Dilps are implicated in mediating the inter-tissue response from the nervous system to the intestines and vice versa[132]. It is interesting that AMPK activation from several tissues causes metabolic remodeling across the whole body. Together, these data point to a feed-forward mechanism where signaling events occur bi-directionally to modulate the fly response to successfully survive stressful stimuli (**Figure 1.6**).

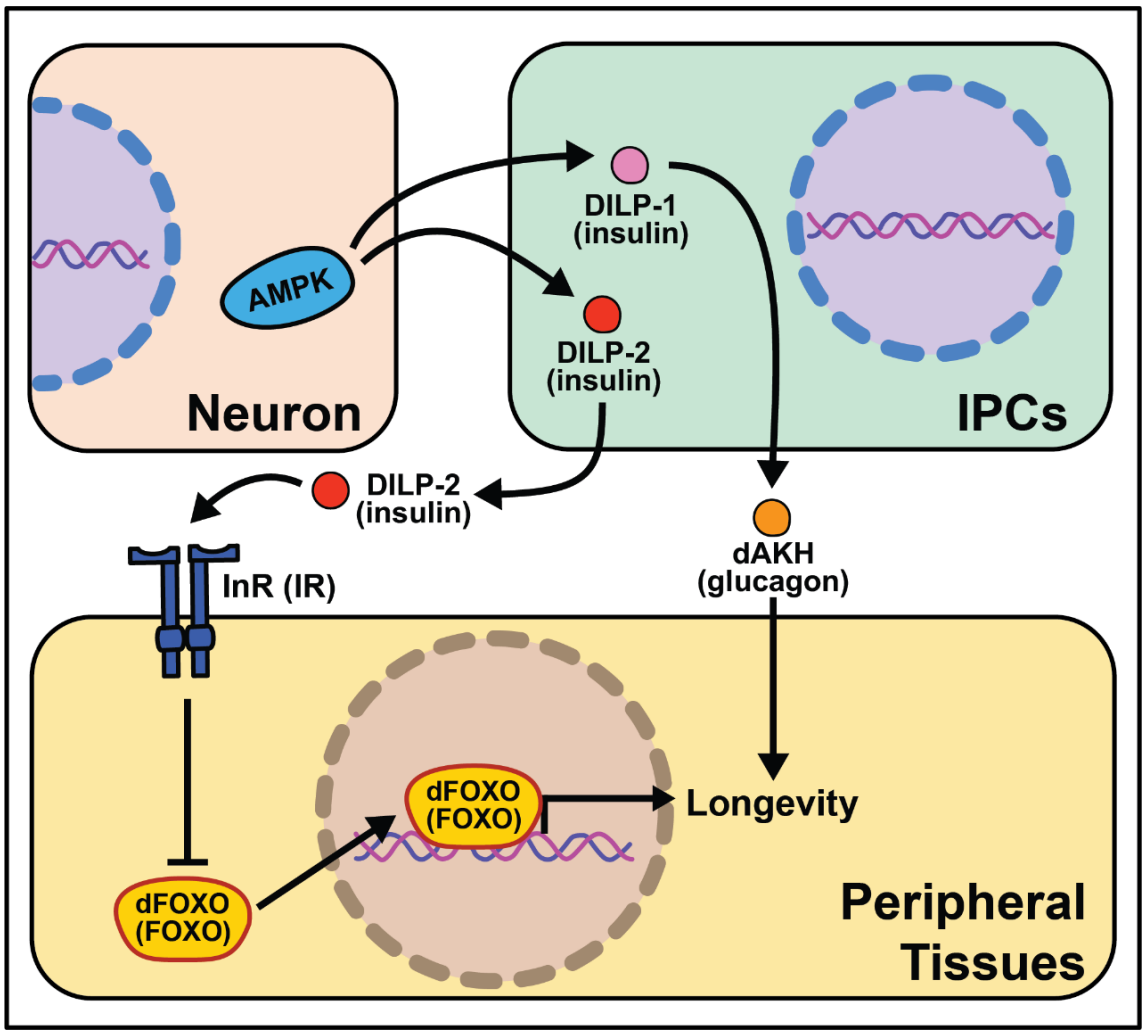


Figure 1.6 Summary of the role energy balance and insulin signaling on cell nonautonomous modulation of longevity in *D. melanogaster*. Mammalian orthologs are listed in parentheses. If there are no parentheses, the name is shared across taxa.

1.2.3.2 Proteostasis signaling pathways

When it was first discovered that knocking-down mitochondrial electron transport chain components in nematodes extends lifespan, it seemed unlikely this phenomenon would be conserved in higher systems. Surprisingly, research using flies (**Figure 1.7**) and mice (later discussed in **Section 1.3**) points to a significant role for mitochondrial function in organismal lifespan. Global knockdown of ETC components in complexes I, III, IV, and V extends fly lifespan, but does not inhibit ETC complex formation or ATP production[133]. Furthermore,

knockdown of complexes I and IV in neurons alone is sufficient to extend lifespan. This led researchers to ask how knockdown of the ETC extends lifespan. Follow up studies show that knockdown of ETC complex I using ND75 RNAi in muscle tissue increases reactive oxygen species (ROS) and activates the mito-UPR and ImpL2 (insulin/IGF binding protein)[134]. Subsequently, upregulation of mito-UPR target genes preserve muscle function while ImpL2 signals to the brain and fat body to decrease global insulin signaling. It is likely both pathways contribute to the longevity phenotype of decreased respiration chain expression. Additional data also suggest that ImpL2 increases lysosomal biogenesis and that autophagy genes are necessary for ND75 knockdown animals to live long. Another datapoint suggesting conservation of this pathway is that knockdown of ETC ND75 in complex I results in smaller flies, a phenotype that is also observed in the nematode ortholog *isp-1* mutants[135].

Modifying the mitochondrial proton gradient by expressing human uncoupling proteins (hUCPs) modulates fly lifespan. Interestingly, the context of when and where the hUCPs are expressed plays a critical role in health and longevity outcomes. hUCP2 targeted to the neurons increases health and longevity while increasing the rate of glycolysis and decreasing ROS production and oxidative damage[136]. Similarly, moderate pan-neuronal overexpression of hUCP3 leads to a modest lifespan extension exclusively in male flies[137]. However, use of a stronger driver that targets hUCP3 pan-neuronally or to the median neurosecretory cells (mNSC) significantly decreases their lifespan. These data suggest that lowering uncoupling mitochondria by high expression of hUCP3 alters mNSC function in a way that increases DILP levels in fly heads and leads to a concomitant decrease in lifespan. Much is left to be done to fully understand the relationship between modulating mitochondria ROS levels and lifespan.

Proteostasis also plays a key role in muscle maintenance with age. While slightly tangential to this review's primary focus on longevity outcomes, the loss of muscle mass often precedes other age-related phenotypes like risks of falling. Throughout life, a fly's muscles accumulate protein aggregates that impair function. Maintenance of proteostasis is enhanced in long-lived animals through elevated activity of FOXO target genes like 4E-BP that increase lysosome/autophagy functions[138]. Interestingly, FOXO signaling through 4E-BP activity in muscle decreases feeding behavior and the release of insulins that delay the age-related accumulation of protein aggregates in other tissues. This result suggests bi-directional cell nonautonomous signaling across tissues with a yet to be discovered signal[138].

Finally, overexpression of the gene hedgehog (*hh*), the Hedgehog signaling pathway ligand in *Drosophila,* extends lifespan through activation of the ER-UPR. While overexpression of hedgehog signaling components in neurons has little effect on lifespan, overexpression in glial cells is sufficient to extend it. Downstream of *hh* overexpression, overexpressing *hsp69* and *hsp40* in glia is sufficient to rescue lifespan in *hh* signaling mutants. Similarly, overexpression of smoothened (*smo)* and *hsp68* in glia partially rescues the lifespan shortening effects of expressing human Aβ42 plaques in *Drosophila* glia. Hh signaling may increase chaperone protein expression in adult glia, which act to maintain the integrity of dopaminergic neurons, leading to increased longevity[139]. Conversely, disrupting this pathway shortens lifespan and decreases the number of dopaminergic neurons[139]. This work parallels nicely with work in *C. elegans* described above in which glial cells modulate aging through the UPR[78]. While such data are compelling, it remains unclear how neuronal and glial subtypes contribute to the lifespan extension of enhanced hedgehog signaling. It is also interesting to consider the conserved role glia cells play in neurotransmission, cell nonautonomous signaling, and longevity.

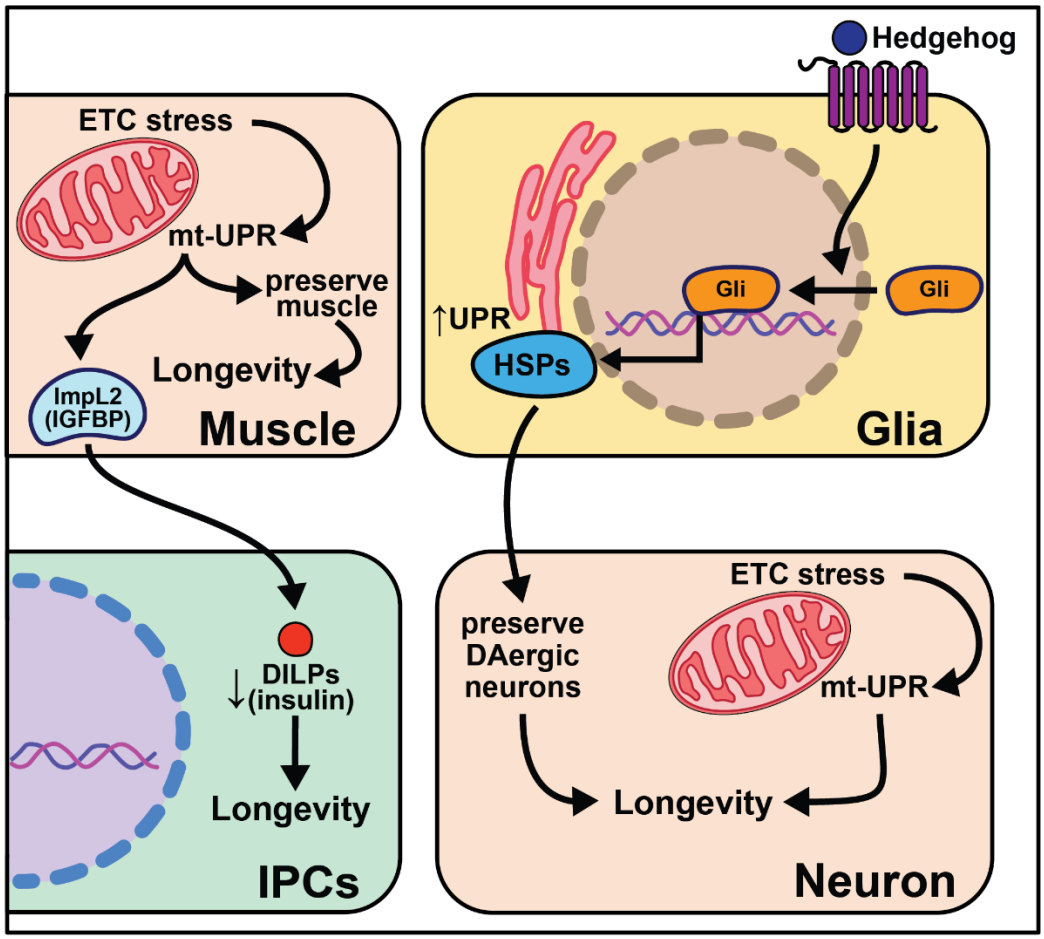


Figure 1.7 Summary of the role of proteostasis in cell nonautonomous modulation of longevity in *D. melanogaster*. Mammalian orthologs are listed in parentheses. If there are no parentheses, the name is shared across taxa.

1.2.3.3 Perception of external stimuli

Research in *Drosophila* has greatly expanded our understanding of the effects of sensory perception on aging. Sensory inputs that relate information about nutrition, conspecifics, and dangerous situations rapidly initiate changes in fly physiology and patterns of aging, often within a few days (**Figure 1.8**). It is known, for example, that a restricted set of olfactory and gustatory neurons influence aging by either promoting or limiting lifespan, fat deposition, or general vigor in old age[112,140]. Sensory perception of specific sugars and amino acids[141,142], as well as social signals such as the health of conspecifics[143] or availability of potential mates[144], is also

important. Conserved neuropeptides and functionally-defined neuronal populations, some associated with psychological conditions such as reward and hunger, are involved in mediating these effects through new candidate cell nonautonomous aging mechanisms[144-146].

Much of this work is centered around the effects of food perception. Exposure of flies to the odor of an important food source (live yeast) as well as knock-out of a critical co-factor for normal olfactory function (*Or83b*/*Orco*) established food perception is sufficient to partially reverse DR-mediated longevity[112]. Loss of Orco function significantly increases fly lifespan. These effects are independent of food intake, activity, respiration, or early-life reproduction, suggesting a direct effect of sensory perception. Mutation of the water sensor, *ppk28*, extends *Drosophila* lifespan by up to 40%, and this effect requires AKH/glucagon receptor[128]. AKH protein levels are higher in *ppk28* mutant animals, and activation of *Akh*-expressing neurons is sufficient to recapitulate the effects of loss of *ppk28* on lifespan. Gustatory perception is also necessary for normal stress resistance and lifespan in a low-glucose environment[140]. Loss of sweet taste receptor *Gr64* produces a sleep-impairment phenotype that is phenocopied by blocking dopamine neurotransmission, and taste-blind flies lived longer than control flies, despite eating more[147]. Conversely, loss of the *Drosophila* trehalose receptor, *Gr5a*, significantly decreases lifespan without altering feeding[129], establishing that taste inputs can modulate lifespan in both directions. Much like some methods of DR-mediated longevity in *C. elegans*, loss of labellar taste bristles requires insulin signaling to extend lifespan in flies[147].

Interestingly, the effects of dietary restriction on *Drosophila* aging are predominantly influenced by dietary composition rather than the overall caloric content of the food[148-151]. Flies exposed to restriction of essential amino acids will choose to switch from a diet comprised primarily of sugar to one primarily of protein[152]. This behavioral switch in feeding preference

requires both serotonin signaling through the 5-HT2A receptor and plasticity of a dopaminergic circuit[52,153]. When flies are allowed to choose the sugar and protein composition of their own diet, they live shorter than when presented with a single, complete diet[52]; an effect that also requires nutrient sensing and signaling through the serotonin receptor 5-HT2A.

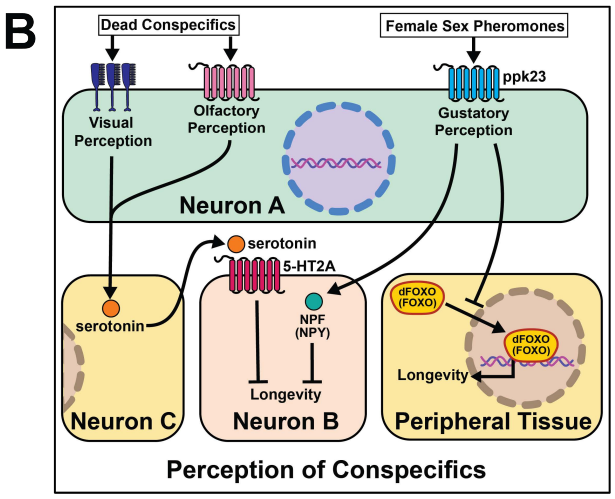
Outside of a flies' ability to assess food quality, several other sensory cues rely on neuronal signaling to modulate lifespan. Exposure to female sex pheromones in the absence of mating causes rapid and reversible declines in fat stores, stress resistance and longevity in male flies[154]. These changes in metabolism and lifespan require taste perception through the gustatory receptor, *ppk23,* as well as neuronal signaling involving the conserved neuropeptide NPF/NPY and FOXO. Moreover, these effects are partially reversed by copulation, suggesting that survival costs of reproduction in male flies are controlled by neural circuits through which reproductive expectation dictates costly precopulatory investment in reproductive success. Related circuits that perceive reproductive reward ameliorate the consequences of this investment if mating is achieved[144]. Because mating decreases both worm and fly lifespan, it's worthwhile to ponder why perception of imminent mating without achieving it causes greater physiological harm to a flies' health. Perhaps upon completing a satisfying activity that is evolutionarily beneficial, like eating or mating, specific neural circuits and signaling peptides reinforce these behaviors, and without these signals only detrimental effects remain.

In addition to cues regarding food availability and reproduction, cues that putatively signal danger are also important. *Drosophila* can visually perceive dead conspecifics in their environment and this experience induces both short- and long-term effects on health and longevity. Exposure to dead flies decreases resistance to starvation, depletes lipid storage, and shortens lifespan[143]. As with protein perception, serotonin signaling via receptor 5-HT2A is

required for death perception to influence lifespan, suggesting a key role for 5-HT2A signaling in lifespan. In addition to death perception, carbon dioxide levels can also act as a danger signal. In *Drosophila, Gr63a* encodes for one of two proteins which make up a CO_2 receptor[155], and flies with a loss of function mutation in *Gr63a* are long-lived. Interestingly, *Gr63a* is expressed on olfactory neurons, and is also required for the odor of live yeast to shorten lifespan. Consequently, nutrient sensing and carbon dioxide sensing could act through interconnected pathways to influence lifespan[156].

A

Intervention	Neuron A	Neuron B	Neuron C
Death Perception	visual neurons, olfactory neurons	unknown	5-HT2A+ neurons
Female Sex Pheromones	leg/wing margin gustatory neurons	NPF+ neurons	NA
Dietary Restriction	gustatory and olfactory neurons	IPCs, DAergic, 5-HT2A+ neurons	NA
CO_2 Perception	ab1C neurons	NA	NA
H_2O Perception	NA	AKH-producing neurons	gustatory neurons



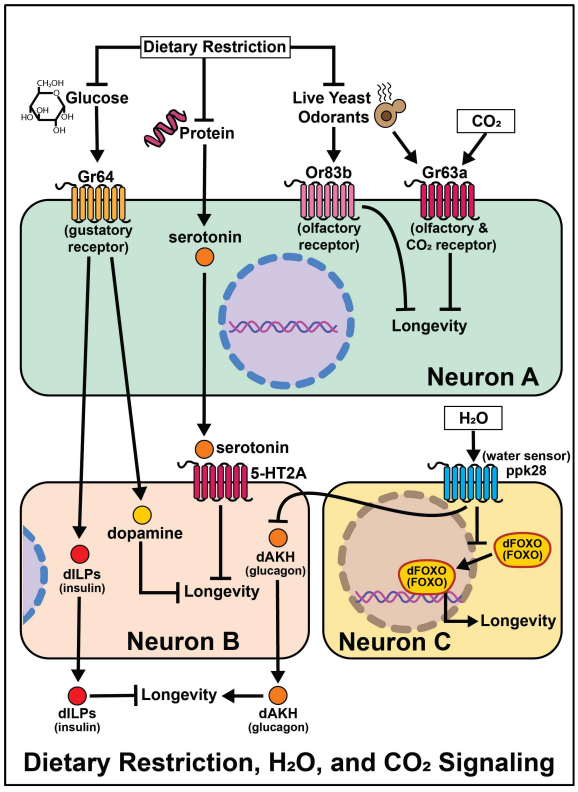


Figure 1.8 Summary of the role of perception on cell nonautonomous modulation of longevity in *D. melanogaster*. Mammalian orthologs are listed in parentheses. If there are no parentheses, the name is shared across taxa.

1.2.4 Mammals

Fewer studies have explored the effects of aging and cell nonautonomous signaling in mammals due to the extended amount of time and effort needed to perform these experiments.

Despite these considerations, a growing body of literature suggests the types of signaling events seen in invertebrates are conserved from worms to mice. These initial findings portend an increase in the number of studies investigating the effects of the nervous system on aging. In this section we will discuss the individual studies performed in mice and compelling evidence that suggests this phenomenon may be conserved in humans (**Figure 1.9**).

Similar to the effects observed in worms and flies, reduced insulin and growth hormone signaling also significantly increase mouse lifespan[157]. Ames dwarf mice, and the similar Snell dwarf mice, each have a single-gene mutation, Prop1 and Pit1, respectively, that impairs anterior pituitary development leading to decreased growth hormone, thyroid stimulating hormone, and prolactin levels. These mice live 40% longer than controls and have decreased plasma IGF-1[40]. However, dwarf mice do become obese in old age, showing that pituitary modulation of aging is independent of body weight regulation. Interestingly, grafting a control pituitary gland in adulthood does not rescue control lifespan in Snell dwarf mice[26]. The mechanism for the longevity of dwarf mice likely involves IGF-1, because similar results have been obtained using the knockout for growth-hormone receptor binding protein (GHR-KO)[158], a heterozygous null mutation of the IGF-I receptor[159], and the knockout of growth hormone releasing hormone (lit/lit mice, mutant for Ghrhr)[26]. Similarly, partial loss of function of IGF-1R in neurons during development leads to reduced growth and lifespan extension[160]. These mice gain slightly more weight with age than WT controls and have higher levels of subcutaneous adipose tissue, higher circulating leptin, and higher circulating lipids. These studies show decreased insulin signaling can alter global metabolism and extend lifespan in mammals. While they do not directly test the effects of other types of neural signaling, this work does confirm that insulin signaling influences lifespan in mice.

Related work in humans suggests insulin regulation, sensitivity, and neuronal excitability all positively correlate with longevity. A transcriptome analysis of cerebral cortex tissue compared >85 year old humans to the <80 year old group. This comparison identified one transcriptional repressor, REST, in which expression positively correlated with longevity[161]. REST negatively regulates neural excitation and FOXO1 expression, and C. *elegans* REST orthologues *spr-3* and *spr-4* are required for *daf-2*/IGFR knockout lifespan extension. The signaling mechanisms between neuronal REST activity and FOXO1 expression in peripheral tissues are not known, but these data provide ample evidence of conserved cell nonautonomous modulation of long-term health.

Similarly, genetic studies of centenarians have identified the locus encoding for tyrosine hydroxylase (TH), insulin (INS), and Insulin Growth Factor 2 (IGF2) as correlative with longevity[162]. TH is the rate-limiting enzyme responsible for producing the neurotransmitter dopamine[163]. This study also looked more closely at the association of specific INS and IGF2 polymorphisms with longevity in humans. Polymorphisms in the subregion spanning TH and INS were significantly associated with lifespan in females, while polymorphisms in the region spanning TH and IGF2 were significant in males. These data support the role of insulin and dopamine signaling in human lifespan, and the gender difference observed may be explained by variations in metabolism between the sexes in old age. Supporting these findings, another research group genotyped a cohort of 90-109 year olds and compared them to ancestry-matched younger people (ages 7-45). The 90+ cohort had a 66% higher incidence of a specific allele of the dopamine D4 receptor (DRD4 7R) which correlated with higher physical activity[164]. Additionally, DRD4 knockout in mice leads to an ~8% decrease in lifespan. It's unclear what

changes in dopaminergic signaling occur in these two populations and whether the increased physical activity is directly linked with the DRD4 allele.

Unlike dwarf mice, mice heterozygous at the insulin receptor substrate 2 (Irs2) locus do not differ from their control counterparts in food intake or body weight, but do have significantly increased insulin sensitivity and live ~25% longer[165]. Knocking out Irs2 in neurons (bIrs2) is sufficient to phenocopy the lifespan extension in the global knockout, and leads to decreased mRNA expression of superoxide dismutase 2 (Sod2) and Foxo1. These results support previous hypotheses that reduced insulin signaling in neurons modulates lifespan by enhanced protection from oxidative stress. It will be interesting to test whether enhanced Irs2 expression in the nervous system shortens mouse lifespan.

Recent studies address questions about initiation and duration of a longevity intervention. Most studies introduce dietary or therapeutic interventions while the mice are young adults[166]. This method is not entirely translatable to humans as most would likely be middle-aged or elderly before adopting a pro-longevity treatment regimen. Many labs are beginning to address this concern by testing the effects of longevity treatments after reaching midlife[41,167]. Applying these principles, supplementing middle-age and elderly mice with intranasally administered recombinant human Hsp70 extends lifespan by ~10% and improves learning and memory during old age[168]. Interestingly, Hsp70-treated mice had higher neuronal density in the temporal cortex and the hippocampus and immunostaining of the cerebral cortex for ribosomal proteins reveals more accumulation of proteasomal subunits in the Hsp70-treated mice. This suggests that Hsp70 promotes proteasomal activity and can extend lifespan in mammals, presumably through both cell autonomous and cell nonautonomous mechanisms.

Within the mammalian brain, the hypothalamus is a key producer of neuropeptides and hormones. It is likely many signals from the hypothalamus are important to relay information from neurosignaling pathways to the rest of the body. Additionally, the hypothalamus is key to maintaining homeostasis in energy balance, blood pressure, oxygenation, body temperature, circadian rhythm and circadian rhythm[169]. Therefore, any perturbations in the environment are likely transmitted from sensory neurons to the hypothalamus. Overexpressing uncoupling protein 2 (UCP2) in mouse hypocretin neurons (Hcrt) increases body temperature specifically in the hypothalamus and leads to a decrease of 0.3-0.5ºC in core body temperature[170]. These transgenic Hcrt-UCP2 mice have the same calorie intake relative to WT controls but live 12-20% longer[170]. These data suggest that neuronal regulation of core body temperature influences lifespan independently of DR and supports cell nonautonomous modulation of aging in mice.

The significant role the hypothalamus plays in cell nonautonomous modulation of aging is further supported by experiments modulating neuronal NF-κB levels in middle-aged mice. NF-κB is a well-studied transcription factor involved with inflammation and the immune response[171]. As aging is correlated with increased inflammation, this study asked whether changes in NF-κB expression with age lead to pro- or anti-aging phenotypes. Middle-aged mice with activated NF-κB in the hypothalamus have slightly shorter lifespan whereas NF-κB inhibition extends lifespan by ~15%[50]. NF-κB inhibition improves maze-learning, muscle endurance, and bone mass while NF-κB knockout in hypothalamic microglia is sufficient to phenocopy the lifespan extension from neural inhibition of NF-κB. Both neuronal and glial hypothalamic NF-κB knockdown also leads to increased gonadotropin-releasing hormone (GnRH) mRNA expression in old mice. GnRH neurons are hypothalamic cells that regulate fertility through pulsatile GnRH release, and importantly, increases in GnRH expression or

treatment of mice with GnRH injection correlates with improved neurogenesis and lifespan. The implication of this study is that increased inflammation from NF-κB expression during aging leads to loss of GnRH release and subsequent diminished health, and that restoring GnRH levels can reverse this effect. Notably, recent work demonstrated that treating mice with an inhibitor of IL-11, a pro-inflammatory cytokine upregulated by NF-κB, can extend mouse lifespan by ~22% and 25% in males and females, respectively[172]. These data not only support a role for the hypothalamus in cell nonautonomous modulation of aging, but also suggest plausible signaling mechanisms (GnRH and/or IL-11 release) for this role.

Recent work further explores the role of the brain in influencing health and longevity in mice. Brain-specific Sirt1 OE (BRASTO) mice live 10-15% longer than controls and have decreased cancer incidence[173]. Middle-aged (20 month) BRASTO mice also exhibit improved healthspan parameters when compared to their aged-matched controls; they are more physically active, have higher core body temperature, consume more oxygen, and have more non-REM sleep. Similar traits are often correlated with increased quality of life in elderly humans[174-176]. While the causative mechanisms behind the improved health and longevity of BRASTO mice are not fully characterized, they show an increase in skeletal muscle mitochondria and mitochondrial functional gene expression in addition to higher mRNA expression of markers of neuronal activity in hypothalamic neurons. Further studies will hopefully identify how SIRT1 expression in the brain changes downstream physiology to improve health and longevity. This will likely involve modulation of neuronal signaling, perhaps due to improved health of neurons in the brain. It will also be interesting to find whether and how these changes are distinct from and overlap with pathways such as insulin-like signaling, that also emanate from the brain. This

study further supports the role of neurons, and hypothalamic neurons in particular, as key modulators of cell nonautonomous aging.

Another focus of aging research in mammals has been cellular senescence, a process characterized by permanent cessation of cellular proliferation. There is a large body of work supporting the hypothesis that the proliferation of senescent cells throughout an animal's lifetime could accelerate their aging via pro-inflammatory secreted compounds. Plasminogen activator inhibitor-1 (PAI-1), a neuronally expressed protein, regulates cellular senescence in mammals[177,178]. In one mouse model of accelerated aging—genetic knockout of the klotho "aging-suppressor" gene—the klotho knockout mice exhibited increased plasma PAI-1 levels when compared to age-matched controls[179]. Knocking out PAI-1 in klotho mutant mice reduces senescence, normalizes telomere length, preserves organ function, and completely rescues their lifespan. These mice are likely short-lived due to accumulation of pro-inflammatory molecules from the "senescence messaging secretome" (SMS) that influences aging through cell nonautonomous signaling. In support of this hypothesis, there is mounting correlative data suggesting elevated PAI-1 levels in humans is strongly associated with aging disease states[180]. While these data are intriguing, more experiments are needed to test whether neuronal SMS mechanistically accelerates aging in mice with normal lifespans.

Cell nonautonomous signaling from senescent cells is another likely mechanism influencing aging. Mammals accumulate senescent cells throughout life, and when chronically present, senescent cells exacerbate age-dependent tissue deterioration due to inflammatory signals dubbed the senescence-associated secretory phenotype (SASP)[181]. However, when transiently present, senescent cells can promote healthy outcomes like optimal wound healing[182]. While the local effects of these signals have been well-studied, their systemic effects remain

unclear[183]. Much work is left to parse out the efficacious effects of senescent cells from SASP, but it is compelling that many anti-aging therapeutics shown to extend mouse lifespan seem to target and kill senescent cells[16]. Whether the lack of these senescent cells is responsible for the pro-longevity effects from these drugs remains unclear. Senolytic compounds have recently entered clinical trials to test their efficacy in treating age-associated diseases[184] and early results show that senolytic therapy improved outcomes in a tauopathy-based mouse model of Alzheimer's[185]. Together, these data indicate senescent cells could represent a local and possibly systemic mechanism for cell nonautonomous modulation of aging.

The process of identifying pro- and anti-aging signaling events such as SASP is accelerated by the use of heterochronic (differently aged) animals sharing a circulatory system either through parabiosis or serum transfer. Incredibly, circulating factors in the blood of young mice can restore cellular function in older mice. Specifically, old mice exposed to young serum show enhanced Notch signaling in satellite cells, increased hepatocyte proliferation, enhanced neurogenesis, decreased incidence of cardiac hypertrophy, and a reduced SASP response[186-190]. Follow-up studies show the TGF-β superfamily member protein GDF11 decreases with age and restoring its levels-alone is sufficient to reverse age-related dysfunction in the skeletal system[191] as well as restoration of the neurogenic niche[188]. Despite the observed benefits of young serum in older mice, an initial study found that young plasma is not able to extend lifespan in aged mice[192]. Together, these results provide the basis for ongoing work identifying the mechanisms of these observations with the hope of showing that defined "youth factors" can improve human healthspan, lifespan, or both. These data highlight the significant role circulating proteins and secreted compounds likely play in modulating aging cell nonautonomously.

Labs with a previous invertebrate focus have begun to explore whether cell nonautonomous signaling pathways are conserved from invertebrates to mammals. To that end, globally knocking out the capsaicin receptor TRPV1 in mice causes no change in body weight or circulating growth hormone (GH)/IGF-1, but increases metabolic activity and energy expenditure and extends lifespan by 10-20%[51]. In worms, knocking out the TRPV-1 orthologues, *osm-9* and *ocr-2*, requires the transcription factor CRTC-1 to influence lifespan. In mouse dorsal root ganglion (DRG) primary neuron cultures, TRPV-1 is also necessary for nuclear translocation of CRTC-1. CRTC-1 interacts with CREB in DRG neurons to regulate secretion of the neuropeptides CGRP and substance P in pancreatic beta cells. The model suggests TRPV-1 knockout mice have reduced CRTC-1 activity which reduces calcitonin gene-related peptide (CGRP) expression and increases pancreatic insulin secretion leading to better glucose tolerance and longevity. It is likely this type of translational study will become more common in the future, establishing which cell nonautonomous pathways of aging are conserved from invertebrates to mammals.

Together, mammalian aging studies show a clear role for cell nonautonomous signaling, but with less detail than in invertebrate organisms. Similar to invertebrates, insulin-like signaling represents the best studied pathway, but additional details are continuously emerging. Whether emanating from whole brain (SIRT1), regions of the brain (e.g. hypothalamic NF-κB and UCP), or from individual tissues throughout the body (SASP, parabiosis), cell nonautonomous modification of systemic aging plays a role in mammals. For many of these pathways, the field is very new and more exciting data will likely come in the future.

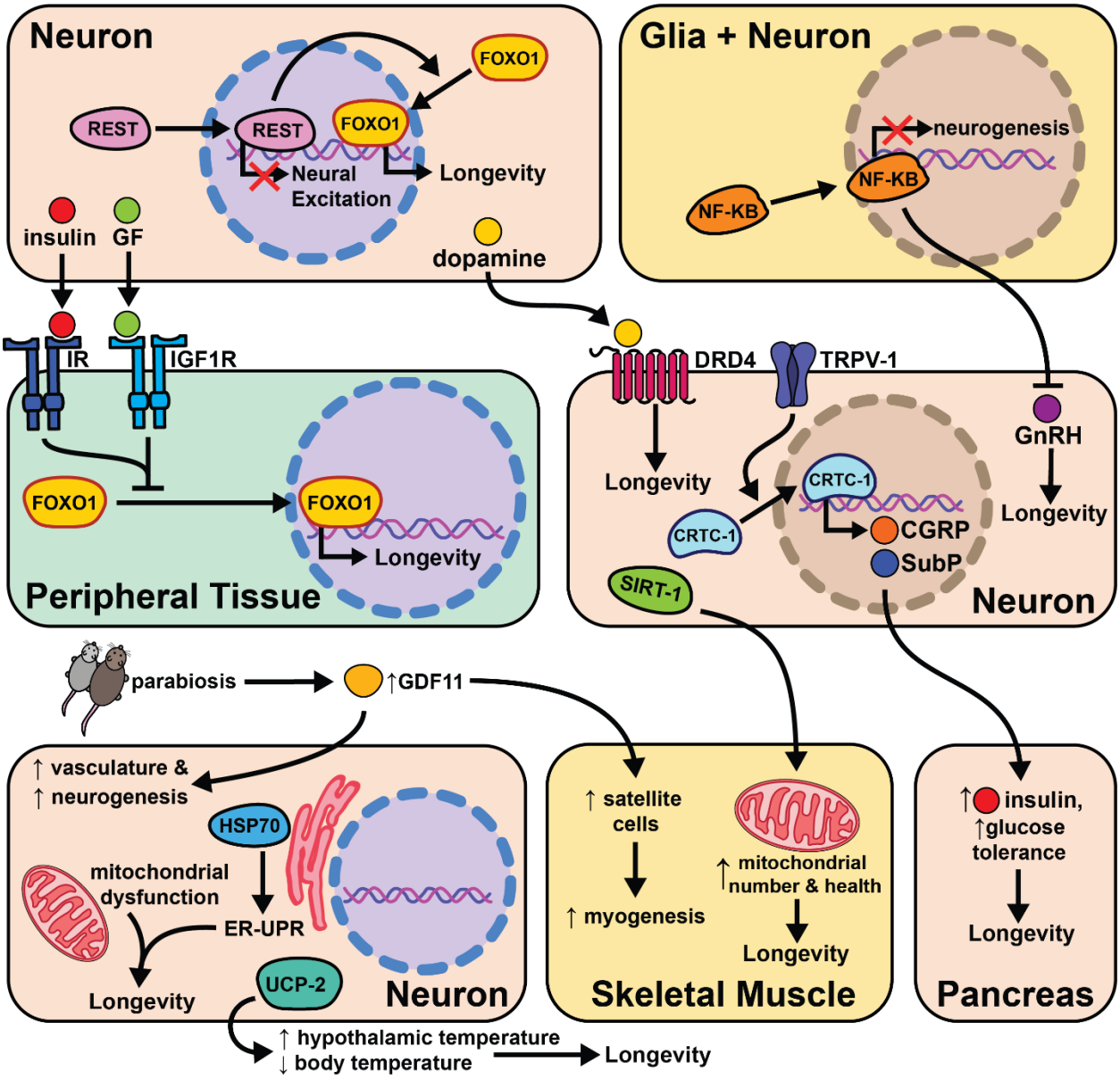


Figure 1.9 The intersection of cell nonautonomous signaling and aging in mammals.

1.2.5 Emerging Concepts in Cell Nonautonomous Signaling and Longevity

The work reviewed here (summarized in **Figure 1.10**) represents a small sliver of the extensive discoveries the aging field has made in the past three decades. Despite cell nonautonomous signaling being a relatively new concept to the field, the critical role the nervous system plays in promoting healthy aging is well-established. Moreover, by understanding how

key signaling tissues evaluate and appropriately integrate large amounts of internal stimuli (energy stores and the allocation of resources) and external stimuli (availability of food/sexual partners and quality), we can target the decision-making processes improve healthspan and lifespan.

Despite the clear role that cell nonautonomous signaling plays in maintaining proteostasis, oxygen homeostasis, food regulation, and overall physiology, there is much we don't know about these areas. All fields, but invertebrate aging research in particular, could follow the lead of the behavior field, where there is convincing data establishing detailed neural circuits and signaling molecules that regulate aspects of behavior. The aging field has occasionally completed similar work, but much less is understood about how cells recognize and relay signals about different types of internal and external environmental stimuli. This is to be expected, as behavioral outcomes are often measurable in seconds or minutes, whereas long-term health and lifespans require weeks or months (for invertebrates) or years (for mammals). Due to time constraints, this is an area where invertebrate research will likely need to lead, but future work should follow up on the translatability of these networks. A subset of invertebrate studies do establish key aspects of these circuits, and if more effort was put into this endeavor, we may also find whether behavior and long-term health interact or are controlled by entirely distinct pathways.

With the establishment of cell nonautonomous regulation of aging in multiple pathways and organisms, there is immense therapeutic potential for this area going forward. Most therapeutics logically target the tissues where physiological change is most important. However, understanding upstream signaling networks provides a unique opportunity to use the natural signals to "trick" key tissues into improving long-term health. This will not necessarily be easy,

as targeting neural circuits using broad drugs (e.g. SSRIs) often has pleiotropic effects, but the better we understand these signaling networks the more specifically we could, in theory, mimic the signal(s). Using a signaling approach to anti-aging therapeutics would allow for induction of hormetic effects without the need for an acute stressor and has great potential to mimic well established longevity interventions such as dietary restriction. It will be of paramount importance, as the field continues to mature, that we test the conservation of these networks from simple worms to complex mammals. It is probable, however, that like the first discovered cell nonautonomous network to influence aging (insulin-like signaling), other pathways will be partially or largely conserved.

Much of the work reviewed here investigates how the nervous system communicates with peripheral tissues to influence aging. This can be thought of as canonical cell nonautonomous signaling. However, recent data from invertebrates supports the idea of non-canonical cell nonautonomous mechanisms where the peripheral tissues use a retrograde signal back to the nervous system to maintain or further modify physiology[138,193-195]. This type of signaling is logical, as organisms require feedback from individual tissues to monitor homeostasis, but the role of retrograde signaling in regulation of aging is not well understood. This concept presents an interesting case for future studies to investigate the circuitry events that occur from the downstream metabolic tissues back to the nervous system. It also provides an opportunity to better understand how cells at the interface of forward and retrograde signaling (i.e. the hypothalamus) make decisions that affect both upstream and downstream physiology.

Another area that will be crucial in future studies will be the identification of epigenetic regulation of these cell nonautonomous networks. While sentinel-like cells such as neurons signal to peripheral tissues to modify stress resistance and longevity, how these pathways

maintain their benefits over time is not well understood. Studies show that just a day of hypoxia[106], for example, can extend lifespan in a worm, but whether that is just due to the persistent benefits of physiological changes made during that day or due to lasting epigenetic changes in peripheral tissues is an open question. The answer will give clues as to whether we could develop therapeutics that are only taken intermittently or whether more continuous treatment is necessary to extend healthspan. Additionally, studies in this area could separate how organisms respond to acute and chronic stress, and whether a series of acute activations of stress responses bring about long-term benefits.

Together, cell nonautonomous regulation of aging represents an exciting area of study that is well-established with many exciting but open questions. The future of this area has great potential to both improve our understanding of the aging process and lead to useful therapeutic advances that improve human health.

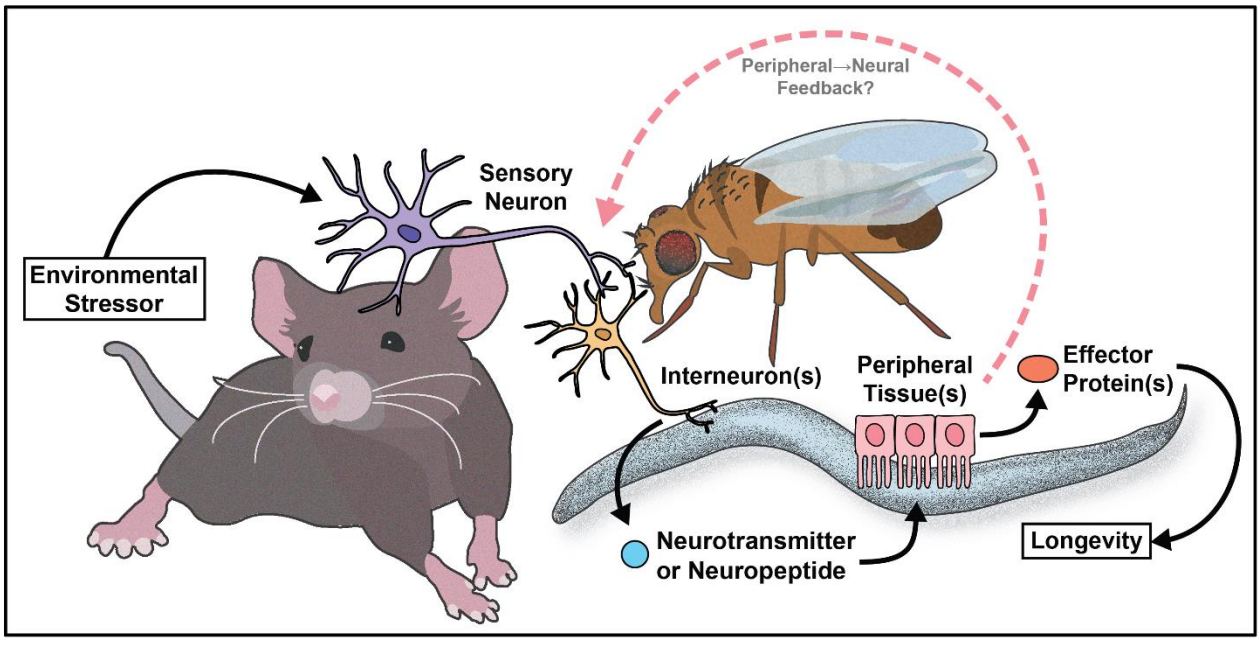


Figure 1.10 Summary model. Perception of environmental stressors by the nervous system activates cell nonautonomous signaling pathways that induce pro-longevity effector proteins in peripheral tissues.

1.3 Potential Obstacles to Anti-Aging Treatments

Longevity interventions often capitalize on the hormetic activation of stress response pathways that can enhance cellular resilience and promote healthy aging. In model organisms, these pathways can be triggered by various environmental stressors, pharmaceutical agents, and genetic modifications. However, while each of these strategies shows promise in theory, their practical implementation in real-world settings presents several challenges. In this section, we will examine the potential obstacles associated with translating longevity interventions into human applications (**Figure 1.11**).

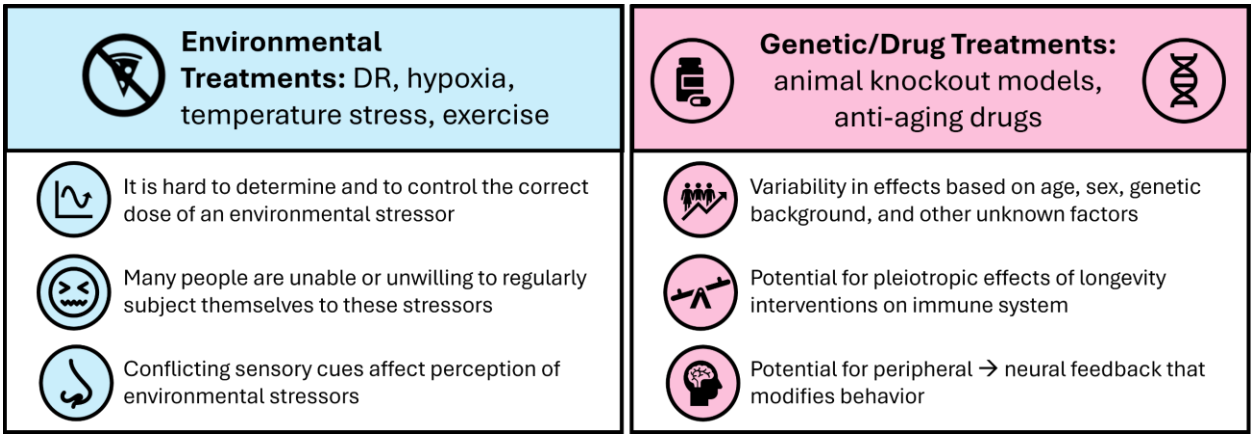


Figure 1.11 A summary of the challenges facing environmental, genetic, and pharmaceutical longevity treatments.

1.3.1 Challenges facing environmental longevity interventions

One potential avenue for anti-aging treatments involves exposing individuals to various physical stressors, such as dietary restriction (DR), exercise, heat stress, or cold stress, all of which activate hormetic stress responses that enhance resilience and healthspan[29]. However, translating these interventions from controlled laboratory environments to real-world settings is difficult for three main reasons. First, it is difficult to achieve consistent application and dosing of an environmental stressor. Second, intentional and repeated stress exposure requires a baseline level of health and great motivation on the part of the individual. Third, while laboratory settings

can carefully regulate these stressors, the environmental factors encountered by individuals in daily life introduce complexities that may significantly affect the efficacy of these interventions.

1.3.1.1 Challenges in dosage and interactions between multiple stressors

The first major challenge in implementing environmental stress exposure as a longevity treatment is the difficulty in controlling the dose of stress, which must be precise to yield beneficial effects without causing harm. Hormesis, by definition, requires a moderate amount of stress to provoke an adaptive response; too little has no effect, and too much can be detrimental[30,32]. In laboratory settings, researchers can carefully manipulate stressors—such as restricting calories by a specific percent of total intake or implementing heat exposure at a specific temperature and duration—to remain within a hormetic range. However, stress exposure in the real world is inherently more unpredictable, and the interaction between different stressors is poorly understood. For example, illness, sleep deprivation, psychological stress, and physical exertion could all interact with environmental stressors in ways that enhance or attenuate their effects. Similarly, there is growing interest in the role of social stressors such as adverse childhood events and socioeconomic status on aging[196]. Overall, it remains unclear how interactions between multiple hormetic and non-hormetic stressors will affect the overall balance needed to optimize health.

Additionally, determining the optimal dose of stress exposure for individuals remains a significant hurdle. While interventions like calorie restriction and exercise have the potential to extend lifespan in various species, the appropriate "dose" of these interventions can vary not only between individuals but also over time for the same individual[197,198]. Additionally, variability in dose-response between individuals in a population can increase with age[199]. This variability makes it difficult to establish clear guidelines for implementing these interventions in a way that

ensures benefits without inducing harm. Pharmaceutical interventions face similar dosing challenges, but environmental stress exposure in daily life is far harder to control and personalize.

1.3.1.2 Behavioral resistance to stress exposure

A second major challenge facing stress-based treatments is the inherent resistance of individuals to voluntarily expose themselves to the kinds of stressors required to extend lifespan. Humans are naturally inclined to avoid discomfort, as evolutionary pressures have shaped behavior to seek safety and conserve energy[200,201]. For example, despite overwhelming evidence that physical exercise and appropriate calorie intake prevents disease and improves health, compliance with these recommendations remains low. According to the Centers for Disease Control and Prevention (CDC), approximately 50% of American adults were trying to reduce their caloric intake as of 2016[202]. However, studies looking at long-term adherence to dietary changes report that only between 5-20% of these attempts are successful[203,204]. Even when dietary change is regularly monitored and enforced as part of a scientific study, it is extremely rare for humans to achieve the 20-40% reduction in caloric intake often employed in scientific studies of DR-mediated longevity. For example, the first human trial examining the effects of calorie restriction on longevity biomarkers aimed for a 25% reduction in calorie intake in healthy, normal-weight subjects. Subjects in this study were also rigorously screened for their likelihood of long-term compliance. Even so, after one year in the study, the average participant only achieved a 12% decrease in caloric intake[33]. Similar difficulties are observed with respect to other lifestyle interventions like exercise. A study by Gjestvang *et al.* found that only 17% of adults who joined a new fitness center still followed a consistent exercise regimen one year later[205]. These surveys suggest that stress-based interventions may only be feasible for a small,

highly motivated subset of the population, making widespread adoption of such approaches unlikely.

1.3.1.3 Conflicting sensory cues influence stress perception in a complex environment

Even for those individuals who are highly motivated to adopt stress-based interventions, the external environment poses additional challenges. In the modern developed world, we are often exposed to cues that signal comfort and safety, which can undermine the effects of environmental stress exposure. For instance, research on dietary restriction in invertebrates has demonstrated that even when organisms are dietary restricted, exposure to food-related cues (such as odors or tastes) can attenuate the lifespan-extending benefits of DR[105,112,206]. While this phenomenon is not well-studied in mammals, these blunting effects in invertebrates are mediated by the highly conserved signaling molecules serotonin and dopamine[52,105,143]. Given that humans are frequently exposed to cues of food availability, such as advertisements, odors, and the widespread consumption of non-nutritive sweeteners, these environmental signals may hinder the effectiveness of DR-based interventions in real-world settings. For example, in 2012, 13% of packaged foods and 35% of beverages were marketed as low-calorie, low-fat, or low-sugar products[207]. The increased consumption of non-nutritive sweeteners (such as aspartame or sucralose), which affect taste perception without providing calories, has further exacerbated this issue, with over 30% of U.S. adults reporting daily consumption of artificial sweeteners as of 2017[208]. These factors suggest that the constant exposure to food cues may blunt the effectiveness of environmental stress interventions like DR in humans, requiring additional studies to understand their impact on health in humans.

Taken together, the challenges associated with stress exposure-based longevity interventions underscore the need for further research into the appropriate dosage of stressors

required to achieve a hormetic response, as well as the impact of conflicting sensory cues. While the controlled environment of the laboratory offers valuable insights, the complexities of real-world stressors and human behavior must be addressed before these interventions can be widely implemented. Consequently, a deeper understanding of how stress exposure interacts with the modern environment and individual variability is crucial for the successful application of longevity strategies based on environmental stress.

1.3.2 Challenges facing pharmaceutical longevity interventions

Developing anti-aging drugs in humans faces several significant challenges, particularly in identifying targets that effectively modulate aging across a heterogenous population. While much progress has been made in understanding molecular mechanisms involved in aging, the complexity of human biology suggests that a one-size-fits-all approach may not be feasible. Pharmaceutical agents targeting hormetic stress-response pathways have shown promise in extending lifespan in animal models such as mice, worms, and flies[209,210]. However, translating these findings into effective human therapies will require identifying the most promising drug targets, understanding variability in drug efficacy across individuals, and overcoming limitations in drug combination strategies.

1.3.2.1 Individual variability and the need for personalized and/or combinatorial approaches

Multiple pharmaceutical agents extend lifespan in non-human mammals by modulating key effectors of different stress-response pathways. Acarbose, rapamycin, and 17 α-estradiol are prime examples of drugs that extend lifespan in mice, though their sites of action and specific mechanisms of action differ significantly. For instance, acarbose likely extends lifespan by inhibiting intestinal enzymes that break down carbohydrates, thereby decreasing the postprandial blood glucose concentrations and reducing insulin signaling[211]. Rapamycin is an inhibitor of the

mechanistic target of rapamycin complex 1 (mTORC1) and promotes autophagy[212]. Finally, 17 α-estradiol is a selective estrogen receptor modulator thought to extend male lifespan by altering estrogen receptor signaling, which influences numerous metabolic and stress-response pathways in non-neuronal tissues[213,214]. While these drugs show promise in extending lifespan in mammals, the debate over which could be the most effective or best intervention for human aging remains unresolved.

One critical challenge in applying these interventions to humans is variability in the efficacy of each treatment based on environment, sex, and genetics: lifespan extension therapies that work effectively in one group of mice may not necessarily produce similar results in humans, nor can they be relied upon to work equally well across the entire population. Even in mouse studies, genetic background, age, and sex can significantly impact the effectiveness of these drugs, suggesting the need for personalized or combinatorial treatment approaches. For example, the proposed anti-aging drug metformin was reported to extend lifespan in female Swiss-H Rappolovo (SHR) mice[215] and male C57BL/6 mice[216], but the Interventions Testing Program (ITP) found no effect of metformin on lifespan in male or female UM-HET3 mice[217]. Similarly, the ITP found 17 α-estradiol extends lifespan in males but not in females[213]. This variability highlights the necessity for multiple FDA-approved and efficacious longevity treatments, each targeting different subsets of the population based on genetic and/or metabolic differences.

Another challenge to consider when translating anti-aging therapies from animal models to humans is the diminishing effect of longevity interventions as one moves up the evolutionary scale. While genetic interventions like knocking down the insulin-like growth factor receptor can double lifespan in *C. elegans*[38], similar interventions tend to have much smaller effects in higher

organisms like mice: the growth hormone-deficient Snell dwarf mouse, one of the longest-lived mouse models, only lives approximately 50% longer than wild-type mice[40]. Activating these longevity pathways via pharmaceutical means decreases the effect on lifespan even further: the largest effect on lifespan observed in the ITP is a 22% increase from acarbose treatment in male mice[213]. This trend suggests that even the most promising longevity drugs may have modest effects on human lifespan. The small magnitude of these effects may be a significant factor in the challenge of translating animal-based findings to humans, as even if a drug has a measurable impact on aging, it may not produce dramatic results.

One option to address these challenges is to tailor interventions to the specific biology of individuals, which will require a better understanding of how different therapies interact and which ones are most likely to produce positive outcomes in each individual. Additionally, there is great interest in combining multiple longevity pharmaceuticals with the hope of achieving an additive effect on health and lifespan. For example, Admasu *et. al* identified two drug combinations that synergistically improve lifespan and healthspan in *C. elegans*. The synergistic effects of both drug combinations required TGF-β signaling and increased levels of monounsaturated fatty acids[218]. Combining multiple anti-aging pharmaceuticals in flies has also proved efficacious. Simultaneous inhibition of mitogen-activated protein kinase kinase, mTOR complex 1, and glycogen synthase kinase-3 acted additively to increase *Drosophila* lifespan by 48%[219]. These data suggest it may be possible to target two or more pathways simultaneously to slow mammalian aging.

However, combining multiple drugs to enhance lifespan or healthspan is complicated by issues such as drug-drug interactions[220,221], variability in individual responses to different dosages[222,223], and increased costs. These challenges are exacerbated by the fact that personalized

dosing regimens for aging interventions are still in early stages and will need to be standardized. As a result, combining multiple drugs to treat aging remains a complex and potentially risky strategy that requires careful consideration of individual responses, drug interactions, and delivery methods.

1.3.2.2 The potential of the nervous system as a target for anti-aging pharmaceuticals

Given these challenges, one potential alternative to a multi-drug approach is to focus on drug targets that could coordinate the regulation of stress-response pathways across various tissues. The nervous system is a promising target for these types of longevity therapeutics because it plays a central role in coordinating diverse physiological processes across the body, influencing metabolic regulation, immune function, and stress resilience. Moreover, research into cell nonautonomous regulation of aging has identified several promising neuronal signals that influence aging in other tissues. For instance, modified serotonin signaling in *C. elegans* and *D. melanogaster* can alter lifespan through multiple downstream mechanisms[52,105,142,143,145,224]. Similarly neuronal signals in worms, flies, and mice can play a crucial role in modifying the insulin/IGF-1 signaling pathway and proteostasis in peripheral tissues[74,78,120,225-228]. These examples suggest that manipulating neural signals upstream of metabolic and stress resistance effectors could be a powerful strategy to influence aging.

Moreover, because the nervous system is composed of highly specialized subsets of cells, limited interventions in neural circuits could have large effects on multiple downstream pathways to affect lifespan. This contrasts with the broader effects of systemic drug interventions, which may require separately targeting multiple pathways or tissues to produce a meaningful impact. Importantly, the FDA has already approved many neuromodulating drugs for psychiatric treatments, and several of these drugs, including trifluoperazine, butaclamol,

thioridazine, and mianserin, have demonstrated lifespan-extending properties in invertebrate models[104,229,230]. This raises the possibility that these drugs could be repurposed for use in anti-aging therapies in humans, with potentially fewer regulatory hurdles compared to novel drug development.

Despite the potential of the nervous system as a target for anti-aging therapeutics, a crucial challenge remains: the need to more fully understand the neural circuits that regulate aging across different tissues. While neuronal signals that influence aging in model organisms have been identified, a detailed mapping of these brain circuits is necessary to identify central regulators of aging. Understanding these circuits will provide insight into how individual neurons and their signaling networks can modulate aging processes in peripheral tissues, ultimately guiding the development of more effective and targeted anti-aging therapies. In conclusion, while there are many obstacles to applying anti-aging pharmaceuticals in humans, focusing on the nervous system as a central hub for regulating aging offers a promising avenue for future research. Identifying neural targets and understanding how they coordinate various longevity pathways may lead to more effective therapies with greater impact on human health and lifespan.

1.3.3 The complex interplay between longevity interventions, reproduction, stress resistance, and behavior

A final challenge in implementing lifespan therapeutics in humans is to mitigate the pleiotropic effects of longevity-promoting stress response pathways. These pathway effects are often not limited to the intended effects on aging, and some may be undesirable or counterproductive. For instance, many longevity interventions divert resources from reproductive health to preserve somatic function, often resulting in reduced fertility[231,232].

Additionally, although these interventions may successfully extend lifespan in controlled laboratory settings, they may impair an organism's ability to cope with real-world stressors, such as infections[233-235]. Both acute and chronic exposure to stress can also profoundly impact behavior and mental well-being[236,237]. For example, calorie restriction in humans has been linked to declines in cognitive performance and increased feelings of dysphoria[238]. Similarly, stresses induced by other longevity interventions, such as heat[239] or hypoxia[240], are not well studied, but have been associated with mental health issues in people.

1.3.3.1 Interactions between anti-aging treatments and reproduction

With respect to reproduction, there is clear evidence that genetic longevity interventions often extend lifespan at the cost of fertility. This is also observed in invertebrates, as worms and flies with germline mutations are long-lived[241]. Similarly, some long-lived mouse strains like Snell and Ames dwarf mice are unable to carry pregnancies to term without hormone supplementation[242]. Encouragingly, this hormone treatment does not block the enhanced health and longevity of Snell Dwarf mice[243], indicating it is possible to separate their longevity and reproductive phenotypes. Additionally, while longevity interventions may not increase total reproductive capacity, some anti-aging drugs are being investigated for their potential to extend the reproductive lifespan[242,244,245]. Overall, the effects of genetic and longevity pharmaceutical interventions on reproduction vary based on the treatment as well as the age and sex of the organism in question. More work is needed to fully decipher the complex interactions between each promising longevity treatment and fertility.

1.3.3.2 Interactions between anti-aging treatments and stress resistance

Much like with reproduction, different genetic and pharmaceutical longevity interventions have varied and complex effects on stress resistance and immune function. While

many genetic longevity interventions also enhance stress resistance in invertebrate models[246], this is not always the case. For example, long-lived *tcer-1* overexpressing worms are more susceptible to pathogen infection than WT worms, while *tcer-1* knockouts are pathogen resistant[247]. Interesting interactions between genetic mimics of dietary restriction and immune function have also been observed: work from the Blackwell lab found that the longevity of dietary restricted worms and *daf-2* knockout worms requires suppression of components of the innate immune response, such a p38 signaling[248]. While this requirement suggests a potential tradeoff between immunity and longevity, multiple studies of dietary restriction in flies report enhanced pathogen resistance following acute dietary restriction[249]. It is also proposed that decreased appetite, a common response to infection across taxa, is a behavioral response to promote enhanced immune function[250]. In mammals, both acute and longer-term dietary restriction interacts with the immune response[251-253], but the consequences of these changes appear to be nuanced and context-dependent.

While some reports have investigated the interactions between dietary restriction or genetic DR mimetics and immune function, very little is known about how promising anti-aging pharmaceuticals alter immune function. One exception to this is rapamycin, although there is still no clear consensus regarding how long-term low dose rapamycin treatment affects immunity. Rapamycin was originally used as immunosuppressant following organ transplantation[254]. Consequently, one might expect chronic rapamycin use to have detrimental effects on immune function. However, the dosage of rapamycin that extends lifespan is much lower than the dose used for intentional immunosuppression[41,212]. In fact, multiple studies suggest that rapamycin could enhance immune function in old age[255,256]. Rapamycin also plays a role in adaptation to physical stress in humans by suppressing muscle protein synthesis after

resistance training[257]. This function can blunt the positive effects of physical activity and would be a clear negative side effect of the drug. Taken together, these data demonstrate clear interactions between longevity treatments, stress resistance, and stress adaptation. Nevertheless, more research is needed to understand the implications of these interactions on health outside of the controlled, pathogen free laboratory environment in which most longevity treatments are tested.

1.3.3.3 Interactions between anti-aging treatments and behavior

With respect to behavioral changes, many studies of novel longevity treatments examine whether movement capacity is enhanced in middle and/or old age as a measure of healthspan[172,258-262]. Work in invertebrate models also demonstrates that more complicated behaviors, like learning and memory, are preserved longer into old age in animals with reduced insulin signaling[263,264]. Additionally, reproductive capacity is often examined as a measure of overall health and fitness[20,265-268]. However, longevity treatments are rarely evaluated for their effects on decision-making and mental state. Nevertheless, many genetic and pharmaceutical longevity interventions activate stress response pathways that are known to elicit behavioral changes that allow an organism to avoid or prepare to endure a stressful environment[236,237,239,240,269,270]. Consequently, there is premise to explore the impact these longevity interventions may have on behavior in young animals.

Many longevity interventions target key metabolic tissues like the liver[271], the hypothalamus[50] and the intestine[213], all of which can directly or indirectly modify mental state and decision-making. While the role of these metabolic tissues in mental state is still poorly understood, there is growing evidence that these tissues affect the nervous system and behavior. For instance, the ketogenic diet, which induces significant metabolic shifts and decreases insulin

signaling, has been used for nearly a century to treat epilepsy, though the precise mechanisms behind its effects on brain function remain unclear[272]. Additionally, metabolic dysfunction, including elevated glucose and triglycerides, is strongly correlated with poor mental health outcomes[273]. This further highlights the broader effects of longevity interventions on behavior. Finally, new and exciting research on the gut-brain axis links many metabolic processes in the gut to changes in brain function and behavior. Metabolites produced by intestinal microbes can act as neuromodulators[274-276], influencing neural activity and mood regulation. Additionally, many neurotransmitters traditionally associated with the brain, such as serotonin and dopamine, are synthesized in the gut and can cross the blood-brain barrier[277]. Each of these examples further emphasizes the role of peripheral metabolism in influencing mental health and behavior.

In conclusion, it is crucial to assess the effects of longevity interventions not only on aging and lifespan but also on reproduction, stress resistance, and behavior. Understanding how these different physiological processes are interrelated and whether they are separable will be essential for developing safe and effective anti-aging treatments. By mapping the mechanisms underlying both longevity and behavioral changes, we can gain insight into the potential trade-offs of these interventions and identify strategies to minimize negative side effects while maximizing benefits. This approach will be key to advancing our understanding of aging and improving the quality of life for individuals undergoing lifespan and healthspan-extending treatments.

1.4 Goals of this Dissertation

In this dissertation, I aim to improve our understanding of the role of cell nonautonomous signaling in aging to address potential challenges facing longevity interventions. In Chapter 2 explores a potential obstacle facing the best-studied environmental longevity intervention,

dietary restriction. Specifically, we examine how exposure to food-like cues in a complex environment attenuates the longevity benefits of dietary restriction in *C. elegans*. Understanding the neural circuits through which perception of environmental food cues influences activation of downstream longevity effectors could aid in the development of longevity interventions that are not affected by external signals.

Chapter 3 continues our exploration of the role of neural signaling in extending lifespan, but this time focusing on the cell nonautonomous circuit through which hypoxia, or a low oxygen environment, extends lifespan in *C. elegans*. In this detailed circuit mapping of a cell nonautonomous longevity pathway, we identify multiple manipulations of neural signals that mimic exposure to hypoxia and extend lifespan in a normoxic environment.

Next, Chapter 4 looks downstream of these environmental longevity interventions and instead focuses on a pro-longevity effector, *fmo-2*, that is activated by both DR and hypoxia to extend lifespan in nematodes. Because 1) these two environmental longevity interventions converge on *fmo-2* induction, and 2) mammalian Fmos are also upregulated in long-lived mice, Fmo overexpression represents a possible target for new longevity treatments. However, we find that altering *fmo-2* expression changes multiple behavioral phenotypes in young adult worms. This chapter focuses on determining whether these behavioral changes are separable from the effects *fmo-2* expression has on aging.

From Chapters 2-4, we can see that *C. elegans* are a valuable model system for mapping cell nonautonomous circuits in relation to lifespan and behavioral outcomes. However, there are some challenges in using nematodes as a model organism. For example, *C. elegans* consume a diet of live OP50 *E. coli* bacteria. Consequently, it can be difficult to determine whether phenotypes observed under various environmental or drug supplementation conditions are due to

alterations in bacterial metabolism or in worm physiology. To address this challenge, we developed a method of metabolically inactivating bacteria without decreasing their nutritional quality. This technique is detailed in Chapter 5. This chapter, which focuses on new methods in *C. elegans* research, also discusses a method developed to automate the quantification of fluorescent images of worms. This process greatly increases the feasibility of large imaging screens, allowing for the identification of key signaling components among many genes of interest.

Finally, Chapter 6 summarizes how this work advances our understanding of the interactions between longevity interventions, conflicting environmental cues, and behavioral effects. However, this thesis represents only a small advancement in our knowledge of how cell nonautonomous signaling pathways modify aging and physiology. Chapter 6 also explores how this work provides a framework for future investigations and proposes additional studies to advance our understanding cell nonautonomous signaling in aging and behavior.

Chapter 2 Touch Limits Lifespan through Neural to Intestinal Signaling[2]

2.1 Foreword

This Chapter builds off of previous work in the lab led by Dr. Hillary Miller and Dr. Shijiao Huang. When I first joined the lab, I assisted Dr. Miller and Dr. Huang in dissecting the neural circuitry through which perception of food smells under DR conditions decreases induction of the pro-longevity enzyme FMO-2 and, in turn, attenuates DR-mediated longevity. Based off our findings related to the role of olfactory perception in longevity, I wondered whether other forms of sensory perception, like mechanosensation, could elicit similar effects. After identifying a method to separate mechanosensory food-like cues from food consumption in *C. elegans*, I found that, much like attractive smells, attractive touch cues decrease both DR-mediated *fmo-2* induction and longevity. This chapter describes our discovery and mapping of an attractive touch cell nonautonomous signaling pathway. This pathway is perceived by the nematode nervous system and communicated to peripheral tissues to effect longevity effectors like FMO-2. While much work remains to explore the implications of this pathway in aging (see Chapter 6), this project begins to address how complex and conflicting sensory cues may affect potential longevity interventions like dietary restriction. I completed the entirety of this work with the exception of Dr. Safa Beydoun performing replicates of key experiments and regular feedback from Dr. Scott Leiser.

[2] In revision at *PNAS* (2025 May; doi: 10.1101/2021.06.18.449022) with authors listed as **Kitto, E.S.**, Beydoun, S., and Leiser, S.F.

2.2 Abstract

In multicellular organisms, sensory perception affects many aspects of behavior and physiology. Perception of environmental stressors like food scarcity often leads to physiological changes that promote survival and slow aging. However, recent work shows that perception of attractive food smells can block the health benefits of dietary restriction in multiple model organisms. While it is known that sensory perception and cell non-autonomous signaling can modulate health and longevity, our knowledge of the specific sensory cues and mechanistic pathways that define this signaling is still limited. Here we find that the sense of touch interacts with nutritional state to modulate lifespan in *C. elegans*. Worms subjected to dietary restriction are shorter-lived when they perceive tactile stimuli that mimic bacterial food and/or protective soil. Touch modulation of dietary restriction requires putative mechanoreceptor proteins, the neurotransmitters dopamine and tyramine/adrenaline, and the neuropeptides INS-11 and GnRH. Ultimately, the touch circuit regulates the longevity effectors DAF-2/IGF1R and FMO-2/FMO5. These results establish a physiological touch circuit and connect neural reward pathways to the growth and reproductive axes. Finding that texture mechanosensation can modulate longevity suggests a role for touch in healthspan and lifespan.

2.3 Introduction

In order to survive and thrive in a changing environment, all organisms must accurately perceive and respond to a wide range of sensory cues. Sight, touch, smell, taste, and sound inform animals of stressors, nutrient availability, and the presence of other organisms. Animals integrate this constant stream of information to respond appropriately to their environment: they must modify their behavior and metabolism to exploit favorable conditions while surviving or fleeing harsh conditions. In recent years, the field of geroscience has found that environmental stressors like dietary restriction (DR)[37], temperature stress[278], and hypoxia[27] can extend lifespan

and healthspan. There is great interest in leveraging these longevity-promoting conditions to improve human health. The most well-studied of these interventions is DR, defined as a reduction in nutrient intake that does not cause malnutrition. DR extends healthspan and lifespan across taxa [37] and there is evidence it can benefit human health[13].

By genetically manipulating sensory perception, scientists have been able to decouple the perception of a stressor from exposure to the stressor itself. Surprisingly, perceiving a stressful environment can extend an organism's lifespan, even under favorable conditions[31]. On the other hand, perceiving attractive smells[105,140,279] and tastes[95,206] decreases the health benefits of DR. Although previous work has shown that smell and taste modulate lifespan, other senses can also indicate the quality of the environment. In the sightless nematode *C. elegans,* tactile cues are especially important for interpreting environmental cues[280]. For example, the sights and textures of food can signal abundant nutrition. Tactile cues can also indicate whether an environment is safe or dangerous, leading to changes in health and lifespan. For example, repeated tapping of the plate *Caenorhabditis elegans* are cultured on decreases their lifespan under normal fed conditions through activation of a fight-or-flight response[58]. On the other hand, the mechanosensation of a food source triggers behavioral changes to remain in the food-rich environment[281]. In mammals, this type of attractive mechanosensory cue could correspond to chewing food, or potentially to other forms of comforting touch like a soft blanket or a hug. But although organisms experience rich mechanosensory stimulation from food and shelter in their natural environment, the role of gentle mechanosensation in longevity is largely unexplored.

In this work, we utilize inedible food-like beads[281] to explore the role of touch in DR-mediated longevity in *C. elegans*. We find that touch modulates DR through a pathway that is distinct from smell, taste, and mechanosensory-driven behavioral circuits. These findings suggest

a role for touch in modulating lifespan. Specifically, our results implicate the neurotransmitters dopamine and tyramine/adrenaline as well as the hormones insulin and Gonadotropin-Releasing Hormone (GnRH) in touch modification of aging. These neural signals ultimately communicate touch information to the intestine, where the longevity effector FMO-2 modulates aging. The involvement of dopamine and tyramine (the *C. elegans* adrenaline homologue) suggests a possible interaction between canonical reward and stress-response circuits associated with these bioamines and longevity. Moreover, these two neuroendocrine signals suggest a central role for the nervous system in balancing lifespan with growth and reproduction under stressful conditions via insulin and GnRH signaling, respectively.

2.4 Mechanosensation attenuates DR-mediated longevity in an *fmo-2* dependent manner.

In order to investigate the role of texture mechanosensation on DR-mediated longevity, we sought an experimental condition that creates a tactile environment attractive to *C. elegans* like food but lacking in other sensory cues. Previous work from the Horvitz lab accomplished this goal by using non-nutritive Sephadex beads to mimic the touch of bacterial food and study *C. elegans'* basal lawn slowing behaviors. Following this protocol from Sawin *et al.*[281], we combined these non-nutritive Sephadex beads with fed and DR conditions (**Fig. 2.1A-B**) to separate the effects of touch perception from other nutrient cues like smell and taste[281]. These beads form a texture similar to a real bacterial lawn, and their average diameter of 50 μm is too large for *C. elegans* to consume. Although these beads are much larger than the 2 μm diameter of a typical *E. coli* cell, *Sawin* et al. found that worms still slowed their movement speed when dopaminergic neurons contacted the Sephadex matrix, suggesting *C. elegans* sense the fake lawn through surface tension or pressure on the cuticle[281]. To confirm worms are unable to eat the beads, we put *C. elegans* on plates with and without GFP-coated beads of the same diameter. We

observed no difference in fluorescence of worms on and off of these beads (**SFig. 2.1A-C**), suggesting *C. elegans* are not consuming either the coating or the beads themselves. To ensure that worms are not responding to any chemical tastants or odors from the Sephadex beads, we performed a chemotaxis assay. This assay tests whether worms placed in the center of a plate exhibit an immediate preference for or avoidance of a region of the plate containing Sephadex, before having a chance to touch the beads. We observed no attraction to nor avoidance of the Sephadex beads or the supernatant in which the beads were suspended (**SFig. 2.1D**).

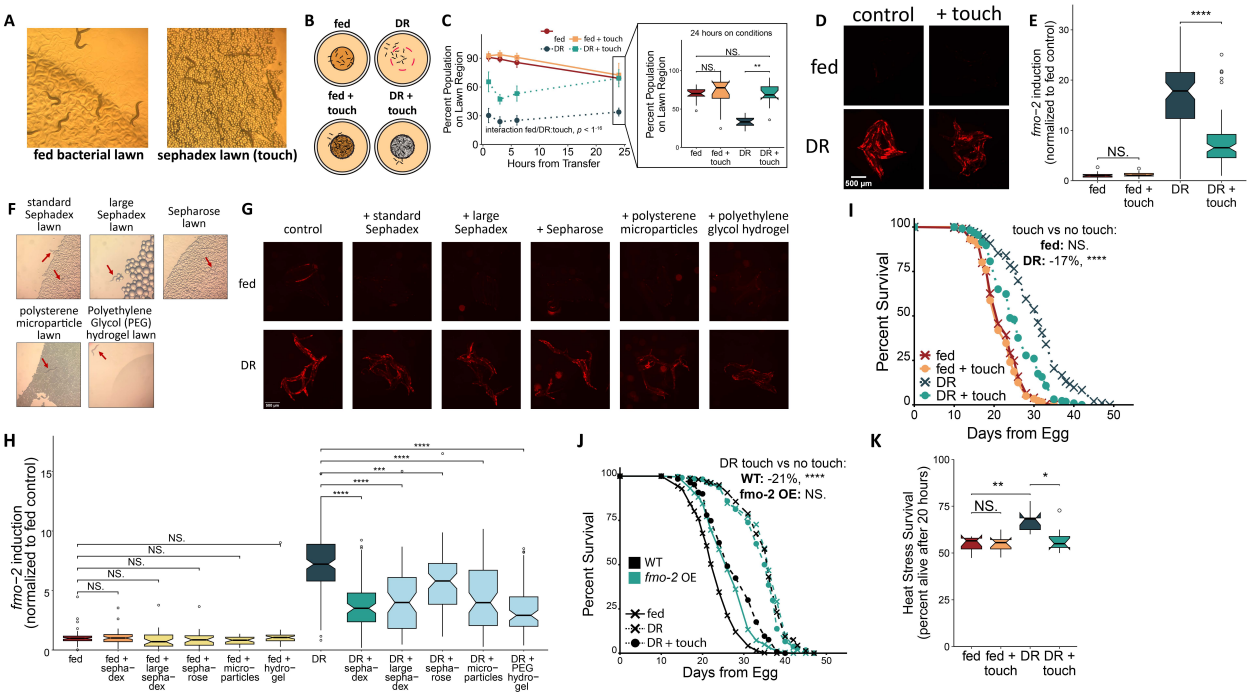
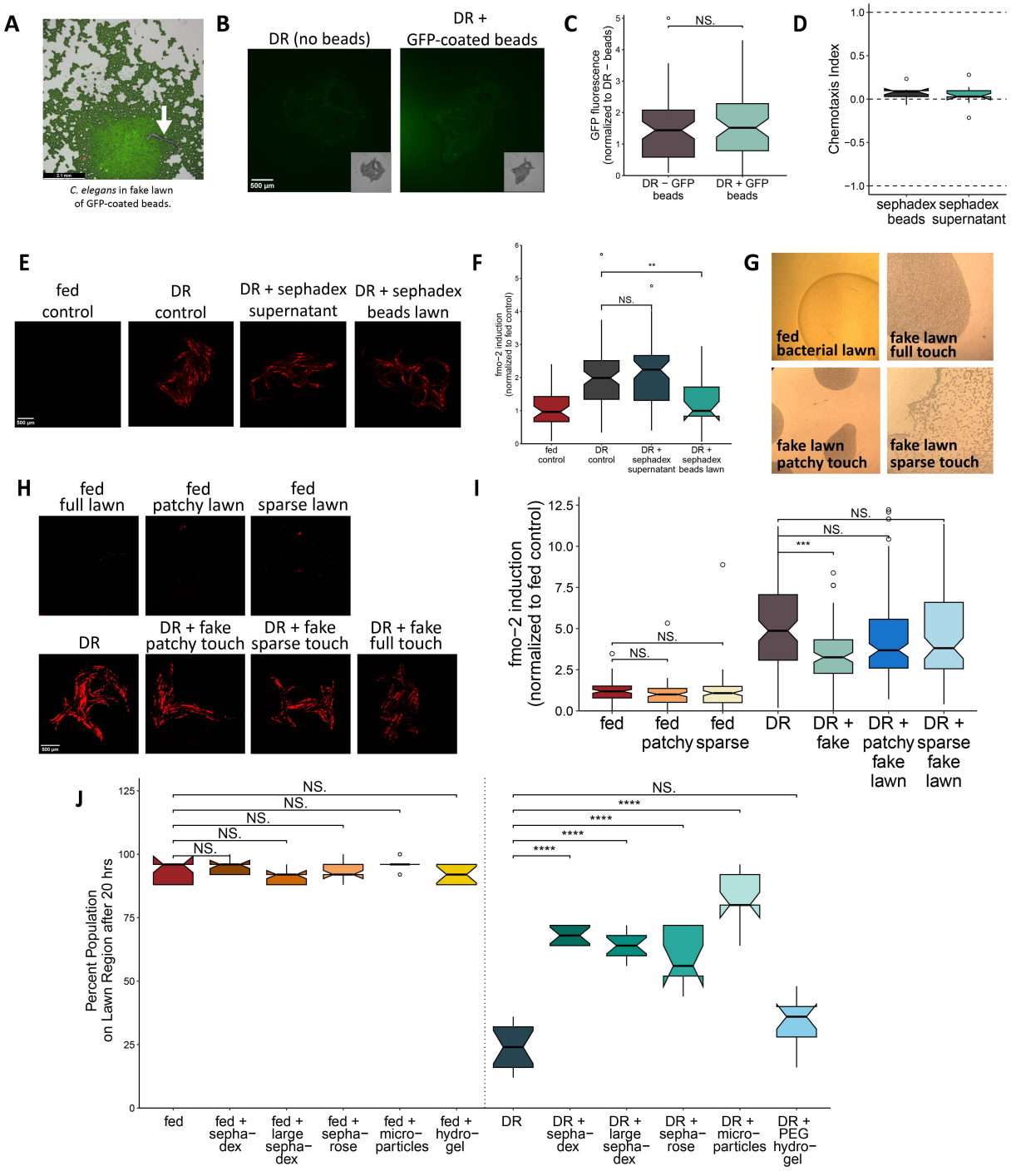


Figure 2.1 Touch blunts DR-mediated longevity through suppression of *fmo-2*. (**A**) Images of *C. elegans* in real and fake bacterial lawns. (**B**) Schematic of fed/DR +/- touch conditions. (**C**) Lawn occupancy on fed/DR +/- touch conditions over time. $N \geq 45$ worms/condition. (**D-E**) Representative images (**D**) and quantification (**E**) of *fmo-2p::mCherry* on fed/DR +/- touch. $N \geq 49$ worms/condition. (**F**) Images of non-Sephadex fake lawn materials. Arrows indicate *C. elegans* in the fake lawns. (**G-H**) Representative Images (**G**) and quantification (**H**) of *fmo-2p::mCherry* on fed/DR +/- different fake lawn materials. $N \geq 32$ worms/condition. (**I-J**) Survival curves of WT (**I**) and *fmo-2* OE (**J**) animals on fed/DR +/- touch. $N \geq 205$ worms/condition. (**K**) Survival of WT worms after 3 hours of heat stress at 37 °C. $N = 9$ plates of 15-20 worms/plate for each condition. The center line on all box plots displays the median, and the boundaries of the box represent the interquartile range. Boxplot statistics are Wilcoxon rank sum test with Bonferroni p-adjustment, two-sided, unpaired. (**I-J**) log rank test. In all panels, NS. = $p > 0.05$, **** = $p < .0001$. All images within one figure panel were taken at the same scale, as indicated by the scale bar in the top left image.

Finally, to confirm that the touch of the fake lawn is attractive to *C. elegans*, we measured lawn occupancy on fed and DR conditions with and without the fake lawn over a period of 24 hours. We found that the addition of the fake lawn does not inhibit lawn occupancy on fed conditions, but *C. elegans* prefer to spend time in the center region of the plate under DR + touch relative to DR alone (**Fig. 2.1C**). Worms also slow upon entering this fake lawn, much like they do a real bacterial lawn[281]. This suggests that the fake lawn is attractive to *C. elegans* in a food availability-dependent manner and meets our criterion for a tactile mimetic of food.


A
C. elegans in fake lawn of GFP-coated beads.
B
DR (no beads)
DR + GFP-coated beads
C
GFP fluorescence (normalized to DR − beads)
NS.
DR − GFP beads
DR + GFP beads
D
Chemotaxis Index
sephadex beads
sephadex supernatant
E
fed control
DR control
DR + sephadex supernatant
DR + sephadex beads lawn
F
fmo−2 induction (normalized to fed control)
**
NS.
fed control
DR control
DR + sephadex supernatant
DR + sephadex beads lawn
G
fed bacterial lawn
fake lawn full touch
fake lawn patchy touch
fake lawn sparse touch
H
fed full lawn
fed patchy lawn
fed sparse lawn
DR
DR + fake patchy touch
DR + fake sparse touch
DR + fake full touch
I
fmo−2 induction (normalized to fed control)
NS.
***
fed
fed patchy
fed sparse
DR
DR + fake
DR + patchy fake lawn
DR + sparse fake lawn
J
Percent Population on Lawn Region after 20 hrs
NS.
****
fed
fed + sepha−dex
fed + large sepha−dex
fed + sepha−rose
fed + micro−particles
fed + hydro−gel
DR
DR + sepha−dex
DR + large sepha−dex
DR + sepha−rose
DR + micro−particles
DR + PEG hydro−gel

Supplemental Figure 2.1 The fake lawn is not edible and does not blunt DR-mediated *fmo-2* induction via chemosensation. (A) *C. elegans* (white arrow) among GFP-coated 20-50 μM beads. (**B-C**) Images (**B**) and quantification (**C**) of WT N2 worms on a DR +/- GFP-coated beads. $N \geq 64$ worms. (**D**) Chemotaxis Assay of WT N2 worms on plates with Sephadex beads or Sephadex-soaked M9 supernatant. N = 9 plates of ≥ 40 worms/plate for each condition. (**E**) Lawn occupancy on fed/DR +/- alternative fake lawns at 20 hours after being placed on conditions. $N \geq 45$ worms/condition. (**F-G)** Images **(F)** and quantification **(G)** of *fmo-2p::mCherry* on fed and DR control conditions as well as DR + 200μL Sephadex media supernatant and DR + 200μL Sephadex beads for 24 hours. $N \geq 71$ worms. (**H**) Images of full, patchy, and sparse lawn configurations. (**I-J**) Representative images (**I**) and quantification (**J**) of *fmo-2p::mCherry* on fed/DR +/- different lawn configurations. $N \geq 99$ worms/condition. (**K-L**) Images (**K**) and quantification (**L**) of *fmo-2p::mCherry* worms on fed and DR conditions +/- different concentrations of the Sephadex fake lawn, ranging from 1x (0.03mg/mL) to 0.25x (0.0075mg/mL). $N \geq 56$ worms per condition. The center line on all box plots displays the median, and the boundaries of the box represent the interquartile range. Boxplot statistics are Wilcoxon rank sum test with Bonferroni p-adjustment, two-sided, unpaired. NS. = $p > 0.05$, *** = $p < .001$. All images within one figure panel were taken at the same scale, as indicated by the scale bar in the top left image.

Based on our previous finding that food smells can decrease DR-mediated longevity by modulating the longevity gene *fmo-2*[105], we next asked whether food-like touch would blunt DR-mediated *fmo-2* induction. FMO-2, a xenobiotic enzyme expressed in the intestine of *C. elegans*, is an effector of DR-mediated longevity[48]. FMO-2 oxygenates substrates with nucleophilic centers, and this oxygenation alters one-carbon metabolism to extend lifespan[282]. Knocking out *fmo-2* prevents DR from extending lifespan and overexpressing *fmo-2* improves lifespan in fed worms. FMOs are structurally conserved from worms to humans, and FMOs are also implicated in DR-mediated longevity in mice[110,283]. Because *fmo-2* expression is induced by DR, and *fmo-2* is required for DR-mediated longevity[48], *fmo-2* induction can be used as a screening tool for the effects various interventions may have on DR-mediated longevity in *C. elegans*[105]. By imaging a single-copy integrated transcriptional *fmo-2* reporter under fed and DR conditions with and without a fake lawn (**Fig. 2.1D-E**), we found that the fake lawn did indeed decrease *fmo-2* induction under DR without affecting fed worms. The data from all *fmo-2p::mCherry* imaging experiments are normalized to the fed control condition. While DR consistently induces *fmo-2* transcription relative to the fed condition, we observe some variability in the fold induction of *fmo-2* under DR due to: 1) seasonal changes temperature and humidity; and 2) basal *fmo-2* induction in fed worms is very low, meaning that slight variations in the fed control between

experiments can lead to variation DR-mediated *fmo-2* induction relative to this control. This DR-mediated *fmo-2* blunting effect was also observed in fake lawns made from a variety of other materials, suggesting the phenotype is not specific to the Sephadex beads used to mimic food touch (**Fig. 2.1F-H**).

In order to determine whether worms prefer to spend time in these materials, like they do the Sephadex fake lawn, we conducted lawn occupancy assays on fed and DR plates +/- each fake lawn alternative (**SFig. 2.1E**). We found that none of these materials decreased preference for a fed lawn. Under DR conditions, worms occupied all alternative materials to a similar degree as they did the Sephadex fake lawn, except for polyethylene glycol (PEG). Additionally, we confirmed that this *fmo-2* blunting effect is not due to a chemosensory property of the Sephadex beads, as worms exposed to the supernatant of beads in water did not exhibit decreased *fmo-2* induction (**SFig. 2.1F-G**).

Next, we asked whether the beads composing the fake lawn had to be in a thick and lawn-like formation to suppress DR-mediated *fmo-2* induction. To answer this question, we measured *fmo-2* induction on DR alone, DR with the fake lawn, DR with a sparse lawn (equal mass of beads distributed in a thin layer), and DR with a patchy lawn (equal mass and concentration of beads distributed in small patches) (**SFig. 2.1H-J**). We found that only the full fake lawn decreased *fmo-2* induction under DR, establishing that the distribution of the fake lawn is crucial in decreasing the DR response, perhaps indicating that the mechanical cues from undergrown or small patches of bacteria do not signal a good source of nutrition to *C. elegans*. Finally, we asked whether the density of the Sephadex beads composing the fake lawn plays a role in DR-mediated *fmo-2* induction. When we measured *fmo-2* induction under fed and DR conditions +/- a fake lawn of the standard bead concentration, 0.5x the standard concentration, or 0.25x the standard

concentration, we found that the standard concentration consistently blunted DR-mediated *fmo-2* induction across three replicates. The fake lawns of lower densities sometimes blunted DR-mediated *fmo-2* induction, but less consistently (**SFig. 2.1K-L**). Together with the sparse lawn, these results indicate that both distribution and density of the fake lawn contribute to the textural properties that blunt DR-mediated *fmo-2* induction.

Finding that the dense fake lawn does blunt expression of the longevity effector *fmo-2* suggests that touch may also blunt the lifespan and stress resistance benefits of DR. After conducting a lifespan assay on the same four conditions, we found that the fake lawn does blunt DR-mediated longevity (**Fig. 2.1I**) but does not shorten fed lifespan. Moreover, this DR-blunting effect was not observed in worms that genetically overexpress *fmo-2* (**Fig. 2.1J**), suggesting that decreased *fmo-2* induction due to mechanosensation causally suppresses DR-mediated longevity. *fmo-2* knockout worms were not examined because *fmo-2* is required for DR to extend lifespan. Dietary restriction not only extends lifespan, but also improves healthspan and stress resistance across taxa[284,285]. To examine the effects of touch on DR-mediated stress resistance, we measured heat stress survival after 24 hours on the conditions of fed/DR +/- touch, followed by three hours at 37 °C then 20 hours of recovery at 20 °C. In this assay, dietary restriction improved heat stress survival compared to fed controls, and touch blunted DR-mediated stress resistance (**Fig. 2.1K**). Together, these results indicate that touch partially abrogates multiple beneficial effects of dietary restriction.

Having identified that the fake lawn blunts DR-mediated longevity in an *fmo-2*-dependent manner, we asked whether canonical mechanoreceptor proteins are required. *C. elegans* respond to touch through >40 putative mechanoreceptor proteins distributed throughout the body wall and nose tip[286]. Both classes of *C. elegans* mechanoreceptor proteins—transient

receptor potential (TRP) and degenerin/epithelial (DEG/ENaC) receptors—are also encoded in mammals[287,288]. To test whether broad inhibition of mechanosensation prevents the fake lawn from blunting DR, we put *fmo-2* reporters on fed, DR, and DR + touch conditions with and without amiloride, a DEG/ENaC inhibitor[289,290]. We found that 250 µM of amiloride consistently blocked our phenotype (**Fig. 2.2A-B**), and that lower doses (10 µM and 100 µM) sometimes blocked the effect, with lower consistency across replicates (**Fig. 2.2A-B**). 250 µM amiloride also prevented touch from abrogating DR-mediated longevity (**Fig. 2.2C**), while 100 µM partially blocked the phenotype and 10 µM had no effect on lifespan (**SFig. 2.2C-D**).

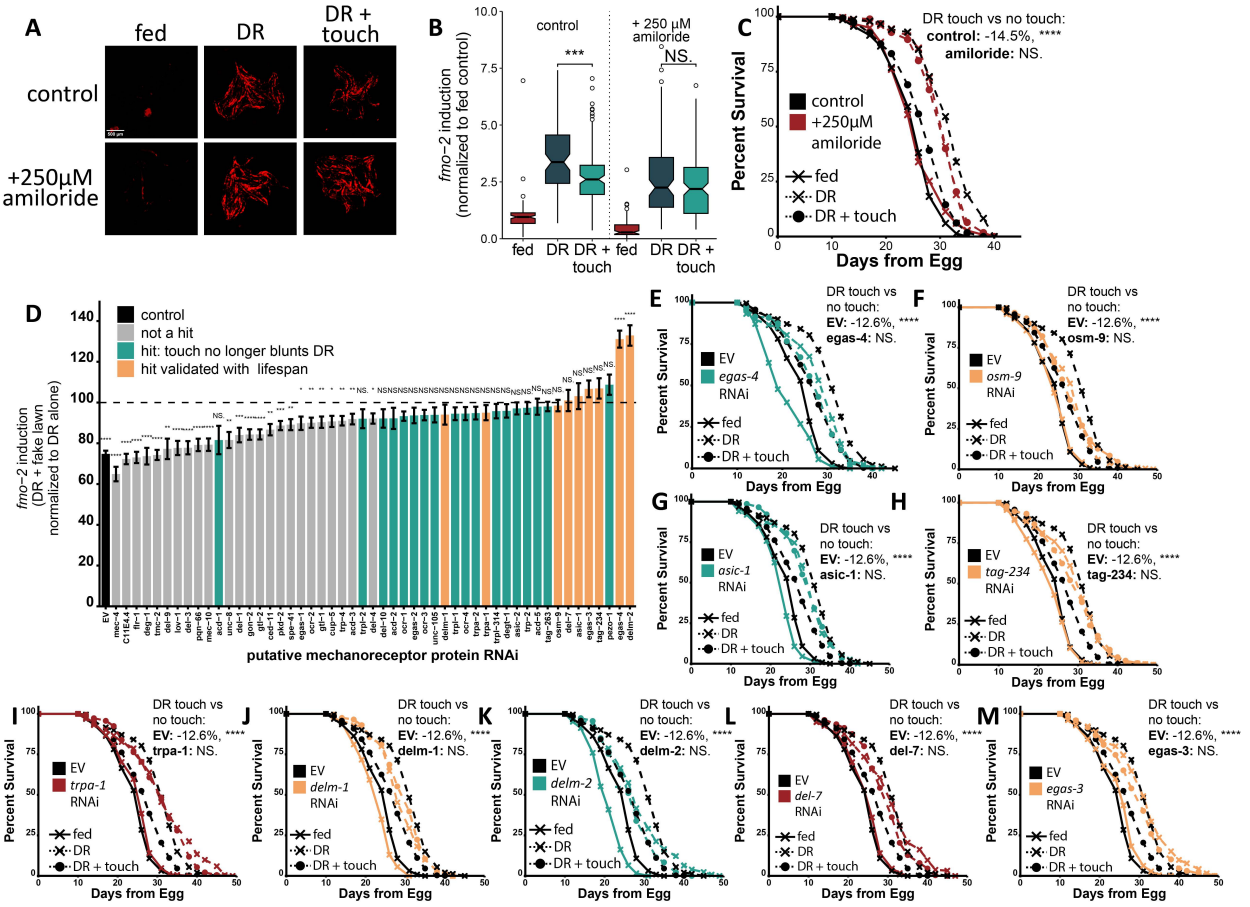
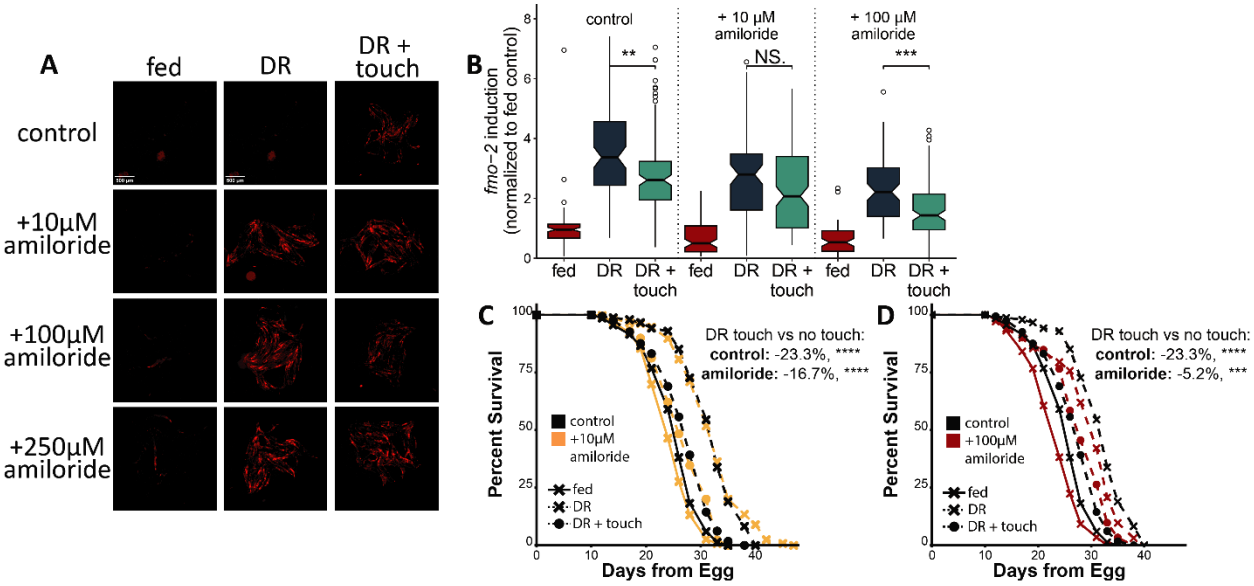


Figure 2.2 Multiple putative mechanoreceptor proteins affect the ability of the fake lawn to blunt DR-mediated longevity. (**A-B**) Representative images (**A**) and quantification (**B**) of *fmo-2p::mCherry* on fed/DR +/- touch, +/- 250 µM amiloride. $N \geq 73$ worms/condition. (**C**) Survival curve of WT animals on fed/DR +/- touch conditions +/- 250 µM amiloride. $N \geq 242$ worms/condition. (**D**) Quantification of *fmo-2* induction in *fmo-2p::mCherry;* MAH677(*sid-1; rgef-1p::sid-1)* on DR + touch as a percent of DR for each putative mechanoreceptor protein knockdown. $N \geq 68$ for DR alone and ≥ 64 for DR + touch. (**E-M**) Survival curves of MAH677(*sid-1; rgef-*

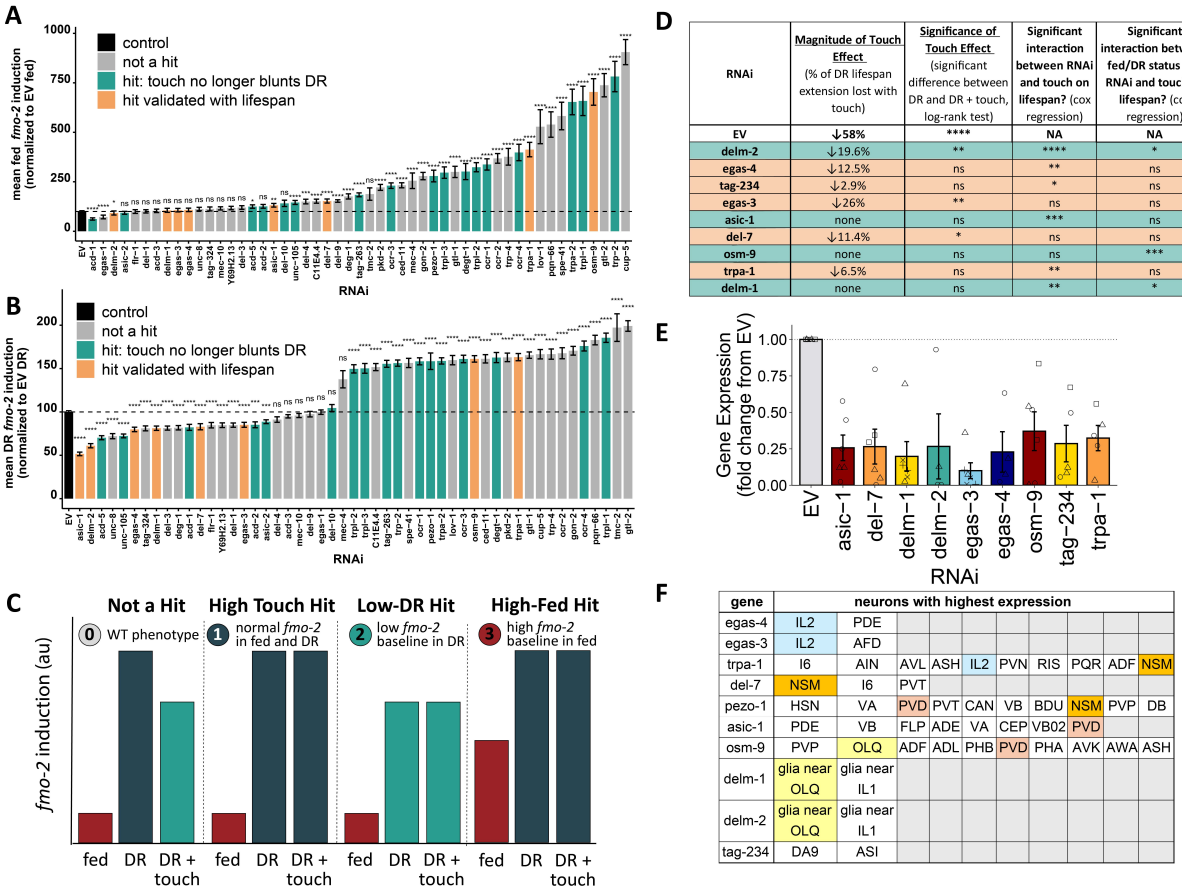
1p::sid-1) on EV or (**E**) *egas-4* ($N \geq 176$), (**F**) *osm-9* ($N \geq 185$), (**G**) *asic-1* ($N \geq 240$), (**H**) *tag-234* ($N \geq 240$), (**I**) *trpa-1* ($N \geq 186$), (**J**) *delm-1* ($N \geq 170$), (**K**) *delm-2* ($N \geq 227$), (**L**) *del-7* ($N \geq 185$), or (**M**) *egas-3* ($N \geq 240$) RNAi, on fed/DR +/- touch conditions. The center line on all box plots displays the median, and the boundaries of the box represent the interquartile range. Boxplot statistics are Wilcoxon rank sum test with Bonferroni p-adjustment, two-sided, unpaired. In all panels, NS. = $p > 0.05$, * = $p < 0.05$, ** = $p < 0.01$, *** = $p < 0.001$, **** = $p < 0.0001$. All images within one figure panel were taken at the same scale, as indicated by the scale bar in the top left image.



Supplemental Figure 2.2 250 µM amiloride has the greatest blocking effect on DR + touch. (**A-B**) Representative images (**A**) and quantification (**B**) of *fmo-2p::mCherry* on fed/DR +/- touch, +/- 10 µM, 100 µM, or 250 µM amiloride. $N \geq 73$ worms/condition. The center line on all box plots displays the median, and the boundaries of the box represent the interquartile range. Boxplot statistics are Wilcoxon rank sum test with Bonferroni p-adjustment, two-sided, unpaired. (**C-D**) Survival curve of WT animals on fed/DR +/- touch conditions +/- 10 µM (**C**) or 100 µM (**D**) amiloride. $N \geq 219$ (**C**) or $n \geq 242$ (**D**) worms/condition. Log-rank tests. In all panels, NS. = $p > 0.05$, * = $p < 0.05$, **** = $p < 0.0001$. All images within one figure panel were taken at the same scale, as indicated by the scale bar in the top left image.

However, amiloride is a broad inhibitor of sodium channels and can also inhibit channels that are not known to have a role in *C. elegans* mechanosensation[291]. We next sought to confirm that the fake lawn effect is due to mechanosensation, to test if TRP channels also contribute, and to determine whether any single putative mechanoreceptor protein is necessary. To answer these questions, we used RNAi to knock down 50 putative *C. elegans* mechanoreceptors[286] with available RNAi clones and measured *fmo-2* induction on fed and DR +/- touch. Our *fmo-2* reporter was crossed with the neuronal-only RNAi uptake strain (MAH677, *sid-1; unc-119p::sid-1)* to facilitate RNAi uptake into neurons and prevent any potential off target effects of

these RNAi in peripheral tissues. We found that knockdown of 25 putative mechanoreceptor proteins prevented touch from blunting DR-mediated *fmo-2* induction (**Fig. 2.2D**) and many knockdowns altered baseline *fmo-2* induction without touch (**SFig. 2.3A-C**). Consequently, some of thegenes that blocked touch blunting of DR-mediated *fmo-2* induction did so by blunting baseline DR to the level of DR + touch in our empty vector (EV) control (low-DR hits, **SFig. 2.3C**). Conversely, other putative mechanoreceptor proteins blocked the touch effect by raising the DR-mediated *fmo-2* induction on DR + touch to the level of DR alone (high-touch hits, **Fig. 2.3C)**. These two types of hits could represent genes that are required for basal DR-mediated *fmo-2* induction and genes that are specifically required for touch perception to lower DR-mediated *fmo-2* induction, respectively. Interestingly, many of these hits also modulate sensory modalities other than mechanosensation. OSM-9, for example, is also important in chemosensation and temperature sensation [292] while TRPA-1 plays a role in nociception and temperature perception[96,293,294].



RNAi	Magnitude of Touch Effect (% of DR lifespan extension lost with touch)	Significance of Touch Effect (significant difference between DR and DR + touch, log-rank test)	Significant interaction between RNAi and touch on lifespan? (cox regression)	Significant interaction between fed/DR status and RNAi and touch on lifespan? (cox regression)
EV	↓58%	****	NA	NA
delm-2	↓19.6%	**	****	*
egas-4	↓12.5%	ns	**	ns
tag-234	↓2.9%	ns	*	ns
egas-3	↓26%	**	ns	ns
asic-1	none	ns	***	ns
del-7	↓11.4%	*	ns	ns
osm-9	none	ns	ns	***
trpa-1	↓6.5%	ns	**	ns
delm-1	none	ns	**	*

gene	neurons with highest expression								
egas-4	IL2	PDE							
egas-3	IL2	AFD							
trpa-1	I6	AIN	AVL	ASH	IL2	PVN	RIS	PQR	ADF	NSM
del-7	NSM	I6	PVT							
pezo-1	HSN	VA	PVD	PVT	CAN	VB	BDU	NSM	PVP	DB
asic-1	PDE	VB	FLP	ADE	VA	CEP	VB02	PVD		
osm-9	PVP	OLQ	ADF	ADL	PHB	PVD	PHA	AVK	AWA	ASH
delm-1	glia near OLQ	glia near IL1								
delm-2	glia near OLQ	glia near IL1								
tag-234	DA9	ASI								

Supplemental Figure 2.3 Knocking down many mechanoreceptors alters baseline fed and DR *fmo-2* induction and longevity with and without touch. (**A-B**) Quantification of MAH677 (*sid-1; rgef-1p::sid-1); fmo-2p::mCherry* on fed (**A**) or DR (**B**) as a percentage of the EV control for each putative mechanoreceptor protein knockdown. $N \geq 47$ (**A**) or $n \geq 68$ (**B**). Bar height shows the mean of 3 biological replicates +/- SEM. Wilcoxon rank sum test with Bonferroni p-adjustment, two-sided, unpaired. (**C**) Schematic summarizing the various ways a putative mechanoreceptor protein knockdown hit could block the touch phenotype. (**D**) Effect of top imaging hits on DR + touch lifespan. (**E**) Gene expression of putative mechanoreceptor protein hits in MAH677 (*sid-1; rgef-1p::sid-1)* worms raised on RNAi targeting each gene compared to control worms raised on empty vector (EV) RNAi for two generations. $N \geq 300$ worms per replicate, or 900 worms per condition. (**F**) Table of up to 10 neurons that have the highest expression of each putative mechanoreceptor hit. Neurons common to multiple hits are colored. Expression data from the Cengen Project[295]. In all panels, NS. = $p > 0.05$, * = $p < 0.05$, ** = $p < 0.01$, *** = $p < 0.001$, **** = $p < 0.0001$. All images within one figure panel were taken at the same scale, as indicated by the scale bar in the top left image.

Based on our imaging screen results, we followed up on nine putative mechanoreceptor protein hits that 1) had the greatest effect size in restoring the induction of *fmo-2* in the DR + touch condition, 2) were consistent across all biological replicates, and 3) included hits from both the DEG/ENaC and the TRP receptor categories. After conducting lifespan assays of the neuronal-specific RNAi uptake strain, MAH677 (*sid-1; rgef-1p::sid-1)* on RNAi for these top

hits, we found that all nine knockdowns either completely (**Fig. 2.2E-J**) or partially (**Fig. 2.2K-M**) prevented touch from blunting DR (Cox regression for an interaction between RNAi and touch, **SFig. 2.3D**). Successful knockdown by the RNAi used in these lifespans was validated via qPCR (**SFig. 2.3E**). Finding that many single putative mechanoreceptor proteins are necessary for the fake lawn to blunt DR-mediated longevity could suggest that either 1) some of these putative mechanoreceptor proteins are acting at downstream points in this circuit rather than directly responding to the fake lawn, or 2) small disruptions to mechanosensory perception may have significant effects on downstream physiology and longevity pathways. An analysis of the expression patterns of these genes reveals a distributed expression pattern of these putative mechanoreceptor proteins among many neurons (**SFig. 2.3F**). However, four candidate neurons (IL2, NSM, PVD, and OLQ) receive input from at least three of the putative mechanoreceptor hits, and all of these cells have established roles in nose touch (IL2, OLQ)[296,297], food sensing (NSM)[298], or general mechanosensation (PVD)[299]. Taken together, these data suggest multiple putative mechanoreceptor protein-expressing neurons may contribute to touch modification of DR-mediated longevity.

2.5 Signaling from dopamine and tyramine is required for touch to regulate longevity.

Upon identifying multiple putative mechanoreceptor proteins that regulate touch attenuation of DR, we sought to determine the neural signals downstream of initial mechanosensory perception. Identifying these signals could point to neural regulators of longevity downstream of sensory perception. To interrogate these signals, we crossed our *fmo-2* reporter with mutants deficient in the synthesis or packaging of each *C. elegans* neurotransmitter[300]. We found that knocking out dopamine synthesis prevented touch attenuation of DR-mediated *fmo-2* induction (**Fig. 2.3A-C**). Additionally, knocking out tyramine and

octopamine synthesis blocked the touch phenotype (**Fig. 2.3A, D-E**). However, knocking out octopamine synthesis alone (**Fig. 2.3A, F-G**) had no effect on suppression of DR-mediated *fmo-2* induction by the fake lawn, suggesting that tyramine but not octopamine is required for this effect. Impairing the synthesis or packaging of serotonin (**SFig. 2.4A-B**), GABA (**SFig. 2.4C-D**), glutamate (**SFig. 2.4E-F**), and acetylcholine (**SFig. 2.4G-H**) also had no effect on the ability of touch to blunt DR. The same effects were observed in lifespan assays: blocking dopamine synthesis (**Fig. 2.3H**) and blocking tyramine and octopamine synthesis (**Fig. 2.3I**) also prevented touch from attenuating DR-mediated longevity while blocking octopamine synthesis alone (**Fig. 2.3J**) did not. Notably, multiple neurotransmitter knockout strains displayed altered baseline levels of *fmo-2* induction under fed and/or DR conditions (**Fig. 2.3E-F, SFig. 2.4D-H**). However, much like the putative mechanoreceptor protein knockdowns (**Fig. 2.2D, SFig. 2.3A-B**), only some of the neurotransmitter knockouts that altered basal *fmo-2* also blocked the touch phenotype. This once again suggests that while some hits may block the food touch effect by preventing a normal response to DR alone, others are highly specific to the DR touch circuit (**SFig. 2.3C**).

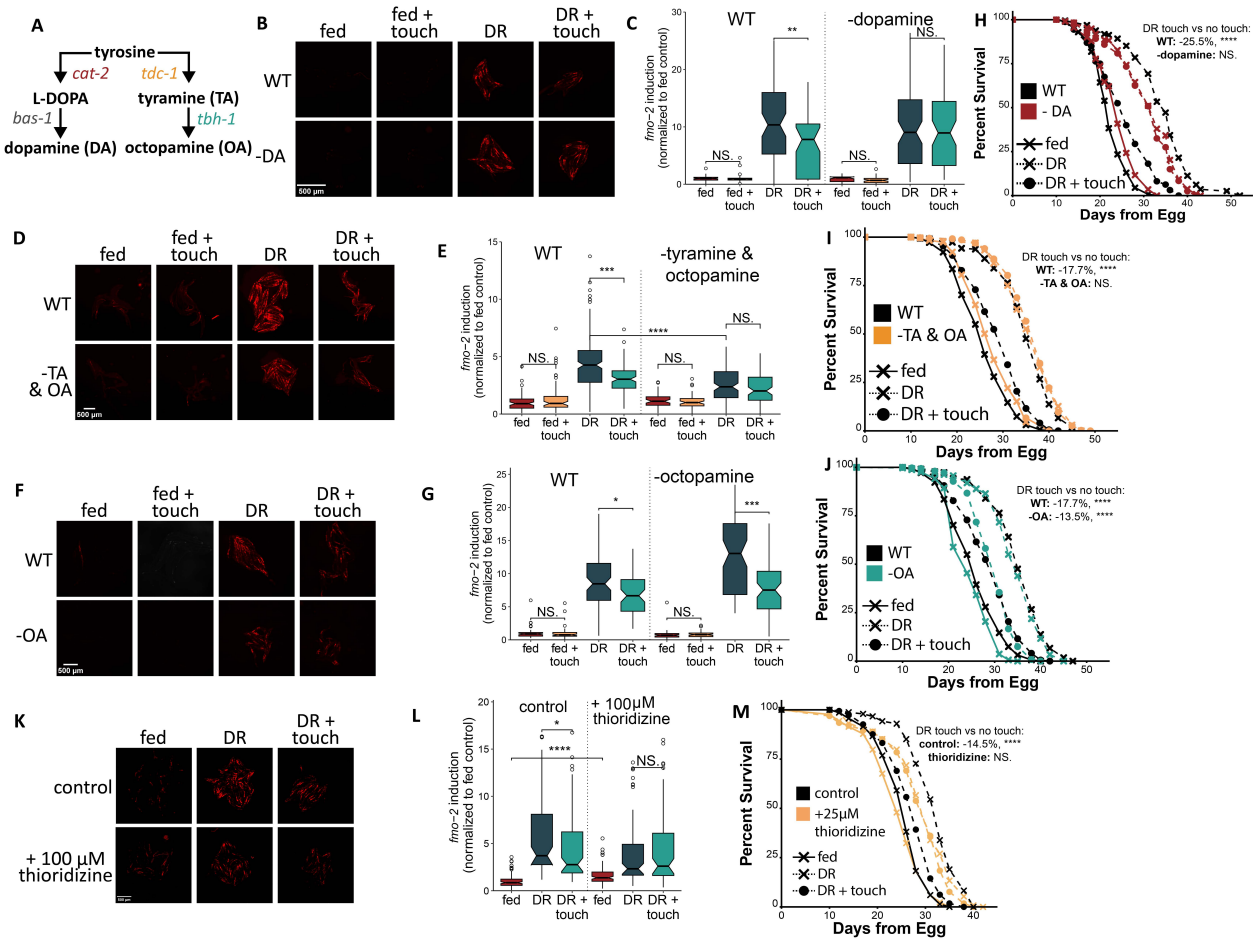
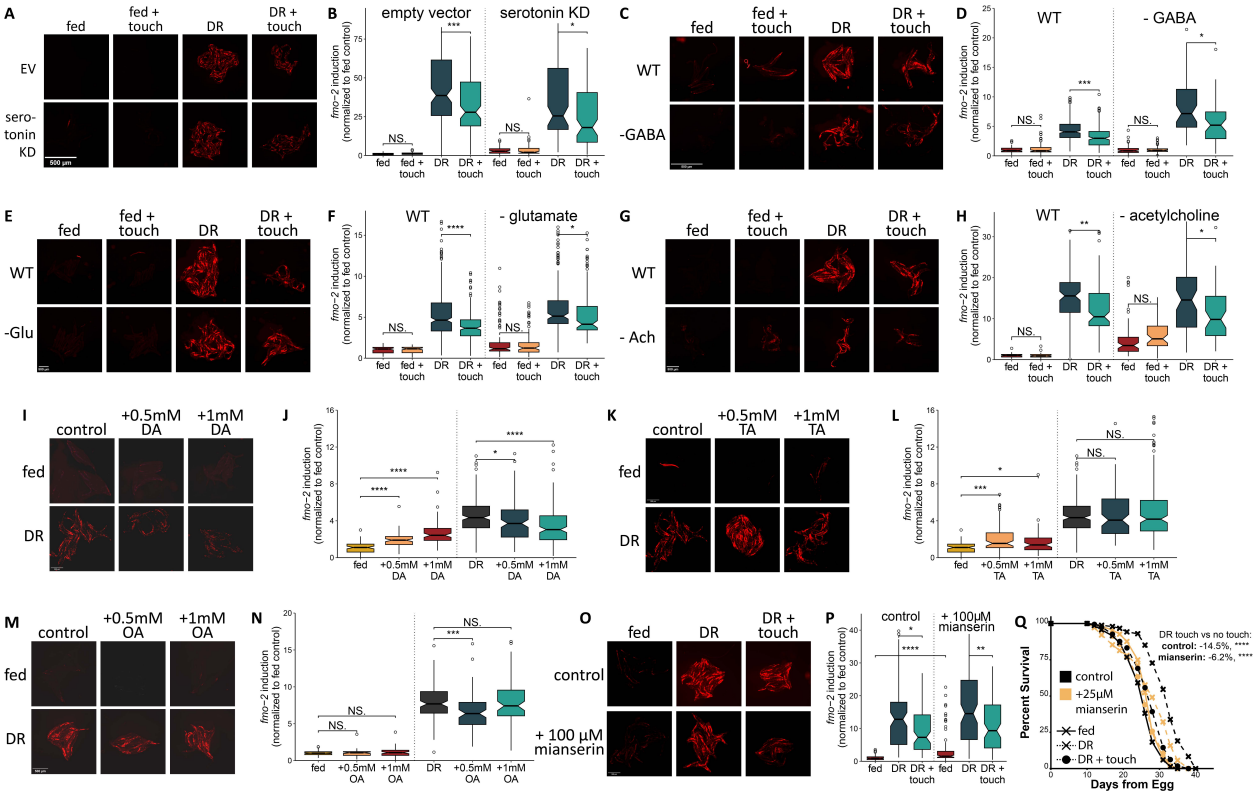


Figure 2.3 The bioamines dopamine and tyramine modulate DR-mediated longevity downstream of touch. (**A**) Diagram of dopamine, tyramine, and octopamine synthesis. (**B-G**) Representative images (**B, D, F**) and quantification (**C, E, G**) of *fmo-2p::mCherry* (WT) and *fmo-2p::mCherry; cat-2(n4547)* (-dopamine, **B-C**), *fmo-2::mCherry; tdc-1(n3419)* (-tyramine & octopamine, **D-E**), or *fmo-2p::mCherry; tbh-1(n3247)* (-octopamine, **F-G**) on fed/DR +/- touch conditions. $N \geq 50$ (**C**), ≥ 54 (**E**), and ≥ 54 (**G**) worms/condition. (**H-J**) Survival curves of WT and *cat-2(n4547)* (-DA) (**H**), *tdc-1(n3419)* (-TA & OA) (**I**), or *tbh-1(n3247)* (-OA) (**J**) animals on fed/DR +/- touch conditions. $N \geq 160$ (**H**), ≥ 225 (**I**), ≥ 225 (**J**) per condition. (**K-L**) Images (**K**) and quantification (**L**) of *fmo-2p::mCherry* on fed/DR +/- touch with or without 100 µM thioridazine. $N \geq 77$ worms per condition. (**M**) Survival curves of WT animals on fed/DR +/- touch conditions with and without 25 µM thioridazine. $N \geq 240$ worms per condition. The center line on all box plots displays the median, and the boundaries of the box represent the interquartile range. Boxplot statistics are Wilcoxon rank sum test with Bonferroni p-adjustment, two-sided, unpaired. (**H-J, M**) Log-rank test. In all panels, NS. = $p > 0.05$, * = $p < 0.05$, ** = $p < 0.01$, *** = $p < 0.001$, **** = $p < 0.0001$. All images within one figure panel were taken at the same scale, as indicated by the scale bar in the top left image.

Interestingly, the production of both dopamine and tyramine (the invertebrate analog of adrenaline) is regulated by food availability. Dopamine release is generally associated with finding food[281,301], but the role of tyramine in signaling nutrient status is less clear[302,303]. To determine whether dopamine and tyramine act as a signal of nutrient abundance or nutrient

scarcity in this circuit, we supplemented our *fmo-2* reporters with exogenous dopamine or tyramine on fed and DR conditions. We expect that adding a signal of nutrient abundance would decrease *fmo-2* induction under DR while adding a signal of nutrient scarcity would increase the DR-response gene *fmo-2* even under fed conditions. When we supplemented *fmo-2* reporters with exogenous dopamine, we observed a dose-dependent increase in *fmo-2* induction under fed conditions and a dose-dependent decrease in *fmo-2* induction under DR conditions. (**SFig. 2.4I-J**). This suggests a complex interaction between dopamine signaling and nutrient perception, and could be consistent with a model in which dopamine release upon perception of touch leads to a decreased DR response. Exogenous tyramine, on the other hand, dose-dependently increased *fmo-2* induction on fed conditions but was not additive with DR-mediated *fmo-2* induction (**SFig. 2.4K-L**). This suggests a model in which the absence of food cues leads to tyramine release, triggering an increased DR response and *fmo-2* induction. However, when worms encounter touch under DR conditions, tyramine release is suppressed to blunt the DR response.

In our previous work on the role of olfaction in DR, we found that two small molecules that antagonize dopamine and serotonin (thioridazine and mianserin, respectively), act as DR-mimetics to extend lifespan [105]. Consistent with our neurotransmitter screen results, we found that thioridazine (**Fig. 2.3K-M**) but not mianserin (**SFig. 2.4M-O**) prevented the fake lawn from blunting DR-mediated *fmo-2* induction (**Fig. 2.3K-L, SFig. 2.4M-N**) and longevity (**Fig. 2.3M, SFig. 2.4O**). These results indicate that DR mimetics acting downstream of food perception may function regardless of external nutrient cues. Moreover, the ability of thioridazine but not mianserin to block touch further supports a role for dopamine, but not serotonin, as an intermediate signal in multiple circuits through which perception regulates DR-mediated longevity.



Supplemental Figure 2.4 Dopamine and tyramine signaling, but not serotonin, GABA, glutamate, or acetylcholine signaling are required for touch to attenuate DR. (**A-B**) Representative images (**A**) and quantification (**B**) of TU3311(*unc-119p::sid-1); fmo-2p::mCherry* on empty vector or *tph-1* RNAi (serotonin KD) on fed/DR +/- touch conditions. $N \geq 61$ worms per condition. (**C-H**) Representative images (**C, E, G**) and quantification (**D, F, H**) of *fmo-2p::mCherry* (WT) and *fmo-2p::mCherry; unc-25(e156)* (-GABA, **C-D**), *fmo-2::mCherry; eat-4(ky5)* (-glutamate, **E-F**), or *fmo-2p::mCherry; unc-17(e113)* (-acetylcholine, **G-H**) on fed/DR +/- touch conditions. $N \geq 50$ (**D**), ≥ 75 (**F**), and ≥ 53 (**H**) worms/condition. (**I-N**) Representative images (**I, K, M**) and quantification (**J, L, N**) of *fmo-2p::mCherry* on DR or fed conditions with or without 0.5mM and 1mM exogenous dopamine (**I-J**), tyramine (**K-L**), and octopamine (**M-N**). $N \geq 153$ (**J**), ≥ 52 (**L**), and ≥ 60 worms/condition. (**O-P**) Representative images (**O**) and quantification (**P**) of *fmo-2p::mCherry* on fed/DR +/- touch conditions with or without 100 µM mianserin. $N \geq 91$ worms per condition. (**Q**) Survival curves of WT animals on fed/DR +/- touch conditions with and without 25 µM mianserin. $N \geq 177$ worms per condition. The center line on all box plots displays the median, and the boundaries of the box represent the interquartile range. Boxplot statistics are Wilcoxon rank sum test with Bonferroni p-adjustment, two-sided, unpaired. (**Q**) Log-rank test. In all panels, NS. = $p > 0.05$, * = $p < 0.05$, ** = $p < 0.01$, *** = $p < 0.001$, **** = $p < 0.0001$. All images within one figure panel were taken at the same scale, as indicated by the scale bar in the top left image.

Once we established the necessity of dopamine and tyramine, we asked which dopaminergic and tyraminergic cells were key players in the DR touch circuit. To determine which dopaminergic neuron(s) signal in this pathway, we rescued dopamine production in each of the three *C. elegans* dopaminergic neuron classes in a dopamine deficient background strain. Because no promoters have been identified that are expressed exclusively in each DAergic neuron class, we rescued *cat-2* expression under promoters active in a subset of neurons that

included only one dopaminergic neuron class. This approach is limited in that *cat-2* may be artificially expressed in some non-dopaminergic neurons, but we expect these neurons will not produce dopamine because they lack *bas-1* activity, which is necessary to convert L-DOPA to dopamine (**Fig. 2.4A**). We found that rescuing dopamine production in all dopaminergic cells and just in the CEP dopaminergic neurons restored WT-like *fmo-2* induction (**Fig. 2.4A-B**) while rescuing dopamine in the ADE or PDE dopaminergic neurons did not (**Fig. 2.4C-D**). Unlike in our imaging experiments, however, we found that rescuing dopamine production in any dopaminergic cell type rescued the effect of touch on DR-mediated longevity (**Fig. 2.4E-H**). Together, these results are consistent with a model in which a subpopulation of dopaminergic neurons play a key role in touch modification of *fmo-2* induction, while neuronal specificity does not contribute to touch modification of lifespan. Alternatively, it is possible that rescuing dopamine synthesis in one dopaminergic neuron class could facilitate reuptake and signaling by other dopaminergic cells. It is also notable that signaling from all three classes of dopaminergic neurons are required for worms to slow upon encountering a bacterial lawn [281], suggesting a complex interaction between the localization of dopamine signaling and various physiological responses to food cues.

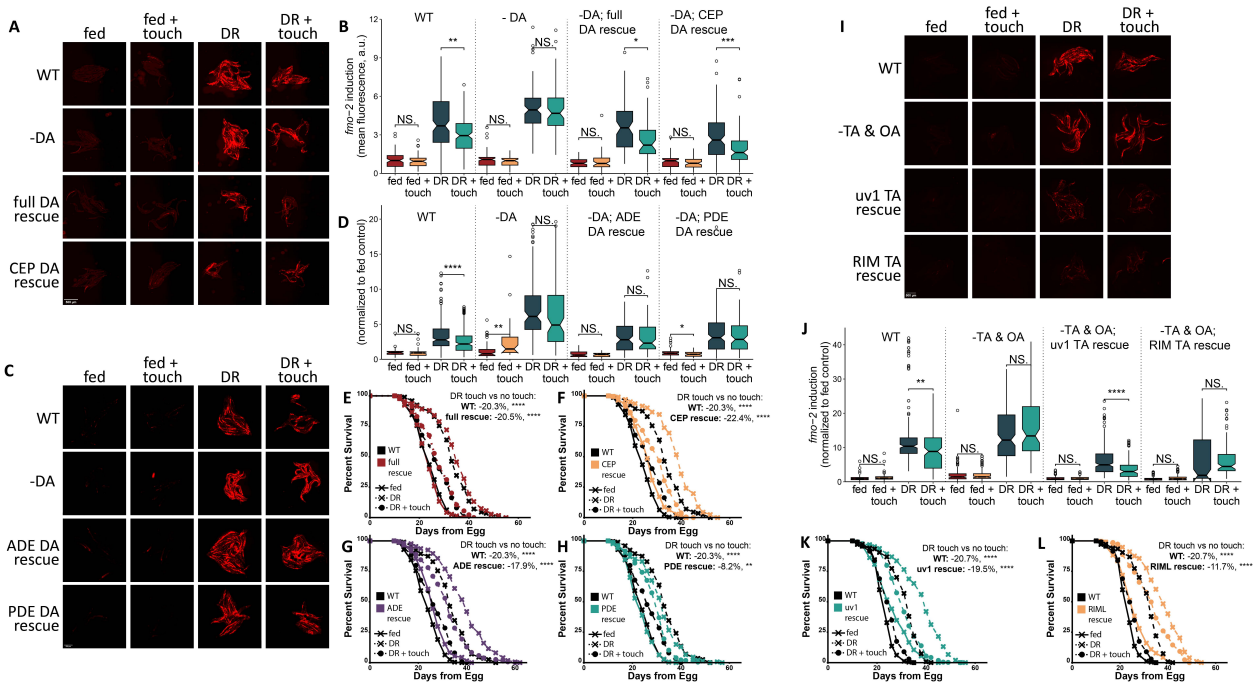


Figure 2.4 Dopamine production from any dopaminergic neuron class and tyramine production from the uv1 neuroendocrine cells is sufficient for touch to blunt DR. (**A-B**) Representative images (**A**) and quantification (**B**) of *fmo-2p::mCherry* (WT), *fmo-2p::mCherry; cat-2(n4547)* (-DA), *fmo-2p::mCherry; cat-2(n4547); Ex[cat-1p::cat-2]* (full DA rescue) and *fmo-2p::mCherry; cat-2(n4547);Ex[swip-10p::cat-2]* (CEP DA rescue) on fed/DR +/- touch conditions. $N \geq 51$ worms per condition. (**C-D**) Representative images (**C**) and quantification (**D**) of *fmo-2p::mCherry* (WT), *fmo-2p::mCherry cat-2(n4547)* (-DA), *fmo-2p::mCherry; cat-2(n4547);Ex[trpa-1p::cat-2]* (ADE DA rescue) and *fmo-2p::mCherry; cat-2(n4547); Ex[tax-2p::cat-2]* (PDE DA rescue) on fed/DR +/- touch conditions. $N \geq 37$ worms per condition. (**E-H**) Survival curves of WT and *cat-2(n4547); Ex[cat-1p::cat-2]* (full DA rescue, **E**), *cat-2(n4547);Ex[swip-10p::cat-2]* (CEP DA rescue, **F**), *cat-2(n4547);Ex[trpa-1p::cat-2]* (ADE DA rescue, **G**), or *cat-2(n4547); Ex[tax-2p::cat-2]* (PDE DA rescue, **H**) animals on fed/DR +/- touch conditions. $N \geq$ 140 (**E**), $\geq$ 140 (**F**), $\geq$ 155 (**G**), and $\geq$ 154 (**H**) per condition. (**I-J**) Representative images (**I**) and quantification (**J**) of *fmo-2p::mCherry* (WT), *fmo-2p::mCherry; tdc-1(n3419)* (-TA & OA), *fmo-2p::mCherry; tdc-1(n3419); Ex[ocr-4p::tdc-1]* (uv1 TA rescue), and *fmo-2p::mCherry; tdc-1(n3419); Ex[gcy-13p::tdc-1]* (RIM TA rescue) on fed/DR +/- touch conditions. $N \geq 66$ worms per condition. (**K-L**) Survival curves of WT and *tdc-1(n3419); Ex[ocr-4p::tdc-1]* (uv1 TA rescue, **K**), or *tdc-1(n3419); Ex[gcy-13p::tdc-1]* (RIM TA rescue, **L**) on fed/DR +/- touch conditions. $N \geq 235$ worms per condition. The center line on all box plots displays the median, and the boundaries of the box represent the interquartile range. Boxplot statistics are Wilcoxon rank sum test with Bonferroni p-adjustment, two-sided, unpaired. (**E-H, K-L**) Log-rank test. In all panels, NS. = $p > 0.05$, * = $p < 0.05$, ** = $p < 0.01$, *** = $p < 0.001$, **** = $p < 0.0001$. All images within one figure panel were taken at the same scale, as indicated by the scale bar in the top left image.

In addition to investigating key dopaminergic neurons, we also asked whether signaling from a specific tyraminergic neuron type was sufficient to restore WT responses to DR + touch. In *C. elegans*, the RIM neuron and uv1 neuroendocrine cells are considered tyraminergic because they express *tdc-1* but not *tbh-1*^{304,305} (**Fig. 2.3A**). To restore tyramine synthesis in each cell type in the *tdc-1* knockout background, we created rescue constructs using the *gcy-13* and

ocr-4 promoters to drive *tdc-1* expression in RIM and uv1 cells, respectively. *gcy-13* expression is specific to only the RIM neuron [306] while *ocr-4* is expressed in the uv1 cells and the OLQ neurons [295,307], although OLQ cells lack *tdc-1* expression required for octopamine and tyramine production. When we tested these cell-specific tyramine rescues on fed/DR +/- touch conditions, we found that only the uv1 cell rescue was sufficient to restore WT-like *fmo-2* induction in response to DR and touch (**Fig. 2.4I-J**). However, we once again observed that rescuing bioamine production in either cell type was sufficient for the fake lawn to blunt DR-mediated longevity (**Fig. 2.4K-L**). Given that only the uv1 rescue restored WT-like *fmo-2* induction and that the uv1 had a larger effect on DR + touch lifespan, we propose that the uv1 cells play a primary role in the touch circuit but that tyramine from the RIM can partially compensate for the loss of uv1 tyramine. However, one limitation to this approach is the possibility of cell nonautonomous effects, where rescuing tyramine synthesis in one cell type drives tyramine reuptake and signaling in other neurons. Interestingly, RIM signaling plays a role in shortening lifespan in response to repeated plate-tapping, suggesting tyramine signaling differs in response to stressful verses food-like touch[58]. Taken together, these data suggest a model in which mechanosensation modulates tyramine release from the uv1 neuroendocrine cells and dopamine release from all dopaminergic neurons, which ultimately send a signal to the intestine to blunt DR-mediated *fmo-2* induction and longevity.

2.6 Insulin and GnRH neuropeptides convey touch signaling to mediate *fmo-2* induction and longevity.

While many dopamine- and tyramine-producing neurons either are primary mechanosensory neurons or receive synaptic input from mechanosensing cells[308], there may be other intermediate signals acting between bioamines and intestinal suppression of *fmo-2*. The *C. elegans* nervous system does not directly innervate peripheral tissues and worms instead secrete

neuropeptide/neuroendocrine signals into the pseudocoelom to communicate with these tissues[309]. To examine whether neuropeptide signaling may facilitate this cell nonautonomous touch signal, we examined the DR + touch *fmo-2* induction response of the dense-core vesicle packing mutant *unc-31*[310]. We found that the fake lawn did not suppress DR-mediated *fmo-2* induction or longevity in *unc-31* mutants (**Fig. 2.5A-C**). We also found that knocking down the pro-neuropeptide maturation and cleavage genes *egl-3* and *egl-21*[309] prevented touch from attenuating DR-mediated *fmo-2* induction (**SFig. 2.5A-B**). Together, these results suggest a possible role for neuropeptides in conveying mechanosensory information from the nervous system to intestinal cells that express the DR effector protein, FMO-2.

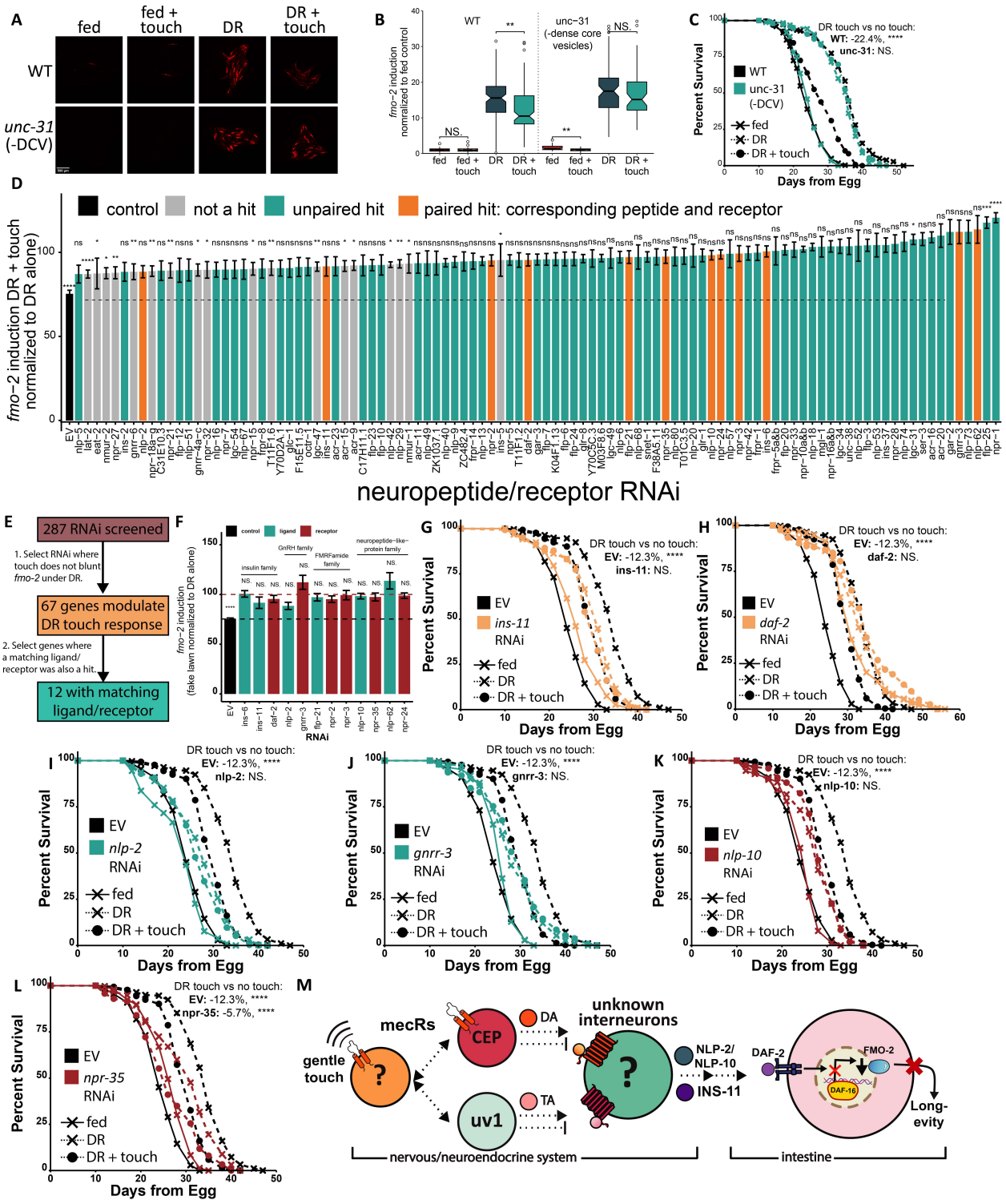
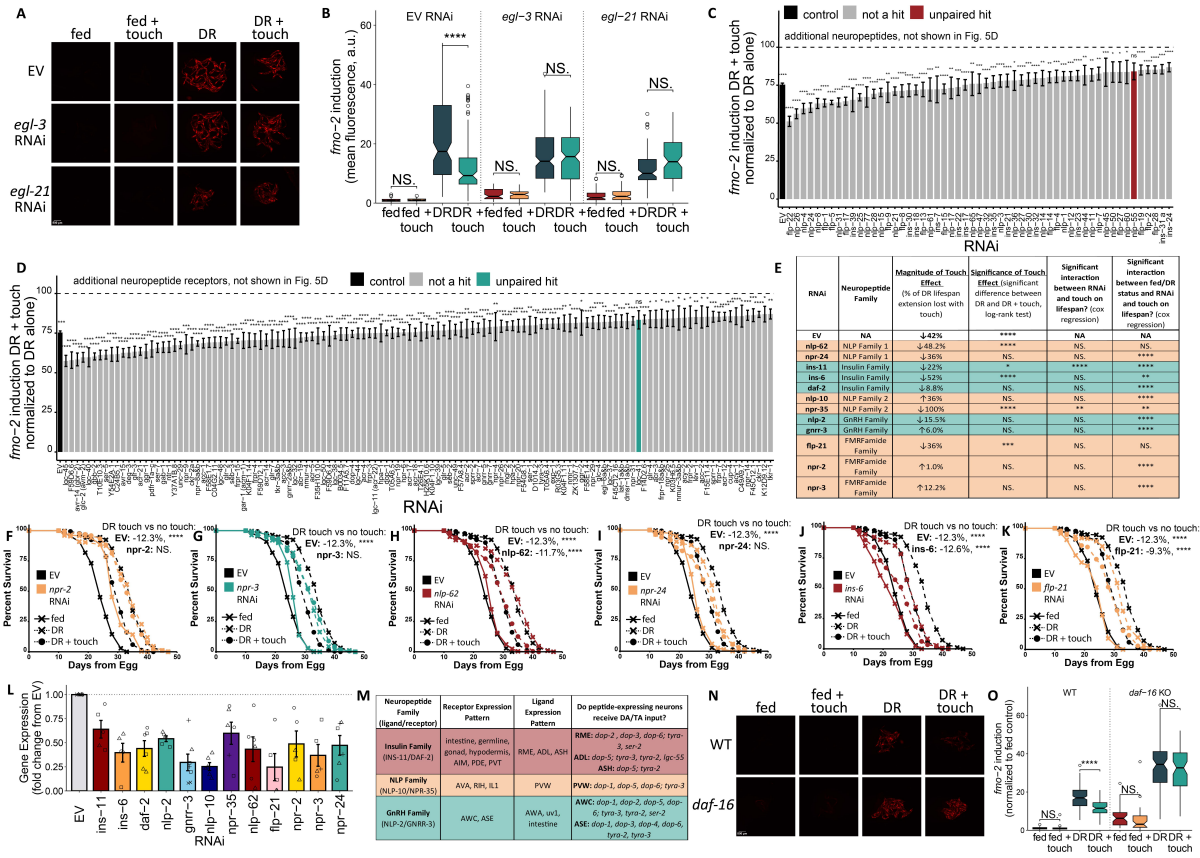


Figure 2.5 Insulin-, GnRH-, and NLP-family neuroendocrine signals are required for touch to blunt DR. (**A-B**) Representative images (**A**) and quantification (**B**) of *fmo-2p::mCherry* (WT) and *fmo-2p::mCherry; unc-31(e169)* (unc-31) on fed/DR +/- touch conditions. $N \geq 51$ worms per condition. (**C**) Survival curves of WT and *unc-31(e169)* worms on fed/DR conditions +/- touch. $N \geq 149$ worms per condition. (**D**) Quantification of *fmo-2p::mCherry; TU3311(unc-119p::sid-1)* on DR + touch as a percent of DR for each neurosignaling knockdown that blocked touch attenuation of DR. $N \geq 54$ for DR alone and ≥ 56 for DR + touch. (**E**) Flow diagram for selecting top

hits. (**F**) *fmo-2* induction on DR + touch as a percent of DR alone on each of the 12 paired hits from (**D**). (**G-L**) Survival curves of TU3311 (*unc-119p::sid-1*) on EV or *ins-11* (**G**), *daf-2* (**H**), *nlp-2* (**I**), *gnrr-3* (**J**), *nlp-10* (**K**), and *npr-35* (**L**) RNAi, on fed/DR +/- touch conditions. $N \geq 242$ (**G**), ≥ 195 (**H**), ≥ 242 (**I**), ≥ 150 (**J**), ≥ 213 (**K**), ≥ 212 (**L**) per condition. (**M**) Diagram of mechanosensory modulation of aging under DR conditions. The center line on all box plots displays the median, and the boundaries of the box represent the interquartile range. Boxplot statistics are Wilcoxon rank sum test with Bonferroni p-adjustment, two-sided, unpaired. (**G-L**) Log rank test. In all panels, NS. = $p > 0.05$, * = $p < 0.05$, ** = $p < 0.01$, *** = $p < 0.001$, **** = $p < 0.0001$. All images within one figure panel were taken at the same scale, as indicated by the scale bar in the top left image.

To identify neuropeptide candidates for this cell nonautonomous signal, we used RNAi to knock down 287 potential neurosignaling ligands and receptors in our *fmo-2* reporter crossed into the neuronal-enhanced RNAi uptake strain, TU3311 (*unc-11p::sid-1)*. Knockdowns resulting in no significant difference between *fmo-2* induction on DR and DR + touch were considered hits. Based on these initial criteria, we identified 85 neurosignaling genes that modified the effect of the fake lawn on DR-mediated *fmo-2* induction (hits in **Fig. 2.5D,** negative data in **SFig. 2.5C-D**). To narrow down this set of potential hits, we eliminated RNAi where results were not consistent across at least 2/3 of replicates. This left us with 67 consistent hits, which we further prioritized by identifying ligand/receptor pairs in which both the ligand and a receptor known to bind to that ligand blocked the DR-touch effect. This final criterion left us with a set of 12 genes falling into 5 groups of ligand/receptor matches (**Fig. 2.5E-F**). Similarly to our putative mechanoreceptor protein RNAi screen, some of these hits blocked the touch phenotype by decreasing baseline DR-mediated *fmo-2* induction to the level of DR + touch while other hits increased *fmo-2* induction on DR + touch to the level of baseline DR-mediated *fmo-2* induction. This suggests that some neuropeptides act as a DR-inhibiting signal and are released in response to touch whereas others act as a DR-promoting signal inhibited by touch.



RNAi	Neuropeptide Family	Magnitude of Touch Effect (% of DR lifespan extension lost with touch)	Significance of Touch Effect (significant difference between DR and DR + touch, log-rank test)	Significant interaction between RNAi and touch on lifespan? (cox regression)	Significant interaction between fed/DR status and RNAi and touch on lifespan? (cox regression)
EV	NA	↓42%	****	NA	NA
nlp-62	NLP Family 1	↓48.2%	****	NS.	NS.
npr-24	NLP Family 1	↓36%	NS.	****	****
ins-11	Insulin Family	↓22%	*	****	****
ins-6	Insulin Family	↓52%	****	NS.	**
daf-2	Insulin Family	↓8.8%	NS.	NS.	****
nlp-10	NLP Family 2	↑36%	NS.	NS.	****
npr-35	NLP Family 2	↓100%	****	**	**
nlp-2	GnRH Family	↓15.5%	NS.	NS.	****
gnrr-3	GnRH Family	↑6.0%	NS.	NS.	****
flp-21	FMRFamide Family	↓36%	***	NS.	NS.
npr-2	FMRFamide Family	↑1.0%	NS.	NS.	****
npr-3	FMRFamide Family	↑12.2%	NS.	NS.	****

Neuropeptide Family (ligand/receptor)	Receptor Expression Pattern	Ligand Expression Pattern	Do peptide-expressing neurons receive DA/TA input?
Insulin Family (INS-11/DAF-2)	intestine, germline, gonad, hypodermis, AIM, PDE, PVT	RME, ADL, ASH	RME: *dop-2 , dop-3, dop-6; tyra-3, ser-2* ADL: *dop-5; tyra-3, tyra-2, igc-55* ASH: *dop-5; tyra-2*
NLP Family (NLP-10/NPR-35)	AVA, RIH, IL1	PVW	PVW: *dop-1, dop-5, dop-6; tyra-3*
GnRH Family (NLP-2/GNRR-3)	AWC, ASE	AWA, uv1, intestine	AWC: *dop-1, dop-2, dop-5, dop-6; tyra-3, tyra-2, ser-2* ASE: *dop-1, dop-3, dop-4, dop-6, tyra-2, tyra-3*

Supplemental Figure 2.5 Many neuroendocrine genes regulate DR-mediated fmo-2 induction and longevity within and independently of the touch pathway. Representative images (**A**) and quantification (**B**) of *fmo-2p::mCherry; MAH677* on fed/DR +/- touch conditions on EV, *egl-3*, or *egl-21* RNAi. $N \geq 57$ worms per condition. (**C-D**) Quantification of *fmo-2p::mCherry; TU3311(unc-119p::sid-1)* on DR + touch as a percent of DR for each neuropeptide (**C**) or neuropeptide receptor (**D**) knockdown that did not block touch attenuation of DR. This represents the negative data from the screen hits shown in **Fig. 5D**. $N \geq 54$ for DR alone and ≥ 56 for DR + touch.(**E**) Effect of top imaging hits on DR + touch lifespan. Log rank tests and cox regression tests with Bonferroni adjustment for comparison across 3 biological replicates. (**F-K**) Survival curves of TU3311 on EV or *npr-2* (**F**), *npr-3* (**G**), *nlp-62* (**H**), *npr-24* (**I**), *ins-6* (**J**), and *flp-21* (**K**) RNAi, on fed/DR +/- touch conditions. $N \geq 176$ (**F**), ≥ 180 (**G**), ≥ 242 (**H**), ≥ 215 (**I**), ≥ 242 (**J**), ≥ 242 (**K**) per condition. (**L**) Gene expression of neuropeptide and neuropeptide receptor hits in TU3311 (*unc-119p::sid-1)* worms raised on RNAi targeting each gene compared to control worms raised on empty vector (EV) RNAi for two generations. $N \geq 300$ worms per replicate, or 900 worms per condition. (**M**) Summary of neurons and tissues that express each neuroendocrine signal hit, as well as whether these neurons receive input from dopamine and/or tyramine. (**L-M**) Representative images (**N**) and quantification (**O**) of *fmo-2p::mCherry* (WT), and *fmo-2p::mCherry; daf-16* (daf-16) on fed/DR +/- touch conditions. $N \geq 34$ worms per condition. The center line on all box plots displays the median, and the boundaries of the box represent the interquartile range. Boxplot statistics are Wilcoxon rank sum test with Bonferroni p-adjustment, two-sided, unpaired. (**F-K**) Log rank test. In all panels, NS. = $p > 0.05$, * = $p < 0.05$, ** = $p < 0.01$, *** = $p < 0.001$, **** = $p < 0.0001$. All images within one figure panel were taken at the same scale, as indicated by the scale bar in the top left image.

When we followed up on these 12 hits with lifespan assays (all touch effects summarized in **SFig. 5E**), we found that 8 of the 12 RNAi imaging hits completely (**Fig. 2.5G-K**, **SFig. 2.5F-G**) or partially (**Fig. 2.5L**) prevented touch from attenuating DR, while the remaining four did

not validate (**SFig. 2.5H-K**). Successful knockdown of all RNAi hits used in lifespans was validated via qPCR (**SFig. 2.5L**). Of the five neuropeptide ligand/receptor families tested, both members of a matching ligand/receptor pair blocked the DR + touch effect in the insulin family (*daf-2, ins-11*), the GnRH family (*nlp-2, gnrr-3*), and one of the two neuropeptide-like protein families (*nlp-10* full block, *npr-35* partial block). Notably, DAF-2 is the only one of these receptors known to be expressed in the intestine (**SFig. 2.5M**)[311], suggesting that *ins-11/daf-2* signaling could be the cell nonautonomous signal conveying mechanosensory information to the intestine. It is also possible that the bioamines dopamine or tyramine signal directly to the intestine via the intestinally-expressed receptors *dop-1* and *tyra-3*, although bioamines are less often packaged in the dense-core vesicles thought to signal to distal tissues[310]. To further validate the role of insulin signaling in the touch-DR pathway, we crossed our *fmo-2* reporter with a mutant of *daf-16*, a key transcription factor acting downstream of DAF-2. We found that, like *ins-11* and *daf-2, daf-16* was required for touch to blunt *fmo-2* induction under DR (**SFig 2.5N-O**). Interestingly, previous work identified a role for *ins-11* in cell nonautonomous signaling from the intestine to the nervous system in response to pathogenic bacteria[312].

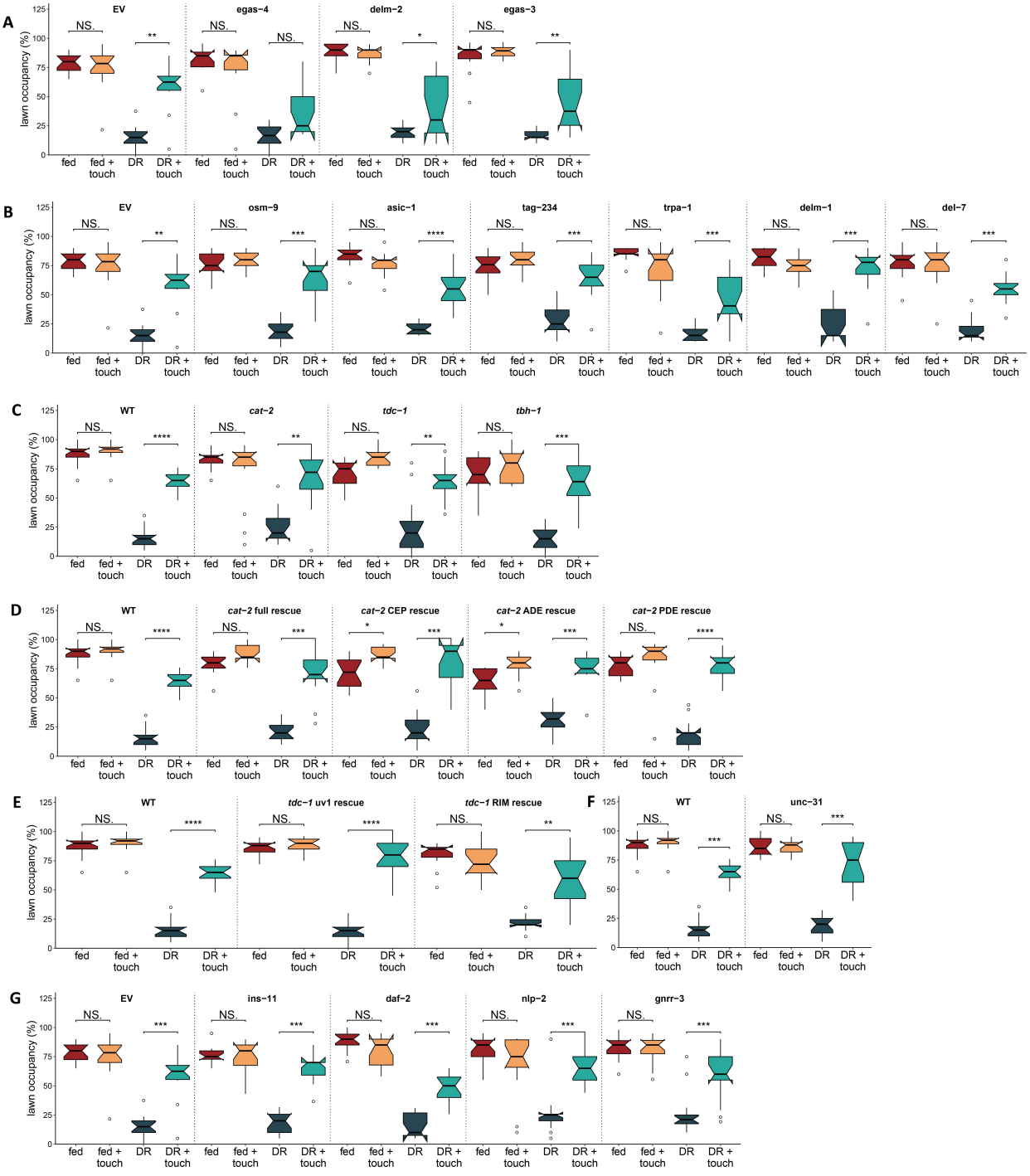
While *ins-11*/*daf-2* signaling is a possible candidate for communication from the nervous system to the intestine, *nlp-2*/GnRH and *nlp-10* signals may integrate touch information within the nervous system and/or germline. Interestingly, *nlp-2*/GnRH is highly expressed in the tyraminergic uv1 cells[295], suggesting a potential integration point between the bioamine and neuropeptide branches of this circuit. Hypothalamic GnRH release is also a direct regulator of reproductive hormones in mammals, and consequently is highly sensitive to nutrient availability[313]. A role for GnRH signaling in aging would also be consistent with the

reproductive/longevity tradeoff in which organisms can either conserve resources for maximum longevity or devote resources to maximize reproduction[314].

After identifying a role for putative mechanoreceptor proteins, the bioamines dopamine and tyramine, and the neuropeptides/neuropeptide receptors *ins-11/daf-2* and *nlp-2/gnrr-3* in touch suppression of DR-mediated longevity, we wondered whether any of these signals may affect longevity by changing the worm's behavior in response to the fake lawn. To answer this question, we measured the lawn occupancy of each of our hits on fed/DR +/- fake lawn conditions. We found that knocking down three of the nine putative mechanosensory protein hits either completely (*egas-4*) or partially (*delm-2, egas-3,* two-way ANOVA lawn occupancy ~ RNAi *condition) prevented lawn occupancy of the fake lawn (**SFig. 2.6A-B**). This result suggests that some putative mechanosensory protein knockdowns may block the effects of the fake lawn on lifespan by causing a behavioral change which reduces the amount of contact animals have with the fake lawn. However, the finding that the remaining six putative mechanosensory protein knockdowns do not change lawn occupancy indicates that some putative mechanoreceptor proteins affect lifespan through mechanisms that are at least partially distinct from mechanosensory driven behaviors.

Aside from the putative mechanoreceptor protein hits, very few signals involved in touch suppression of DR-mediated longevity had any effect on lawn occupancy behavior. Among our bioamine signaling hits, knocking down dopamine and tyramine signaling did not change occupancy of the fake lawn on DR conditions. However, the *cat-2* and *tdc-1* knockout strains did exhibit a trend towards lower occupancy of the normal fed lawn relative to WT worms (**SFig. 2.6C**). Interestingly, rescuing dopamine synthesis in either the CEP or the ADE neurons increased lawn occupancy on fed + fake lawn conditions back to the level of the WT control,

suggesting that dopamine signaling in these neurons may contribute to behaviors driven by lawn texture (**SFig. 2.6D**). However, the neuron specific rescues of *tdc-1* in either RIM or uv1 cells had no effect on lawn occupancy (**SFig. 2.6E**). Finally, lawn occupancy was unaffected by blocking dense core vesicle packaging (**SFig. 2.6F**) or by knocking down the top neuropeptide hits, *ins-11, daf-2, nlp-2,* or *gnrr-3* (**SFig. 2.6G**). Together, these results indicate that putative mechanoreceptor proteins and dopamine signaling may play a role in both behavioral and longevity responses to the fake lawn, but that these circuits diverge at the level of tyramine and neuropeptide signaling.



Supplemental Figure 2.6 Some signals involved in touch attenuation of DR-mediated longevity also modify lawn occupancy behavior. (**A-B**) Lawn occupancy of MAH677 *(sid-1; rgef-1p::sid-1)* worms on fed/DR +/- touch conditions after two generations on empty vector (EV) or *egas-4, osm-9, asic-1, tag-234, trpa-1, delm-1, delm-2, del-7,* or *egas-3* RNAi. $N \geq 45$ worms/condition. (**C**) Lawn occupancy of WT, *cat-2 (n4547), tdc-1 (n3419),* and *tbh-1(n3247)* worms on fed/DR +/- touch conditions. $N \geq 45$ worms/condition. (**D**) Lawn occupancy of WT, *cat-2 (n4547); [cat-1p::CAT-2]), cat-2 (n4547); [swip-10p::CAT-2], cat-2 (n4547); [tax-2p::CAT-2],* and *cat-2 (n4547); [trpa-1p::CAT-2]* worms on fed/DR +/- touch conditions. $N \geq 45$ worms/condition. (**E**) Lawn occupancy of WT, *tdc-1(n3419); Ex[gcy-13p::tdc-1,* and *tdc-1(n3419); Ex[ocr-4p::tdc-1]* worms on fed/DR +/- touch conditions. $N \geq$

45 worms/condition. (**F**) Lawn occupancy of WT, and *unc-31(e169)* worms on fed/DR +/- touch conditions. $N \geq 45$ worms/condition. (**G**) Lawn occupancy of TU3311 *(unc-119::sid-1)* worms on fed/DR +/- touch conditions after two generations on empty vector (EV) or *ins-11, daf-2, nlp-2,* or *gnrr-3* RNAi. $N \geq 45$ worms/condition. The center line on all box plots displays the median, and the boundaries of the box represent the interquartile range. Boxplot statistics are Wilcoxon rank sum test with Bonferroni p-adjustment, two-sided, unpaired. In all panels, NS. = $p > 0.05$, **** = $p < .0001$.

2.7 Discussion

Taken together, our data support a model in which touch activates multiple putative mechanoreceptor proteins that modulate signaling from dopaminergic neurons and tyraminergic uv1 cells. These bioamines then modify neuroendocrine signaling through NLP-2/GnRH, NLP-10, and INS-11. Ultimately, this food-touch circuit decreases intestinal *fmo-2* induction and longevity under DR conditions (**Fig. 2.5M**). While we found that each component of this model is required for the DR-touch circuit, the order and tissue-specificity of these signals remains unclear. For example, it is possible that the key mechanoreceptor protein-expressing neurons signal to downstream bioaminergic neurons, or that the dopaminergic and mechanoreceptor protein-expressing CEP neurons fill both of these roles. This role for dopaminergic neuron(s) like the CEP as a key mechanosensory cell and as a bioamine signaling in this pathway would be consistent with previous work on touch-mediated behavioral circuits[315,316]. Moreover, there could be crosstalk between multiple putative mechanoreceptor protein-expressing within this circuit.

Another key limitation of this work is the absence of data demonstrating that the putative mechanoreceptor proteins required for this circuit are directly activated by changes in stretch or surface tension from encountering the fake lawn. Given that some of these genes are expressed on non-canonical touch responsive neurons, it is possible that these proteins are modifying the touch mediated longevity circuit through an indirect mechanism of action. Future work should follow up on these putative mechanoreceptor proteins and the neurons they are expressed in with measurements of neuronal activity, such as calcium imaging, to test whether these channels alter signaling in response to physical stimuli.

Additionally, it remains to be determined whether the bioamines dopamine and tyramine act in series or in parallel within this pathway, and if these bioaminergic signals converge with each other and/or additional neuropeptidergic signals on a key interneuron. More work is also required to determine the epistasis and cell-specificity of dopaminergic and tyraminergic signaling in this pathway. Given the unexpected result that rescuing dopamine or tyramine in any dopaminergic or tyraminergic cell type was sufficient to rescue touch attenuation of DR-mediated longevity, it would be beneficial to generate cell-specific dopamine and tyramine knockouts. These strains could be used to determine if bioamine production from any single cell type is necessary for touch suppression of DR and would not be limited by potential cell nonautonomous effects possible in rescue strains.

Finally, INS-11/DAF-2 signaling is indicated as the neuronal to intestinal signal in our working model, but we have not confirmed that DAF-2/DAF-16 acts in the intestine within this pathway. Although there is much future work needed to completely understand this pathway, these findings support a growing literature on the role of sensory perception in healthy aging. Under dietary restriction conditions specifically, food-like smells[105,140,279] and tastes[95,206] attenuate DR-mediated longevity. In this work, we identify a role for mechanosensation in DR and connect sensory perception to known (bioamines, insulin, FMO-2) and novel (GnRH, NLP-10) longevity-modifying signals.

The finding that touch negatively impacts DR-mediated longevity raises interesting questions about the effects of non-nutritive food cues in humans. Humans often experience mechanosensory food perception in the absence of nutrient intake, such as chewing gum or consuming high volume diet foods with non-nutritive fillers. For example, 13% of packaged foods and 35% of beverages purchased in 2012 were marketed as low calorie, low fat, or low

sugar foods[207]. In particular, consumption of non-nutritive sweeteners is rising with greater than 30% of American adults consuming artificial sweeteners daily[208] as of 2017. This increase in non-nutritive food cues suggests a need for studies of food perception on the health benefits of DR in mammals.

While technically challenging, future work in this area should focus on identifying interneurons acting downstream of multiple modes of sensory perception that modulate aging. Currently, it remains unclear whether discrete environmental stimuli that regulate aging act through convergent or parallel pathways to modify lifespan. Additionally, it is notable that perception of food-like smell, taste, or touch alone is not sufficient to completely block the DR response. This suggests that either 1) different modes of food perception are integrated under fed conditions to completely suppress a DR response, or 2) metabolic changes that occur under nutrient scarcity are also accounted for when determining the magnitude of the DR-response. Examining the interplay between metabolic and sensory signals of nutrient scarcity could lead to key insights regarding the maximum effect sensory perception can have on longevity.

2.8 Materials and Methods

2.8.1 Strains and Growth Conditions

C. elegans were maintained following standard procedures[317] in 20 °C temperature-controlled incubators. Nematodes were fed *Escherichia coli* (OP50) seeded on solid nematode growth medium (NGM) plates. For maintenance and lifespans, worms were transferred gently with a platinum wire pick. A list of strains and RNAi conditions used in this study can be found in **Tables 2.1 and 2.2,** respectively. All genotypes were confirmed using PCR and all RNAi imaging hits were sequence-validated before use in lifespans.

Table 2.1, RNAi

RNAi	Figure	Library
pezo-1	2D (mechanoreceptor screen)	Vidal
tmc-2	2D (mechanoreceptor screen)	Vidal
mec-10	2D (mechanoreceptor screen)	Ahringer
mec-4	2D (mechanoreceptor screen)	Ahringer
deg-1	2D (mechanoreceptor screen)	Ahringer
del-1	2D (mechanoreceptor screen)	Ahringer
unc-8	2D (mechanoreceptor screen)	Ahringer
unc-105	2D (mechanoreceptor screen)	Ahringer
flr-1	2D (mechanoreceptor screen)	Ahringer
asic-1	2D (mechanoreceptor screen)	Ahringer
F26A3.6	2D (mechanoreceptor screen)	Ahringer
T28F2.7	2D (mechanoreceptor screen)	Ahringer
F23B2.3	2D (mechanoreceptor screen)	Ahringer
C24G7.1	2D (mechanoreceptor screen)	Ahringer
C24G7.2	2D (mechanoreceptor screen)	Ahringer
C24G7.4	2D (mechanoreceptor screen)	Ahringer
tag-324	2D (mechanoreceptor screen)	Vidal
C27C12.5	2D (mechanoreceptor screen)	Ahringer
T28D9.7	2D (mechanoreceptor screen)	Ahringer
C18B2.6	2D (mechanoreceptor screen)	Ahringer
C46A5.2	2D (mechanoreceptor screen)	Ahringer
Y69H2.11	2D (mechanoreceptor screen)	Ahringer
Y69H2.2	2D (mechanoreceptor screen)	Ahringer
Y69H2.13	2D (mechanoreceptor screen)	Ahringer
F55G1.12	2D (mechanoreceptor screen)	Ahringer
T28B8.5	2D (mechanoreceptor screen)	Ahringer
asic-2	2D (mechanoreceptor screen)	Ahringer
tag-263	2D (mechanoreceptor screen)	Ahringer
C11E4.4	2D (mechanoreceptor screen)	Ahringer
F25D1.4	2D (mechanoreceptor screen)	Ahringer
trp-1	2D (mechanoreceptor screen)	Ahringer
trp-2	2D (mechanoreceptor screen)	Vidal
spe-41	2D (mechanoreceptor screen)	Ahringer
osm-9	2D (mechanoreceptor screen)	Ahringer
ocr-1	2D (mechanoreceptor screen)	Ahringer
ocr-2	2D (mechanoreceptor screen)	Ahringer
ocr-4	2D (mechanoreceptor screen)	Vidal
trpa-1	2D (mechanoreceptor screen)	Ahringer
trpa-2	2D (mechanoreceptor screen)	Ahringer
gtl-1	2D (mechanoreceptor screen)	Ahringer
gtl-2	2D (mechanoreceptor screen)	Ahringer
gon-2	2D (mechanoreceptor screen)	Ahringer

Y38C1AB.2/6	2D (mechanoreceptor screen)	Vidal
lov-1	2D (mechanoreceptor screen)	Ahringer
pkd-2	2D (mechanoreceptor screen)	Vidal
cup-5	2D (mechanoreceptor screen)	Ahringer
pqn-66	2D (mechanoreceptor screen)	Ahringer
ced-11	2D (mechanoreceptor screen)	Vidal
F56F11.5	2D (mechanoreceptor screen)	Ahringer
W03B1.2	2D (mechanoreceptor screen)	Ahringer
T05A6.5	5D (neurosignaling screen)	Ahringer
lat-1a&b	5D (neurosignaling screen)	Ahringer
nlp-11	5D (neurosignaling screen)	Ahringer
flp-13	5D (neurosignaling screen)	Ahringer
nlp-30	5D (neurosignaling screen)	Ahringer
unc-49	5D (neurosignaling screen)	Ahringer
lgc-37	5D (neurosignaling screen)	Ahringer
ins-37	5D (neurosignaling screen)	Ahringer
ins-18	5D (neurosignaling screen)	Ahringer
nlp-12	5D (neurosignaling screen)	Ahringer
unc-38	5D (neurosignaling screen)	Ahringer
acr-11	5D (neurosignaling screen)	Ahringer
ser-3	5D (neurosignaling screen)	Ahringer
ckr-1	5D (neurosignaling screen)	Ahringer
nmur-4	5D (neurosignaling screen)	Ahringer
cup-4	5D (neurosignaling screen)	Ahringer
flp-23	5D (neurosignaling screen)	Ahringer
flp-24	5D (neurosignaling screen)	Ahringer
gar-2	5D (neurosignaling screen)	Ahringer
npr-14	5D (neurosignaling screen)	Ahringer
ins-24	5D (neurosignaling screen)	Ahringer
ins-6	5D (neurosignaling screen)	Ahringer
exp-1	5D (neurosignaling screen)	Ahringer
glc-4	5D (neurosignaling screen)	Ahringer
acr-7	5D (neurosignaling screen)	Ahringer
F14D2.6	5D (neurosignaling screen)	Ahringer
ins-32	5D (neurosignaling screen)	Ahringer
lat-2	5D (neurosignaling screen)	Ahringer
unc-13	5D (neurosignaling screen)	Ahringer
acy-1	5D (neurosignaling screen)	Ahringer
npr-19	5D (neurosignaling screen)	Ahringer
nlp-26	5D (neurosignaling screen)	Ahringer
tkr-1	5D (neurosignaling screen)	Ahringer
ins-23	5D (neurosignaling screen)	Ahringer
flp-4	5D (neurosignaling screen)	Ahringer
nlp-5	5D (neurosignaling screen)	Ahringer

npr-20	5D (neurosignaling screen)	Ahringer
nlp-16	5D (neurosignaling screen)	Ahringer
ggr-1	5D (neurosignaling screen)	Ahringer
npr-27	5D (neurosignaling screen)	Ahringer
ins-17	5D (neurosignaling screen)	Ahringer
Y54E2A.1	5D (neurosignaling screen)	Ahringer
glr-4	5D (neurosignaling screen)	Ahringer
T05A6.4	5D (neurosignaling screen)	Ahringer
nlp-29	5D (neurosignaling screen)	Ahringer
npr-15	5D (neurosignaling screen)	Ahringer
ZK1307.7	5D (neurosignaling screen)	Ahringer
ins-30	5D (neurosignaling screen)	Ahringer
npr-29	5D (neurosignaling screen)	Ahringer
npr-31	5D (neurosignaling screen)	Ahringer
hpa-2	5D (neurosignaling screen)	Ahringer
seb-2	5D (neurosignaling screen)	Ahringer
nmr-1	5D (neurosignaling screen)	Ahringer
frpr-4	5D (neurosignaling screen)	Ahringer
ins-11	5D (neurosignaling screen)	Ahringer
lgc-34	5D (neurosignaling screen)	Ahringer
frpr-14	5D (neurosignaling screen)	Ahringer
F58E1.4	5D (neurosignaling screen)	Ahringer
F54G8.1	5D (neurosignaling screen)	Ahringer
T11F1.2	5D (neurosignaling screen)	Ahringer
T11F1.6	5D (neurosignaling screen)	Ahringer
acy-2	5D (neurosignaling screen)	Ahringer
ins-21	5D (neurosignaling screen)	Ahringer
ins-22	5D (neurosignaling screen)	Ahringer
C04G2.11	5D (neurosignaling screen)	Ahringer
lev-1	5D (neurosignaling screen)	Ahringer
dop-1	5D (neurosignaling screen)	Ahringer
npr-8a&b	5D (neurosignaling screen)	Ahringer
B0034.5	5D (neurosignaling screen)	Ahringer
acc-3	5D (neurosignaling screen)	Ahringer
F45C12.1	5D (neurosignaling screen)	Ahringer
F45C12.16	5D (neurosignaling screen)	Ahringer
frpr-7	5D (neurosignaling screen)	Ahringer
sprr-1	5D (neurosignaling screen)	Ahringer
acr-3	5D (neurosignaling screen)	Ahringer
lgc-11 (acr-22)	5D (neurosignaling screen)	Ahringer
flp-5	5D (neurosignaling screen)	Ahringer
nlp-7	5D (neurosignaling screen)	Ahringer
gnrr-4a-c	5D (neurosignaling screen)	Ahringer

npr-6	5D (neurosignaling screen)	Ahringer
egl-6a&b	5D (neurosignaling screen)	Ahringer
nmur-1	5D (neurosignaling screen)	Ahringer
nmur-2	5D (neurosignaling screen)	Ahringer
ntr-1	5D (neurosignaling screen)	Ahringer
nlp-27	5D (neurosignaling screen)	Ahringer
lgc-48	5D (neurosignaling screen)	Ahringer
K04F1.13	5D (neurosignaling screen)	Ahringer
flp-21	5D (neurosignaling screen)	Ahringer
npr-2	5D (neurosignaling screen)	Ahringer
npr-3	5D (neurosignaling screen)	Ahringer
flp-10	5D (neurosignaling screen)	Ahringer
Y37A1B.8	5D (neurosignaling screen)	Ahringer
lgc-39	5D (neurosignaling screen)	Ahringer
C49A9.7	5D (neurosignaling screen)	Ahringer
C50F7.1	5D (neurosignaling screen)	Ahringer
ckr-2a	5D (neurosignaling screen)	Ahringer
ins-35	5D (neurosignaling screen)	Ahringer
acr-17	5D (neurosignaling screen)	Ahringer
gar-1 (acm-1)	5D (neurosignaling screen)	Ahringer
F38A5.11	5D (neurosignaling screen)	Ahringer
nlp-32	5D (neurosignaling screen)	Ahringer
npr-26	5D (neurosignaling screen)	Ahringer
octr-1	5D (neurosignaling screen)	Ahringer
nlp-33	5D (neurosignaling screen)	Ahringer
C17H11.1	5D (neurosignaling screen)	Ahringer
R03G5.3	5D (neurosignaling screen)	Ahringer
K03H6.5	5D (neurosignaling screen)	Ahringer
dop-4	5D (neurosignaling screen)	Ahringer
nlp-3	5D (neurosignaling screen)	Ahringer
H25K10.6	5D (neurosignaling screen)	Ahringer
pdfr-1a-c	5D (neurosignaling screen)	Ahringer
tkr-3a&b	5D (neurosignaling screen)	Ahringer
flp-8	5D (neurosignaling screen)	Ahringer
ZC482.4	5D (neurosignaling screen)	Ahringer
nlp-25	5D (neurosignaling screen)	Ahringer
flp-9	5D (neurosignaling screen)	Ahringer
nlp-17	5D (neurosignaling screen)	Ahringer
lgc-54	5D (neurosignaling screen)	Ahringer
F35H10.10	5D (neurosignaling screen)	Ahringer
gnrr-5	5D (neurosignaling screen)	Ahringer
C24B5.1	5D (neurosignaling screen)	Ahringer
D1014.2	5D (neurosignaling screen)	Ahringer
acr-23	5D (neurosignaling screen)	Ahringer

F15E11.4	5D (neurosignaling screen)	Ahringer
F15E11.5	5D (neurosignaling screen)	Ahringer
F57A8.4	5D (neurosignaling screen)	Ahringer
F59D6.4	5D (neurosignaling screen)	Ahringer
F59D6.6	5D (neurosignaling screen)	Ahringer
K12D9.12	5D (neurosignaling screen)	Ahringer
ser-1	5D (neurosignaling screen)	Ahringer
frpr-8	5D (neurosignaling screen)	Ahringer
hpa-1	5D (neurosignaling screen)	Ahringer
K04F1.10	5D (neurosignaling screen)	Ahringer
K04F1.11	5D (neurosignaling screen)	Ahringer
K04F1.14	5D (neurosignaling screen)	Ahringer
lgc-40	5D (neurosignaling screen)	Ahringer
nlp-36	5D (neurosignaling screen)	Ahringer
tyra-3	5D (neurosignaling screen)	Ahringer
npr-9	5D (neurosignaling screen)	Ahringer
gnrr-7	5D (neurosignaling screen)	Ahringer
npr-4	5D (neurosignaling screen)	Ahringer
npr-32	5D (neurosignaling screen)	Ahringer
ins-7	5D (neurosignaling screen)	Ahringer
ins-2	5D (neurosignaling screen)	Ahringer
frpr-1	5D (neurosignaling screen)	Ahringer
dmsr-1a&b	5D (neurosignaling screen)	Ahringer
F11A5.7	5D (neurosignaling screen)	Ahringer
npr-33	5D (neurosignaling screen)	Ahringer
acr-2	5D (neurosignaling screen)	Ahringer
nlp-14	5D (neurosignaling screen)	Ahringer
npr-7	5D (neurosignaling screen)	Ahringer
gnrr-2a&b	5D (neurosignaling screen)	Ahringer
acc-2	5D (neurosignaling screen)	Ahringer
lgc-32	5D (neurosignaling screen)	Ahringer
mgl-1	5D (neurosignaling screen)	Ahringer
glr-7	5D (neurosignaling screen)	Ahringer
lgc-41	5D (neurosignaling screen)	Ahringer
nmur-3a&b	5D (neurosignaling screen)	Ahringer
gnrr-6	5D (neurosignaling screen)	Ahringer
npr-25	5D (neurosignaling screen)	Ahringer
frpr-5a&b	5D (neurosignaling screen)	Ahringer
T01C3.5	5D (neurosignaling screen)	Ahringer
T26E4.1	5D (neurosignaling screen)	Ahringer
Y70C5C.3	5D (neurosignaling screen)	Ahringer
ZK1037.1	5D (neurosignaling screen)	Ahringer
nlp-20	5D (neurosignaling screen)	Ahringer
lgc-49	5D (neurosignaling screen)	Ahringer

C31E10.3	5D (neurosignaling screen)	Ahringer
F59D12.1	5D (neurosignaling screen)	Ahringer
npr-21	5D (neurosignaling screen)	Ahringer
gnrr-3	5D (neurosignaling screen)	Ahringer
nlp-1	5D (neurosignaling screen)	Ahringer
glc-1	5D (neurosignaling screen)	Ahringer
flp-12	5D (neurosignaling screen)	Ahringer
ggr-2	5D (neurosignaling screen)	Ahringer
npr-28	5D (neurosignaling screen)	Ahringer
sprr-2	5D (neurosignaling screen)	Ahringer
seb-3	5D (neurosignaling screen)	Ahringer
nlp-2	5D (neurosignaling screen)	Ahringer
frpr-18a&b	5D (neurosignaling screen)	Ahringer
Y70D2A.1	5D (neurosignaling screen)	Ahringer
eat-2	5D (neurosignaling screen)	Ahringer
acr-20	5D (neurosignaling screen)	Ahringer
T10E10.3	5D (neurosignaling screen)	Ahringer
ins-5	5D (neurosignaling screen)	Ahringer
F58E1.7	5D (neurosignaling screen)	Ahringer
hlh-30	5D (neurosignaling screen)	Ahringer
ins-39	5D (neurosignaling screen)	Ahringer
nlp-44	5D (neurosignaling screen)	Ahringer
nlp-45	5D (neurosignaling screen)	Ahringer
nlp-47	5D (neurosignaling screen)	Ahringer
nlp-49	5D (neurosignaling screen)	Ahringer
nlp-50	5D (neurosignaling screen)	Ahringer
nlp-51	5D (neurosignaling screen)	Ahringer
nlp-52	5D (neurosignaling screen)	Ahringer
nlp-53	5D (neurosignaling screen)	Ahringer
nlp-55	5D (neurosignaling screen)	Ahringer
nlp-57	5D (neurosignaling screen)	Ahringer
nlp-60	5D (neurosignaling screen)	Ahringer
nlp-61	5D (neurosignaling screen)	Ahringer
nlp-62	5D (neurosignaling screen)	Ahringer
nlp-65	5D (neurosignaling screen)	Ahringer
nlp-67	5D (neurosignaling screen)	Ahringer
nlp-68	5D (neurosignaling screen)	Ahringer
nlp-73	5D (neurosignaling screen)	Ahringer
nlp-74	5D (neurosignaling screen)	Ahringer
nlp-77	5D (neurosignaling screen)	Ahringer
nlp-80	5D (neurosignaling screen)	Ahringer
flp-27	5D (neurosignaling screen)	Ahringer
frpr-2	5D (neurosignaling screen)	Ahringer
glr-3	5D (neurosignaling screen)	Ahringer

nlp-8	5D (neurosignaling screen)	Ahringer
nlp-4	5D (neurosignaling screen)	Ahringer
nlp-15	5D (neurosignaling screen)	Ahringer
ser-5	5D (neurosignaling screen)	Ahringer
flp-22	5D (neurosignaling screen)	Ahringer
acr-19	5D (neurosignaling screen)	Ahringer
unc-29	5D (neurosignaling screen)	Ahringer
mgl-2	5D (neurosignaling screen)	Ahringer
glc-2 (avm-2)	5D (neurosignaling screen)	Ahringer
avr-14 (gbr-2)	5D (neurosignaling screen)	Ahringer
acr-5	5D (neurosignaling screen)	Ahringer
lgc-38	5D (neurosignaling screen)	Ahringer
lgc-50	5D (neurosignaling screen)	Ahringer
glr-2	5D (neurosignaling screen)	Ahringer
acr-21	5D (neurosignaling screen)	Ahringer
gbb-2	5D (neurosignaling screen)	Ahringer
acr-14	5D (neurosignaling screen)	Ahringer
flp-15	5D (neurosignaling screen)	Ahringer
nlp-21	5D (neurosignaling screen)	Ahringer
flp-14	5D (neurosignaling screen)	Ahringer
gab-1	5D (neurosignaling screen)	Ahringer
lgc-45	5D (neurosignaling screen)	Ahringer
avr-15	5D (neurosignaling screen)	Ahringer
ser-7	5D (neurosignaling screen)	Ahringer
frpr-15	5D (neurosignaling screen)	Ahringer
acr-18	5D (neurosignaling screen)	Ahringer
nlp-24	5D (neurosignaling screen)	Ahringer
deg-3	5D (neurosignaling screen)	Ahringer
acr-4	5D (neurosignaling screen)	Ahringer
lgc-44	5D (neurosignaling screen)	Ahringer
frpr-3	5D (neurosignaling screen)	Ahringer
glr-5	5D (neurosignaling screen)	Ahringer
flp-17	5D (neurosignaling screen)	Ahringer
nlp-28	5D (neurosignaling screen)	Ahringer
acc-1	5D (neurosignaling screen)	Ahringer
flp-1	5D (neurosignaling screen)	Ahringer
nlp-31	5D (neurosignaling screen)	Ahringer
npr-1	5D (neurosignaling screen)	Ahringer
lgc-31	5D (neurosignaling screen)	Ahringer
npr-16a&b	5D (neurosignaling screen)	Ahringer
flp-7	5D (neurosignaling screen)	Ahringer
glr-8	5D (neurosignaling screen)	Ahringer
flp-2	5D (neurosignaling screen)	Ahringer
flp-3	5D (neurosignaling screen)	Ahringer

lgc-47	5D (neurosignaling screen)	Ahringer
npr-18a-g	5D (neurosignaling screen)	Ahringer
npr-10a&b	5D (neurosignaling screen)	Ahringer
acr-9	5D (neurosignaling screen)	Ahringer
acr-12	5D (neurosignaling screen)	Ahringer
nlp-6	5D (neurosignaling screen)	Ahringer
npr-24	5D (neurosignaling screen)	Ahringer
M03F8.6	5D (neurosignaling screen)	Ahringer
snet-1	5D (neurosignaling screen)	Ahringer
nlp-13	5D (neurosignaling screen)	Ahringer
nlp-9	5D (neurosignaling screen)	Ahringer
acr-16	5D (neurosignaling screen)	Ahringer
flp-6	5D (neurosignaling screen)	Ahringer
gar-3	5D (neurosignaling screen)	Ahringer
glr-1	5D (neurosignaling screen)	Ahringer
nlp-42	5D (neurosignaling screen)	Ahringer
nlp-10	5D (neurosignaling screen)	Ahringer
nlp-40	5D (neurosignaling screen)	Ahringer
nlp-18	5D (neurosignaling screen)	Ahringer
npr-42	5D (neurosignaling screen)	Ahringer
ins-31 a	5D (neurosignaling screen)	Ahringer
acr-15	5D (neurosignaling screen)	Ahringer
flp-19	5D (neurosignaling screen)	Ahringer
flp-28	5D (neurosignaling screen)	Ahringer
flp-20	5D (neurosignaling screen)	Ahringer
npr-5	5D (neurosignaling screen)	Ahringer
flp-25	5D (neurosignaling screen)	Ahringer
daf-2	5D (neurosignaling screen)	ordered from BioSource
npr-35	5D (neurosignaling screen)	Ahringer
npr-37	5D (neurosignaling screen)	Ahringer
npr-43	5D (neurosignaling screen)	Ahringer
flp-16	5D (neurosignaling screen)	Ahringer
tph-1	S3A	Ahringer
egl-3	S5A	Vidal
egl-21	S5A	Vidal

Table 2.1 RNAi used in this work.

Table 2.2, Strains

Strain Description	Strain	Identifier	Outcross
WT	wild-type	N2	≥4
fmo-2p::mCherry	*[(pCF150) (fmo-2p::mCherry + H2B::GFP) + Cbr-unc-119(+)] II*	LZR01	≥4

fmo-2 ubiquitous overexpressor	*seaSi39 [(pCFJ448) (eft-3p::fmo-2 + H2B::GFP) + Cbr-unc-119(+)] I.*	KAE9	≥4
fmo-2p::mCherry; MAH677 neuronal only RNAi uptake	*sqIs71 [rgef-1p::GFP + rgef-1p::sid-1]*	LZR250	≥4
MAH677 neuronal only RNAi uptake	*[(pCF150) (fmo-2p::mCherry + H2B::GFP) + Cbr-unc-119(+)] II; sqIs71 [rgef-1p::GFP + rgef-1p::sid-1]*	MAH677	≥4
fmo-2p::mCherry; cat-2 (n4547)	*[(pCF150) (fmo-2p::mCherry + H2B::GFP) + Cbr-unc-119(+)] II; cat-2 (n4547)*	LZR206	≥4
fmo-2p::mCherry; tdc-1 (n3419)	*[(pCF150) (fmo-2p::mCherry + H2B::GFP) + Cbr-unc-119(+)] II; tdc-1 (n3419)*	LZR251	≥4
fmo-2p::mCherry; tbh-1(n3247)	*[(pCF150) (fmo-2p::mCherry + H2B::GFP) + Cbr-unc-119(+)] II; tbh-1(n3247)*	LZR252	≥4
fmo-2p::mCherry; unc-17 (e113)	*[(pCF150) (fmo-2p::mCherry + H2B::GFP) + Cbr-unc-119(+)] II; unc-17 (e113)*	CB113	≥4
fmo-2p::mCherry; unc-25(e156)	*[(pCF150) (fmo-2p::mCherry + H2B::GFP) + Cbr-unc-119(+)] II; unc-25(e156)*	CB156	≥4
fmo-2p::mCherry; eat-4(ky5)	*[(pCF150) (fmo-2p::mCherry + H2B::GFP) + Cbr-unc-119(+)] II; eat-4(ky5)*	MT6308	≥4
cat-2 (n4547)	*cat-2 (n4547)*	MT15620	≥4
tdc-1 (n3419)	*tdc-1 (n3419)*	MT13113	≥4
tbh-1(n3247)	*tbh-1(n3247)*	MT9455	≥4
cat-2(-) + CEP,PDE,ADE rescue	*cat-2 (n4547); [cat-1p::CAT-2]*	LZR240	≥4
cat-2(-) + CEP rescue	*cat-2 (n4547); [swip-10p::CAT-2]*	LZR244	≥4
cat-2(-) + ADE rescue	*cat-2 (n4547); [tax-2p::CAT-2]*	LZR237	≥4
cat-2(-) + PDE rescue	*cat-2 (n4547); [trpa-1p::CAT-2]*	LZR242	≥4
fmo-2p::mCherry; cat-2(-) + CEP,PDE,ADE rescue	*[(pCF150) (fmo-2p::mCherry + H2B::GFP) + Cbr-unc-119(+)] II; cat-2 (n4547); [cat-1p::CAT-2]*	LZR213	≥4
fmo-2p::mCherry; cat-2(-) + CEP rescue	*[(pCF150) (fmo-2p::mCherry + H2B::GFP) + Cbr-unc-119(+)] II; cat-2 (n4547); [swip-10p::CAT-2]*	LZR210	≥4
fmo-2p::mCherry; cat-2(-) + ADE rescue	*[(pCF150) (fmo-2p::mCherry + H2B::GFP) + Cbr-unc-119(+)] II; cat-2 (n4547); [tax-2p::CAT-2]*	LZR212	≥4

fmo-2p::mCherry; cat-2(-) + PDE rescue	*[(pCF150) (fmo-2p::mCherry + H2B::GFP) + Cbr-unc-119(+)] II; cat-2 (n4547); [trpa-1p::CAT-2]*	LZR211	≥4
TU3311; fmo-2p::mCherry	*[(pCF150) (fmo-2p::mCherry + H2B::GFP) + Cbr-unc-119(+)] II; uIs60 [unc-119p::YFP + unc-119p::sid-1]*	LZR45	≥4
TU3311	*uIs60 [unc-119p::YFP + unc-119p::sid-1]*	TU3311	≥4
fmo-2p::mCherry; daf-16 (mu86)	*[(pCF150) (fmo-2p::mCherry + H2B::GFP) + Cbr-unc-119(+)] II; daf-16(mu86)*	LZR258	≥4
tdc-1(-) + RIM rescue	*tdc-1(n3419); Ex[gcy-13p::tdc-1]*	LZR259	≥4
tdc-1(-) + uv1 rescue	*tdc-1(n3419); Ex[ocr-4p::tdc-1]*	LZR260	≥4
fmo-2p::mCherry; tdc-1(-) + RIML rescue	*[(pCF150) (fmo-2p::mCherry + H2B::GFP) + Cbr-unc-119(+)] II; tdc-1(n3419); Ex[gcy-13p::tdc-1]*	LZR261	≥4
fmo-2p::mCherry; tdc-1(-) + uv1 rescue	*[(pCF150) (fmo-2p::mCherry + H2B::GFP) + Cbr-unc-119(+)] II; tdc-1(n3419); Ex[ocr-4p::tdc-1]*	LZR262	≥4
unc-31	*unc-31(e169)*	CB169	≥4
unc-31; fmo-2p::mCherry	*unc-31(e169); [(pCF150) (fmo-2p::mCherry + H2B::GFP) + Cbr-unc-119(+)] II*	LZR263	≥4

Table 2.2 Strains used in this work.

2.8.2 tdc-1 Rescue Constructs

Plasmid construction and microinjection was conducted by Suny Biotech to generate both *tdc-1* rescue constructs. In designing the plasmids, we used the *ocr-4* promoter to drive cDNA of TDC-1::SL2::GFP in the uv1 neuroendocrine cells. To express cDNA of TDC-1::SL2::GFP in the RIM neuron, we used the *gcy-13* promoter. All plasmids were verified via restriction digest and sanger sequencing, and ApE files are available upon request. Plasmids were microinjected by Suny Biotech using the co-injection marker *myo-2*p::GFP and 3 transgenic lines were tested in each experiment.

2.8.3 Fake Lawn Preparation

G-200 Sephadex beads (Sigma G5050) were suspended S-basal buffer at a concentration of 30mg/ml and autoclaved for 45 minutes. For fed + touch plates, OP50 bacteria was grown overnight to an optical density (OD_{600}) of 3.0, then pelleted at 3000 *rcf* for 20 minutes. The supernatant was discarded and replaced with the Sephadex in S-basal, then the mixture was vortexed until the pellet was dissolved. 200 µL was seeded onto the center of a 60 mm diameter NGM plate. For DR + touch conditions, autoclaved Sephadex in S-basal was added directly to the center of the NGM plate (overnight imaging experiments) or the autoclaved Sephadex in S-basal was used to resuspend a pellet from a diluted concentration of bacteria (DR lifespan experiments). For fed controls and DR lifespan controls, the bacterial pellet was resuspended in S-basal instead of S-basal + Sephadex. For DR imaging controls, 200 µL autoclaved S-basal was added directly to the plate.

2.8.4 RNAi Knockdown

The RNAi feeding bacteria were grown from the Ahringer and Vidal *C. elegans* RNAi feeding libraries. All RNAi plasmids used for lifespan assays were sequenced to verify the correct target sequence. RNAi used for large screens (putative mechanoreceptor protein and neuroendocrine signaling screens) were not sequenced initially, but any hits that moved on to the validation stage were sequence-verified and qPCR validated. Animals in RNAi knockdown conditions were progeny from two generations of adults on the RNAi. RNAi bacteria was seeded on NGM plates supplemented with 1 mM β-D-isothiogalactopyranoside (IPTG) and 25 µg/mL carbenicillin. Previous work has found that the RNAi feeding bacteria (HT115 strain of *E. coli*) can alter worm lifespan relative to a diet of OP50[318,319]. These differences should be noted when comparing lifespans conducted on RNAi relative to lifespans on OP50.

2.8.5 Drug Treatments

For all experiments with supplementation of exogenous small molecules (exogenous dopamine, exogenous tyramine, amiloride, thioridazine, and mianserin), the small molecule was dissolved in solid agar plates. Each compound was added to agar once it had cooled to < 55 ˚C and before it was poured into plates. All drugs were purchased from Sigma-Aldrich and were initially dissolved in milliQ water at 2 mM (mianserin), or 100 mM concentration (thioridazine, amiloride, dopamine, and tyramine), aliquoted, and stored at -20 ˚C.

2.8.6 Lifespan Measurements

Lifespan assays were conducted as previously described[320] with the exception of the fake lawn conditions (see fake lawn preparation). In short, 10-15 gravid adults were left on NGM plates for a 3-4 hour timed egg lay and then removed. Once the progeny of these adults reached late L4/early adult stage of development, they were transferred to NGM plates with 33 µL of 150 mM fluorodeoxyuridine (FUdR) and 100 µL of 50 mg/mL Ampicillin per 100 mL NGM. The FUdR prevents development of progeny and the Ampicillin prevents bacterial growth. 60-80 worms were placed on each NGM + FUdR + AMP plate seeded with concentrated bacteria (5x for OP50 fed lifespans, 0.5x OP50 (10^9 CFU/mL) for DR lifespans), and at least two plates per strain per condition were used for each lifespan replicate. In all DR lifespans, OP50 in the fed and DR conditions was resuspended in S-media to prevent bacterial growth. In the DR and DR + touch conditions, worms were kept on 5x fed bacteria until day 2 of adulthood, when they were transferred to fresh DR or DR + touch plates every other day for four transfers. This form of DR is referred to as solid DR (sDR)[321]. Worms on fed and fed + touch conditions were transferred to fresh fed plates at the same time as each DR transfer. Animals were removed from the experiment and counted as dead when they did not move in response to a gentle touch from a platinum wire pick under a dissection microscope. Lifespans were scored at least 3 times per

week until all animals were dead. A 'fence' of 75 µL of 100 mM palmitic acid (Sigma-Aldrich) dissolved in 100% ethanol was also applied to the edge of each lifespan plate to prevent fleeing. While FUdR can extend lifespan, FUdR was used in all lifespan plates to prevent matricide under DR conditions[322]. NGM lifespans without FUdR were attempted to test the necessity of FUdR for the touch phenotype, but were not successful due to excessive matricide and fleeing under the DR conditions. Data were plotted by R version 4.3.1 and Adobe Illustrator 2022.

2.8.7 RNAi Lifespans

RNAi lifespan assays were performed like other lifespans with the exception of the initial timed egg-lay (TEL) and the food concentrations. To ensure maximum knockdown on RNAi, a first generation of worms was TEL'ed on RNAi for 3-4 hours. The progeny from this TEL were left on RNAi plates to develop into gravid adults and were then used for a second TEL on the same RNAi conditions. Progeny from the second-generation TEL were then used for the lifespan assay. RNAi bacteria (HT115) is AMP resistant and can grow slowly on AMP lifespan plates during the assay. To maintain equivalent amounts of bacterial availability over the course of the lifespan, RNAi lifespan plates are seeded with 2x concentrated bacteria for fed conditions and 0.1x concentrated bacteria for DR conditions, from a starting optical density (OD_{600}) of 3.0.

2.8.8 Slide Microscopy

Fluorescent images in this study were taken using Leica Application Suite X (LASX) software and a Leica scope with > 15 worms per treatment at ≥ 35x magnification. For representative images displayed in the figures, worms were paralyzed in 0.5 M sodium azide (NaN_3) and imaged once residual liquid evaporated and the worms clumped together. For quantification of these images and for imaging screens, the same method was used but after the residual sodium azide had evaporated, individual worms were gently pushed apart until they were no longer

touching one another. Fluorescent mean comparisons were then quantified using R code to identify individual worms and measure fluorescent intensity[323]. The mean fluorescent intensity of the background (all non-worm pixels) was subtracted from the mean fluorescence of each worm. All outputs from this R code were manually quality controlled to eliminate any non-worm objects that were misidentified. This code will be provided upon request to the corresponding author. Data were plotted by R version 4.3.1 and Adobe Illustrator 2022. The brightness of fluorescent images of clumped worms was increased to an equal degree across all images compared to one another in ImageJ bundled with 64-bit Java 1.8.0.

2.8.9 Lawn Occupancy Measurements

For lawn occupancy measurements, worms were grown to gravid adults, then washed off of NGM plates in M9 and pelleted at 1,000 *rcf* for 1 minute. At least 10 worms per plate were then pipetted onto the edge of a 35 mm diameter NGM plates seeded with 100 µL of fed, fed + touch, DR, and DR + touch media (see Fake Lawn Preparation). Five 35 mm plates were used for each condition for each replicate. Worms were left on these conditions for 24 hours, and a picture of each plate was taken using Leica Application Suite X (LASX) software and a Leica scope at 7.3x magnification at 1, 3, 6, and 24 hours after placement on conditions. For fed, fed + touch, and DR + touch conditions, the Cell Counter application on Image J was used to click on and count each worm in the lawn region and off the lawn region (FIJI Is Just ImageJ bundled with 64-bit Java 1.8.0). For DR conditions, the average area covered by a fed lawn was calculated as a circle with a diameter of 850 pixels. A circle of this size was drawn in ImageJ and placed in the center of the image of the plate. Worms within the circle were counted as “on the lawn” and worms outside of this circle, near the plate perimeter, were counted as “off the lawn”. Data were plotted by R version 4.3.1 and Adobe Illustrator 2022.

2.8.10 Chemotaxis Assays

For chemotaxis assays, unseeded NGM plates were separated into four quadrants using a marker on the bottom of the plate. A circle with a 5 mm radius was drawn in the center of the plate and within each quadrant, a dot was marked in the middle of the quadrant 5 mm from the edge of the plate rim. 5 µL of 0.5 M sodium azide was pipetted onto each of the four dots (one per quadrant). Two quadrants opposite from one another were designated as control quadrants, and 2 were designated as treatment quadrants. In the treatment quadrants, 10 µL of either 0.03 g/mL Sephadex in M9 or the supernatant of Sephadex soaked in M9 was pipetted on top of the sodium azide. In the control quadrants, 10 µL of M9 (not soaked in Sephadex) was pipetted on top of the sodium azide. Immediately after preparing the plates, gravid adults were washed off of NGM plates in M9 and pelleted at 1,000 *rcf* for 1 minute. At least 40 worms per plate were then pipetted onto the 5 mm radius circle in the center of each chemotaxis plate. After one hour, the number of worms in the control and treatment quadrants were counted under a dissection microscope. Chemotaxis Index was calculated by subtracting the number of worms on all control quadrants from the number of worms on all treatment quadrants, then dividing that by the total number of worms on the plate. Data were plotted by R version 4.3.1 and Adobe Illustrator 2022.

2.8.11 Heat Stress Assays

Worms were synchronized from eggs and grown to gravid adults, then 25 worms were transferred to three plates of fed/DR +/- touch conditions using a platinum wire pick. Worms remained on these conditions for 24 hours at 20 °C and were then transferred to fed plates at 37 °C for three hours. Animals were removed from the touch conditions before heat stress exposure because the Sephadex fake lawn could act as a thermal insulator from the heat. Worms were allowed to recover at 20 °C after heat exposure and were then scored for heat stress survival.

Worms that moved in response to gentle touch with a platinum wire pick were considered alive. Data were plotted by R version 4.3.1 and Adobe Illustrator 2022.

2.8.12 Statistical Analysis

The center line on all box plots displays the median, and the boundaries of the box represent the interquartile range. Boxplot statistics are Wilcoxon rank sum test with Bonferroni p-adjustment, two-sided, unpaired. Comparisons between more than two conditions in imaging and lawn occupancy experiments were done using ANOVA. For comparisons between two conditions, a Wilcoxon rank sum test (two-sided, unpaired) was used with a Bonferroni p-adjustment to account for three biological replicates. p values are $*p < 0.05$, $**p < 0.01$, $***p < 0.001$, and $****p<0.0001$. For lifespan assays, the statistical groupwise and pairwise comparisons across survivorship curves were performed using the survfit survival analysis package in R. *P* values comparing two survival curves were acquired using the log-rank analysis. *P* values indicating an interaction between multiple experimental variables and across >2 survival curves were performed using the survivalMPL package in R to perform a Cox regression analysis between covariates of interest. Tests done with data from multiple biological variables were adjusted with a Bonferroni p value correction. p values are $*p < 0.05$, $**p < 0.01$, $***p < 0.001$, and $****p<0.0001$. Exact *N*s for each experiment are included in the source data files and minimum *N*s for each plot are included in the figure legends.

Chapter 3 The Hypoxic Response Extends Lifespan through a Bioaminergic and Peptidergic Neural Circuit.[3]

3.1 Foreword

After exploring the cell nonautonomous signaling mechanisms through which food-like cues modify dietary restriction-mediated longevity in Chapter 2, Chapter 3 focuses on a different environmental longevity intervention—hypoxia. Foundational work leading to this project was first conducted by Dr. Scott Leiser in the lab of Dr. Matt Kaeberlein. In this study, Dr. Leiser found that both dietary restriction and hypoxia, two previously identified longevity interventions in *C. elegans*, require the intestinal enzyme FMO-2 to extend lifespan. Additionally, *fmo-2* overexpression is sufficient to improve healthspan and lifespan in *C. elegans* under fed, normoxic conditions. Some key elements of the cell nonautonomous hypoxia-mediated *fmo-2* induction pathway were also discovered in this paper, leading to a model in which hypoxia leads to hypoxia-inducible factor 1 (HIF-1) stabilization in serotonergic neurons modifies serotonin signaling and alters the activity of *ser-7*-expressing neurons to ultimately induce *fmo-2* in the intestine.

Dr. Shijiao Huang, a Research Investigator in the Leiser lab, then began a follow-up study on the hypoxia-mediated *fmo-2* induction pathway in order to identify more specific components of this circuit. When Dr. Huang left the group to start her own laboratory, I took

[3] Submitted to *Current Biology* with authors listed as **Elizabeth S. Kitto***, Shijiao Huang*, Mira Bhandari, Cassie Tian, Rebecca L. Cox, Safa Beydoun, Emily Wang, Danielle Shave, Hillary A. Miller, Sarah A. Easow, Ella Henry, Megan L. Schaller, Scott F. Leiser. * indicates co-first authorship.

over this project as co-first author. While Dr. Huang did the initial work to start this project in the lab and designed many of the transgenic *C. elegans* strains used in this study, I collected much of the data appearing in the final manuscript, put together the figures and wrote the paper. Together, this chapter identifies neurons and neuronal signals within the hypoxia-mediated longevity pathway, providing information that could help future investigations identify key neural drivers of aging rate (see Chapter 6, Future Directions).

3.2 Abstract

A coordinated response to stress is crucial for promoting the short- and long-term health of an organism. The perception of stress, frequently through the nervous system, can lead to physiological changes that are fundamental to maintaining homeostasis. Activating the response to low oxygen, or hypoxia, extends healthspan and lifespan in *C. elegans*. However, despite some positive impacts, negative effects of the hypoxic response in specific tissues prevent translation of their benefits in mammals. Thus, it is imperative to identify which components of this response promote longevity. Here, we interrogate the cell nonautonomous hypoxic response signaling pathway. We find that HIF-1-mediated signaling in ADF serotonergic neurons is both necessary and sufficient for lifespan extension. Signaling through the serotonin receptor SER-7 in the GABAergic RIS interneurons is necessary in this process. Our findings also highlight the involvement of additional neural signaling molecules, including the neurotransmitters tyramine and GABA, and the neuropeptide NLP-17, in mediating longevity effects. Finally, we demonstrate that oxygen- and carbon-dioxide-sensing neurons act downstream of HIF-1 in this circuit. Together, these insights develop a circuit for how the hypoxic response cell nonautonomously modulates aging and suggests valuable targets for modulating aging in mammals.

3.3 Introduction

The global population is aging at an unprecedented rate, posing significant challenges for healthcare systems worldwide[324]. The increasing burden of age-related diseases such as cardiovascular disease, diabetes, and neurodegeneration[4] highlights the pressing need to improve healthspan, defined as the disease-free period of life[261]. Work over the past several decades has led to a better understanding of the conserved molecular and cellular mechanisms that regulate lifespan. One promising avenue has been the identification of environmental stressors that, when applied in a controlled manner, activate stress-response pathways to promote longevity. These interventions, including calorie restriction, exercise, hypoxia, heat shock, and cold exposure, extend lifespan and healthspan[13,27,37,278]. These stress-response pathways induce hormesis, a phenomenon in which a low dose of a stressor results in adaptive beneficial effects on cellular function[29,30]. Hormesis and the underlying stress-responses that promote longevity converge on cellular pathways, including oxidative stress, insulin signaling, autophagy, and protein homeostasis[325], to promote longevity.

Multicellular organisms secrete a highly conserved set of neuromodulators including neurotransmitter and neuropeptide signals from the central nervous system. These signals integrate information about the organism's external environment and internal state, and coordinate a physiological response in peripheral tissues. Within the context of aging, bioamine neurotransmitters contribute to the activation of many well-studied stress response mechanisms that promote longevity. For example, serotonin signaling modulates the mitochondrial unfolded protein response in *C. elegans*[75], and regulates how food perception contributes to dietary restriction-mediated longevity in worms[105] and flies[112]. Dopamine also modifies the longevity benefits of dietary restriction in invertebrates[105,326], and polymorphisms in the dopamine D4 receptor are associated with longevity in humans[164]. Finally, adrenaline and its invertebrate

analog, tyramine, have been linked to changes in the aging rate in both nematodes[58,81,326,327] and mammals[51]. Hormone signals such as insulin[328-330], growth factors[159,160], and GnRH[50,326] also contribute to longevity pathways across taxa. This growing body of work has led to great interest in manipulating longevity-promoting neural circuits to improve health[31]. While significant research effort focuses on pathways like autophagy, insulin signaling, and proteostasis in the context of aging, the role of hypoxia remains relatively underexplored. Currently, no longevity-promoting agents have been reported to target the hypoxic response.

The hypoxic response is highly conserved across species[331-333], highlighting the relevance of this pathway in other organisms, including humans. In *C. elegans*, activating the hypoxic response by knocking down or mutating the E3 ubiquitin ligase von hippel-lindau-1 (VHL-1)[334] protein or stabilizing the hypoxia-inducible factor-1 (HIF-1) transcription factor[27,48] is sufficient to extend lifespan. All of these interventions—environmental hypoxia, VHL-1 knockdown, and HIF-1 stabilization—require the intestinal enzyme flavin-containing monooxygenase-2 (*fmo-2)* to extend lifespan in *C. elegans*[48]. Hypoxic conditions also extend lifespan in a short-lived progeria mouse model[335], and epidemiological studies indicate a correlation between hypoxia exposure and longevity[336,337]. However, the physiological changes induced by the hypoxic response are broad and involve adaptations such as increased vascularization, metabolic rewiring, and changes in cell survival pathways. In mammals, some of these same adaptations can be detrimental, as mutations in components of the hypoxic response have been linked to conditions like cancer and cardiovascular disease[338-341]. This presents a key challenge: while hypoxia-induced longevity in a post-mitotic invertebrate model like *C. elegans* is promising, some of the mechanisms involved may not be directly translatable to mammals without causing deleterious side effects. Therefore, a mechanistic understanding of the individual cells, neural

circuits, and pathways that mediate the beneficial but not detrimental effects of hypoxia on aging is essential to determine whether this circuit could be leveraged to improve human health.

Our previous work in *C. elegans* identified that stabilization of HIF-1 in neurons is sufficient to extend lifespan through the serotonin receptor, SER-7. This pathway eventually leads to the induction of *fmo-2*, a longevity gene expressed in the intestine[48,110]. In this study, we uncover key neural components of the hypoxic response longevity circuit. Within this circuit, we identify individual cells, signals, and receptors necessary and/or sufficient to extend lifespan downstream of the hypoxic response. More specifically, we find serotonin signaling in the ADF serotonergic neurons is both necessary and sufficient to extend lifespan through the hypoxic response. This pathway signals through the serotonin receptor SER-7 in the RIS interneuron, which is also essential for hypoxia-mediated longevity. We further demonstrate additional neurotransmitters (GABA and tyramine), and a neuropeptide (NLP-17) are critical for mediating these longevity effects. Finally, we identify that oxygen sensing neurons (URX, AQR, PQR and BAG) act downstream of neuronal HIF-1 in this circuit. Our insights into this longevity pathway provide a mechanistic understanding of how the hypoxic response delays aging and improves health.

3.4 Results

3.4.1 Serotonin signaling through the ADF neuron and the SER-7 receptor are necessary and sufficient for the hypoxic response to extend lifespan.

Induction of the hypoxic response by targeted genetic manipulations can increase lifespan in *C. elegans.* These manipulations include decreasing activity of the VHL-1 E3 ubiquitin ligase that targets the transcription factor HIF-1 for degradation under hypoxia[334] or by a mutation that stabilizes HIF-1 (HIF-1^{P621A})[27,48] (**Fig. 3.1A**). We previously found that stabilizing HIF-1 in

serotonergic neurons is sufficient to extend lifespan[48]. To determine which serotonergic neurons initiate HIF-1-mediated longevity, we generated strains with a nondegradable HIF-1 variant (HIF-1^{P621A})[48,342] expressed under promoters specific to each of *C. elegans'* three primary serotonergic neuron types—the ADF, NSM, and HSN neurons[343]. These transgenic worms were then crossed into the *hif-1* null background to ensure that HIF stabilization in one neuron type could not feedback to modify HIF-1 activity in other cells. When we measured the lifespan of each strain relative to WT and *hif-1* knockout controls, we observed that stabilizing HIF-1 in the ADF or NSM neurons significantly extended lifespan by 26% and 23%, respectively (**Fig. 3.1B-C**). HIF-1 stabilization in the HSN neurons had a smaller effect but significantly extended lifespan by 9% (**Fig. 3.1D**). This result indicates that modifying signaling in any serotonergic neuron is sufficient to induce some level of hypoxic response-mediated longevity. These data suggest that serotonergic neurons can partially substitute for each other to promote longevity in this pathway. In summary, the ADF and/or NSM serotonergic neurons play an essential role in hypoxic response-mediated longevity.

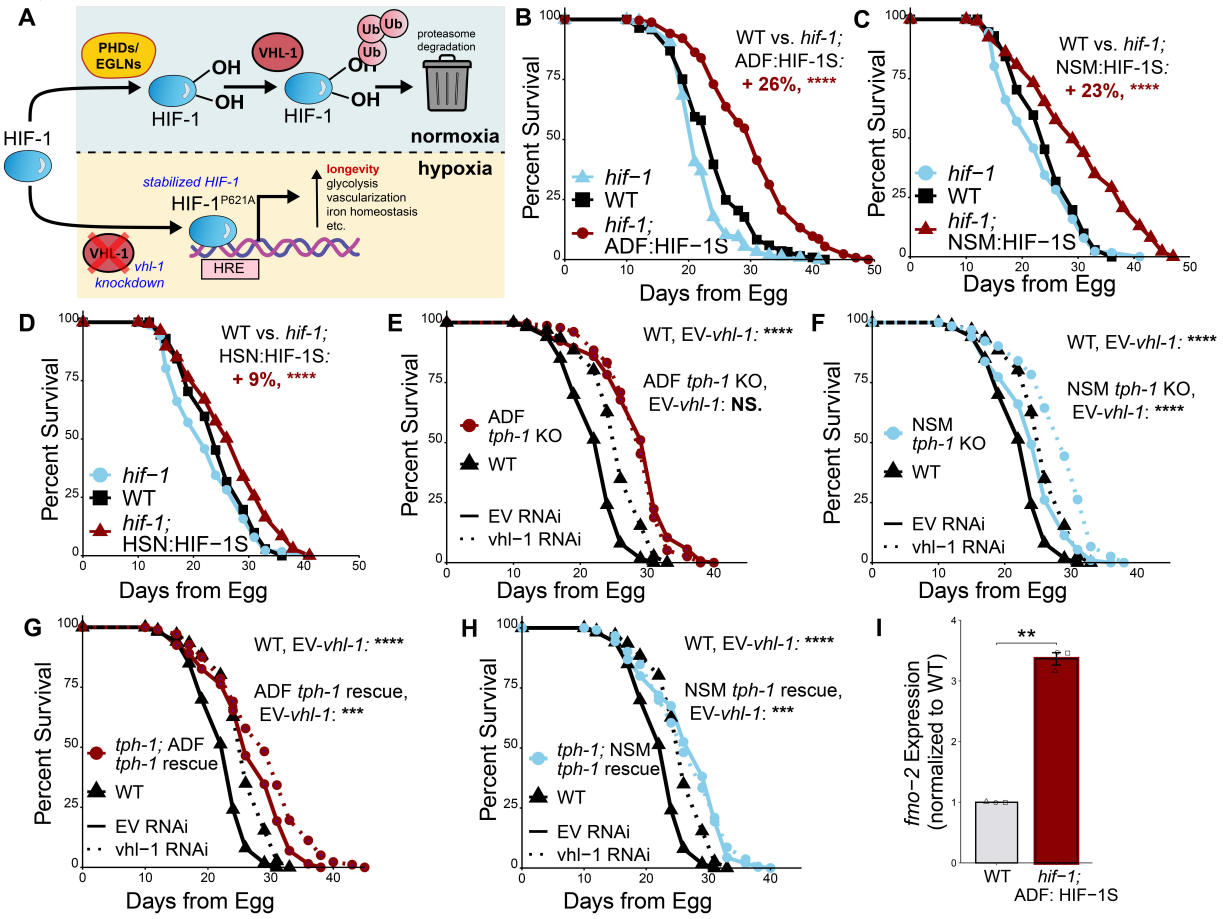
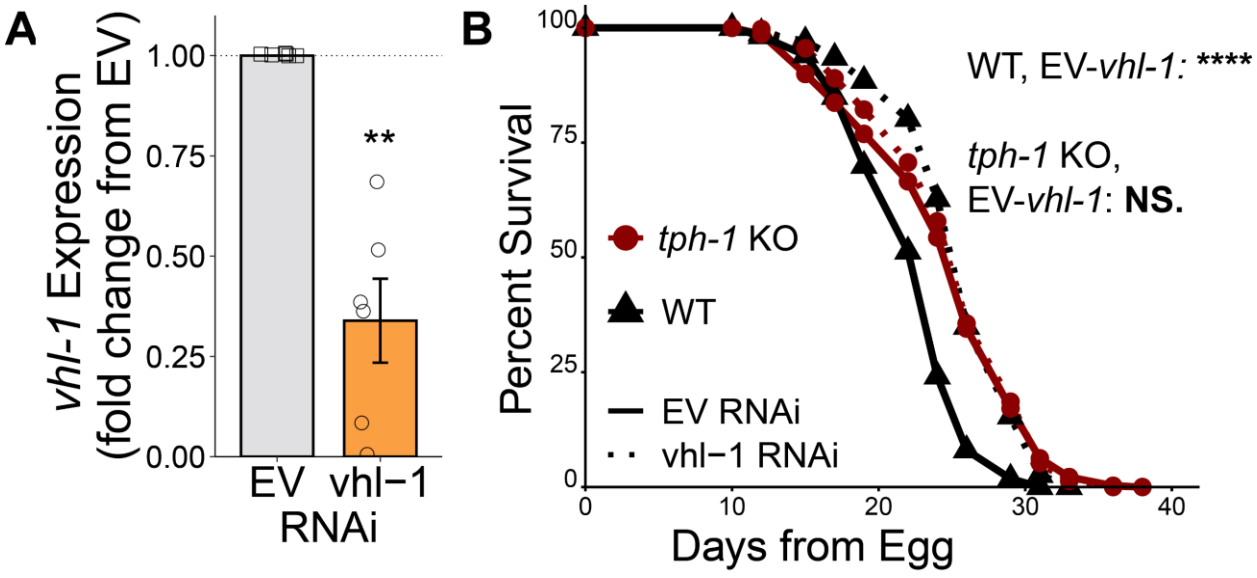


Figure 3.1 ADF serotonergic neurons are necessary and sufficient to extend lifespan downstream of the hypoxic response. (**A**) Diagram of the conserved hypoxic response and genetic approaches to activate it, *vhl-1* knockdown and HIF-1 stabilization. (**B-D**) Survival curves of WT, *hif-1(ia4)* knockout, *hif-1(ia4);* ADF::HIF-1S (**B**), *hif-1(ia4);* NSM::HIF-1S (**C**), and *hif-1(ia4);* HSN::HIF-1S (**D**) worms. $N \geq 256$ (**B**), $N \geq 188$ (**C**), and $N \geq 188$ (**D**) worms per condition. (**E**) Survival curves of WT and ADF:*tph-1* knockout worms on empty vector (EV) or *vhl-1* RNAi. $N \geq 143$ worms per condition. (**F**) Survival curves of WT and NSM:*tph-1* knockout worms on empty vector (EV) or *vhl-1* RNAi. $N \geq 193$ worms per condition. (**G**) Survival curves of WT and *tph-1(mg280);* ADF:*tph-1* rescue worms on empty vector (EV) or *vhl-1* RNAi. $N \geq 178$ worms per condition. (**H**) Survival curves of WT and *tph-1(mg280);* NSM:*tph-1* rescue worms on empty vector (EV) or *vhl-1* RNAi. $N \geq 160$ worms per condition. (**I**) Gene expression of *fmo-2* in WT and *hif-1(ia4);* ADF:HIF-1S worms. Significance in panels B-H is from a log-rank test comparing median survival. Significance in panel I is from a Student's t-test (unpaired, two-tailed). In all panels, three replicates were plotted together, and all statistics include a Bonferroni correction for multiple comparisons. NS. = $p > 0.05$, * = $p < 0.05$, ** = $p < 0.01$, *** = $p < 0.001$, and **** = $p < 0.0001$.

To further test the necessity of the most impactful (for lifespan) serotonergic neurons in hypoxia-mediated longevity, we used transgenic animals in which *tph-1*, the rate-limiting enzyme in serotonin synthesis, was knocked out exclusively in the ADF or the NSM serotonergic neurons[105,344]. We then measured the lifespans of these strains on empty vector (EV) and *vhl-1* RNAi to determine the necessity of ADF and NSM serotonergic signaling in *vhl-1*-

mediated longevity. Successful RNAi knockdown was confirmed with qPCR validation (**SFig. 3.1A**). We found that serotonin synthesis in ADF but not NSM neurons was required for *vhl-1* knockdown to extend lifespan (**Fig. 3.1E-F**). This indicates that while HIF stabilization in multiple serotonergic neurons can extend lifespan, ADF serotonin signaling is required for lifespan extension in response to *vhl-1* knockdown.

To test if serotonin production in a single neuron type is sufficient for the hypoxic response to extend lifespan, we rescued *tph-1* expression in a *tph-1* null background using promoters specific to the ADF or the NSM neurons[105]. The lifespans of these strains on EV or *vhl-1* RNAi were then measured. As expected and consistent with our previous publication[48], the lifespan of the *tph-1* knockout strain was not extended by *vhl-1* knockdown (**SFig. 3.1B).** Consistent with the ADF neuron's requirement for hypoxic response-mediated longevity (**Fig. 3.1E-F**), serotonin synthesis in the ADF neurons was sufficient for *vhl-1* knockdown to extend lifespan while NSM serotonin synthesis was not (**Fig. 3.1G-H**). The enzyme *fmo-2* is induced in the intestine under hypoxia and is required for lifespan extension by environmental hypoxia, HIF-1 stabilization, or *vhl-1* depletion[48]. To test whether ADF-specific HIF-1 stabilization also induces *fmo-2*, we measured *fmo-2* transcription in this strain using qPCR. We found that ADF HIF-1 stabilization significantly induced *fmo-2* expression relative to WT controls (**Fig. 3.1I**), suggesting a model in which ADF signaling extends lifespan through the same mechanism as *vhl-1* knockdown and environmental hypoxia. Together, these data indicate that while HIF-1 stabilization in any serotonergic neuron is sufficient to extend lifespan, only ADF serotonin production is necessary and sufficient for *vhl-1*-mediated longevity. This suggests that under normal physiological conditions the serotonergic ADF neurons propagate a signal in response to whole body stabilized HIF-1.



Supplemental Figure 3.1 *tph-1* is required for *vhl-1* mediated longevity. (**A**) Gene expression of *vhl-1* in worms on *vhl-1* RNAi compared to control worms on empty vector (EV) RNAi for two generations. $N \geq 200$ worms per replicate, or 1200 worms per condition. The top of the bar represents the mean of the population and error bars indicate standard error of the mean (SEM). (**B**) Survival curve of WT, *vhl-1(ok161)*, *tph-1(mg280),* and *vhl-1(ok161); tph-1(mg280)* worms. $N \geq 338$ worms per condition. Significance is from a log-rank test comparing median survival. In all panels, NS. = $p > 0.05$, * = $p < 0.05$, ** = $p < 0.01$, *** = $p < 0.001$, and **** = $p < 0.0001$. Three replicates were plotted together, and all statistics include a Bonferroni correction for multiple comparisons.

After identifying ADF neurons as the most central serotonergic neurons in hypoxic response-mediated longevity, we next sought to determine the downstream receptor responding to serotonin signaling from ADF neurons. *C. elegans* have six known serotonin receptors—SER-1, SER-4, SER-5, SER-7, MOD-1, and LGC-50. Of these six receptors, our previous findings showed that *ser-7* expression is required for hypoxia to induce *fmo-2* and extend lifespan[48]. SER-7 is a G protein-coupled receptor (GPCR) with high sequence identity to the 5-HT$_7$ receptor in mammals[345,346]. SER-7 is thought to be expressed in 27 of *C. elegans'* 302 neurons[295] and contributes to many aspects of physiology such as reproduction and pharyngeal pumping[345]. Consequently, broad manipulation of SER-7 signaling is not an ideal method for exclusively modifying aging. To identify more specific targets for lifespan extension within this pathway, we asked whether *ser-7* expression in any subset of neurons is sufficient to rescue the hypoxic response in a *ser-7* null background.

We created transgenic strains with *ser-7* expression under the control of 11 different cell-specific promoters in a *ser-7* null background. These promoters were selected to rescue *ser-7* expression in the following neuronal populations: whole-body rescue (*ser-7p::ser-7)*, interneuron rescue (*glr-1p::ser-7)*, bioaminergic neuron rescue (*cat-1p::ser-7)*, glutamatergic neuron rescue (*eat-4p::ser-7*), GABAergic neuron rescue (*unc-47p::ser-7*), cholinergic neuron rescue (*unc-17p::ser-7*), sensory neuron rescue (*osm-6p::ser-7*), GABAergic motor neuron rescue (*unc-25p::ser-7*), cholinergic motor neuron rescue (*acr-2p::ser-7*), M3 and M4 neuron rescue (*ceh-28p::ser-7*), and intestinal rescue (*vha-6p::ser-7*) in a *ser-7* null background. To measure whether *ser-7* expression restores a WT-like hypoxic response, we injected each construct into *ser-7* null worms crossed with a single-copy transcriptional reporter for *fmo-2 (fmo-2p::mCherry)*. Because *fmo-2* is induced by and required for hypoxia-mediated longevity[48], we utilized its induction as an efficient screening tool to identify components of this longevity pathway.

We first confirmed that *ser-7* knockout attenuates *vhl-1*-mediated *fmo-2* induction (**Fig. 3.2A**). The whole-body rescue of SER-7 expression under the endogenous *ser-7* promoter restored *fmo-2* induction to 91% of WT controls (**Fig. 3.2A**). Of the 10 cell-specific *ser-7* rescues, expression in interneurons, bioaminergic neurons, glutamatergic neurons, or GABAergic neurons fully rescued *vhl-1*-mediated *fmo-2* induction to ≥ 100% of the WT control response (**Fig. 3.2A**, pink bars). *ser-7* rescue in GABAergic motor neurons or in sensory neurons showed a partial rescue (defined as a 50-99% increase from *fmo-2* induction in the *ser-7* knockout) (**Fig. 3.2A**, orange bars). In contrast, rescuing *ser-7* in cholinergic motor neurons, cholinergic neurons, M3 and M4 neurons, or in the intestine did not rescue (**Fig. 3.2A,** gray bars). Taken together, 6 of the 10 cell-specific *ser-7* rescues at least partially restored *vhl-1*-

mediated *fmo-2* induction, including some that have no known overlap in *ser-7* expression patterns. Collectively, these data suggest that serotonin receptor *ser-7* expression in multiple neurons may be sufficient to convey the hypoxic signal to the intestine and induce *fmo-2*.

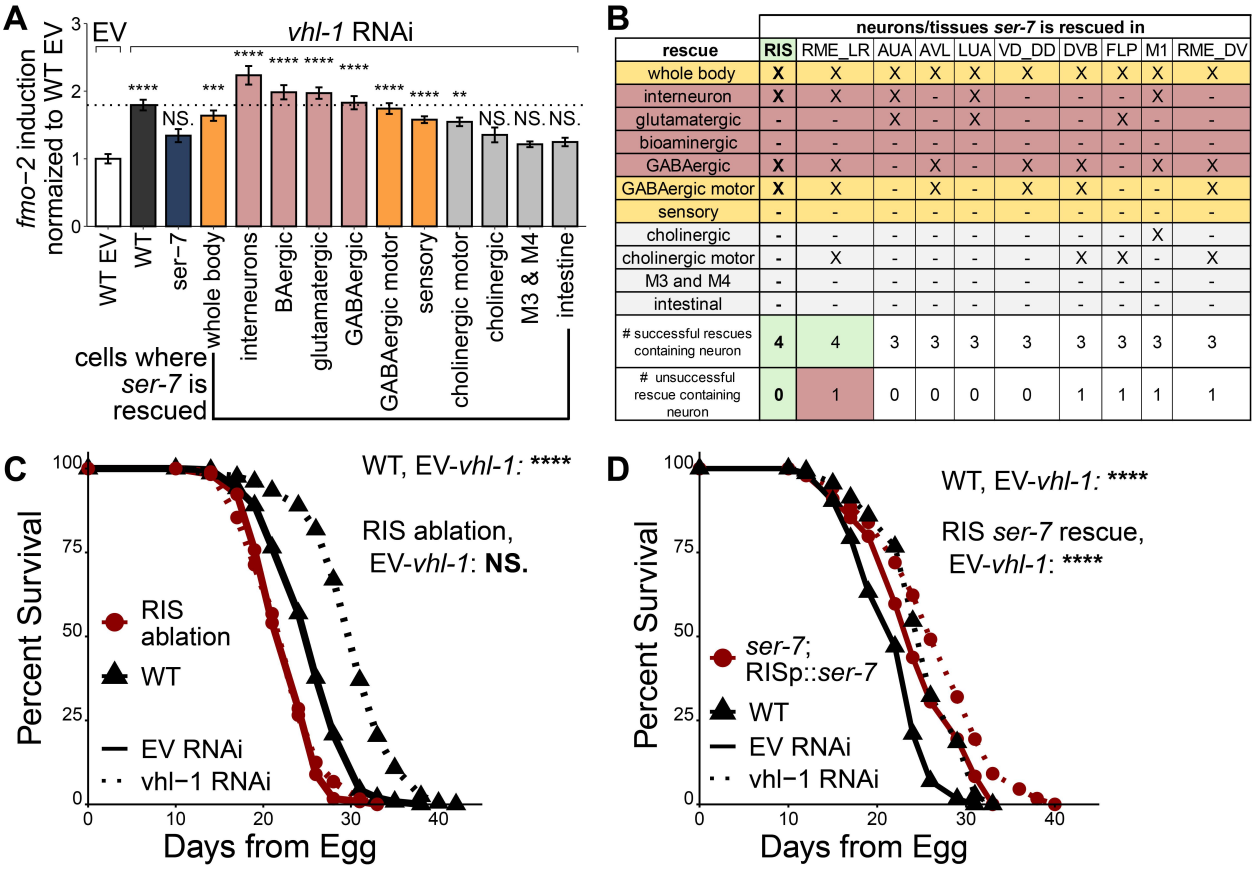


Figure 3.2 *ser-7* expression in the GABAergic RIS neuron is required for hypoxia to extend lifespan. (**A**) Quantification of *fmo-2p::mCherry* (WT positive control), *fmo-2p::mCherry; ser-7(tm1325)* knockout (negative control), and *fmo-2p::mCherry; ser-7(tm1325)* knockouts with *ser-7* rescued in the whole body (*ser-7p::ser-7)*, interneurons (*glr-1p::ser-7)*, bioaminergic neurons (*cat-1p::ser-7)*, glutamatergic neurons (*eat-4p::ser-7*), GABAergic neurons (*unc-47p::ser-7*), GABAergic motor neurons (*unc-25p::ser-7*), sensory neurons (*osm-6p::ser-7*), cholinergic motor neurons (*acr-2p::ser-7*), cholinergic neurons (*unc-17p::ser-7*), M3 & M4 neurons (*ceh-28p::ser-7*), and the intestine (*vha-6p::ser-7*) on empty vector (EV, WT control shown) or *vhl-1* RNAi (all strains shown). Bar height indicates the mean fluorescence on *vhl-1* RNAi of each genotype normalized to the empty vector control value from that genotype. The dashed line indicates the *vhl-1*-mediated *fmo-2* induction of WT positive control. $N \geq 45$ worms per condition. Error bars indicate SEM. Significance is from a two-way ANOVA (*fmo-2* induction ~ genotype*RNAi) and post-hoc Tukey HSD test (unpaired, two-tailed). Stars signify results from this post-hoc test comparing the *fmo-2* induction of each strain on EV RNAi the *fmo-2* induction of that strain on *vhl-1* RNAi. (**B**) A table showing the 10 *ser-7* expressing candidate neurons and their expression patterns among the *ser-7* cell-specific strains that successfully rescued *fmo-2* induction in Fig. 2A. Pink rows indicate rescues that full restored *vhl-1* mediated *fmo-2* induction, orange rows indicate rescues that partially restored *vhl-1*-mediated *fmo-2* induction, and gray rows signify unsuccessful rescue constructs from the data in Fig. 2A. (**C**) Survival curve of WT and RIS ablation (*Ex[srsx-18p::caspase-3(p12)-nz]; Ex[srsx-18p::cz-caspase-3 (p17)]; srsx-18p::GFP*) worms on empty vector (EV) and *vhl-1* RNAi. $N \geq 192$ worms per condition. (**D**) Survival curve of WT and *ser-7 (tm1325); ser-7* rescue in the RIS neuron (*flp-11p::ser-7*) worms on EV and *vhl-1* RNAi. $N \geq 144$ worms per condition.

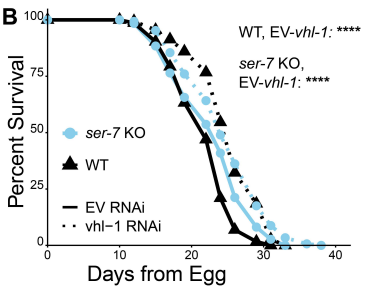
Significance in panels C-D is from a log-rank test comparing median survival. In all panels, NS. = $p > 0.05$, * = $p < 0.05$, ** = $p < 0.01$, *** = $p < 0.001$, and **** = $p < 0.0001$. In all panels, three replicates were plotted together, and all statistics include a Bonferroni correction for multiple comparisons.

We compiled a table containing the top candidates for the *ser-7* neuron based on which rescue constructs restored *ser-7* expression (simplified table in **Fig. 3.2B**, full table in **SFig. 3.2A**). We hypothesized that neurons present in many of the successful rescue constructs would be most important in the hypoxia longevity circuit. Conversely, we hypothesized that candidate neurons within rescues that did not restore a WT-like hypoxia response are less likely to be important (**Fig. 3.2B**; **SFig. 3.2A**). We acknowledge that this analysis strategy is biased toward neurons rescued in a greater proportion of the transgenic strains, which could lead to false negatives. From this analysis, we identified 10 neurons that were rescued in 3-4 of the 6 successful rescue constructs (**Fig. 3.2B**). Five of these neurons (DVB, FLP, M1, RME_LR, and RME_DV) were also present in unsuccessful rescue constructs, so they were not considered for follow-up experiments. Of the remaining five neurons (RIS, AUA, AVC, LUA, and VD_DD), the top candidate was the RIS neuron, because RIS was present in the highest number (4 as shown in **Fig. 3.2B**) of successful rescue constructs.

A

	neurons/tissues SER-7 is rescued in																														
rescue	RIS	RME_LR	AUA	AVL	LUA	VD_DD	DVB	FLP	M1	RME_DV	I2	I4	I5	I6	MI	PLM	I3	IL1	M3	M5	NSM	VC_4_5	M2	MC	intestine	I1	PDA	M4
whole body	X	X	X	X	X	X	X	X	X	X	X	X	X	X	X	X	X	X	X	X	X	X	X	X	X	X	X	X
interneuron	X	X	X	-	X	-	-	-	X	-	-	X	-	-	-	-	-	-	-	-	-	-	-	-	-	-	-	-
glutamatergic	-	-	X	-	X	-	-	X	-	-	X	-	X	X	X	X	-	X	X	X	-	-	-	-	-	-	-	-
bioaminergic	-	-	-	-	-	-	-	-	-	-	-	-	-	-	-	-	-	-	-	-	X	X	-	-	-	-	-	-
GABAergic	X	X	-	X	-	X	X	-	X	X	-	-	-	-	-	-	X	-	-	-	-	-	-	-	-	-	-	-
GABAergic motor	X	X	-	X	-	X	X	-	-	X	-	-	-	-	-	-	-	-	-	-	-	-	-	-	-	-	-	-
sensory	-	-	-	-	-	-	-	-	-	-	-	-	-	-	-	-	-	X	-	-	-	-	-	-	-	-	-	-
cholinergic	-	-	-	-	-	-	-	-	X	-	-	-	-	-	-	-	X	-	-	X	-	X	X	X	-	X	X	X
cholinergic motor	-	X	-	-	-	-	X	X	-	X	-	-	-	-	-	-	-	X	-	-	X	X	-	-	-	X	X	X
M3 and M4	-	-	-	-	-	-	-	-	-	-	-	-	-	-	-	-	-	-	X	-	-	-	-	-	-	-	-	X
intestinal	-	-	-	-	-	-	-	-	-	-	-	-	-	-	-	-	-	-	-	-	-	-	-	-	X	-	-	-
# successful rescues containing neuron	4	4	3	3	3	3	3	3	3	3	2	2	2	2	2	2	2	2	2	2	2	2	1	1	1	1	1	1
# unsuccessful rescue containing neuron	0	1	0	0	0	0	1	1	1	1	0	0	0	0	0	0	1	1	1	1	1	2	1	1	1	2	2	3

B



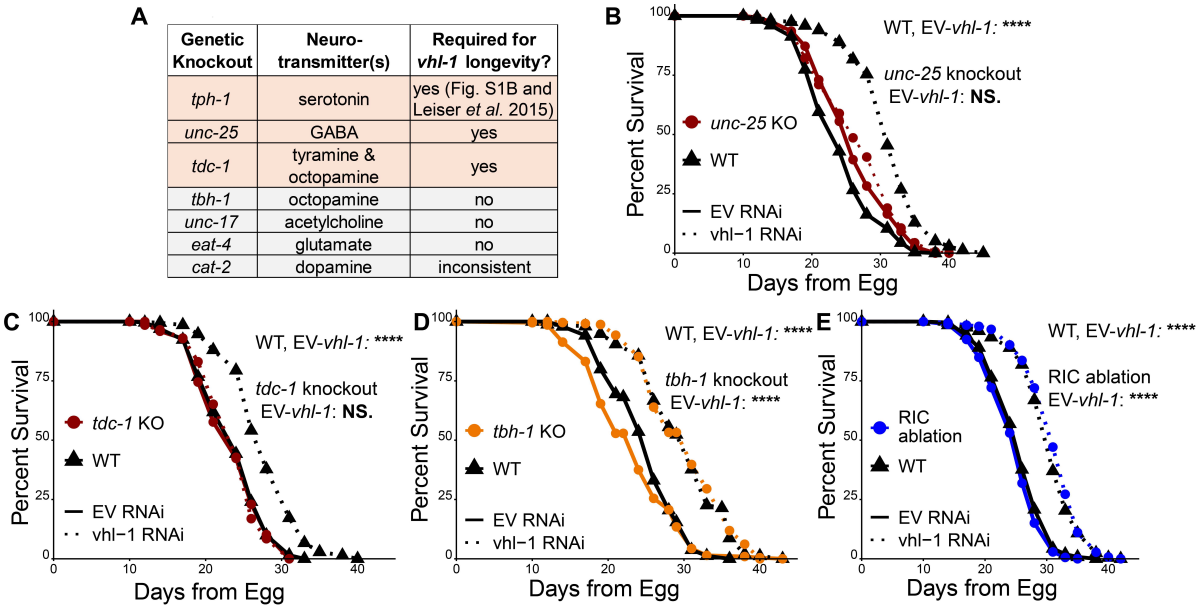
Supplemental Figure 3.2 *ser-7* expression in each *ser-7* expressing neuron is rescued by at least one construct, and *ser-7* is required for *vhl-1*-mediated longevity. (**A**) A table showing all *ser-7* expressing candidate neurons, and which constructs in Fig. 2A restored *ser-7* expression in these neurons. Pink rows indicate rescues that fully restored *vhl-1* mediated *fmo-2* induction, orange rows indicate rescues that partially restored *vhl-1*-mediated *fmo-2* induction, and gray rows signify unsuccessful rescue constructs from the data in panel A. (**B**) Survival curve of WT, and *ser-7(tm1325)* worms on empty vector (EV) and *vhl-1* RNAi. $N \geq 259$ worms per condition. Significance is from a log-rank test comparing median survival. Cox Regression for an interaction between the effect of *ser-7 (tm1325)* knockout and *vhl-1* RNAi knockdown on lifespan. $p = 0.003$, **. NS. = $p > 0.05$, * = $p < 0.05$, ** = $p < 0.01$, *** = $p < 0.001$, and **** = $p < 0.0001$. Three replicates were plotted together, and all statistics include a Bonferroni correction for multiple comparisons.

To validate whether the RIS neuron is a key signaling cell in hypoxia-mediated longevity, we first genetically ablated the RIS neuron to test its necessity. Our results showed that *vhl-1* RNAi does not extend lifespan of RIS ablated worms, indicating that the RIS neuron is completely required for *vhl-1* knockdown to extend lifespan (**Fig. 3.2C**). To test the sufficiency of RIS signaling, we next rescued *ser-7* expression in the RIS neuron in the *ser-7* null background under the *flp-11* promoter. *flp-11* is expressed in the RIS neuron[347] and uv1 neuroendocrine cells[348] that do not endogenously express *ser-7*[295]. We first confirmed that *ser-7* knockout worms are partially required for *vhl-1* RNAi to extend lifespan (**SFig. 3.2B**, Cox Regression, $p = 0.003$, **). Significantly, *ser-7* rescue in the RIS neuron (*ser-7; flp-11p::ser*-7) restores the lifespan extension by *vhl-1* RNAi to the same degree as WT worms (**Fig. 3.2D**). These data suggest that *ser-7* expression in the RIS neuron only is sufficient for *vhl-1*-mediated longevity. However, one limitation of this approach is that non-physiological expression of *ser-7* in the uv1 cells could play a role in restoration of a WT-like hypoxic response. Together, these data are consistent with a model where hypoxic conditions stabilize HIF-1 in the ADF neurons, which modify serotonin signaling to the SER-7 receptor on the RIS interneuron.

3.4.2 Tyraminergic signaling from the RIM neuron and the tyramine receptor TYRA-3 are required for vhl-1 knockdown to extend lifespan.

After identifying neuron subtypes involved in serotonin signaling downstream of the hypoxic response, we next set out to identify whether other neurotransmitters act in the pathway. To answer this question, we obtained mutants deficient in the production of each type of neurotransmitter in *C. elegans* (**Fig. 3.3A**) and measured their lifespan on control and *vhl-1* RNAi. Out of the six neurotransmitters we tested, blocking the production of GABA (*unc-25*, **Fig. 3.3B**) or tyramine + octopamine (*tdc-1,* **Fig. 3.3C**) attenuated longevity on *vhl-1* RNAi. The

requirement of GABA is consistent with our finding that *ser-7* expression on the GABAergic RIS neuron is also necessary for hypoxic response-mediated longevity (**Fig. 3.2**), connecting the serotonergic and GABAergic components of this circuit.



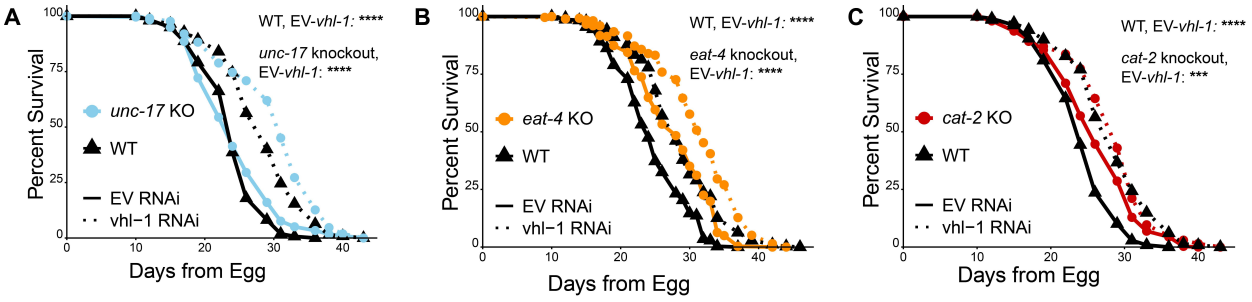
Genetic Knockout	Neuro-transmitter(s)	Required for *vhl-1* longevity?
tph-1	serotonin	yes (Fig. S1B and Leiser *et al.* 2015)
unc-25	GABA	yes
tdc-1	tyramine & octopamine	yes
tbh-1	octopamine	no
unc-17	acetylcholine	no
eat-4	glutamate	no
cat-2	dopamine	inconsistent

Figure 3.3 GABA and tyramine synthesis are required for the hypoxic response to extend lifespan. (**A**) Summary table of the necessity of each *C. elegans* neurotransmitter for *vhl-1* RNAi-mediated longevity. (**B-E**) Survival curves of WT and *unc-25(e156)* (GABA deficiency) (**B**), *tdc-1(n3419)* (tyramine + octopamine deficiency) (**C**), *tbh-1(n3247)* (octopamine deficiency) (**D**), and RIC ablation (*Ex[tbh-1p::caspase-3(p12)-nz]; Ex[tbh-1p::cz-caspase-3 (p17)]; tbh-1p::GFP*) (**E**) worms on empty vector (EV) and *vhl-1* RNAi. $N \geq 310$ (**B**), ≥ 201 (**C**), ≥ 258 (**D**), and ≥ 258 (**E**) worms per condition. Significance in panels B-E is from a log-rank test comparing median survival. NS. = $p > 0.05$, * = $p < 0.05$, ** = $p < 0.01$, *** = $p < 0.001$, and **** = $p < 0.0001$. In all panels, three replicates were plotted together, and all statistics include a Bonferroni correction for multiple comparisons.

Tyramine (analogous to mammalian adrenaline[349]) is synthesized from tyrosine by tyrosine decarboxylase (*tdc-1*) and can be further converted to octopamine (analogous to mammalian noradrenaline) by tyramine β-hydroxylase (*tbh-1*) in *C. elegans*[304]. Therefore, the *tdc-1* knockout is deficient in both tyramine and octopamine synthesis (**Fig. 3.3C**) and the *tbh-1* knockout (**Fig. 3.3D**) is only deficient in octopamine synthesis. Since worms lacking only octopamine (*tbh-1*, **Fig. 3.3D**) were long-lived on *vhl-1* RNAi but worms lacking both tyramine and octopamine (*tdc-1*, **Fig. 3.3C**) were not, we can conclude that tyramine is required for the hypoxic response to extend lifespan. To further test whether tyramine but not octopamine is

involved in this pathway, we generated a strain in which the primary octopamine-producing neuron, RIC[304], is genetically ablated. We found that the RIC neuron is not required for *vhl-1*-mediated longevity (**Fig. 3.3E**), further supporting that tyramine but not octopamine is a key neurotransmitter in the hypoxic response longevity circuit.

In addition to octopamine (*tbh-1,* **SFig. 3.3C**), we also observed that acetylcholine (*unc-17*, **SFig. 3.3A**) and glutamate (*eat-4*, **SFig. 3.3B**) were not required for lifespan extension by *vhl-1* RNAi. Our lifespans of the dopamine synthesis mutant *cat-2* indicated that dopamine is inconsistently required for the hypoxic response to extend lifespan. In three biological replicates, we observed a full requirement, partial requirement, and no requirement for dopamine synthesis in *vhl-1* RNAi-mediated longevity. When analyzed together, the net result suggests that dopamine is partially required for *vhl-1*-mediated longevity (**SFig. 3.3C**, Cox Regression for interaction between genotype and *vhl-1* RNAi, $p < 0.0001$, ****). We did not follow up on dopamine due to the inconsistency. Together, the results from this neurotransmitter screen support the conclusion that in addition to serotonin, both GABA and tyramine play a role in hypoxic response-mediated longevity.



Supplemental Figure 3.3 Acetylcholine, glutamate, and dopamine synthesis are not fully required for *vhl-1* RNAi to extend lifespan. (**A-C**) Survival curves of WT and *unc-17(e113)* (acetylcholine deficiency) (**A**), *eat-4(ky5)* (glutamate deficiency) (**B**), and *cat-2(n4547)* (dopamine deficiency) (**C**) worms on empty vector (EV) and *vhl-1* RNAi. $N \geq 213$ (**A**), ≥ 274 (**B**), and ≥ 270 (**C**) worms per condition. (**C**) Cox Regression for an interaction between genotype and *vhl-1* RNAi, $p < 0.0001$, ****. Significance in all panels is from a log-rank test comparing median survival. NS. = $p > 0.05$, * = $p < 0.05$, ** = $p < 0.01$, *** = $p < 0.001$, and **** = $p < 0.0001$. In all panels, three replicates were plotted together, and all statistics include a Bonferroni correction for multiple comparisons.

Nematodes synthesize GABA in 26 of 302 neurons while tyramine is only synthesized in two cells[300]. As a result, identifying highly specific components of tyraminergic signaling is more feasible than mapping GABAergic signaling components. Therefore, we sought to determine the tyramine-producing neuron(s) and tyramine receptor(s) that contribute to hypoxic response-mediated longevity. In *C. elegans*, the two canonically tyraminergic cell types (the RIM neuron and the uv1 neuroendocrine cells) express *tdc-1* but not *tbh-1*[300]. To determine which tyraminergic cell(s) act in the hypoxic response pathway, we expressed *tdc-1* under promoters specific to either RIM or uv1 in a *tdc-1* null background[326]. We then measured whether the lifespans of these tyramine rescue strains could be extended by *vhl-1* RNAi. Our results showed that *vhl-1* RNAi extended lifespan in the RIM rescue strain (**Fig. 3.4A**), but not in the uv1 rescue (**Fig. 3.4B**). This finding demonstrates that tyramine synthesis in the RIM neuron is sufficient for *vhl-1* RNAi to extend lifespan. Notably, both tyramine rescue constructs lived longer than WT controls (**Fig. 3.4A-B**). This could indicate that altering tyramine signaling modifies lifespan both within and independently of the *vhl-1*-mediated longevity pathway.

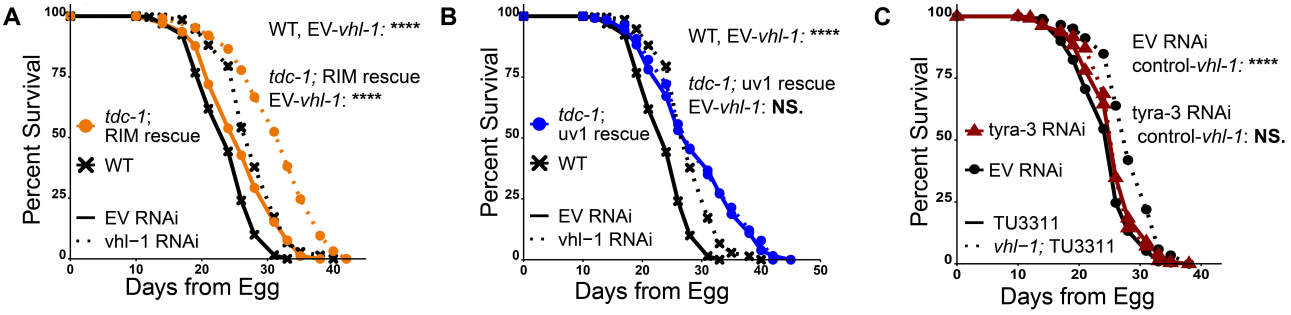
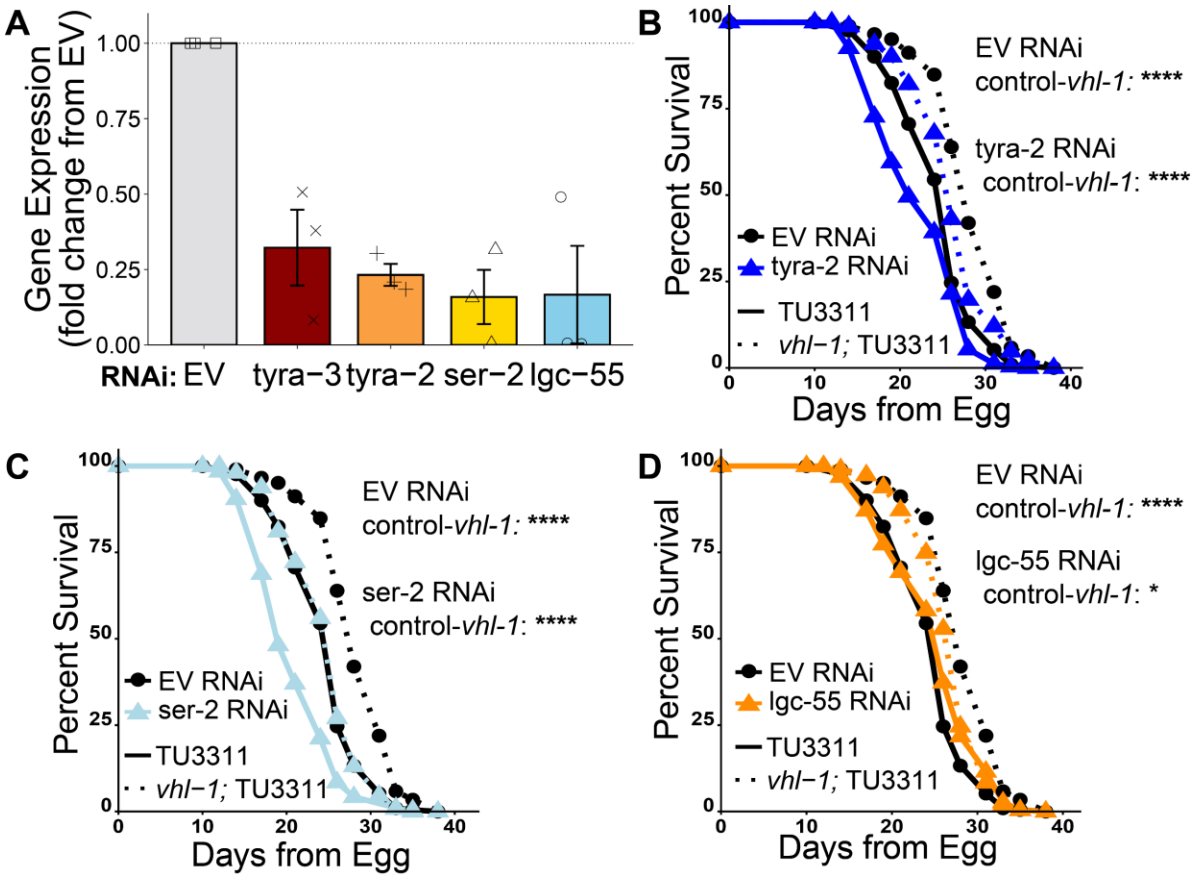


Figure 3.4 The RIM neuron and the tyramine receptor *tyra-3* act in the hypoxic response-mediated longevity pathway. (**A-B**) Survival curves of WT, RIM rescue (*tdc-1 (n3419);* Ex[*ocr-4p::tdc-1]*) (**A**), and uv1 *tdc-1* rescue (*tdc-1 (n3419);* Ex[*gcy-13p::tdc-1]*) (**B**) strains on empty vector (EV) and *vhl-1* RNAi. $N \geq 126$ (**A**) and $N \geq 140$ (**B**) worms per condition. (**C**) Survival curves of TU3311(*unc-119p::sid-1)* and *vhl-1(ok161);* TU3311(*unc-119p::sid-1*) worms on empty vector (EV) and *tyra-3* RNAi. $N \geq 215$ worms per condition. Significance in all panels is from a log-rank test comparing median survival. NS. = $p > 0.05$, * = $p < 0.05$, ** = $p < 0.01$, *** = $p < 0.001$, and **** = $p < 0.0001$. In all panels, three replicates were plotted together, and all statistics include a Bonferroni correction for multiple comparisons.

To identify the tyramine receptor(s) necessary in the hypoxic response-mediated longevity pathway, we used RNAi to knockdown each of *C. elegans'* four known tyramine receptors[350-353] (**Fig. 3.4C**). Since tyramine receptors are mostly expressed in neurons, and RNAi uptake into some neurons is less efficient than other cell types, we used a strain with enhanced neuronal RNAi uptake (TU3311, *unc-119p::sid-1*) crossed into *vhl-1* knockout worms. This neural enhanced RNAi uptake strain was not used previously in this work for *vhl-1* RNAi experiments because *vhl-1* RNAi knockdown extends lifespan in WT worms[48]. The generated *vhl-1; unc-119p::sid-1* strain was long-lived compared to the control strain *unc-119p::sid-1* (**Fig. 3.4C**). Successful RNAi knockdown was validated via qPCR (**SFig. 3.4A**). Our lifespan results show that the tyramine receptor *tyra-3* was fully required for *vhl-1*-mediated longevity (**Fig. 3.4C**), but the tyramine receptors *tyra-2* and *ser-2* were not (**SFig. 3.4B-C**). Another tyramine receptor, *Igc-55,* showed a partial requirement for *vhl-1*-mediated longevity (**SFig. 3.4D**). Although there was a lifespan extension by *vhl-1* on *Igc-55* RNAi (**SFig. 3.4D**), we did observe a significant interaction between *lgc-55* knockdown and genotype on lifespan (Cox Regression, $p < 0.0001$, ****), indicating a partial requirement. In summary, these data indicate that tyramine signaling from the RIM neuron to the TYRA-3 receptor is required for hypoxic response-mediated longevity, while the LGC-55 receptor may play a partial role. Interestingly, TYRA-3 is highly expressed on the low oxygen/high carbon dioxide-sensing BAG neuron as well as in the intestine[295,354], the site of *fmo-2* induction during hypoxia[48].



Supplemental Figure 3.4 *tyra-2* and *ser-2* are not necessary for *vhl-1*-mediated longevity, while *lgc-55* is partially required. (**A**) Gene expression of *tyra-3, tyra-2, ser-2,* and *lgc-55* in TU3311(*unc-119p::sid-1)* worms raised on RNAi targeting each gene compared to control worms raised on empty vector (EV) RNAi for two generations. $N \geq 300$ worms per replicate, or 900 worms per condition. The top of the bar represents the mean of the population and error bars indicate standard error of the mean (SEM). (**B-D**) Survival curves of TU3311(*unc-119p::sid-1)* and *vhl-1(ok161);* TU3311(*unc-119p::sid-1*) worms on empty vector (EV) and *tyra-2* (**B**), *ser-2* (**C**), or *lgc-55* (**D**) RNAi. Cox Regression for an interaction between *lgc-55* knockdown and *vhl-1* knockout on lifespan in the TU3311background strain. $p < 0.0001$, ****. $N \geq 215$ worms per condition. Significance is from a log-rank test comparing median survival. NS. = $p > 0.05$, * = $p < 0.05$, ** = $p < 0.01$, *** = $p < 0.001$, and **** = $p < 0.0001$. In all panels, three replicates were plotted together, and all statistics include a Bonferroni correction for multiple comparisons.

3.4.3 Oxygen and carbon dioxide sensing neurons act downstream of serotonin signaling.

Given that *tyra-3* is highly expressed in the canonical low-oxygen sensing neuron BAG[295], we next explored whether neurons responsible for sensing high- and low-oxygen conditions are essential for hypoxic response-mediated longevity. *C. elegans* have four oxygen sensory neurons: the URX, PQR, and AQR neurons detect high levels of oxygen[354], the BAG neuron responds to low levels of oxygen[355] and high levels of carbon dioxide[356] (**Fig. 3.5A**). We

hypothesized that these oxygen sensing cells may perceive hypoxic conditions and help initiate the hypoxic response. Alternatively, these oxygen sensing neurons could modify behavior in response to hypoxia but not play a role in longevity. We found that *vhl-1* knockdown was unable to extend lifespan when we genetically ablated the three high-oxygen sensing neurons (URX, AQR, PQR, **Fig. 3.5B**). Interestingly, the low O_2/high CO_2 responsive BAG neurons were also required for *vhl-1*-mediated longevity (**Fig. 3.5C**). We next crossed the URX/AQR/PQR ablation worms or BAG ablation worms into *C. elegans* with HIF-1 stabilized in the ADF neurons. Ablation of either the URX/PQR/AQR or the BAG neurons abrogated lifespan extension in the ADF HIF-1 stabilized worms. This suggests that oxygen sensing neurons act downstream of ADF HIF-1 stabilization in this pathway (**Fig. 3.5D-E**).

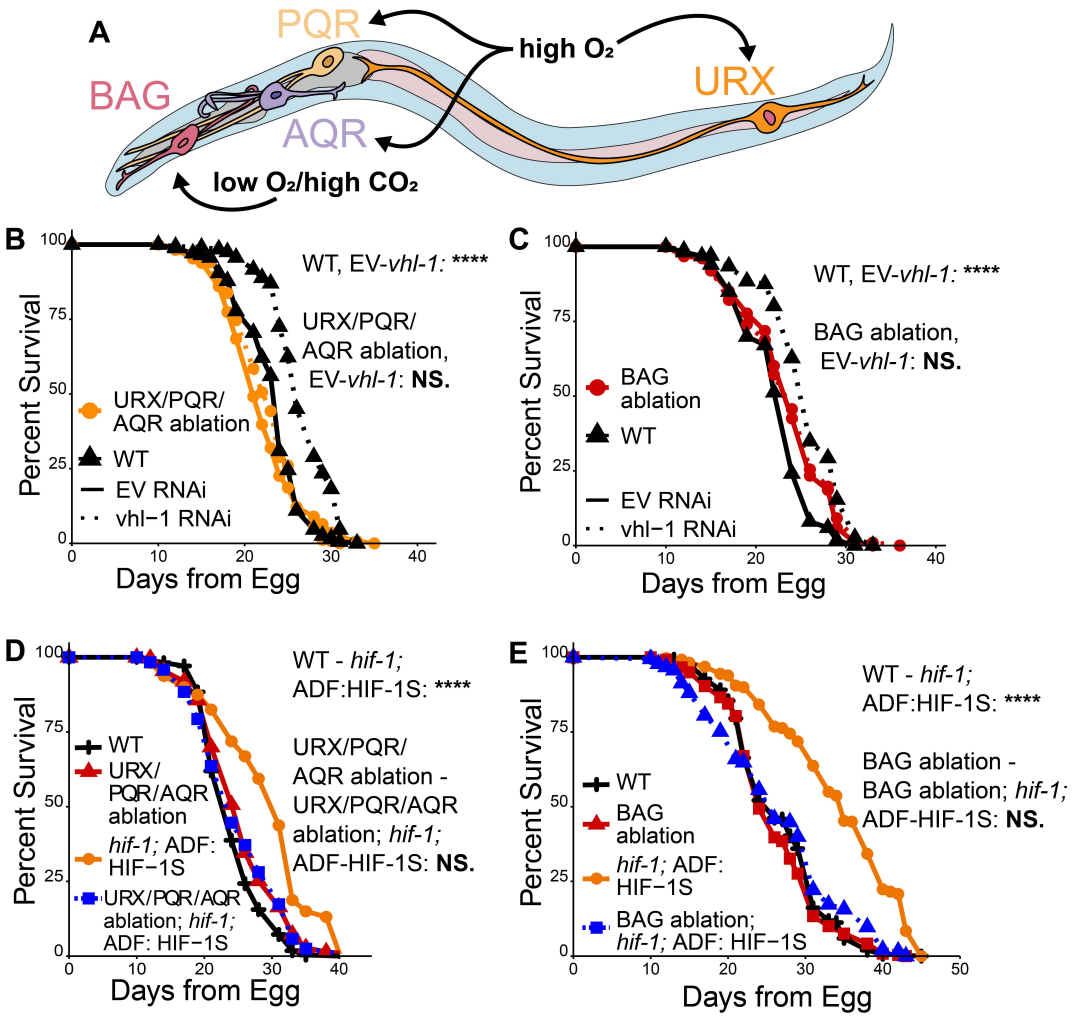


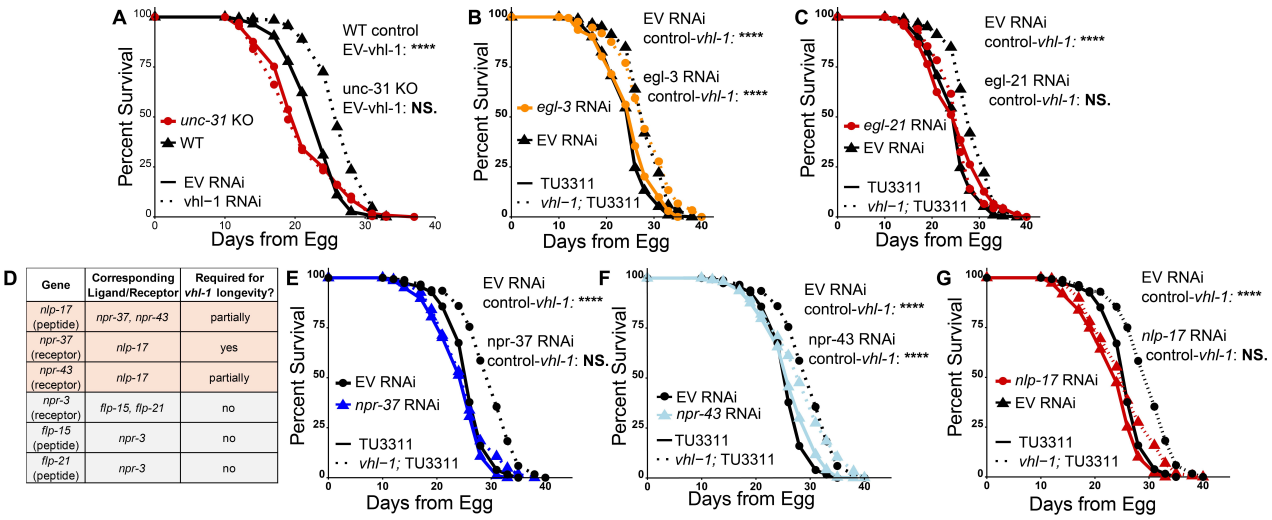
Figure 3.5 High- and low-oxygen sensing neurons are important for hypoxic response-mediated longevity. (**A**) Diagram of oxygen sensing neurons in *C. elegans*. (**B**) Survival curves of WT and URX/PQR/AQR ablated worms (*qaIs2241 [gcy-36::egl-1 + gcy-35::GFP + lin-15(+)]*) on empty vector (EV) and *vhl-1* RNAi. $N \geq 279$ worms per condition. (**C**) Survival curves of WT and BAG ablated worms (*Ex[gcy-31p::caspase-3(p12)-nz]; Ex[gcy-31p::cz-caspase-3 (p17)]; gcy-31p::GFP*) on empty vector (EV) and *vhl-1* RNAi. $N \geq 188$ worms per condition. (**D**) Survival curves of WT, *hif-1(ia4);* ADF-HIF-1S, URX/PQR/AQR (*qaIs2241 [gcy-36::egl-1 + gcy-35::GFP + lin-15(+)]*) ablation, and URX/PQR/AQR (*qaIs2241 [gcy-36::egl-1 + gcy-35::GFP + lin-15(+)]*) ablation; *hif-1(ia4);* ADF-HIF-1S worms. $N \geq 150$ worms per condition. (**E**) Survival curves of WT, *hif-1(ia4);* ADF-HIF-1S, BAG (*Ex[gcy-31p::caspase-3(p12)-nz]; Ex[gcy-31p::cz-caspase-3 (p17)]; gcy-31p::GFP*) ablation, and BAG (*Ex[gcy-31p::caspase-3(p12)-nz]; Ex[gcy-31p::cz-caspase-3 (p17)]; gcy-31p::GFP*) ablation; *hif-1(ia4);* ADF-HIF-1S worms. $N \geq 186$ worms per condition. Significance in all panels is from a log-rank test comparing median survival. NS. = $p > 0.05$, * = $p < 0.05$, ** = $p < 0.01$, *** = $p < 0.001$, and **** = $p < 0.0001$. In all panels, three replicates were plotted together, and all statistics include a Bonferroni correction for multiple comparisons.

3.4.4 The neuropeptide NLP-17 and its receptors contribute to vhl-1-mediated longevity.

After identifying neurons, neurotransmitters, and neuroreceptors acting in the hypoxic response longevity circuit, we wondered how this neural circuit ultimately propagates

information about hypoxic conditions to the intestine and induces the pro-longevity gene *fmo-2*. The *C. elegans* nervous system does not directly innervate the intestine. Instead, neurosignaling molecules bind to receptors on peripheral tissues through packaging in dense-core vesicles and subsequent release into and diffusion through pseudocoelomic fluid[357,358]. These dense-core vesicles are packaged with a wide variety of neuropeptide signals, although there is also evidence that bioaminergic neurotransmitters like serotonin, dopamine, and adrenaline/noradrenaline can also signal through this dense-core vesicle mechanism[358-360].

We first tested if inducing the hypoxic response through *vhl-1* RNAi extends lifespan in a mutant strain lacking the dense-core vesicle packaging gene *unc-31*. We observed that *unc-31* was required for *vhl-1* knockdown to extend lifespan (**Fig. 3.6A**). To examine whether neuropeptide signals carried by dense-core vesicles are involved, we knocked down two neuropeptide processing enzymes—*egl-3* and *egl-21*[309]. Successful knockdown was validated with qPCR (**SFig. 3.5A**). Interestingly, *egl-21* but not *egl-3* was required for *vhl-1*-mediated longevity (**Fig. 3.6B-C**). This could be because *egl-21* is the only enzyme known to perform the carboxypeptidase E cleavage step of neuropeptide processing[361], while there are four known proprotein convertases with similar function to *egl-3*[309,362].

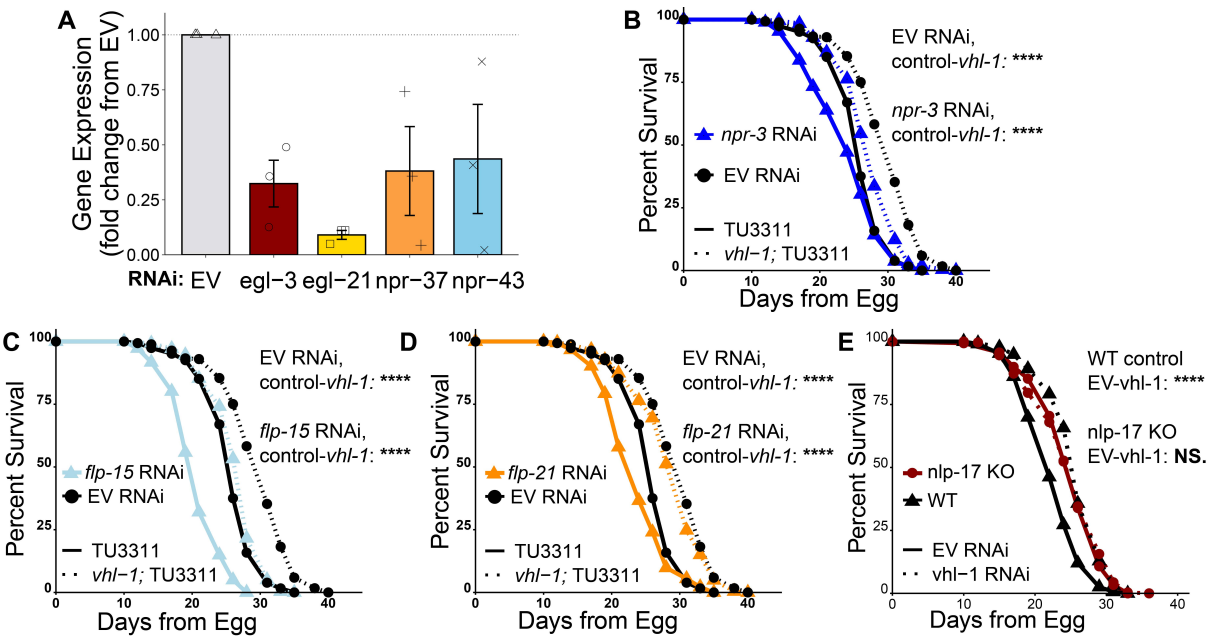


Gene	Corresponding Ligand/Receptor	Required for *vhl-1* longevity?
nlp-17 (peptide)	*npr-37, npr-43*	partially
npr-37 (receptor)	*nlp-17*	yes
npr-43 (receptor)	*nlp-17*	partially
npr-3 (receptor)	*flp-15, flp-21*	no
flp-15 (peptide)	*npr-3*	no
flp-21 (peptide)	*npr-3*	no

Figure 3.6 The neuropeptide *nlp-17* and its receptors *npr-37* and *npr-43* are required for hypoxic response-mediated longevity. (**A**) Survival curves of *unc-31(e169)* and WT worms on empty vector (EV) and vhl-1 RNAi. $N \geq 242$ worms per condition. (**B-C**) Survival curves of TU3311 (*unc-119p::sid-1)* and *vhl-1(ok161);* TU3311 (*unc-119p::sid-1)* worms on empty vector (EV) and *egl-3* (**B**) or *egl-21* (**C**) RNAi. $N \geq 209$ worms (**B**) and $N \geq 185$ worms (**C**) per condition. (**D**) Summary table of two sets of neuropeptide ligands/receptors that blunted *vhl-1*-mediated lifespan. (**E-G**) Survival curves of TU3311 (*unc-119p::sid-1)* and *vhl-1(ok161);* TU3311 (*unc-119p::sid-1)* worms on empty vector (EV) and *npr-37* (**E**), *npr-43* (**F**), or *nlp-17* (**G**) RNAi. $N \geq 288$ worms (**E**), $N \geq 309$ worms (**F**), and $N \geq 309$ worms (**G**) per condition. Significance in panels A-C and E-G are from log-rank test comparing median survival. Cox Regression for a significant interaction between *npr-43* knockdown and *vhl-1* knockout on lifespan, $p < 0.01$, **. Cox regression for a significant interaction between *nlp-17* knockdown and *vhl-1* knockout on lifespan, $p < 0.05$, *. NS. = $p > 0.05$, * = $p < 0.05$, ** = $p < 0.01$, *** = $p < 0.001$, and **** = $p < 0.0001$. In all panels, three replicates were plotted together, and all statistics include a Bonferroni correction for multiple comparisons.

We next tested a group of 6 genes corresponding to neuropeptide/receptor binding pairs that blunted hypoxic response-mediated *fmo-2* induction (**Fig. 3.6D**). These genes, along with their corresponding receptors, were targeted for RNAi and tested for lifespan in TU3311 (*unc-119p::sid-1*) and TU3311 (*unc-119p::sid-1*); *vhl-1 (ok161)* strains. We found that the *npr-3* receptor and it's ligands, *flp-15* and *flp-21* were not required for *vhl-1*-mediated longevity. (**SFig. 3.5B-D**). However, knocking down the neuropeptide *nlp-17* partially blocked *vhl-1*-mediated longevity (**Fig. 3.6E**, Cox regression $p < 0.05$). Consistently, knocking down *nlp-17*'s receptors also completely (*npr-37*, **Fig. 3.6F**) or partially (*npr-43*, **Fig. 3.6G**, Cox regression $p < 0.001$) blocked *vhl-1*-mediated longevity. Successful knockdown of *npr-37* and *npr-43* was validated with qPCR (**SFig. 3.5A**). The *nlp-17* ligand result was validated using a genetic knockout (*nlp-*

17 (ok3461)), which completely prevented *vhl-1* knockdown from extending lifespan (**SFig. 3.5E**). Together, these data suggest a role for NLP-17 signaling in hypoxic response-mediated longevity.



Supplemental Figure 3.5 qPCR validation of RNAi hits from Figure 5, and neuropeptide screen hits that did not validate. (**A-B**) Gene expression of (**A**) *egl-3, egl-21, npr-37,* and *npr-43* in TU3311 (*unc-119p::sid-1)* worms raised on RNAi targeting each gene compared to control worms raised on empty vector (EV) RNAi for two generations. $N \geq 300$ worms per replicate, or 900 worms per condition. The top of the bar represents the mean and error bars represent SEM. (**B-D**) Survival curves of TU3311 (*unc-119p::sid-1)* and *vhl-1(ok161);* TU3311 (*unc-119p::sid-1)* worms on empty vector (EV) and *npr-3* (**B**), *flp-15* (**C**), or *flp-21* (**D**) RNAi. $N \geq 191$ worms (**B**), $N \geq 181$ worms (**C**), and $N \geq 183$ worms (**D**) per condition. (**E**) Survival curves of *nlp-17(ok3461)* on empty vector (EV) or vhl-1 RNAi. $N \geq 275$ worms per condition. Significance in panels B-E are from log-rank test comparing median survival. NS. = $p > 0.05$, * = $p < 0.05$, ** = $p < 0.01$, *** = $p < 0.001$, and **** = $p < 0.0001$. In all panels, 2-3 replicates were plotted together, and all statistics include a Bonferroni correction for multiple comparisons.

Taken together, these results support a model in which HIF-1 stabilization in the ADF serotonergic neurons leads to modified serotonin signaling from the ADF to the SER-7 expressing and GABA-producing RIS neuron (**Fig. 3.7**). Oxygen sensing neurons act downstream of HIF-1 stabilization in the ADF neuron in the hypoxic response longevity circuit. Tyramine produced by the RIM neuron and neuropeptide (NLP-17) signaling are also required for the hypoxic response to extend lifespan, although it remains unclear whether these signals act

upstream, downstream, or in parallel to the serotonergic and GABAergic components in this pathway.

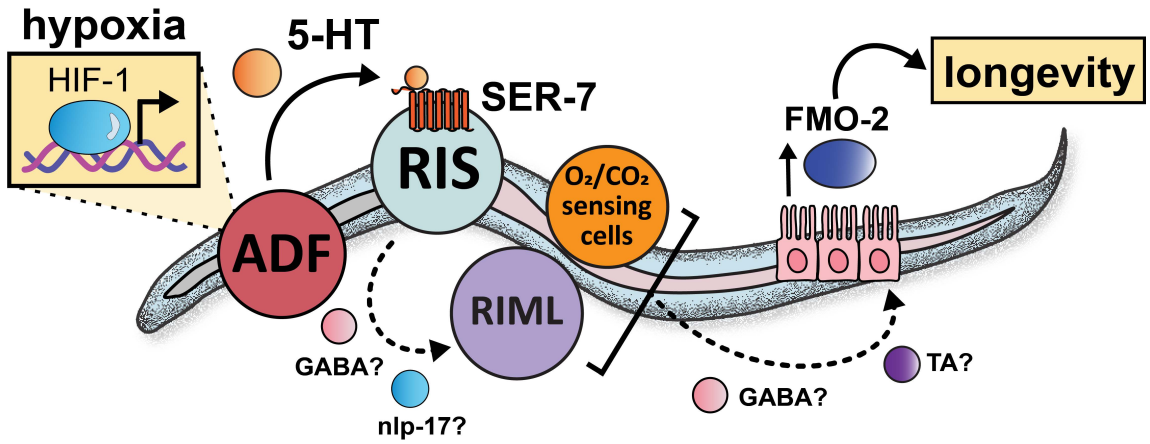


Figure 3.7 Working model of the hypoxia-mediated longevity pathway.

3.5 Discussion

In this study, we interrogated a complex signaling pathway through which genetic induction of the hypoxic response extends lifespan in *C. elegans*. Within this pathway, we demonstrate that: 1) stabilization of HIF-1 in the ADF serotonergic neurons modifies signaling to the SER-7 receptor on the GABAergic and neuropeptidergic RIS neuron (**Fig. 3.1-3.2**); 2) tyraminergic signaling through the RIM neuron and the TYRA-3 receptor (**Fig. 3.3-3.4**) are required for hypoxic response-mediated longevity; 3) oxygen and carbon-dioxide sensory neurons act downstream of HIF-1 stabilization and serotonergic ADF neurons to extend lifespan (**Fig. 3.5**); and 4) in addition to neurotransmitter signals, the neuropeptide NLP-17 and its receptors NPR-37 and NPR-43 are required for the hypoxic response to extend lifespan (**Fig. 3.6**). Ultimately, these neural signals converge on the intestine, to activate FMO-2 and extend lifespan (working model summarized in **Fig. 3.7**).

The hypoxic response is highly conserved across species, highlighting the potential relevance of this pathway in other organisms, including humans. In nematodes, activating the

hypoxic response promotes health and longevity. However, the physiological changes induced by the hypoxic response are broad and involve adaptations that can drive tumorigenesis in mammals. Therefore, a mechanistic understanding of the individual cells, signals, and circuits that mediate the beneficial effects of hypoxia is essential. In this work, the discovery that HIF-1 stabilization in the ADF neurons extends lifespan by 26% demonstrates the potential for targeted manipulations within this pathway to have large effects on lifespan. Additionally, our data identify a previously unknown role for tyramine/adrenaline in the hypoxic response as well as establish NLP-17, a neuropeptide with no previous known function, as a signal in *vhl-1*-mediated longevity. This work also demonstrates that the oxygen sensing AQR, PQR, URX, and BAG neurons act downstream of the serotonergic ADF neuron in the hypoxic response, indicating an interaction between internal and external oxygen sensing mechanisms in longevity. Together, the mapping of these cells, signaling molecules, and receptors in the hypoxic response lays the foundation to discover druggable targets that selectively modulate aging in humans without negative side effects.

Other studies in *C. elegans* have also identified neural networks involving the hypoxic response. For example, previous work found a role for HIF-1 in hypoxia-mediated behaviors, such as food-dependent hyperoxia (excessive oxygen) avoidance[363]. Hyperoxia avoidance requires *hif-1* expression both in the neurons and the tyraminergic uv1 neuroendocrine cells. Interestingly, serotonin signaling from the ADF neuron is also required for WT-like hyperoxia avoidance[363]. While this HIF-1-mediated behavioral circuit has parallels with the HIF-1-mediated longevity circuit interrogated in this work, these pathways do diverge: the key tyraminergic cell type implicated in hyperoxia avoidance is the uv1 gonadal neuroendocrine cells, while the RIM tyraminergic neurons played a role in longevity (**Fig. 3.4**). Together, the

partial overlap between this behavioral and longevity circuit implies that modifying neural signaling to induce the hypoxic response and extend lifespan may also alter behavioral phenotypes. Future research in this area should interrogate exactly where these and any other HIF-1-mediated circuits overlap and diverge.

While this study identifies many neural signals required for *vhl-1* knockdown or knockout to extend lifespan, one key limitation of this work is the potential differences between genetic and environmental methods of inducing the hypoxic response. While *vhl-1* knockdown or knockout leads to HIF-1 stabilization by blocking its proteasomal degradation, it also results in hydroxylated but stable HIF-1. This contrasts with environmental hypoxia, in which HIF-1 remains stable because it cannot be hydroxylated. While HIF-1 is stabilized and localized to the nucleus in both cases, there are differences in transcriptional outcomes between stable hydroxylated and unhydroxylated states[364,365]. Additionally, we did not explore the effects of alternative genetic activators of the hypoxic response such as PHD/EGL mutants, which may provide further insight into how different manipulations of the hypoxic response impact longevity.

The circuit-mapping approaches employed in this work are also impacted by limitations in cell-specific genetic modifications and in the use of RNAi knockdown. For example, cell-specific rescue constructs can sometimes lead to unintended rescues in other cell types due to cell nonautonomous signaling. Because all serotonin-producing neurons also express the serotonin reuptake transporter *mod-5*, serotonin produced by one cell in our rescue strains could be taken up by other serotonin-producing neurons, leading to unintended signaling effects. This may also be true of the uv1 and RIM tyraminergic rescue strains, although little is known about tyramine reuptake in *C. elegans*. Additionally, although RNAi experiments were validated using

sequence confirmation and qPCR, not all RNAi hits were corroborated with genetic knockouts. This leaves open the possibility that RNAi-induced knockdown effects differ from complete genetic ablation, or that production of a given RNAi may modify bacterial metabolism in a way that indirectly modifies the hypoxic response in *C. elegans*. Finally, while the use of RNAi knockdown and genetic knockouts establishes the necessity of many signals within the hypoxia-mediated longevity circuit, the exact directionality of these signals remains unclear. It is possible that increased, decreased, or pulsatile changes in signaling through these bioamines and neuropeptides are required for the hypoxic response to extend lifespan. Future work in this area could use tools to measure or modify neuronal activity, such as calcium imaging or optogenetics, to begin answering these questions.

While many individual neurosignaling components are essential for the hypoxic response to extend lifespan, their epistasis is unclear. Future work in this area should focus on manipulating various components of this network in a manner that we would expect to mimic hypoxia and extend lifespan. This will allow us to narrow down which signals are necessary only to adapt to hypoxia, and which are sufficient to extend lifespan in a normoxic environment. One notable target for further exploration is the SER-7 expressing RIS neuron, which plays a role in sleep[366] and stress resistance[367]. Moreover, optogenetically increasing RIS activity can extend lifespan under normoxic conditions[368].

While our understanding of this circuit is still incomplete, our findings point to several promising signaling components that could be targeted for longevity interventions. Manipulating serotonin and tyramine/adrenaline signaling pathways may offer strategies for extending lifespan, with minimal pleiotropic effects if precisely controlled. These neural targets have great potential for longevity therapeutics due to 1) the small number of neurons that can control aging-

related pathways in the entire organism; 2) the availability of FDA-approved pharmaceuticals that target individual bioaminergic transporters and receptors[104,229,230]; and 3) the high conservation of neurotransmitter biology between invertebrates and mammals[300,305,309]. Further research into how these pathways can be modulated in a targeted manner could spur development of interventions that promote healthy aging and delay the onset of age-related diseases.

3.6 Methods

3.6.1 Strains and Growth Conditions

C. elegans were cultured according to established protocols[48]. In brief, worms were grown at 20 °C on standard solid nematode growth media (NGM). Throughout their lifespan, the worms were fed *E. coli* OP50, except during RNA interference (RNAi) experiments, where *E. coli* HT115 was used to deliver double-stranded RNA. Transfers of worms were carried out using a platinum wire, unless stated otherwise. The RNAi strains employed are listed in Table 3.1, while the strains used in the experiments are provided in Table 3.2. Genotypes were verified through PCR, and RNAi imaging results were confirmed by sequencing and quantitative PCR (qPCR) before proceeding with the experiments.

3.6.2 Generating transgenic strains

3.6.2.1 Neuron-specific stabilized HIF-1 strains

We used the following promoters to drive cDNA of HIF-1 (P621A)::SL2::GFP in three serotonergic neuronal populations: ADF neurons (*srh-142p::* HIF-1 (P621A)), NSM neurons (*ceh-2p::* HIF-1 (P621A)), HSN neurons (*ham-2p::* HIF-1 (P621A)). All plasmids were verified via restriction digest and sanger sequencing, and ApE files are available upon request. Plasmids

were microinjected to *hif-1(ia4)* KO strain by Suny Biotech using the co-injection marker *myo-2p*::GFP and 2-3 transgenic lines were tested in each experiment.

3.6.2.2 Neuron-specific tph-1 rescues

The pKA805[*srh-142p*::TPH-1] and pKA807[*ceh-2p::*TPH-1] constructs were generously provided by Dr. Kaveh Ashrafi. These constructs were injected at ~50 ng/µL) with fluorescent co-injection marker *myo-2p*::mNeonGreen (15 ng/µL) or *sur-5p*::*sur-5::*NLSGFP (20 ng/µL) and junk DNA (up to 100 ng/µL) into gonads of day 1 gravid adult hermaphrodites. Standard protocols were followed to isolate and obtain stable over-expression mutants[369].

3.6.2.3 ser-7 rescue strains

Plasmid construction and microinjection was conducted by Suny Biotech to generate all *ser-7* rescue constructs. In designing the plasmids, we used the following promoters to drive cDNA of SER-7::SL2::GFP in different neuronal populations: full rescue (*ser-7p::ser-7)*, interneuron rescue (*glr-1p::ser-7)*, bioaminergic neuron rescue (*cat-1p::ser-7)*, glutamatergic neuron rescue (*eat-4p::ser-7*), GABAergic neuron rescue (*unc-47p::ser-7*), GABAergic motor neuron rescue (*unc-25p::ser-7*), sensory neuron rescue (*osm-6p::ser-7*), cholinergic motor neuron rescue (*acr-2p::ser-7*), cholinergic neuron rescue (*unc-17p::ser-7*), M3 & M4 neuron rescue (*ceh-28p::ser-7*), and intestinal rescue (*vha-6p::ser-7*). All plasmids were verified via restriction digest and sanger sequencing, and ApE files are available upon request. Plasmids were microinjected by Suny Biotech using the co-injection marker *myo-2p::*GFP and 2-3 transgenic lines were tested in each experiment.

3.6.2.4 RIS, RIC, and BAG neuronal ablation strains

For RIS neuronal ablation strains, we purchased donor plasmid *mec-18p*::caspase-3 (p12)::nz [TU#813] (Plasmid #16082) and *mec-18p* cz::caspase-3 (p17) [TU#814] from Addgene (Plasmid

#16083), and used Gibson cloning (NEB) to replace *mec-18p* with *srsx-18p*. Three constructs *srsx-18p*::caspase-3(p12)::nz, *srsx-18p*::cz::caspase-3(p17), and *srsx-18p*::GFP were co-injected with fluorescent co-injection marker *myo-3p*::GFP (20 ng/µL) into the *wild-type N2* strain to generate RIS genetic ablation strains. Similarly, for RIC ablation strain, *tbh-1p* was constructed into TU#813 and TU#814 to replace *mec-18p*. Three constructs *tbh-1p*::caspase-3(p12)::nz, *tbh-1p*::cz::caspase-3(p17), and *tbh-1p*::GFP were co-injected with fluorescent co-injection marker *myo-3p*::GFP (20 ng/µL) into the *wild-type N2* strain to generate RIC genetic ablation strains. For BAG ablation strain, *gcy-31p* was constructed into TU#813 and TU#814 to replace *mec-18p*. Three constructs *gcy-31p*::caspase-3(p12)::nz, *gcy-31p*::cz::caspase-3(p17), and *gcy-31p*::GFP were co-injected with fluorescent co-injection marker *myo-3p*::GFP (20 ng/µL) into the *wild-type N2* strain to generate BAG genetic ablation strains. All plasmids were verified via restriction digest and sanger sequencing. ApE files available upon request. Plasmid construction and microinjection was conducted by Suny Biotech.

3.6.2.5 RIM and uv1 tdc-1 rescue strains

Plasmid construction and microinjection was conducted by Suny Biotech to generate both *tdc-1* rescue constructs. In designing the plasmids, we used the *ocr-4* promoter to drive cDNA of TDC-1::SL2::GFP in the uv1 neuroendocrine cells. To express cDNA of TDC-1::SL2::GFP in the RIML neuron, we used the *gcy-13* promoter. All plasmids were verified via restriction digest and sanger sequencing, and ApE files are available upon request. Plasmids were microinjected by Suny Biotech using the co-injection marker *myo-2*p::GFP.

3.6.3 RNAi Knockdown

For all RNAi knockdowns, worms were exposed to the RNAi treatment for two generations to achieve optimal knockdown. All RNAi clones were sourced from the Vidal RNAi library. Each RNAi clone was sequence-verified.

3.6.4 Quantitative PCR

For RNAi validation experiments, RNA was isolated from day 1 adult worms that had been grown on RNAi for two generations. For measuring *fmo-2* induction in the *hif-1(ia4);* ADF::HIF-1S strain, worms were grown on OP50, synchronized, and collected at day 1 of adulthood. RNA extraction was performed using the Direct-zol RNA Miniprep Kit (Zymo), and cDNA synthesis was carried out with the Biorad iScript cDNA Synthesis Kit. Gene expression was assessed using the SYBR Green quantitative RT-PCR (qRT-PCR) system (BioRad), with mRNA levels normalized to the housekeeping genes cdc-42 and Y45FD10.4. Primers for RNAi validation were designed to target the 3' UTR of each gene to avoid amplification of the bacterially produced RNAi. Gene expression was quantified using standard curves.

3.6.5 Lifespan Measurements

Lifespan assays were conducted following previously described protocols[48]. Briefly, 10-15 gravid adults were transferred to NGM plates for a three-hour timed egg lay, after which they were removed. Once the progeny reached day 1 of adulthood, 60-80 worms were placed on NGM plates containing 33 µL of 150 mM fluorodeoxyuridine (FUdR) and 100 µL of 50 mg/mL ampicillin per 100 mL of NGM. FUdR inhibits progeny development, while ampicillin prevents bacterial contamination. NGM + FUdR + Ampicillin plates were seeded with concentrated bacteria (5x for OP50-fed lifespan assays). At least two plates per strain and condition were used for each lifespan replicate. Worms were considered dead when they failed to respond to a gentle touch with a platinum wire under a dissection microscope. Lifespan data were recorded at least

three times a week until all worms were dead. To prevent escape, a barrier of 75 µL of 100 mM palmitic acid (Sigma-Aldrich) dissolved in 100% ethanol was applied along the edges of each lifespan plate. Data were analyzed using R version 4.3.1 and visualized in Adobe Illustrator 2022.

3.6.6 RNAi Lifespans

RNAi lifespan assays were performed similarly to standard lifespan assays, with modifications to the initial timed egg lay (TEL) procedure and food concentrations. To ensure maximal RNAi knockdown, worms were first TEL'ed for 3 hours on RNAi plates. The progeny from this TEL were left on RNAi plates to develop into gravid adults and then used for a second TEL under the same RNAi conditions. Progeny from the second-generation TEL were then used for the lifespan assay. RNAi bacteria (HT115) are ampicillin-resistant and can grow slowly on AMP-containing lifespan plates. To maintain consistent bacterial availability throughout the lifespan assay, RNAi plates were seeded with bacteria at 2x concentration, starting from an optical density (OD_{600}) of 3.0.

3.6.7 Fluorescent Slide Microscopy

Fluorescent images for this study were captured using a Leica M165F fluorescent microscope, controlled by Leica Application Suite X (LASX) software. A minimum of 15 worms per condition were imaged at a magnification of at least 70x. For image quantification, individual worms were carefully separated to ensure they did not touch. Custom R code[323] was then used to create a pixel mask of each worm from the brightfield image and measure the fluorescent intensity of that region in the corresponding fluorescent image. The background fluorescence was subtracted from the mean fluorescence values. Data were analyzed using R version 4.3.1 and visualized in Adobe Illustrator 2022.

3.6.8 Statistical Analysis

The height of all bar plots represents the mean value for each condition, with error bars indicating the standard error of the mean (SEM). For comparisons involving more than two conditions, one-way ANOVA followed by post-hoc Tukey HSD tests (2-tailed, unpaired) were used to assess interactions between variables and determine statistical differences between conditions. Significance levels are indicated as *$p < 0.05$, **$p < 0.01$, ***$p < 0.001$, and ****$p < 0.0001$. For lifespan assays, statistical comparisons of survivorship curves were performed using the survfit survival analysis function in R. The log-rank test was used to compare two survival curves. To assess interactions across multiple experimental variables and for comparisons involving more than two survival curves, a Cox regression analysis was conducted using the survivalMPL package in R. For experiments with multiple biological replicates, p-values were adjusted using the Bonferroni correction. Exact sample sizes (Ns) for each experiment are provided in the source data files, and minimum sample sizes for each plot are specified in the figure legends.

3.7 Acknowledgements and Funding

Funding Sources:

National Institutes of Health grant F31AG084146-01 (ESK)

National Science Foundation Graduate Research Fellowship Program DGE1841052 (ESK)

National Institutes of Health grant R01AG058717 (SFL)

3.8 Supplementary Tables

RNAi	Figure(s)	Library
vhl-1	1,2,3,4,5,6,7	Vidal
tyra-3	4	Vidal
tyra-2	S4	Vidal
lgc-55	S4	Vidal
ser-2	S4	Vidal
egl-3	6	Vidal
egl-21	6	Vidal
npr-37	6	Vidal
npr-43	6	Vidal
npr-3	S5	Vidal
flp-15	S5	Vidal
flp-21	S5	Vidal

Table 3.1 RNAi used in this work.

Strain Description	Strain	Source	Identifier	Outcross
WT	wild-type	CGC	N2	≥4
hif-1 knockout	*hif-1 (ia4)*	CGC	ZG31	≥4
hif-1; NSM::HIF-1S	*hif-1 (ia4); Ex[ceh-2p::hif-1(P621A)]*	this paper		≥4
hif-1; HSN::HIF-1S	*hif-1 (ia4); Ex[ham-2p::hif-1(P621A)]*	this paper		≥4
hif-1; ADF::HIF-1S	*hif-1 (ia4); Ex[srh-142p::hif-1(P621A)]*	this paper		≥4
tph-1 knockout	*tph-1 (mg280)*	CGC	MT15434	≥4
ADF::*tph-1* knockout	*kySi56 IV; kyEx4077[srh-142::nCre]*	Cori Bargmann	CX13571	≥4
NSM::*tph-1* knockout	*kySi56 IV; kyEx4057[ceh-2::nCre]*	Cori Bargmann	CX13572	≥4
vhl-1 knockout	*vhl-1 (ok161)*	CGC	CB5602	≥4
ADF *tph-1* rescue	*tph-1(mg280); pKA805[srh-142p::TPH-1]*	Miller *et al* 2022	LZR008	≥4
NSM *tph-1* rescue	*tph-1(mg280); pKA807[ceh-2p::TPH-1]*	Miller *et al* 2022	LZR009	≥4

ser-7 knockout	*ser-7 (tm1325)*	CGC	DA2100	≥4
whole body *ser-7* rescue	*ser-7 (tm1325); Ex[ser-7p::ser-7]*	this paper		≥4
glutamatergic neuron *ser-7* rescue	*ser-7 (tm1325); Ex[eat-4p::ser-7]*	this paper		≥4
cholinergic motor neuron *ser-7* rescue	*ser-7 (tm1325); Ex[acr-2p::ser-7]*	this paper		≥4
bioaminergic neuron *ser-7* rescue	*ser-7 (tm1325); Ex[cat-1p::ser-7]*	this paper		≥4
sensory neuron *ser-7* rescue	*ser-7 (tm1325); Ex[osm-6p::ser-7]*	this paper		≥4
cholinergic neuron *ser-7* rescue	*ser-7 (tm1325); Ex[unc-17p::ser-7]*	this paper		≥4
interneuron *ser-7* rescue	*ser-7 (tm1325); Ex[glr-1p::ser-7]*	this paper		≥4
GABAergic neuron *ser-7* rescue	*ser-7 (tm1325); Ex[unc-47p::ser-7]*	this paper		≥4
GABAergic motor neuron *ser-7* rescue	*ser-7 (tm1325); Ex[unc-25p::ser-7]*	this paper		≥4
M3 and M4 neuron *ser-7* rescue	*ser-7 (tm1325); Ex[ceh-28p::ser-7]*	this paper		≥4
intestinal *ser-7* rescue	*ser-7 (tm1325); Ex[vha-6p::ser-7]*	this paper		≥4
RIS neuron ablation	*Ex[srsx-18p::caspase-3(p12)-nz]; Ex[srsx-18p::cz-caspase-3 (p17)]; srsx-18p::GFP*	this paper		≥4
unc-17 knockout	*unc-17 (e113)*	this paper	CB113	≥4
unc-25 knockout	*unc-25(e156)*	this paper	CB156	≥4

eat-4 knockout	*eat-4(ky5)*	this paper	MT6308	≥4
tdc-1 knockout	*tdc-1 (n3419)*	CGC	MT13113	≥4
tbh-1 knockout	*tbh-1(n3247)*	CGC	MT9455	≥4
cat-2 knockout	*cat-2 (n4547)*	CGC	MT15620	≥4
RIC neuron ablation	*Ex[tbh-1p::caspase-3(p12)-nz]; Ex[tbh-1p::cz-caspase-3 (p17)]; tbh-1p::GFP*	this paper		≥4
tdc-1(-) + RIML rescue	*tdc-1(n3419); Ex[gcy-13p::tdc-1]*	Kitto et al 2024	LZR259	≥4
tdc-1(-) + uv1 rescue	*tdc-1(n3419); Ex[ocr-4p::tdc-1]*	Kitto et al 2024	LZR260	≥4
neuronal enhanced RNAi uptake strain	*uIs60 [unc-119p::YFP + unc-119p::sid-1]*	CGC	TU3311	≥4
vhl-1 knockout; neuronal enhanced RNAi uptake strain	*vhl-1 (ok161); uIs60 [unc-119p::YFP + unc-119p::sid-1]*	this paper		≥4
URX, AQR, PQR ablation	*qaIs2241 [gcy-36::egl-1 + gcy-35::GFP + lin-15(+)].*	CGC	CX7102	≥4
BAG ablation	*Ex[gcy-31p::caspase-3(p12)-nz]; Ex[gcy-31p::cz-caspase-3 (p17)]; gcy-31p::GFP*	this paper		≥4
URX, AQR, PQR ablation; *hif-1* knockout; ADF::HIF-1S	*qaIs2241 [gcy-36::egl-1 + gcy-35::GFP + lin-15(+)]; hif-1(ia4); Ex[srh-142p::hif-1(P621A)]*	this paper		≥4
BAG ablation; *hif-1* knockout; ADF::HIF-1S	*Ex[gcy-31p::caspase-3(p12)-nz]; Ex[gcy-31p::cz-caspase-3 (p17)]; gcy-31p::GFP; hif-1 (ia4); Ex[srh-142p::hif-1(P621A)]*	this paper		≥4

unc-31 knockout	*unc-31 (e169)*	CGC	CB169	≥4
nlp-17 knockout	*nlp-17 (ok3461)*	CGC	RB2498	≥4

Table 3.2 Strains used in this work.

Chapter 4 Metabolic Regulation of Behavior by the Intestinal Enzyme *fmo-2*.[4]

4.1 Foreword

In Chapters 2-3, we examined the cell nonautonomous signaling pathways through which two types of environmental signals—food availability and oxygen levels—induce intestinal *fmo-2* and extend lifespan in *C. elegans*. Both of these environmental conditions (dietary restriction and hypoxia) not only extend lifespan in *C. elegans*, but also elicit acute and chronic behavioral changes across different species. Because *fmo-2* acts downstream of both pathways, and because *fmo-2* overexpression is a promising longevity intervention, we wondered whether changes in *fmo-2* expression could also result in altered behavior. To answer these questions, I developed a new project in the lab looking at behavioral differences between wild type (WT), *fmo-2* knockout, and *fmo-2* overexpressing worms. This chapter details these behavioral changes and seeks to determine whether the mechanisms through which *fmo-2* affects behavior and lifespan are overlapping or distinct. I planned and collected the majority of the data for this project, with some help performing experimental replicates from many other lab members. Dr. Leiser gave input regularly along the way, and I drafted and edited the manuscript. Overall, this work suggests a working model for *fmo-2* mediated behavioral change, but future experiments are

[4] In revision at *Science Advances* with authors listed as **Elizabeth S. Kitto**, Safa Beydoun, Ella Henry, Megan L. Schaller, Mira Bhandari, Sarah A. Easow, Angela M. Tuckowski, Marshall B. Howington, Ajay Bhat, Aditya Sridhar, Eugene Chung, Scott F. Leiser

needed to further validate this model and to investigate the effects of other longevity interventions on behavior across taxa (see Chapter 6, Future Directions).

4.2 Abstract

Many elements of an organism's behavior are completely intertwined with the health of the animal. Over a long period of time, health status is also indicative of lifespan, with improved health correlating with a longer life. However, the relationship between longevity and behavior remains relatively unexplored. Here, we report that modification of a single longevity gene downstream of dietary restriction and hypoxia, dramatically alters behavior in *Caenorhabditis elegans*. We discovered that altered expression of flavin-containing monooxygenase (*fmo-2)* leads to altered sensory perception and decision-making in a variety of behavioral paradigms. Surprisingly, many of these changes are in the same direction, as both the *fmo-2* knockout and overexpressing animals explored novel environments less than WT worms. This cell non autonomous signaling pathway is likely due to changes in tryptophan metabolism, where loss of *fmo-2* requires the tryptophan metabolite serotonin and overexpressed *fmo-2* requires the tryptophan metabolite quinolinic acid. Notably, interventions that rescue exploratory behavior also rescue some, but not all of the other behavioral, reproductive, and longevity phenotypes. Considering that *fmo-2* is a well-established responder to energy stress, these results suggest a unique mechanism for gut metabolism to communicate positive satiety signals and negative depressive signals to the organism by modifying an essential amino acid. They also establish a new role for *fmo-2* in behavior and demonstrate the importance of examining pleiotropic effects in promising longevity interventions.

4.3 Introduction

Within the last 30 years, there has been a growing interest in researching environmental and genetic factors that determine the rate of aging across taxa[370]. The ability of environmental factors to slow aging was first reported in 1935, when McCay *et al* published that caloric restriction extends lifespan in rodents[371]. In 1983, the first genetic mutants with increased lifespan were identified by Klass *et al*[17], showing it is possible to identify physiological drivers of aging and to manipulate these pathways to extend lifespan. In the ensuing decades, many physiological circuits that modify the aging process have been identified in multiple model organisms. These interventions, including dietary restriction (DR)[22], temperature stress[23,24], insulin signaling[21,25,26], and hypoxia[27,28], share a common theme in that they activate stress response pathways without damaging the organism. This concept of mild stressors activating beneficial stress response pathways to improve health and longevity is known as hormesis[30]. However, the ability of a stressor to induce a beneficial hormetic effect depends on the baseline health of the organism, the dose of the stressor, and levels of other, co-occurring environmental stressors[32].

Consequently, environmental manipulations that extend lifespan are often impractical solutions to improving healthspan on a population-wide scale. Interventions like dietary restriction (DR) and other stressors can have low compliance, are difficult to titrate to each individual, and elicit broad physiological changes that affect phenotypes other than aging[33-36]. One potential solution to these implementation problems is to activate stress-response pathways via genetic or pharmaceutical interventions. For example, DR extends lifespan across taxa through multiple mechanisms including decreased insulin and mammalian target of rapamycin (mTOR) signaling[37]. Genetic manipulations that reduce insulin and growth hormone signaling

mimic DR to extend lifespan across taxa[38-40]. Pharmaceutical interventions such as rapamycin can also mimic DR by inhibiting mTOR signaling to improve health[41]. Currently, much work is focused on identifying pro-longevity circuits downstream of environmental interventions, with the idea that targeted pharmaceutical manipulation of these pathways is a more practical solution than administering stressors like DR to human patients[42].

Similarly, genes acting downstream of multiple longevity interventions are of particular interest because they could be highly specific modulators of aging and may be more likely to extend lifespan in a diverse population. One such gene is flavin-containing monooxygenase. In *C. elegans, fmo-2* expression is required for the longevity interventions dietary restriction and hypoxia to extend lifespan, and overexpression of *fmo-2* is sufficient to extend lifespan by modifying one-carbon and tryptophan metabolism[282]. Moreover, FMOs 1) are structurally conserved from worms to humans, 2) are upregulated in multiple long-lived mouse models[109,110,372], 3) improve stress resistance in human cells when overexpressed[373], 4) are induced by multiple FDA-approved pharmaceuticals, and 5) promote healthspan in *C. elegans* and mammalian cell culture[105,230]. Together, these results make Fmos an important gene family to understand for their conserved role in health and longevity.

Genetic and pharmaceutical interventions that extend lifespan through a single gene (e.g., Fmo) are more practical and targeted than environmental longevity interventions. However, it remains unclear whether these strategies will also have pleiotropic effects on other areas of physiology such as reproduction, stress resistance, and behavior. For example, many longevity interventions decrease fertility by directing resources towards preserving somatic function over germline health[231]. Additionally, some of these interventions may extend lifespan in a highly controlled laboratory environment but reduce an organism's ability to withstand real-world

stressors like pathogens[233-235]. Acute and chronic stress exposure also has profound effects on behavior and mental state[236,237]. For example, attempts to restrict calories in humans can lead to decreased cognitive performance and dysphoria[238]. Stresses induced by other longevity interventions, like heat stress[239] and hypoxic stress[240] are also linked to negative mental health outcomes in people.

Many longevity interventions extend lifespan by acting on key metabolic tissues like the liver[271] and intestine[213]. While the role of these tissues in neurosignaling and mental state is not well understood, there is growing evidence that these tissues directly and indirectly affect the nervous system and behavior. For example, broad metabolic changes induced by a ketogenic diet have been used since the 1920s to treat epilepsy, although the mechanism of this treatment is still not fully understood[272]. Additionally, general metabolic dysfunction—characterized by elevated circulating glucose and triglycerides—is also correlated with poor mental health outcomes[273]. Lastly, a growing interest in the gut-brain axis has revealed that metabolites produced by intestinal microbes can act as neuromodulators[274-276] and alter behavior. Many canonical neurotransmitters are also synthesized in the intestine and able to cross the blood-brain barrier[277], pointing to an essential role for peripheral metabolism in neuronal activity. Consequently, it is essential to examine potential interactions between lifespan and behavior in longevity interventions that target these metabolically active tissues.

In this work, we explore how the pro-longevity gene *fmo-2* modifies *C. elegans* behavior, and whether these behavioral effects are separable from *fmo-2*'s role in longevity. We find that modifying *fmo-2* expression leads to a variety of reproductive, sensory perception, and decision-making-related behaviors in *C. elegans*. In particular, *fmo-2* expression changes result in decreased exploration of a novel environment. Our data suggest this low exploration phenotype

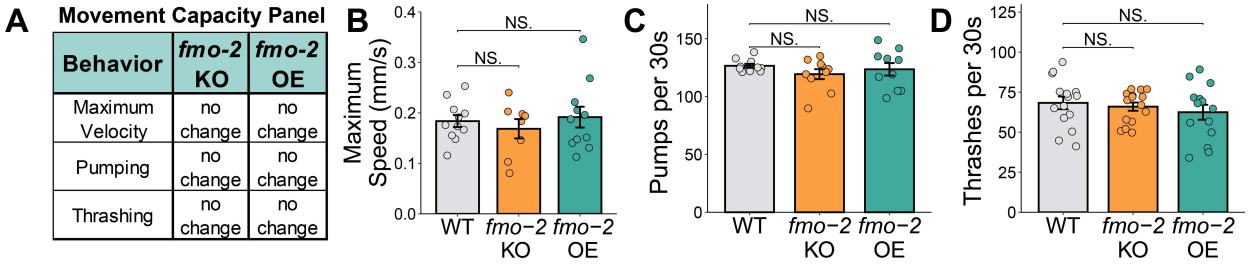
results from FMO-2's role in oxygenating tryptophan to produce N-formyl kynurenine. In *fmo-2* knockout animals, the loss of this activity pushes tryptophan metabolism towards production of the neurotransmitter serotonin. Conversely, overexpression of *fmo-2* increases tryptophan flux towards the kynurenine-derived neuromodulators quinolinic acid and kynurenic acid. In our working model, accumulation of serotonin in the *fmo-2* knockout and quinolinic acid in the *fmo-2* overexpressor leads to decreased exploration. This low-exploration phenotype can be rescued genetically by blocking serotonin synthesis or quinolinic acid production in the *fmo-2* knockout and overexpressor, respectively. Interestingly, the genetic interventions that rescue *fmo-2* mediated behavioral effects also rescue some, but not all of the other behavioral and aging-related phenotypes observed in these strains. Together, these results point toward a central role for *C. elegans* FMO-2 and tryptophan metabolism in modifying longevity and behavior that serves as an example for how longevity, metabolism and behavior can be intertwined.

4.4 Results

4.4.1 fmo-2 expression alters C. elegans sensory perception, foraging, and reproductive behavior.

To investigate how the metabolic enzyme *fmo-2* affects "mental state," we measured a panel of behaviors using strains with modified *fmo-2* expression. We initially created two panels of behavioral assays to run on wild-type (WT), *fmo-2* knockout (KO) and *fmo-2* overexpressing (OE) animals at day 1 of adulthood. The first of these panels was designed to test locomotor ability to ensure that differences in movement capacity would not interfere with measurements of more complex behaviors tested in the second panel. In our resulting data (**SFig. 4.1A**), we observed no differences in maximum speed (**SFig. 4.1B**), pumping (**SFig. 4.1C**), or thrashing

(**SFig. 4.1D**) between WT, KO, and OE animals. These results support that KO and OE animals have a similar ability to physically move in different environments during young adulthood.



Supplemental Figure 4.1 *fmo-2* knockout and overexpressing animals have normal movement capacity during young adulthood. (**A**) A summary of the movement capacity of *fmo-2* knockout and *fmo-2* overexpressing animals relative to WT. (**B**) Quantification of the maximum speed of WT, *fmo-2* knockout, and *fmo-2* overexpressing worms over a 30-minute video recording. $N \geq 8$ worms per condition. (**C-D**) Quantification of the pumping (**C**) and thrashing (**D**) rates of WT, *fmo-2* knockout, and *fmo-2* overexpressing animals. $N \geq 10$ (**C**) or $N \geq 15$ (**D**) worms per condition. In all bar plots, the top of the bar represents the mean of the population and error bars indicate standard error of the mean (SEM). In all panels, NS. = $p > 0.05$. Significance for all panels is from a one-way ANOVA and post-hoc Tukey HSD test (unpaired, two-tailed). All panels show one representative replicate. Raw data from all three replicates can be found in supplemental data files.

Having established no obvious differences in locomotor ability, we moved to a second panel of behaviors designed to assess mental state, sensory perception, and foraging decisions. Here, we observed multiple interactions between *fmo-2* expression and behavior (**Fig. 4.1A**). With respect to sensory perception, no changes were observed in responses to gentle touch (**Fig. 4.1B**) or harsh touch in either strain (**Fig. 4.1C**), indicating normal mechanosensation. Strikingly, both the KO and OE exhibited greatly reduced chemotaxis responses to both an attractive compound (diacetyl, **Fig. 4.1D**) and to an aversive compound (1-octanol, **Fig. 4.1E**). Surprisingly, these differences were not in opposite directions, as we expected from a knockout and overexpression model. Rather, both strains showed diminished responses to the attractive and aversive compounds. This decreased sensitivity to chemical attractants and repellants could indicate either a deficit in the worms' ability to detect these compounds, or a general apathy towards these chemicals. More broadly, these results suggest a novel role for an intestinal metabolic enzyme in modifying behaviors governed by multiple neural circuits.

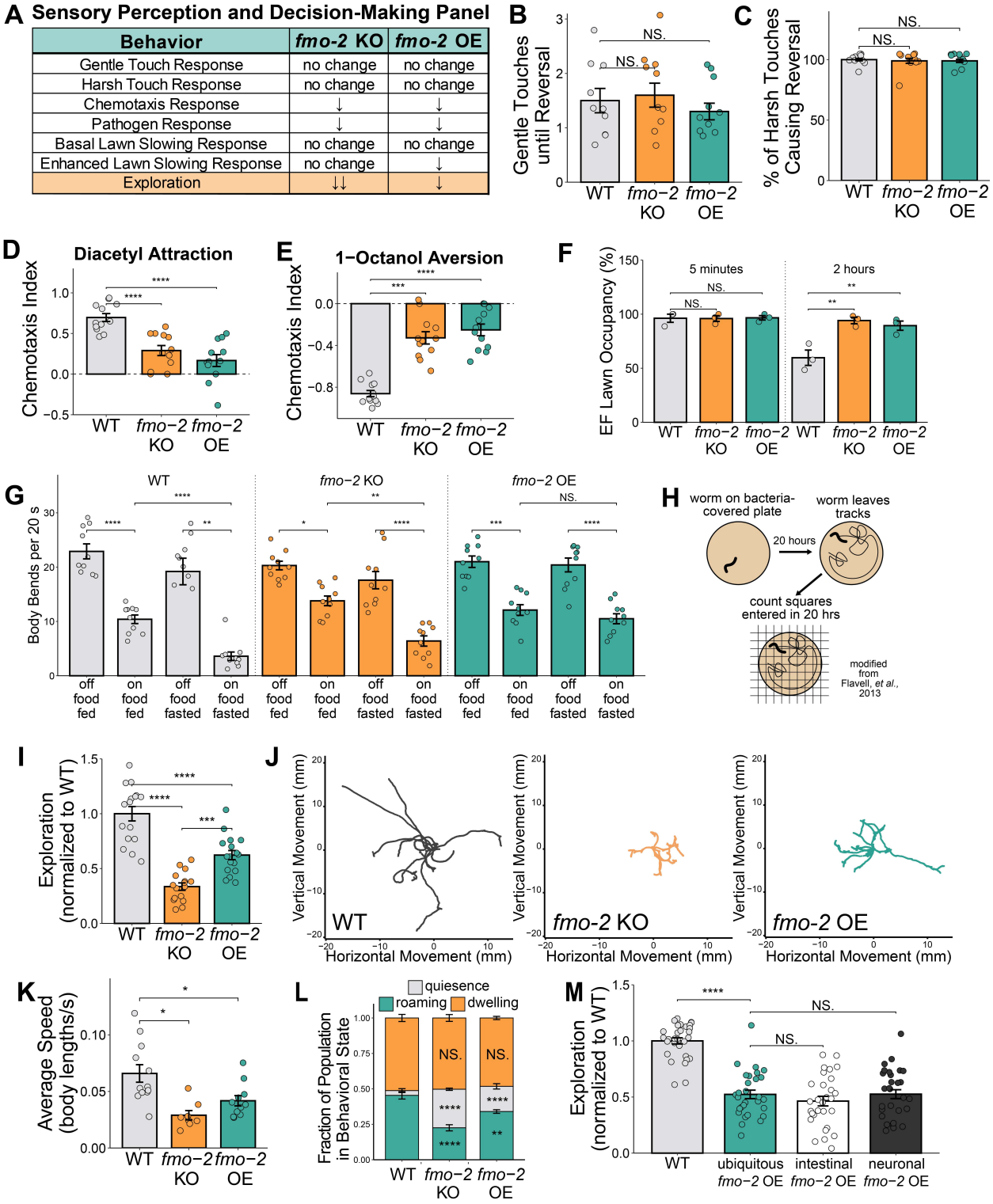


Figure 4.1 *fmo-2* expression alters *C. elegans* sensory perception, foraging, and reproductive behavior. (**A**) A summary of sensory perception and decision-making related behavioral changes in *fmo-2* knockout and *fmo-2* overexpressing worms, relative to WT controls. (**B-C**) Quantification of the gentle touch response (**B**) and harsh touch response (**C**) in WT, *fmo-2* knockout, and *fmo-2* overexpressing worms. $N = 10$ worms per condition. (**D-E**) Quantification of the chemotaxis response to the attractant diacetyl (**D**) and the repellent 1-octanol (**E**) in WT, *fmo-2* knockout, and *fmo-2* overexpressing worms. $N \geq 237$

worms per condition. (**F**) Quantification of the percent of WT, *fmo-2* knockout, and *fmo-2* overexpressing worms that remained on a pathogenic lawn of *Enterococcus faecalis* after 5 minutes and 2 hours of exposure. $N \geq 85$ worms per condition. (**G**) Quantification of the basal and enhanced slowing response in WT, *fmo-2* knockout, and *fmo-2* overexpressing worms. $N = 10$ worms per condition. (**H**) Diagram of the exploratory behavior assay. (**I**) Quantification of exploration in WT, *fmo-2* knockout, and *fmo-2* overexpressing worms. $N \geq 16$ worms per condition. (**J**) Traces of the paths WT, *fmo-2* knockout, and *fmo-2* overexpressing worms traveled over a 30-minute video. $N \geq 10$ worms per condition, and each path from a single worm was normalized to begin at point (0,0). (**K**) The average speed of worms recorded for (**J**). (**L**) Quantification of the fraction of a population of WT, *fmo-2* knockout, or *fmo-2* overexpressing worms in quiescent, roaming, and dwelling behavioral states. Significance compares each behavioral state to the fraction of the population in that state in the WT control group. $N \geq 52$ worms per condition. (**M**) Quantification of exploration of WT worms compared to ubiquitous *fmo-2* overexpressors (*eft-3p::fmo-2*), intestinal *fmo-2* overexpressors (*elt-2p::fmo-2*), and neuronal *fmo-2* overexpressors (*rab-3p::fmo-2*). In all bar plots, the top of the bar represents the mean of the population and error bars indicate standard error of the mean (SEM). In all panels, NS. = $p > 0.05$, * = $p < 0.05$, ** = $p < 0.01$, *** = $p < 0.001$, and **** = $p < 0.0001$. Significance for all panels except F and L is from a one-way ANOVA and post-hoc Tukey HSD test (unpaired, two-tailed). In panels F and L, a 2-way ANOVA was run (fraction of population ~ genotype*behavioral state (**L**) and lawn occupancy ~ genotype*timepoint (**F**)). Panels B, C, G, I, J, K, and M show one representative replicate. Raw data from all three replicates can be found in supplemental data files. Panels D, E, F, and L plot data from three replicates together. Statistics for these panels include a Bonferroni correction for multiple comparisons.

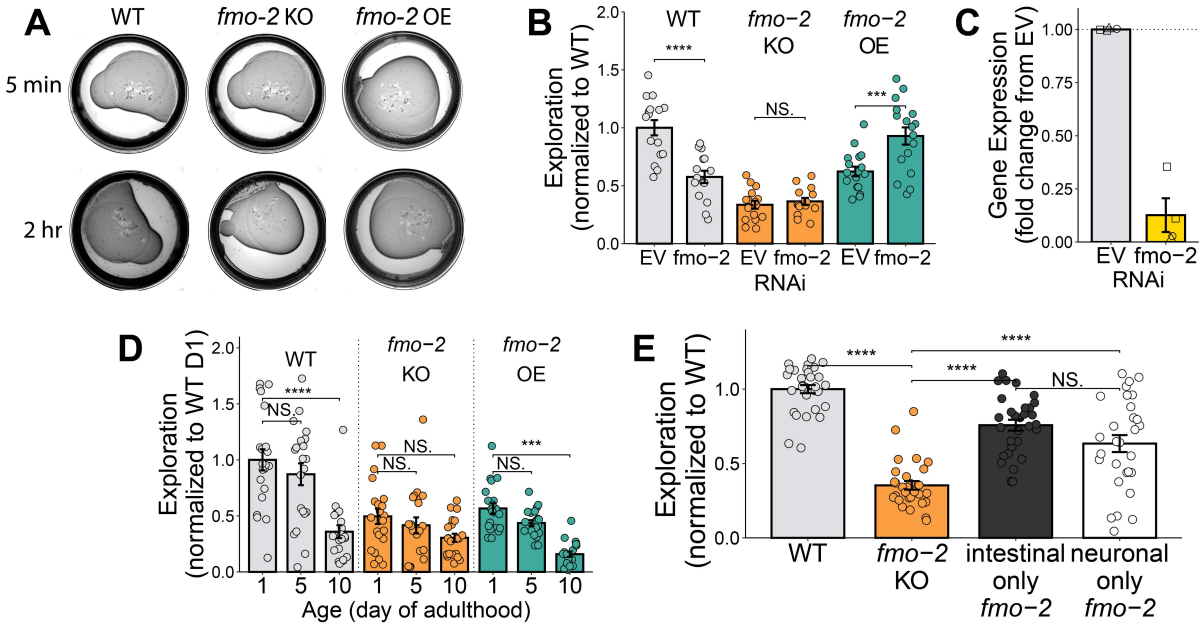
In addition to altered chemotaxis responses, we observed significant changes to foraging and decision-making behaviors. To measure a type of negative environment decision-making behavior, we performed a pathogen fleeing assay, where WT worms generally avoid a lawn of harmful bacteria[374]. In congruence with the hypothesis that these strains are apathetic to negative environments, both the *fmo-2* knockout and overexpressor show higher occupancy than WT on a lawn of pathogenic *Enterococcus faecalis* (EF) bacteria after two hours of exposure (**Fig. 4.1F**, representative images **SFig. 4.2A**). To examine foraging behavior, we assessed both typical foraging behavior and the starvation response in *C. elegans* by measuring the movement speed of the worm upon finding food[281]. The basal slowing response, which indicates the difference in movement speed of well-fed animals before and after they encounter a bacterial lawn, was unchanged between WT, KO, and OE animals, suggesting that they recognize food appropriately. However, the OE animals did not display an enhanced slowing response, which measures lawn-slowing in animals that have been fasted for 30 minutes prior to testing (**Fig. 4.1G**). This suggests that the OE animals are insensitive to the behavioral effects of brief fasting, potentially because *fmo-2* overexpression is already mimicking a chronic DR state. Together, these results indicate that changes to intestinal *fmo-2* activity are sufficient to modify an organism's perception of and/or response to positive and negative environmental signals.

Finally, we tested WT, KO, and OE worms on an assay of exploratory behavior[375]. This assay encompasses movement over time as represented by the tracks left by a single worm on a 35 mm diameter plate completely covered with bacterial food. At the end of the exploration period, the worm is removed and the plate with its tracks is overlayed with a grid of squares. The number of squares the worm entered are counted to quantify the region of the plate explored by the worm (**Fig. 4.1H**). In this exploration assay, we observed a 47% decrease in exploration in the OE relative to WT, and an even more pronounced 62% decrease in exploration in the KO (**Fig. 4.1I**). To validate this low-exploration phenotype using another method, we next recorded worm movement on 35 mm plates completely covered in a bacterial lawn and quantified mean speed over 30 minutes. We observed that the paths taken by the *fmo-2* knockouts and overexpressors as well as their mean speed correlated with the changes observed in the initial exploration assay: both *fmo-2* mutants stayed closer to their point of origin than WT worms and displayed lower mean speed over the 30-minute period (**Fig. 4.1J-K**). This result, coupled with the behavioral results discussed above, suggests that animals with modified expression of *fmo-2* exhibit substantial changes in response to environmental cues despite a normal ability to move. These changes result in a decreased behavioral response regardless of the direction of *fmo-2* (KO or OE), consistent with a complex mechanism of action.

In order to identify the mechanism of these behavioral changes, we chose to primarily focus on exploratory behavior for three reasons: 1) there is a significant difference between the phenotype of the KO and OE; 2) there is a robust change in exploration in both strains; and 3) this behavior reflects both sensory perception of the environment and decision-making in response to these cues. To begin interrogating how *fmo-2* expression modifies exploration, we first examined the amount of time a worm spends in three distinct behavioral states: quiescence,

roaming, and dwelling[376]. Quiescence has been equated to a sleep-like state, where worms do not move at all. Dwelling worms exhibit a local-search foraging pattern, where they turn frequently and stay in one area. Roaming worms turn infrequently and explore more widely from their point of origin. We observed decreased roaming and increased quiescence in both the KO and OE but saw no changes in dwelling behavior. This shift from roaming to quiescence was greater in KO, which could explain the decrease in KO exploration relative to the OE (**Fig. 4.1L**). These results indicate that *fmo-2* expression changes exploration by shifting behavioral state rather than globally decreasing movement, again pointing to a more nuanced mechanism of action.

To further test the relationship between *fmo-2* expression and low exploration, we performed RNAi knockdown of *fmo-2* on WT, KO, and OE animals (**SFig. 4.2B**). *fmo-2* RNAi did indeed decrease exploration in WT worms, but to a lesser extent than fully knocking out *fmo-2*. Successful knockdown with *fmo-2* RNAi was validated with qPCR (**SFig. 4.2C**). As expected, *fmo-2* RNAi had no effect on the KO. Interestingly, *fmo-2* RNAi did partially rescue the low exploration of the OE, supporting the idea that high *fmo-2* expression is responsible for its low-exploration phenotype. Together, these results support a 'goldilocks' model for *fmo-2* expression in behavior, where a limited window of expression results in normal exploration.



Supplemental Figure 4.2 The effects of *fmo-2* expression on exploratory behavior persist through mid-adulthood and both neural and intestinal *fmo-2* expression contribute to changes in exploratory behavior. (**A**) Representative images of pathogenic lawn occupancy, quantified in (**Fig. 1F**). (**B**) Exploration of WT, *fmo-2* knockout, and *fmo-2* overexpressing animals on empty vector (EV) or *fmo-2* RNAi. $N \geq 16$ worms per condition. (**C**) Gene expression of *fmo-2* in worms raised on *fmo-2* RNAi compared to control worms raised on empty vector (EV) RNAi for two generations. $N \geq 200$ worms per replicate, or 800 worms per condition. (**D**) Quantification of the exploration of WT, *fmo-2* knockout, and *fmo-2* overexpressing worms at days 1, 5, and 10 of adulthood. $N \geq 21$ worms per condition. (**E**) Exploration of WT, *fmo-2* knockout, intestinal *fmo-2* rescue (*fmo-2(ok2147); elt-2p::fmo-2*), and neuronal *fmo-2* rescue (*fmo-2(ok2147); rab-3p::fmo-2*) strains. $N \geq 29$ worms per condition. In all bar plots, the top of the bar represents the mean of the population and error bars indicate standard error of the mean (SEM). In all panels, NS. = $p > 0.05$, * = $p < 0.05$, ** = $p < 0.01$, *** = $p < 0.001$, and **** = $p < 0.0001$. Significance for all panels is from a one-way (panel E) or two-way (panels B,C,D) ANOVA and post-hoc Tukey HSD test (unpaired, two-tailed). All panels show one representative replicate except for panel C, which includes all replicates. Raw data from three individual replicates for each experiment can be found in supplemental data files.

We next tested the specificity of the low exploration phenotype. To test for age-specificity, we aged WT, KO, and OE worms to middle age and measured their exploratory behavior. We observed a significant decrease in exploration with age in WT and OE, but not in KO worms (**SFig. 4.2D**). To measure tissue-specificity, we examined the sufficiency of *fmo-2* OE in individual tissues. Because *fmo-2* is primarily an intestinal enzyme but behavior is primarily governed by the nervous system, we measured the exploratory behavior of neuronal-specific and intestinal-specific *fmo-2* overexpressors. We found that overexpression in either tissue was sufficient to decrease exploratory behavior (**Fig. 4.1M**). Conversely, to examine the necessity of *fmo-2* in each tissue for normal exploratory behavior, we re-expressed *fmo-2* under a

neuronal or an intestinal specific promoter in the *fmo-2* null background. This approach led to strains with *fmo-2* expression absent only in the intestine or in the nervous system, respectively. We observed a significant rescue of exploratory behavior in in both strains. (**SFig. 4.2E**). Together, these results are consistent with a mechanism in which *fmo-2* activity in either tissue changes metabolism in a way that modifies neural signaling and, in turn, alters behavior. Specifically, FMO-2 could either produce or limit a behavior modulating molecule, across the lifespan, and within multiple tissues.

4.4.2 fmo-2 expression interacts with tryptophan metabolism to alter exploratory behavior.

Given that intestinal *fmo-2* over- and under-expression can modify both behavior and longevity, we next sought to establish the specificity of and substrate(s) responsible for these effects. To test for specificity, we asked whether modifying the expression of other flavin-containing monooxygenases with similar activities could also change exploration. We tested the behavior of *fmo-1* or *fmo-4* KO and OE because they are structurally the most similar to FMO-2. Interestingly, we found that fmo-*1* and *fmo-4* KO and OE worms exhibited normal exploratory behavior (**Fig. 4.2B**), suggesting the behavioral role is specific to FMO-2. Upon testing the three enzymes for substrate specificity, we found that FMO-1 and FMO-4 act on many of the same substrates as FMO-2, with the notable exception of tryptophan, which is specific to *C. elegans* FMO-2 (**Fig. 4.2A**). These data are consistent with a model in which altered oxygenation of tryptophan, the only identified substrate unique to FMO-2, may be responsible for the behavioral effects of *fmo-2* expression.

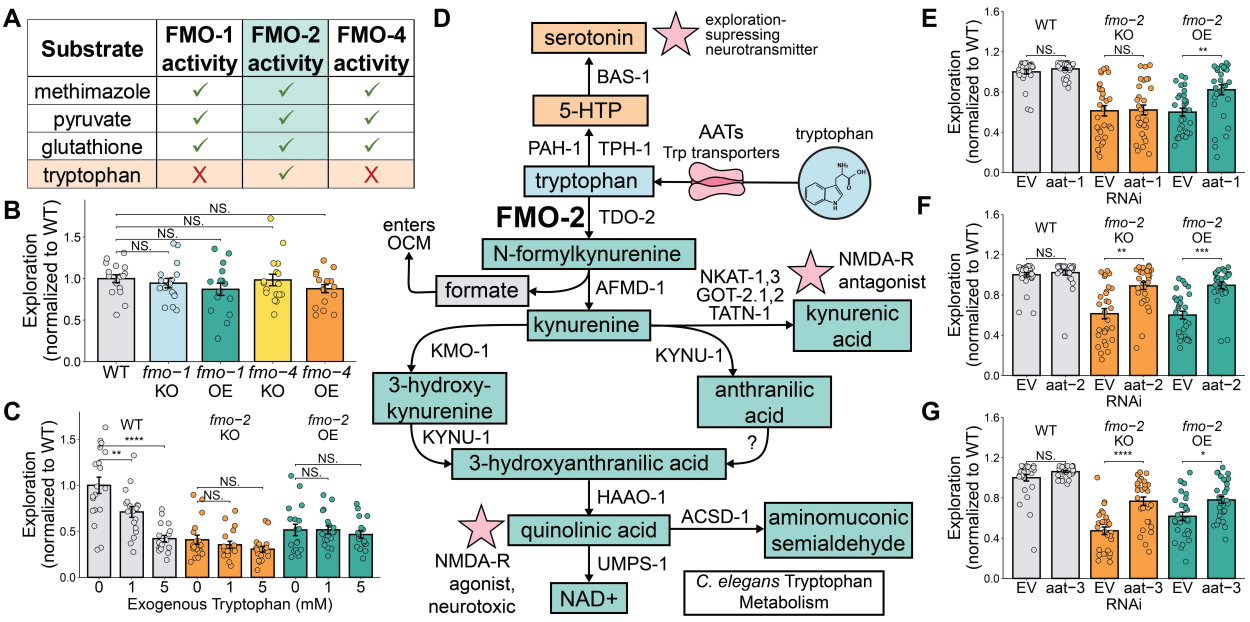
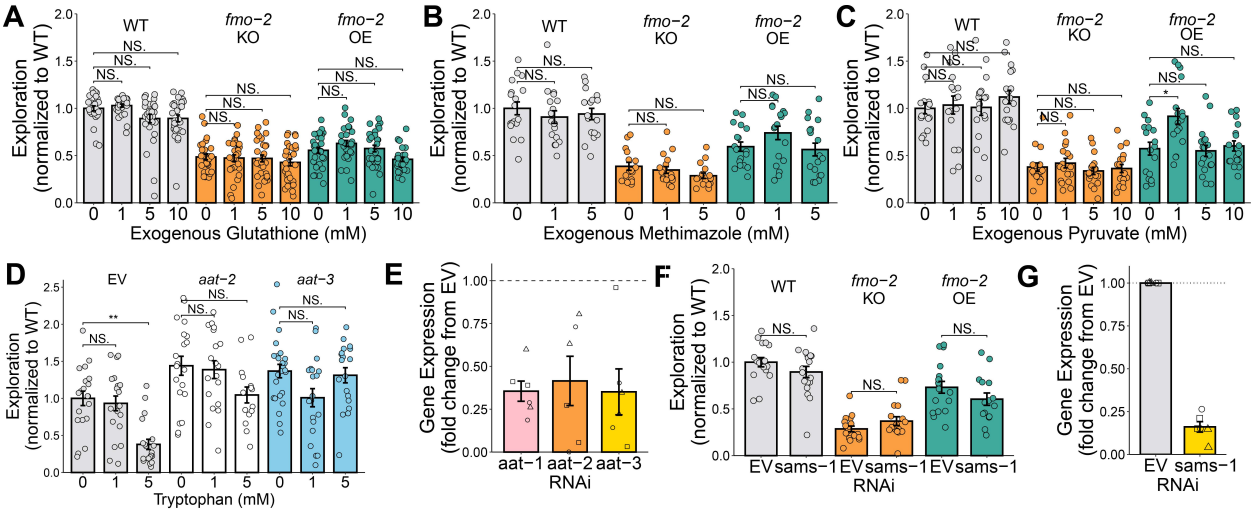


Figure 4.2 *fmo-2* expression interacts with tryptophan metabolism to alter exploratory behavior. (**A**) A summary of the enzymatic activities of *C. elegans* FMO-1, FMO-2, and FMO-4 on the substrates methimazole, pyruvate, glutathione, and tryptophan. K_{cat} and K_m values can be found in the supplemental data files. (**B**) Quantification of the exploration of *fmo-1* knockout *(ok405), fmo-1* overexpressing (*eft-3p::fmo-1*), *fmo-4* knockout (*ok294*), and *fmo-4* overexpressing (*eft-3p::fmo-4*) worms. $N \geq 16$ worms per condition. (**C**) Exploration of WT, *fmo-2* knockout, and *fmo-2* overexpressing worms after supplementation from egg on plates with 0, 1, or 5 mM tryptophan in the agar. $N \geq 18$ worms per condition. (**D**) A diagram of tryptophan uptake and metabolism in *C. elegans.* (**E-G**) Quantification of the exploration of WT, *fmo-2* knockout, and *fmo-2* overexpressing worms on empty vector (EV) or *aat-1* (**E**), *aat-2* (**F**), and *aat-3* (**G**) RNAi. $N \geq 29$ (**E**), ≥ 27 (**F**), ≥ 29 (**G**) worms per condition. In all bar plots, the top of the bar represents the mean of the population and error bars indicate standard error of the mean (SEM). In all panels, NS. = $p > 0.05$, * = $p < 0.05$, ** = $p < 0.01$, *** = $p < 0.001$, and **** = $p < 0.0001$. Significance for all panels is from a one-way (panel B) or two-way (panels C,E,F,G) ANOVA and post-hoc Tukey HSD test (unpaired, two-tailed). All panels show one representative replicate. Raw data from all three replicates can be found in supplemental data files.

Consequently, we sought to determine whether FMO-2's activity on tryptophan or on any other individual substrate is involved in *fmo-2* mediated behavioral change. To test whether the behavioral changes of *fmo-2* KO and OE are specific to tryptophan and or any other known FMO-2 substrates, we measured the effects of supplementing each established FMO-2 substrate on exploration. We found that only tryptophan supplementation dose dependently decreased WT exploration (**Fig. 4.2C**), with no significant effect from glutathione, methimazole, or pyruvate (**SFig. 4.3A-C**). Notably, the reduction in exploration observed in *fmo-2* KO and OE worms was not additive with the decrease caused by exogenous tryptophan, suggesting that altered tryptophan metabolism through *fmo-2* affects exploratory behavior via the same mechanism (**Fig. 4.2C**). These data indicate a specific role for the highly-conserved amino acid tryptophan in *fmo-*

2 mediated behavioral change.



Supplemental Figure 4.3 Supplementation with glutathione, methimazole, and pyruvate do not modify exploration, knocking down *aat-2* and *aat-3* blocks tryptophan-mediated decreases in exploration, and *sams-1* does not interact with *fmo-2* to modify exploration. (**A-C**) Exploration of WT, *fmo-2* knockout, and *fmo-2* overexpressing worms after supplementation from egg with glutathione (**A**), methimazole (**B**), and pyruvate (**C**). $N \geq 29$ (**A**), ≥ 21 (**B**), and ≥ 20 (**C**) worms per condition. (**D**) Exploration of WT worms raised on empty vector (EV), *aat-2*, and *aat-3* RNAi on 0, 1, and 5 mM tryptophan from egg. $N \geq 25$ worms per condition. (**E**) Gene expression of *aat-1*, *aat-2*, and *aat-3* in worms raised on *aat-1, aat-2,* and *aat-3* RNAi compared to control worms raised on empty vector (EV) RNAi for two generations. $N \geq 200$ worms per replicate, or 1200 worms per condition. (**F**) Exploration of WT, *fmo-2* knockout, and *fmo-2* overexpressing worms on empty vector (EV) or *sams-1* RNAi. $N \geq 17$ worms per condition. (**G**) Gene expression of *sams-1* in worms raised on *sams-1* RNAi compared to control worms raised on empty vector (EV) RNAi from L3 stage. $N \geq 200$ worms per replicate, or 1200 worms per condition. In all bar plots, the top of the bar represents the mean of the population and error bars indicate standard error of the mean (SEM). In all panels, NS. = $p > 0.05$, * = $p < 0.05$, ** = $p < 0.01$, *** = $p < 0.001$, and **** = $p < 0.0001$. Significance for all panels is from a two-way ANOVA and post-hoc Tukey HSD test (unpaired, two-tailed). All panels except E and G show one representative replicate. Raw data from all three replicates can be found in supplemental data files. Panels E and G shows all replicates plotted together.

To confirm that tryptophan uptake is required for exogenous tryptophan supplementation to decrease exploration, we grew WT worms on RNAi against the two best-validated *C. elegans* tryptophan transporters (**Fig. 4.2D**), *aat-2* and *aat-3*[377,378]. We observed that worms with either transporter knocked down were resistant to the behavioral effects of exogenous tryptophan (**SFig. 4.3D**), suggesting that tryptophan uptake into cells is required for decreased exploration. This indicates a metabolic mechanism of action, rather than behavioral change resulting from sensory perception of amino acid(s) in the environment.

Having established that tryptophan supplementation is sufficient to decrease exploration in WT worms, we next asked whether tryptophan was necessary for low exploration in the KO

and OE. To reduce tryptophan uptake, we again used RNAi to knockdown AATs with high similarity to mammalian homologues—*aat-1, aat-2,* and *aat-3*[377]. We observed that knockdown of all three AATs tested partially rescued the exploratory behavior of the OE (**Fig. 4.2E-G**), while *aat-2* and *aat-3* knockdown partially rescued the KO (**Fig. 4.2F-G**). Interestingly, AAT-1 also transports the tryptophan metabolite kynurenic acid[378], suggesting a potential role for kynurenic acid in the decreased exploration of the *fmo-2* OE but not the KO. All RNAi knockdowns were validated with qPCR for expression of the targeted gene (**SFig. 4.3E**). These data indicate that tryptophan uptake is at least partially required for *fmo-2* expression to modify exploration.

We next asked how *fmo-2* expression interacts with tryptophan metabolism to modify exploration. Previous work from our lab found that FMO-2 oxygenates tryptophan to form N-formyl-kynurenine *in vitro*. N-formyl-kynurenine is then converted into kynurenine by formidase (*afmd-1*), which also releases formate as a byproduct (**Fig. 4.2D**). This formate can enter the folate cycle, potentially altering the flux of the One Carbon Metabolism (OCM) cycle and modifying lifespan[282]. To test whether *fmo-2* modifies behavior indirectly through this interaction with OCM, we used RNAi to knock down *sams-1* and decrease SAM synthesis. We observed no change in exploration after *sams-1* knockdown (**SFig. 4.3F-G**), indicating that the behavioral effects of *fmo-2* are more likely directly related to tryptophan metabolism rather than OCM. Again, these results suggest that 1) tryptophan metabolites likely play a key role in *fmo-2* mediated behavioral change, and 2) the mechanisms of *fmo-2* mediated longevity and behavioral change may be separable.

4.4.3 Knocking out fmo-2 suppresses exploratory behavior by modifying serotonin signaling.

Having ruled out changes in OCM as a mechanism of *fmo-2* mediated behavioral change, we asked whether the accumulation or depletion of any tryptophan-derived metabolites could lead to low exploration in these strains. Based on the role of *fmo-2* in the tryptophan metabolism pathway (**Fig. 4.2D**), we hypothesized that knocking out *fmo-2* may increase tryptophan flux towards serotonin, which is known to decrease exploration[375]. To test whether *fmo-2* expression modifies serotonin production, we crossed the KO and OE with a transcriptional reporter for *tph-1*, the rate-limiting enzyme in neuronal serotonin synthesis from tryptophan[343]. We observed a 40% increase in *tph-1* expression in the KO and no change in *tph-1* expression in the OE (**Fig. 4.3A-B**). *tph-1* is expressed in two pairs of neurons in the head (ADF and NSM), and one pair of neurons near the vulva (HSN) that contribute to egg laying[343]. When the fluorescence intensity of *tph-1* was measured in individual serotonergic neurons, we again did not observe any changes in the OE (**SFig. 4.4A-C**). However, the KO displayed increased *tph-1* expression in the NSM but not in the ADF or HSN neurons (**SFig. 4.4D-F**). Interestingly, the NSM acts as a key signal in multiple foraging-related behavioral circuits[281,298,379]. Serotonin production in the NSM, but not the ADF and HSN, has also been shown to increase quiescent behavior at the expense of roaming behavior[380], as is observed in the *fmo-2* knockout worms (**Fig. 4.1L**). These data are consistent with higher serotonin production in the KO and no change in serotonin production in the OE.

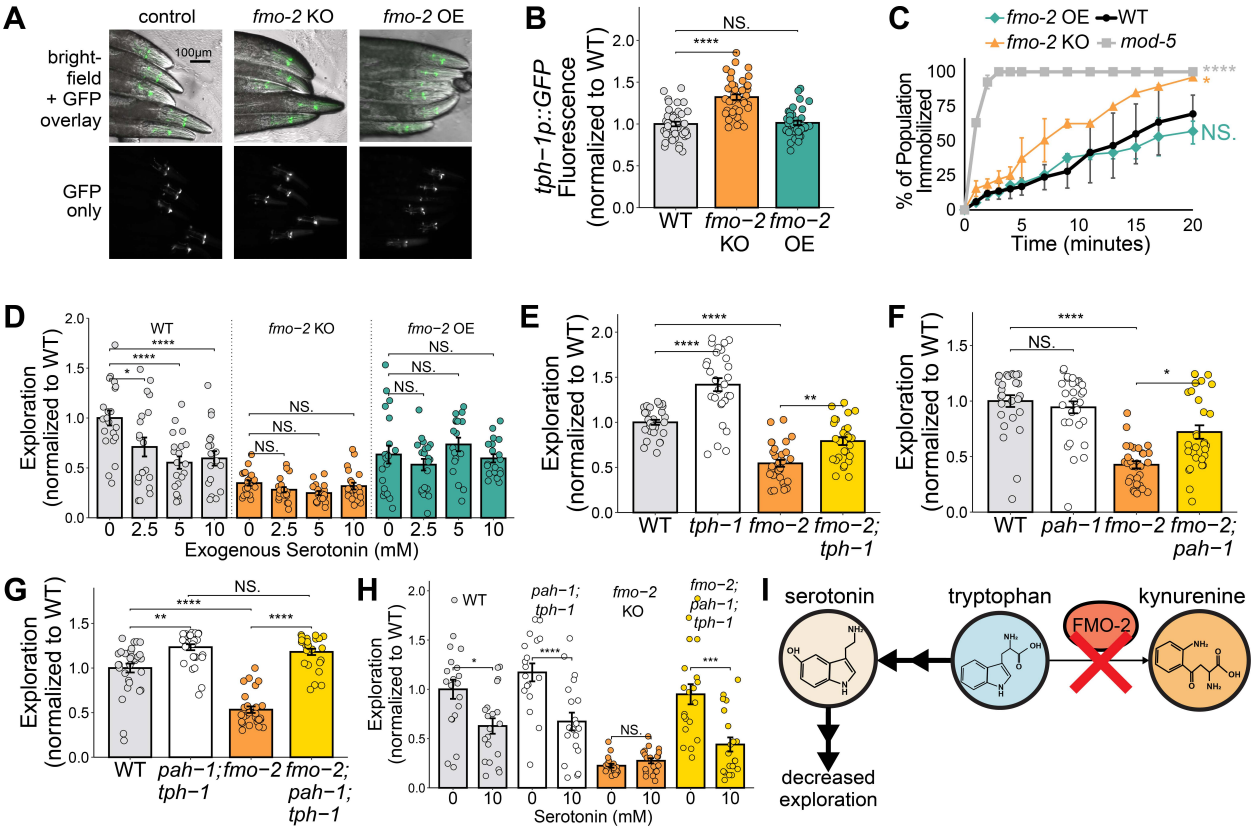
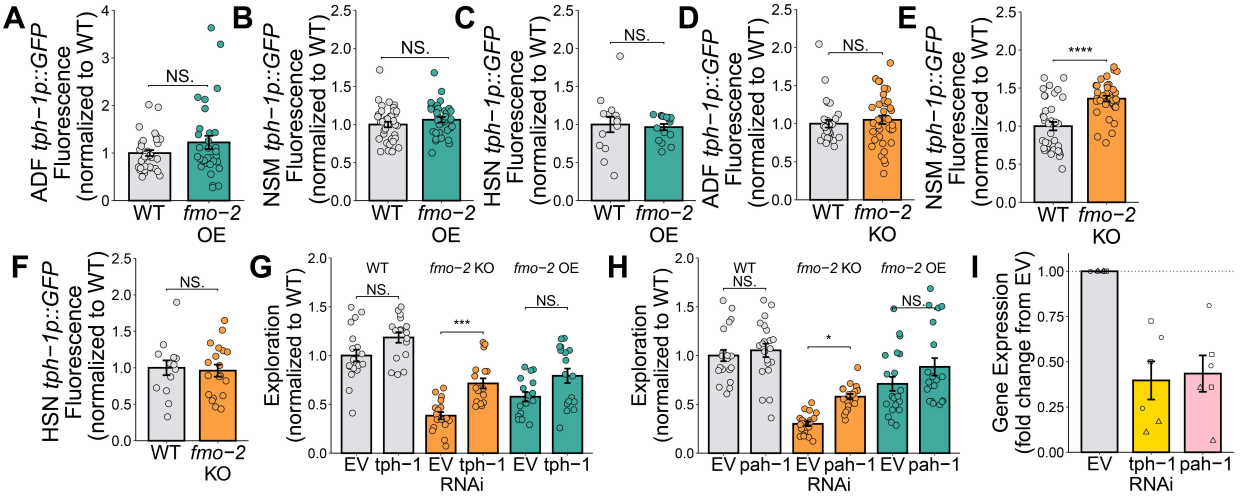


Figure 4.3 Knocking out *fmo-2* suppresses exploratory behavior by modifying serotonin signaling. (**A-B**) Representative images (**A**) and quantification of mean head fluorescence (**B**) of *zdls13 (tph-1p::GFP), fmo-2(ok2147); zlds13(tph-1p::GFP),* and *fmo-2* overexpressor *(eft-3p::fmo-2); zdls13 (tph-1p::GFP). N* ≥ 23 worms per condition. (**C**) Quantification of the immobilization of WT, *fmo-2* knockout, *fmo-2* overexpressor, and *mod-5(n3314)* in 30 M serotonin in M9 buffer over a 20-minute period. *N* ≥ 128 worms per genotype. (**D**) Exploration of WT, *fmo-2* knockout, and *fmo-2* overexpressing worms on 0, 2.5, 5, and 10 mM exogenous serotonin from egg. *N* ≥ 18 worms per condition. (**E**) Exploration of WT, *tph-1(mg280)*, *fmo-2(ok2147),* and *tph-1(mg280); fmo-2(ok2147)* worms. *N* ≥ 28 worms per condition. (**F**) Exploration of WT, *pah-1(syb3601)*, *fmo-2(ok2147),* and *pah-1(syb3601)*; *fmo-2(ok2147)* worms. *N* ≥ 28 worms per condition. (**G**) Exploration of WT, tph-1(mg280); *pah-1(syb3601)*, *fmo-2(ok2147),* and *tph-1(mg280); pah-1(syb3601)*; *fmo-2(ok2147)* worms. *N* ≥ 27 worms per condition. (**H**) Exploration of WT, *tph-1(mg280); pah-1(syb3601)*, *fmo-2(ok2147),* and *tph-1(mg280); pah-1(syb3601)*; *fmo-2(ok2147)* worms on 0 or 10 mM exogenous serotonin from egg. *N* ≥ 19 worms per condition. (**I**) Working model of the mechanism through which *fmo-2* knockout decreases exploration. In all bar plots, the top of the bar represents the mean of the population and error bars indicate standard error of the mean (SEM). In all panels, NS. = $p > 0.05$, * = $p < 0.05$, ** = $p < 0.01$, *** = $p < 0.001$, and **** = $p < 0.0001$. Significance for all panels is from a one-way (panels B, C, E, F, G) or two-way (panels D,H) ANOVA and post-hoc Tukey HSD test (unpaired, two-tailed). All panels show one representative replicate. Raw data from all three replicates can be found in supplemental data files.

Since increased transcription of *tph-1* does not necessarily lead to higher levels of serotonin, we further examined whether the behavioral changes mediated by *fmo-2* are linked to altered serotonin. To test the likelihood of high serotonin in the KO, we performed a serotonin immobilization assay in which worms are placed in a high concentration (30 M) serotonin solution. Worms with high baseline levels of extrasynaptic serotonin, like the serotonin reuptake

transporter knockout *mod-5*, are immobilized faster than WT in this assay[381]. We observed that the KO was indeed immobilized faster than WT, while immobilization of the OE did not differ from WT (**Fig. 4.3C**). These results suggest the KO has elevated extrasynaptic serotonin availability while the OE does not. Consequently, the low exploration of the OE cannot be explained by altered serotonin availability, but the low exploration of the KO could be due to increased serotonin signaling.



Supplemental Figure 4.4 Knocking out f*mo-2* increases *tph-1p::GFP* fluorescence in the NSM neurons and knocking down *tph-1* or *pah-1* partially rescues the exploration of the *fmo-2* knockout. (**A-C**) Quantification of the mean fluorescence of *tph-1p::GFP* in a WT and *fmo-2* overexpressing background in the (**A**) ADF, (**B**) NSM, and (**C**) HSN neurons. $N \geq 29$ (**A**), ≥ 28 (**B**), and ≥ 22 (**C**), neurons per condition. (**D-F**) Quantification of the mean fluorescence of *tph-1p::GFP* in a WT and *fmo-2* knockout background in the (**D**) ADF, (**E**) NSM, and (**F**) HSN neurons. $N \geq 33$ (**D**), ≥ 36 (**E**), and ≥ 19 (**F**), neurons per condition. (**G**) Exploration of WT, *fmo-2* knockout, and *fmo-2* overexpressing worms on empty vector (EV) or *tph-1* RNAi. $N \geq 17$ worms per condition. (**H**) Exploration of WT, *fmo-2* knockout, and *fmo-2* overexpressing worms on empty vector (EV) or *pah-1* RNAi. $N \geq 24$ worms per condition. (**I**) Gene expression of *tph-1* and *pah-1* in worms raised on *tph-1* and *pah-1* compared to control worms raised on empty vector (EV) RNAi for two generations. $N \geq 200$ worms per replicate, or 1200 worms per condition. In all bar plots, the top of the bar represents the mean of the population and error bars indicate standard error of the mean (SEM). In all panels, NS. = $p > 0.05$, * = $p < 0.05$, ** = $p < 0.01$, *** = $p < 0.001$, and **** = $p < 0.0001$. Significance in panels G and H is from a one-way (panel J) or two-way (panels G, H) ANOVA and post-hoc Tukey HSD test (unpaired, two-tailed). Significance for panels A-F is from a Wilcox test (two-tailed, unpaired). All panels show one representative replicate panel I, which shows all replicates together. Raw data from individual three replicates can be found in supplemental data files.

To confirm whether increased serotonin availability is sufficient to suppress exploration and that the low exploration of the OE is not driven by flux of tryptophan away from serotonin, we supplemented WT, KO, and OE worms with exogenous serotonin. Exogenous serotonin decreased WT exploration, but did not alter the exploration of the KO and OE (**Fig. 4.3D**). These

data suggest that high serotonin is not additive with low *fmo-2* in decreasing exploration. Additionally, the inability of serotonin supplementation to rescue the OE indicates that low serotonin is not likely causing the OE's behavioral change.

After finding that supplementing WT worms with exogenous serotonin is sufficient to phenocopy the low exploration of the KO, we next sought to test the necessity of serotonin signaling in the KO's low exploration phenotype. To test the necessity of serotonin, we first used RNAi to knockdown *tph-1* or *pah-1* expression in WT, KO, and OE animals. Like mammals, *C. elegans* produce serotonin in neurons and in peripheral tissues such as the intestine. Neuronal serotonin production requires *tph-1*, while peripheral serotonin production requires *pah-1*^{382}. Blocking *tph-1* partially rescued the exploratory behavior of the KO, and we observed an insignificant trend towards increased exploration in WT and OE worms on *tph-1* RNAi ($p = 0.16$ and $p = 0.09$, respectively) (**SFig. 4.4G**). *pah-1* knockdown had no effect on exploration in the WT or OE animals, but also partially rescued the exploration of the KO (**SFig. 4.4H**). Both RNAi knockdowns were qPCR validated (**SFig. 4.4I**). Together, these data indicate that decreasing serotonin synthesis in either the nervous system or in peripheral tissues partially reverses the effects of *fmo-2* KO on exploration. This again supports a model in which global metabolic changes driven by *fmo-2* expression modify neurotransmitter production to alter behavior.

To confirm our RNAi knockdown data, we knocked out either *tph-1*, *pah-1*, or both in the *fmo-2* KO background. Again, we observed that knocking out each gene partially rescued the exploration of the *fmo-2* KO (**Fig. 4.3E-F**). However, when we knocked out both *tph-1* and *pah-1* in the *fmo-2* KO background, we observed a complete rescue of exploratory behavior to the level of the *pah-1; tph-1* control (**Fig. 4.3G**). Moreover, the exploration of *fmo-2; pah-1; tph-1*

was reversed back towards baseline *fmo-2* knockout exploration levels by supplementation with exogenous serotonin (**Fig. 4.3H**), suggesting *pah-1; tph-1* knockout directly mediates KO exploration via serotonin availability. Together, these data suggest a model in which knocking out *fmo-2* increases serotonin production in neurons and/or in the intestine, which consequently lowers exploration (**Fig. 4.3I**). This model reflects a novel role for Fmos in modulating a highly conserved neurotransmitter with broad impacts on health and behavior.

4.4.4 Increased quinolinic acid lowers exploratory behavior in the fmo-2 overexpressor.

We next sought to interrogate the mechanism of tryptophan-mediated behavioral change in the OE. Because the OE did not display decreased *tph-1* expression and was not rescued by exogenous serotonin, we wondered whether *fmo-2* OE could instead increase flux towards kynurenine-derived metabolites that decrease exploration. To test this hypothesis, we used RNAi to knockdown all genes involved in tryptophan-kynurenine metabolism. WT, KO, and OE worms were grown on either empty vector (EV) or *tdo-2*, *afmd-1*, *nkat-1, nkat-3, tatn-1, got-2.1, got-2.2, kmo-1, kynu-1, haao-1, acsd-1,* or *umps-1* RNAi for two generations and then their exploratory behavior was measured. Successful knockdown of each gene was confirmed via qPCR (**SFig. 4.5A**). The first hit from this RNAi screen was *tdo-2*, a gene that acts in the same step as *fmo-2* in *C. elegans* tryptophan metabolism (**Fig. 4.2D**). Interestingly, *tdo-2* knockdown did not alter WT or KO exploration but did partially rescue the OE (**Fig. 4.4A**). This finding is consistent with a model in which increased TDO-2 and/or FMO-2 activity pushes tryptophan towards the kynurenine pathway which decreases exploration. Consequently, knocking down *tdo-2* partially compensates for *fmo-2* overexpression to rescue exploratory behavior.

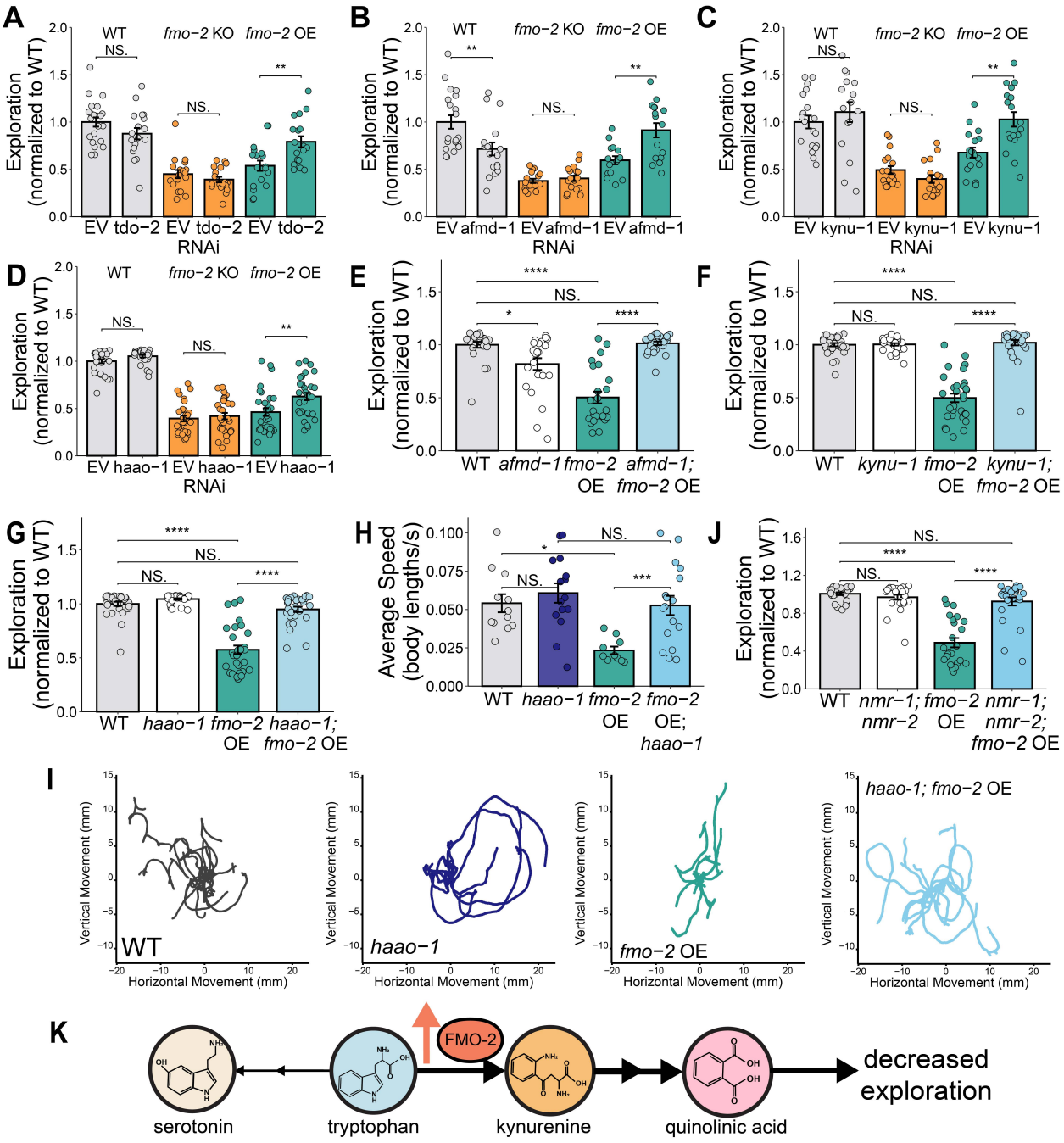
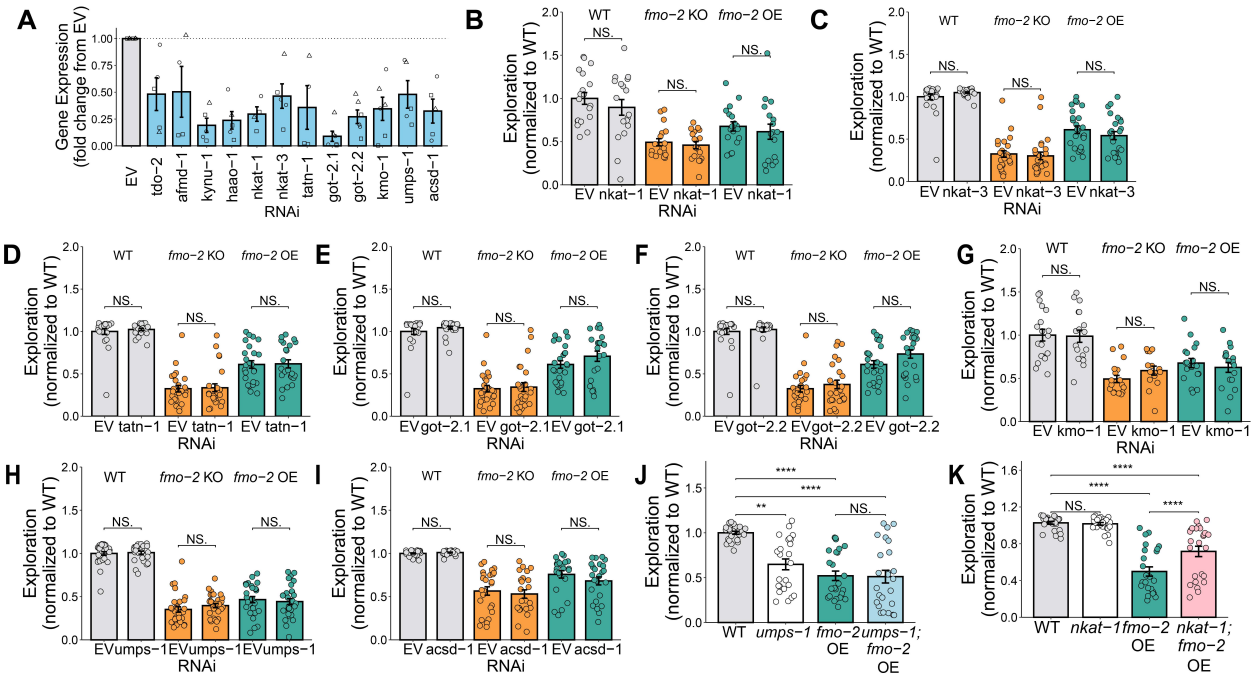


Figure 4.4 The kynurenine metabolites quinolinic and kynurenic acid contribute to exploratory behavior changes in the *fmo-2* overexpressor. (**A-D**) Exploration of WT, *fmo-2* knockout, and *fmo-2* overexpressing worms on empty vector (EV) or (**A**) *tdo-2*, (**B**), *afmd-1*, (**C**), *kynu-1*, and (**D**) *haao-1* RNAi. $N \geq 18$ (**A**), ≥ 16 (**B**), ≥ 16 (**C**), and ≥ 29 (**D**) worms per condition. (**E**) Exploration of WT, *afmd-1(tm4547)*, *fmo-2* overexpressor, and *afmd-1(tm4547); fmo-2* overexpressor worms. $N \geq 24$ worms per condition. (**F**) Exploratory behavior of WT, *kynu-1(tm4924)*, *fmo-2* overexpressor, and *kynu-1(tm4924); fmo-2* overexpressor worms. $N \geq 30$ worms per condition. (**G**) Exploration of WT, *haao-1(tm4627)*, *fmo-2* overexpressor, and *haao-1(tm4627); fmo-2* overexpressor worms. $N \geq 28$ worms per condition. (**H-I**) The average speed (**H**) and paths traveled (**I**) over a 30-minute video recording. $N \geq 10$ worms per condition, and each path from a single worm was normalized to begin at point (0,0). (**J**) Exploration of WT, *nmr-1(ak4); nmr-2(ok3324)*, *fmo-2* overexpressor, and *nmr-1(ak4); nmr-2(ok3324); fmo-2* overexpressor worms. $N \geq 24$ worms per condition. (**K**) Working model of how *fmo-2* overexpression decreases exploratory behavior. In all bar plots, the top of the bar represents the mean of the population and error bars indicate standard error of the mean (SEM). In all panels, NS. = $p > 0.05$, * = $p < 0.05$, ** = $p < 0.01$, *** = $p < 0.001$, and **** = $p <$

0.0001. Significance in panels A-H and J is from a one-way (panels E-H and J) or two-way (panels A-D) ANOVA and post-hoc Tukey HSD test (unpaired, two-tailed). All panels show one representative replicate. Raw data from all three replicates can be found in supplemental data files.

Downstream of *fmo-2* and *tdo-2* (**Fig. 4.2D**), we identified three knockdowns that partially rescued the exploratory behavior of the OE: *afmd-1, kynu-1, and haao-1* (**Fig. 4.4B-D**), while the remaining genes had no effect on behavior (**SFig. 4.5B-I**). Because *afmd-1* knockdown partially rescued OE exploration, it is likely that a buildup of kynurenine or kynurenine metabolites is responsible for the *fmo-2* overexpressor behavior, rather than a buildup of N-formylkynurenine, the direct product of FMO-2 oxygenating tryptophan[48]. Interestingly, *afmd-1* knockdown also blunted exploration in WT, and had no effect on the KO (**Fig. 4.4B**). The second knockdown to partially rescue OE exploration was *kynu-1*, suggesting that kynurenic acid and 3-hydroxykynurenine are unlikely to be responsible for the OE's low-exploration phenotype. The third and final RNAi knockdown to partially rescue the *fmo-2* overexpressor was *haao-1*, which converts 3-hydroxykynurenic acid to quinolinic acid (**Fig. 4.4C**). Quinolinic acid can then be made into NAD+ by *umps-1* or into aminomuconic semialdehyde by *acsd-1*. Neither *umps-1* nor *acsd-1* knockdown rescued the *fmo-2* overexpressor (**SFig. 4.5H-I**), indicating that decreasing quinolinic acid synthesis is sufficient to rescue the *fmo-2* overexpressor. Taken together, the RNAi knockdown screen supports a model in which *fmo-2* OE increases quinolinic acid which in turn decreases exploration.



Supplemental Figure 4.5 Additional data from the tryptophan metabolism RNAi knockdown and knockout screen. (**A**) Gene expression of *tdo-2, afmd-1, kynu-1, haao-1, nkat-1, nkat-3, tatn1, got-2.1, got-2.2, kmo-1, umps-1,* and *acsd-1* in worms raised on each RNAi compared to control worms raised on empty vector (EV) RNAi for two generations. $N \geq 200$ worms per replicate, or 800 worms per condition. (**B-I**) Exploration of WT, *fmo-2* knockout, and *fmo-2* overexpressor worms on empty vector (EV) or (**B**) *nkat-1*, (**C**) *nkat-3*, (**D**) *tatn-1*, (**E**) *got-2.1*, (**F**) *got-2.2*, (**G**) *kmo-1*, (**H**) *umps-1*, and (**I**) *ascd-1* RNAi. $N \geq 17$ (**B**), ≥ 24 (**C**), ≥ 23 (**D**), ≥ 22 (**E**), ≥ 25 (**F**), ≥ 16 (**G**), ≥ 27 (**H**), and ≥ 23 (**I**) worms per condition. (**J**) Exploration of WT, *umps-1(zu456)*, *fmo-2* overexpressor, and *umps-1(zu456); fmo-2* overexpressor worms. $N \geq 24$ worms per condition. (**K**) Exploration of WT, *nkat-1(ok585)*, *fmo-2* overexpressor, and *nkat-1(ok585); fmo-2* overexpressor worms. $N \geq 25$ worms per condition. In all bar plots, the top of the bar represents the mean of the population and error bars indicate standard error of the mean (SEM). In all panels, NS. = $p > 0.05$, * = $p < 0.05$, ** = $p < 0.01$, *** = $p < 0.001$, and **** = $p < 0.0001$. Significance in all panels is from a one-way (panels K-J) or two-way (panels B-I) ANOVA and post-hoc Tukey HSD test (unpaired, two-tailed). All panels show one representative replicate panel A, which shows all replicates together. Raw data from individual three replicates can be found in supplemental data files.

Since knockdown of *afmd-1*, *kynu-1,* and *haao-1* only partially rescued the behavior of the OE, we validated our results using genetic knockouts. We found that knocking out *afmd-1* slightly decreased WT exploration, but rescued *fmo-2* OE exploration to the level of *afmd-1* alone (**Fig. 4.4E**). Knocking out either *kynu-1* or *haao-1* fully rescued the *fmo-2* OE without affecting WT exploration (**Fig. 4.4F-G**). *haao-1; fmo-2* OE worms also displayed similar movement patterns and average speed to WT worms over a 30-minute video recording (**Fig. 4.4H-I**). The ability of these kynurenine metabolism enzyme knockouts to completely rescue the *fmo-2* OE indicates the kynurenine-derived neuromodulator quinolinic acid is required for this strain's low exploration.

We also used genetic knockouts to confirm our negative data from *umps-1* and *nkat-1* RNAi. The *fmo-2* OE was crossed into an *umps-1* knockout background because NAD plays a role in energy balance and longevity pathways[383,384], and we wanted to test whether altered energy availability might drive changes in exploration. However, crossing the OE into an *umps-1* knockout strain also failed to rescue exploration (**SFig. 4.5J**). In fact, loss of *umps-1* in WT animals decreased exploration, further supporting a model where quinolinic acid production suppresses exploration. Much like with the *fmo-2* KO, the role of *fmo-2* OE in regulating neuromodulator availability implicates metabolically active tissues as important drivers of neural signaling and behavioral state.

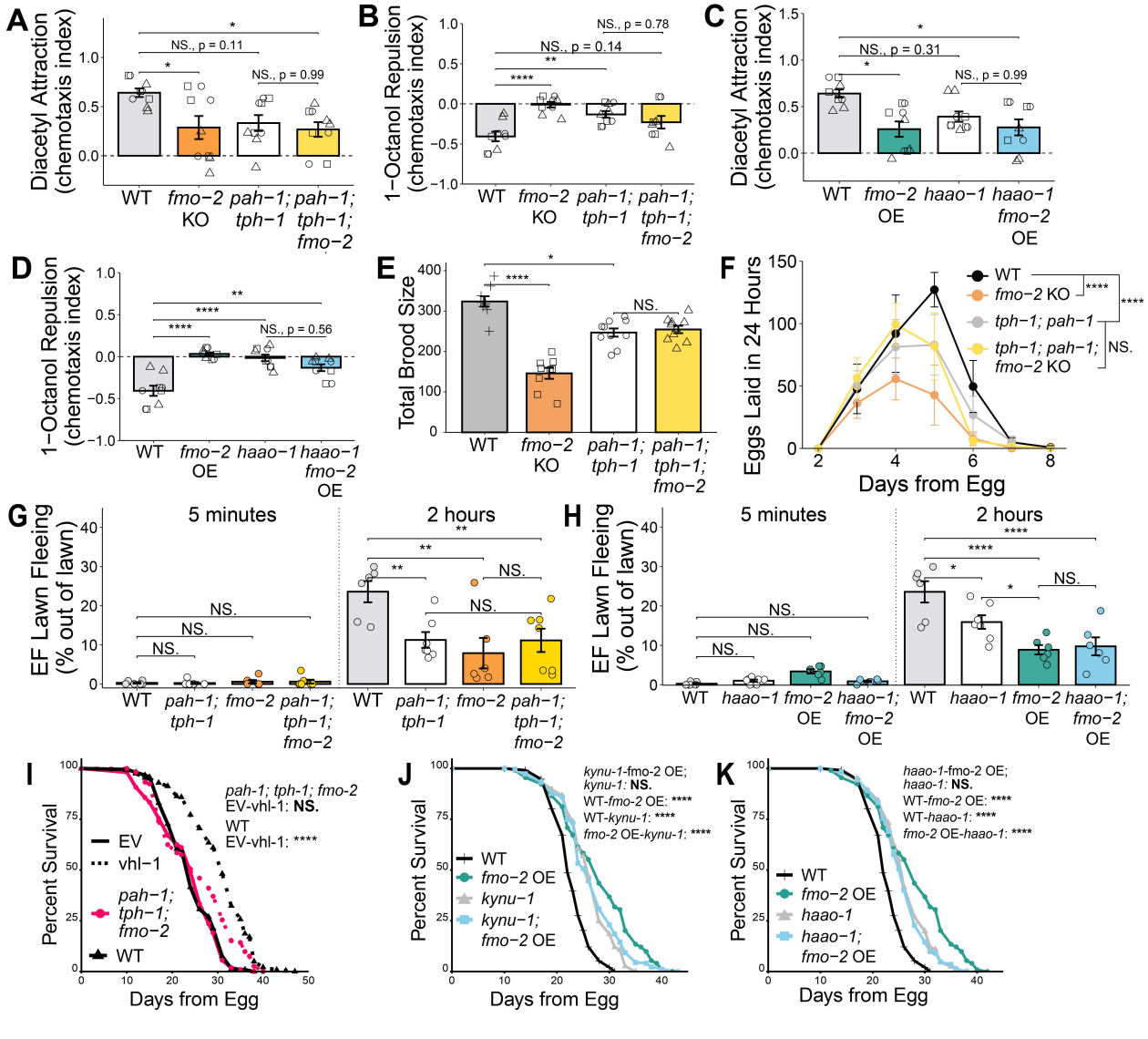
The *haao-1* and *umps-1* knockout data indicate that quinolinic acid is necessary for the low exploration of the OE and sufficient to decrease exploration in WT. However, we were surprised to see that blocking kynurenic acid production through knockdown of *nkat-1, nkat-3, tatn-1, got-2.1,* or *got-2.2* had no effect on exploratory behavior, considering that kynurenic acid plays a role in *C. elegans* feeding behavior[385] (**SFig. 4.5B-F**). To confirm this result, we also crossed the *fmo-2* OE into an *nkat-1* null background. *nkat-1* was chosen over the other kynurenic acid synthesis genes because *nkat-1* is expressed in the nervous system and is known to modify other behaviors in *C. elegans*[378,386]. Interestingly, we observed a bimodal distribution in the exploration of the *fmo-2* OE; *nkat-1* worms. Approximately half of these animals were not affected by *nkat-1* knockout, while the other half of the population was rescued by blocking neuronal kynurenic acid synthesis (**SFig. 4.5K**). This result could suggest that the buildup of kynurenic acid is responsible for the decreased exploration in some, but not all OE worms. However, it is also possible that knocking down two or more of these genes simultaneously would be required to prevent kynurenic acid buildup and rescue exploration in all OE animals.

Having established a role for quinolinic and kynurenic acid in the low exploration of the *fmo-2* OE, we next examined the shared receptor of these two neuromodulators, glutamatergic NMDA receptors. Quinolinic acid agonizes NMDA receptors, which can lead to excitotoxicity of NMDA receptor-expressing neurons. In contrast, kynurenic acid is a competitive inhibitor at the glutamatergic binding site in NMDA receptors. *C. elegans* only have one NMDA receptor, a heterotetramer of the *nmr-1* and *nmr-2* subunits[387,388]. Since both quinolinic acid synthesis kynurenic acid synthesis affected exploration in *fmo-2* OE animals, it is imperative to better understand their roles. We overexpressed *fmo-2* in an *nmr-1; nmr-2* null background and measured exploratory behavior. We observed that knocking out the NMDA receptor completely rescues the exploration of *fmo-2* overexpressors (**Fig. 4.4J**), supporting a model in which quinolinic acid buildup drives glutamatergic neuron excitotoxicity that decreases exploration in *fmo-2* OE (**Fig. 4.4K**). In this scenario, blocking kynurenic acid synthesis through *nkat-1* knockout could rescue some animals by either 1) leading to downregulation of the NMDA receptor, or 2) through eliminating the effects of high kynurenic acid at other receptor types to increase exploration via a different mechanism. These data indicate a complicated role for *fmo-2* expression in altering kynurenine metabolism to modify neurosignaling and behavior.

4.4.5 The mechanisms through which fmo-2 expression effects exploratory behavior, other behaviors, and longevity are partially but not completely overlapping.

After determining that blocking serotonin production rescues KO animal exploration and blocking quinolinic acid synthesis rescues OE animals, we wondered if these manipulations could also rescue the other behavioral changes observed in these strains (**Fig. 4.1**). To answer this question, we first measured the chemotaxis responses of *fmo-2; pah-1; tph-1* and *haao-1; fmo-2* OE to attractive and repellant compounds. We found that blocking serotonin production

decreased attraction to diacetyl (**Fig. 4.5A**) and reduced repulsion from 1-octanol (**Fig. 4.5B**) independently of *fmo-2*. All three strains showed a similarly reduced chemotaxis response to the attractant diacetyl (**Fig. 4.5A**). However, knocking out *pah-1* and *tph-1* in the *fmo-2* KO background did rescue the KO response to 1-octanol to the level of the *pah-1; tph-1* strain (**Fig. 4.5B**). We also measured the chemotaxis responses of *haao-1* and *haao-1; fmo-2* OE. *haao-1* exhibited a decreased response to both the attractant and the repellant to a degree similar to the *fmo-2* OE. Consequently, knocking out *haao-1* did not rescue the chemotaxis behavior of the OE (**Fig. 4.5C-D**). These data suggest that modifying multiple points in the tryptophan metabolism pathway, through the activity of *fmo-2* or other key enzymes, is sufficient to modify behavioral outcomes.



L

restores phenotype to WT?

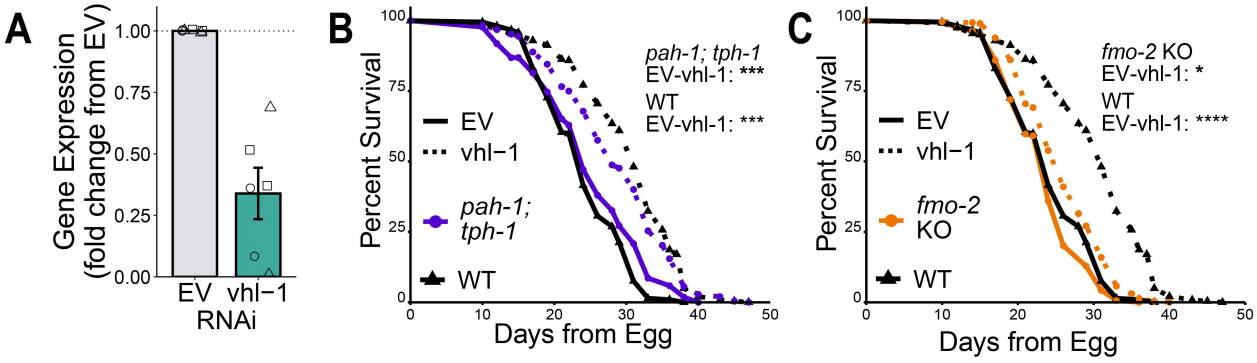
Intervention	explo-ration	brood size	mean velocity	chemo-taxis	pathogen fleeing	lifespan
↓ 5-HT in *fmo-2* KO	✓	✓	X	X	X	X
↓ QA in *fmo-2* OE	✓	NA	✓	X	X	~

Figure 4.5 The mechanisms through which *fmo-2* expression affects exploratory behavior, other behaviors, and longevity are partially but not completely overlapping. (**A-B**) Quantification of the chemotaxis response to the attractant diacetyl (**A**) and the repellent 1-octanol (**B**) in WT, *tph-1(mg280); pah-1(syb3601)*, *fmo-2(ok2147),* and *tph-1(mg280); pah-1(syb3601)*; *fmo-2(ok2147)* worms. $N \geq 400$ worms per condition. (**C-D**) Quantification of the chemotaxis response to the attractant diacetyl (**C**) and the repellent 1-octanol (**D**) in WT, *haao-1(tm4627)*, *fmo-2* overexpressor, and *haao-1(tm4627); fmo-2* overexpressor worms. $N \geq 590$ worms per condition. (**E-F**) Quantification of total brood size (**E**) and eggs laid each day of the reproductive lifespan (**F**) in WT, *pah-1(syb3601)*; *tph-1(mg280), fmo-2(ok2147),* and *pah-1(syb3601); tph-1(mg280)*; *fmo-2(ok2147)* worms. $N \geq 7$ worms per condition. (**G**) Quantification of the percent of WT, *pah-1(syb3601)*; *tph-1(mg280), fmo-2(ok2147),* and *pah-1(syb3601); tph-1(mg280)*; *fmo-2(ok2147)* worms that remained on a pathogenic lawn of *Enterococcus faecalis* after 5 minutes and 2 hours of exposure. $N \geq 350$ worms per condition. (**H**) Quantification of the percent of WT, *haao-*

1(tm4627), *fmo-2* overexpressor, and *haao-1(tm4627); fmo-2* overexpressor worms that remained on a pathogenic lawn of *Enterococcus faecalis* after 5 minutes and 2 hours of exposure. $N \geq 350$ worms per condition. (**I**) Survival curve of WT and *tph-1(mg280); pah-1(syb3601)*; *fmo-2(ok2147)* worms on empty vector (EV) or *vhl-1* RNAi. $N \geq 229$ worms per condition. (**J**) Survival curve of WT, *kynu-1(tm4924)*, *fmo-2* overexpressor, and *kynu-1(tm4924); fmo-2* overexpressor worms. $N \geq 226$ worms per condition. (**K**) Survival curve of WT, *haao-1(tm4627)*, *fmo-2* overexpressor, and *haao-1(tm4627); fmo-2* overexpressor worms. $N \geq 226$ worms per condition. (**L**) A summary of the behavioral and aging-related phenotypes that were rescued by blocking serotonin synthesis in *fmo-2* knockout worms or by blocking quinolinic acid synthesis in *fmo-2* overexpressing animals. In all bar plots, the top of the bar represents the mean of the population and error bars indicate standard error of the mean (SEM). In all panels, NS. = $p > 0.05$, * = $p < 0.05$, ** = $p < 0.01$, *** = $p < 0.001$, and **** = $p < 0.0001$. Significance in panels A-F is from a one-way ANOVA and post-hoc Tukey HSD test (unpaired, two-tailed). Significance in panels G-H is from a two-way ANOVA (lawn occupancy~genotype*timepoint) and post-hoc Tukey HSD test (unpaired, two-tailed). Significance in panels I-K is from a log-rank test comparing median survival. Panels E-F show one representative replicate. Raw data from all three replicates can be found in supplemental data files. Panels A-D and G-K plot data from three replicates together. Statistics for these panels include a Bonferroni correction for multiple comparisons.

To further test whether tryptophan metabolism is a common mechanism of *fmo-2* mediated behavioral and physiological change, we looked at reproductive egg laying behavior in the *fmo-2* KO and the *fmo-2; pah-1; tph-1* strains. Previous work on the role of *fmo-2* in *C. elegans* shows that knocking out *fmo-2* decreases brood size, or reproductive capacity, while overexpressing *fmo-2* has no effect[48]. Much like in the chemotaxis assay, *pah-1; tph-1* displayed decreased brood size relative to WT. Interestingly, knocking out *tph-1* and *pah-1* in the *fmo-2* KO background rescued the brood size of the KO to the level of *pah-1; tph-1* (**Fig. 4.5E-F**). These results indicate that the mechanism through which *fmo-2* KO alters exploration and reproduction may partially overlap. However, this was not the case for pathogen fleeing behavior. As previously observed, both the KO and OE were less likely to flee a pathogenic lawn of *E. faecalis* than WT worms. Similarly to our chemotaxis response results, the modifications to tryptophan metabolism that rescued *fmo-2* KO and OE exploration (*pah-1; tph-1* knockout and *haao-1* knockout, respectively), resulted in decreased pathogen fleeing independently of *fmo-2* expression. Consequently, these interventions did not rescue the pathogen response behavior of the KO or OE (**Fig. 4.5G-H**). Overall, these data suggest that the kynurenine metabolic pathway has multiple distinct mechanisms, including *fmo-2* OE, where modulation of this pathway affects behavior. However, altered serotonin signaling may contribute to both the reproduction and exploration phenotypes of the KO.

To test how behavior and longevity are linked, we asked whether the mechanism of *fmo-2*-mediated behavioral changes is distinct from *fmo-2* mediated effects on longevity. *fmo-2* is required for hypoxia to extend lifespan in *C. elegans*[48]. Because high serotonin drives behavioral changes in the *fmo-2* knockout, we asked whether high serotonin is also the reason that *fmo-2* KO is not long-lived under hypoxia. To answer this question, we examined the lifespan of *pah-1; tph-1*, and *fmo-2; pah-1; tph-1* on empty vector (EV) and *vhl-1* RNAi, a hypoxia mimetic. Successful RNAi knockdown was validated with qPCR (**SFig. 4.6A**). We found that the lifespans of both WT and *pah-1; tph-1* worms were extended by *vhl-1* RNAi (**SFig. 4.6B**), but that *fmo-2* KO and *fmo-2; pah-1; tph-1* lifespans were no longer extended by *vhl-1* RNAi (**SFig. 4.6C, Fig. 4.5I**). This is consistent either with *fmo-2* acting downstream of serotonin signaling in hypoxia-mediated longevity, or with *fmo-2* affecting hypoxia-mediated longevity through a serotonin-independent mechanism. Importantly, this result also indicates that the effects of *fmo-2* KO on exploratory behavior and on longevity are separable.



Supplemental Figure 4.6 *vhl-1* RNAi extends lifespan in WT and *pah-1; tph-1* but this effect is partially blocked by *fmo-2* knockout. (**A**) Gene expression of *vhl-1* in worms raised on *vhl-1* RNAi compared to control worms raised on empty vector (EV) RNAi for two generations. $N \geq 200$ worms per replicate, or 1200 worms per condition. (**B**) Survival curve of WT and *pah-1(syb3601); tph-1(mg280)* worms on empty vector (EV) or *vhl-1* RNAi. $N \geq 229$ worms per condition. (**C**) Survival curve of WT and *fmo-2(ok2147)* worms on empty vector (EV) or *vhl-1* RNAi. $N \geq 197$ worms per condition. In all panels, NS. = $p > 0.05$, * = $p < 0.05$, ** = $p < 0.01$, *** = $p < 0.001$, and **** = $p < 0.0001$. Significance in panels B-C is from a log-rank test comparing median survival on EV to *vhl-1* RNAi for each genotype. All panels plot data from three replicates together. Statistics for these panels include a Bonferroni correction for multiple comparisons.

While *fmo-2* activity is required for environmental interventions like hypoxia to extend lifespan, overexpression of *fmo-2* is also sufficient to extend lifespan in *C. elegans*[48]. To test

whether the longevity phenotype of the *fmo-2* overexpressor is separable from the low exploration phenotype, we measured the lifespan of *fmo-2* OE in the *kynu-1* knockout or *haao-1* knockout backgrounds. Notably, work from the Sutphin lab found that both *kynu-1* and *haao-1* knockouts are long-lived due to a buildup of the kynurenine-derived metabolite 3-hydroxyanthranilic acid (3HAA), which activates the oxidative stress response[389]. We find that both *kynu-1* and *haao-1* extended lifespan relative to WT but were not as long-lived as the *fmo-2* OE (**Fig. 5I-K**). Interestingly, lifespans of *kynu-1; fmo-2* OE and *haao-1; fmo-2* OE were not different from *kynu-1* or *haao-1* alone, but shorter-lived than the *fmo-2* OE (**Fig. 5J-K**). Consequently, rescuing the exploratory behavior of the *fmo-2* OE does mitigate the longevity benefits of *fmo-2* OE, but does not suppress lifespan to the level of WT worms. Together, these findings highlight 1) the complex interplay between behavior and longevity; and 2) the essential role of tryptophan metabolism in both the behavioral and lifespan effects of *fmo-2*.

Overall, these data indicate that maintaining regular flux through tryptophan metabolism—either through the activity of FMO-2 or other key enzymes—is essential for typical behavioral and aging-related outcomes. FMO-2 plays a critical role in this metabolic pathway, as knocking out *fmo-2* modifies exploratory behavior and brood size requiring serotonin signaling. However, manipulations that restore some elements of WT-like behavior in the *fmo-2* KO, like blocking serotonin synthesis, disrupt the balance of tryptophan metabolism in other ways, leading to distinct behavioral effects (**Fig. 4.5L**). Similarly, the effects of *fmo-2* OE on exploratory behavior can be rescued by blocking quinolinic acid synthesis, but this intervention also modifies tryptophan metabolism in a manner that has consequences on chemotaxis and pathogen fleeing behaviors (**Fig. 4.5L**). Finally, many of these changes to tryptophan metabolism through *fmo-2* and other pathway components interact with longevity as well as multiple

behaviors. Ideally, this circuit could be manipulated in a way where healthspan and lifespan are extended but WT-like behaviors are preserved. The closest intervention to meeting this goal may be the long-lived *haao-1; fmo-2* OE worms, which maintain some of the longevity benefits of *fmo-2* OE but display normal exploratory behavior. Together, these results provide a promising start in optimizing metabolic pathways for both health and behavioral goals, but also highlight the additional work needed to untangle the effects of longevity interventions on behavioral and other physiological adaptations.

4.5 Discussion

In this work, we establish multiple behavioral changes that occur in response to modified expression of the longevity gene *fmo-2* in *C. elegans* (**Fig. 4.1**). Notably, we do not observe opposite behavioral effects of *fmo-2* KO and OE, as one might expect from a knockout and overexpression model. Taken together, our data suggest a model in which altering *fmo-2* expression in either direction decreases exploratory behavior by changing flux through tryptophan metabolism (**Fig. 4.2**). In the case of the *fmo-2* KO, tryptophan that would normally be oxygenated into *N*-formyl-kynurenine is instead diverted towards increased serotonin synthesis. Elevated serotonin is sufficient to decrease exploration in WT worms and blocking serotonin production is sufficient to fully rescue the exploratory behavior of the KO (**Fig. 4.3**). In contrast, the OE increases flux of tryptophan towards kynurenine-derived metabolites including the NMDA receptor agonist quinolinic acid. Blocking any gene required for quinolinic acid synthesis and knocking out the NMDA receptor itself is sufficient to rescue exploratory behavior in *fmo-2* OE worms (**Fig. 4.4**). After identifying manipulations to the tryptophan metabolism pathway that can rescue the exploratory behavior of the KO and OE, we tested whether these manipulations also rescue other behavioral and longevity phenotypes of each strain.

Interestingly, we found that knocking out and overexpressing *fmo-2* affects multiple behaviors and longevity through partially overlapping and partially distinct mechanisms (**Fig. 4.5**). Collectively, our data indicate a broad role for *C. elegans fmo-2* in multiple areas of physiology, including behavior and longevity.

Previous work on flavin-containing monooxygenases in *C. elegans* and in mammalian models has primarily focused on the role of FMOs in the immune response[390,391], endogenous metabolism[372,373,392,393], and more recently in health and longevity[48,230,282,394]. However, *C. elegans fmo-2* was recently identified in a screen for genes required for aversion-resistant ethanol seeking behavior[395]. Moreover, two environmental conditions that induce *fmo-2*, hypoxia[396] and dietary restriction[397] have also been found to modify behavioral responses in *C. elegans*. FMOs have also been proposed to play a role in neurodegeneration in mammals[372,398]. In this work, we identify multiple behavioral responses that require *fmo-2*, suggesting a broad role for FMOs in mental state and behavior.

Notably, the behavioral effects of both knocking out and overexpressing *fmo-2* interact with tryptophan metabolism. We were initially surprised to find that knocking out *fmo-2* could be sufficient to modify serotonin synthesis, given that other enzymes such as *tdo-2* can also metabolize tryptophan into *N*-formyl-kynurenine. However, *C. elegans tdo-2* is primarily expressed in the hypodermis whereas *fmo-2* is lowly expressed in the nervous system and highly expressed in the intestine[399]. This could suggest that tryptophan metabolism can have varied effects on behavior in different tissues. Additionally, only about 1-2% of tryptophan is thought to be metabolized into serotonin and other non-kynurenine metabolites[400], suggesting a small change in tryptophan availability could lead to amplified changes in levels of trace neuromodulators like serotonin. More work in this area is needed to understand both the tissue-

specific effects of altered tryptophan metabolism and in understanding the movement of tryptophan-derived metabolites between tissues.

A growing body of research has also linked dysregulated tryptophan metabolism and elevated quinolinic acid with depression, schizophrenia, and neurodegeneration[400-403]. These investigations of the relationship between kynurenine metabolites and mental state often focus on the activity of indoleamine dioxygenases (IDOs) and tryptophan dioxygenases (TDOs) in this pathway. However, the finding that *fmo-2* overexpression can drive this type of dysregulated tryptophan metabolism suggests a potentially overlooked role for FMOs in mental state. Previous work from our lab has found that tryptophan is also an *in vitro* substrate of mammalian Fmo5[282], suggesting the effects of *C. elegans* FMO-2 on tryptophan metabolism could be translatable to mammalian models. Much like *C. elegans fmo-2*, mammalian Fmo5 is lowly expressed in brain tissue[404] and highly expressed in the liver and intestine in mice and humans[405].

In addition to highlighting a novel role for FMOs in mental state, this work indicates the importance of considering pleiotropic effects of potential longevity interventions. Much like *fmo-2* overexpression, many other genetic and pharmaceutical longevity interventions target stress-response pathways that coordinate broad physiological changes across multiple tissues[31,406]. While it is relatively common to measure the effects of new longevity interventions on movement and reproductive capacity[231,232,314,407], other more nuanced changes in behavior are not often examined. Future work should measure the effects of promising longevity interventions on a greater variety of behavioral assays to determine which interventions are most specific to aging and whether additional concurrent interventions may be required to mitigate negative behavioral effects. Overall, additional work is needed to 1) better understand the role of FMOs in mental state, and 2) consider the behavioral effects of additional promising longevity interventions.

4.6 Methods

4.6.1 Strains and Growth Conditions

C. elegans were cultivated using standard, previously described methods[48]. Briefly, all worms were maintained at 20 °C on solid nematode growth media (NGM). Worms were fed *E. coli* OP50 throughout life, except in experiments using double stranded (ds) RNAi (*E. coli* HT115). Worm transfers were conducted using a platinum wire unless otherwise specified. RNAi used are listed in Table 4.1 and strains used are listed in Table 4.2. All genotypes were confirmed using PCR and all RNAi imaging hits were sequence-validated and qPCR-validated before use.

4.6.2 Pumping Assays

Pumping was measured in day 2 gravid adults, as previously described[48]. The number of pumps per 30 seconds was measured in at least 10 worms under 100x magnification. Because food availability is known to change pumping rate, only worms on the bacterial lawn were considered in this assay. Data were plotted by R version 4.3.1 and Adobe Illustrator 2022.

4.6.3 Thrashing Assays

Thrashing was measured in day 2 gravid adults, as previously described[48]. Briefly, approximately 10 worms were placed in a droplet of M9 solution. Once worms began moving at a maximum rate, their body bends were counted for 30 seconds. Data were plotted by R version 4.3.1 and Adobe Illustrator 2022.

4.6.4 30-minute Video Recordings for Speed and Movement Patterns

On day 1 of adulthood, 10-15 worms of each genotype were placed in the center of a 35 mm petri dish that was completely covered in 350 µL of OP50 bacteria (bacteria was grown overnight to an optical density (OD_{600} 3.0). Worms were placed above the bright light source at

the base of the microscope used for video recording for 10 minutes to acclimate to the light, and then 30-minute video recordings were started. Videos were taken at 3.65x magnification, and at 1 frame per second on a Leica M165F microscope using Leica Application Suite X (LASX) software and 4x4 binning. The videos were analyzed using the wrMTrck multiple object tracker plugin (wrMTrck_Batch v1.04) on FIJI[408] (FIJI Is Just ImageJ bundled with 64-bit Java 1.8.0) to measure average speed, maximum speed, worm area, total distance traveled, and distance from the point of origin. Raw x and y coordinates were also exported from wrMTrck to create the plots of worm paths over the course of the 30-minute videos. Not all worm paths lasted the full 30-minute duration of the video due to fleeing and collisions. In cases when worms fled the plate and were no longer visible during the video, the data from that worm was included if the on-plate duration was ≥10 minutes. In cases where worms collided and wrMTrck failed to correctly determine which worm was which after the event, the data for those worms before the collision was included if the duration was ≥ 10 minutes. In all data analysis using wrMTrck data, we confirmed that there was no significant difference in average path duration per condition. To generate paths plots, the starting location of each worm was normalized to x = 0, y = 0. For each subsequent frame, the normalized x, y coordinate was determined by calculating the change in x and y position from the preceding to the current frame. Data were plotted by R version 4.3.1 and Adobe Illustrator 2022.

4.6.5 Gentle Touch Response Assay

Measuring the response of different strains to a gentle touch (eyebrow hair) was performed as previously described[409]. 10 day 2 gravid adult worms were each stroked 10 times with an eyebrow hair, and touches were alternated from head to tail. Because no differences were observed between anterior and posterior touch response in any strain, head and tail touches were

combined in calculating the number of touches until a response. A response was considered a change in movement direction away from the touched part of the worm or ceasing movement towards the direction of the touch. The average number of touches until a response was calculated for each worm. Data were plotted by R version 4.3.1 and Adobe Illustrator 2022.

4.6.6 Harsh Touch Response Assay

Measuring the response of different strains to a harsh touch (platinum wire pick) was performed as previously described[409]. 10 day 2 gravid adult worms were each touched 10 times with a platinum wire pick and touches were alternated from head to tail. Because no differences were observed between anterior and posterior touch response in any strain, head and tail touches were combined in calculating the percent of touches that elicited a response. A response was considered a change in movement direction away from the touched part of the worm or ceasing movement towards the direction of the touch. The percent of harsh touches that produced a response was calculated for each worm. Data were plotted by R version 4.3.1 and Adobe Illustrator 2022.

4.6.7 Chemotaxis Assay

For chemotaxis assays, unseeded NGM plates were separated into four quadrants using a marker on the bottom of the plate. A circle with a 5 mm radius was drawn in the center of the plate and within each quadrant, a dot was marked in the middle of the quadrant 5 mm from the edge of the plate rim. 5 µL of 0.5 M sodium azide was pipetted onto each of the four dots (one per quadrant). Two quadrants opposite from one another were designated as control quadrants, and 2 were designated as treatment quadrants. In the treatment quadrants, 10 µL of diacetyl or 1-octanol was pipetted on top of the sodium azide. In the control quadrants, 10 µL of ethanol was pipetted on top of the sodium azide. Immediately after preparing the plates, gravid adults were washed off of

NGM plates in M9 and pelleted at 1,000 *rcf* for 1 minute. At least 40 worms per plate were then pipetted onto the 5 mm radius circle in the center of each chemotaxis plate. After one hour, the number of worms in the control and treatment quadrants were counted under a dissection microscope. Chemotaxis Index was calculated by subtracting the number of worms on all control quadrants from the number of worms on all treatment quadrants, then dividing that by the total number of worms on the plate. The attractant diacetyl and the repellent 1-octanol were applied at a dilution of 1:1000 compound to ethanol. Data were plotted by R version 4.3.1 and Adobe Illustrator 2022.

4.6.8 Pathogen Fleeing Assay

A flask containing 1x Brain Heart Infusion Broth (BHI, BD Difco) supplemented with 100 µg/mL Rifampicin (Thermo Scientific Chemical) was inoculated with *Enterococcus faecalis* OG1RF (ATCC) and incubated for 18 hours with shaking at 37 °C. From this culture, 100 µL of the 1x *E. faecalis* culture was seeded onto 35 mm BHI agar (BD Difco) plates containing Rifampicin and a palmitic acid fence (0.5 g palmitic acid in 50 mL of 100% ethanol), followed by incubation at 37 °C for 18 hours. The palmitic acid fence was added to prevent worms from fleeing onto the sides of the plate and desiccating. After incubation, the plates were allowed to cool to room temperature before adding the worms. At day 1 of adulthood, approximately 100 worms were placed in the center of freshly prepared *E. faecalis* lawns and incubated at 25 °C until imaging at 5-minute, 2-hour, and 20-hour timepoints. Brightfield images were captured at each timepoint at 0.365x magnification using a Leica fluorescent microscope. The images were analyzed using ImageJ software, where the number of worms on and off the *E. faecalis* lawn was counted, and the percentage of lawn occupancy was calculated. Data were plotted by R version 4.3.1 and Adobe Illustrator 2022.

4.6.9 Basal and Enhanced Slowing Response Assay

The basal and enhanced lawn slowing response assay was conducted as previously described by Sawin et al[281]. All measurements were performed on standard 60 mm diameter NGM plates, either seeded with 200 µL *E. coli* OP50 in a ring on the outside of the plate, or unseeded in control conditions. Plates were allowed to dry overnight before the assay. To measure the locomotory rate of fed animals, well-fed gravid worms at day 1 of adulthood were transferred off of NGM plates in M9 buffer and twice. Approximately 5 worms at a time were then pipetted into the unseeded portion of the plate and residual buffer was absorbed with a Kimwipe. After 5 minutes of acclimatization, the body bends of each animal were recorded over 20s intervals until all animas had entered the region containing bacteria. To measure the behavior of fasted animals, the same procedure was followed but worms were first transferred to an NGM plate without food for one hour. Data were plotted by R version 4.3.1 and Adobe Illustrator 2022.

4.6.10 Brood Size Assay

For each replicate, 10 worms per condition from a timed egg-lay were plated individually on 35 mm NGM plates as L4s, before egg-laying began. Once egg-laying began, mothers were transferred daily to new plates until no new eggs were laid for two days. Eggs were allowed to grow to L3 before counting. Worms which fled up the sides of the plate and could not be recovered during the assay were excluded from measurements of total brood size. However, preceding days in which the worm was on the plate for a full 24 hours were included in calculations of average eggs laid per day. Data were plotted by R version 4.3.1 and Adobe Illustrator 2022.

4.6.11 Exploration Assays

Exploration assays were performed as previously described by Flavell et al[375]. Individual worms from a timed egg lay were transferred at young adulthood to a 35 mm NGM agar plate completely covered with *E. coli* OP50 (350 µL). Images were taken of each plate using an iPad attached to a brightfield microscope. A custom ImageJ java script was used to enhance the contrast of each image to an equal degree to improve visibility of worm tracks through the bacteria and to overlay a grid of uniform-size across the image. The number of squares entered by the worm tracks were counted for each worm, with the maximum number of squares possible being 109. 20-30 worms were assayed for each condition. Worms that fled the plate during the assay were excluded from analysis. Data were plotted by R version 4.3.1 and Adobe Illustrator 2022.

4.6.12 Exploration Assays with Metabolite/Compound Supplementation

For all supplemented compounds, the specified dose of the compound was incorporated into the agar of 60 mm NGM plates, and worms were TEL'ed and grown on these specialty plates from egg. At young adulthood, worms were removed from the supplemented plates and placed on exploration plates (described above). The exploration assay was performed as indicated, with the exception that images were taken after three hours to reduce regression to control-like behavior after many hours off of plates with the supplemented compound. Data were plotted by R version 4.3.1 and Adobe Illustrator 2022.

4.6.13 Behavioral State Assays

At day 1 of adulthood, 10-20 worms in each condition were transferred to a standard 60 mm NGM plate seeded with *E. coli* OP50 bacteria. Animals were allowed to acclimate to the new plate for 30 minutes, then an iPad attached to a brightfield microscope was used to record a 15-second video of the plate. An experimenter blinded to the plate condition then scored each worm

on the plate as roaming (moving quickly with few turns), dwelling (moving around a local area with frequent turns), or quiescent (minimal to no movement) over the 15-second period. The percentage of the population in each state during that period was then calculated. Data were plotted by R version 4.3.1 and Adobe Illustrator 2022.

4.6.14 Generating tissue-specific fmo-2 overexpressors

Plasmid construction and microinjection was conducted by Suny Biotech to generate both tissue-specific *fmo-2* overexpression constructs. In designing the plasmids, we used the *elt-2* promoter to drive genomic DNA of FMO-2::SL2::GFP in the intestine. To express genomic DNA of FMO-2::SL2::GFP in neurons, we used the *rab-3* promoter. All plasmids were verified via restriction digest and sanger sequencing, and ApE files are available upon request. Plasmids were microinjected by Suny Biotech using the co-injection marker myo-2p::GFP and 3 transgenic lines were tested in each experiment.

4.6.15 RNAi Knockdown

For most RNAi knockdowns, worms were placed on the RNAi for two generations to ensure maximal knockdown. However, *sams-1* RNAi severely stunted development, so worms were placed on *sams-1* RNAi at L3 stage then assayed as gravid adults. All RNAi clones were taken from the Vidal RNAi library. All RNAi was sequence-verified and successful knockdown was also qPCR validated.

4.6.16 Quantitative PCR for RNAi validation

RNAi was isolated from day 1 adult worms that have been on the RNAi for two generations (with the exception of *sams-1*, see above). A Direct-zol RNA miniprep kit (Zymo) was used for RNA extraction, and cDNA was generated using the Biorad iScript cDNA Synthesis Kit.

Expression levels were measured with the SYBER Green (BioRad) quantitative RT-PCR (qRT-PCR) system, and mRNA levels were normalized to the housekeeping genes *cdc-42* and *Y45FD10.4*. Primers for RNAi validation were designed to span the 3' UTR of each transcript to prevent amplification of the bacterially-produced RNAi. Gene expression was calculated using standard curves.

4.6.17 Enzymatic Activity Assay

The oxygenation activity of FMO-2 was assessed using a method described previously[282,410]. In brief, the consumption of NADPH was monitored spectrophotometrically at 340 nm, using the molar extinction coefficient of 6.22 mM^{-1} cm^{-1} to determine substrate oxygenation. The assay buffer contained 25 mM sodium phosphate (pH 8.5), 0.5 mM diethylenetriaminepentaacetic acid (DETAPAC), 0.5 mM NADPH, 0.04 μM FMO-2, and excess FAD. For tryptophan, the final concentrations were 100, 250, 500, 750 μM, and 1, 2.5, 5, 7.5, and 10 mM. For MMI, the final concentrations were 100, 300, and 600 μM, along with 1, 3, 5, 7, 10, and 30 mM. To assess NADPH oxidation rates by FMO, NADPH concentrations of 10, 30, 100, 300, 500, and 700 μM, as well as 1 and 1.5 mM, were used. All experiments were performed at 30 °C with shaking. Kinetic parameters (e.g., kcat and Km) were determined by fitting the rate of turnover versus substrate concentration to the Michaelis-Menten equation, using GraphPad Prism (version 9.1.0). FMO-2 protein was purchased from GenScript, while NADPH (10107824001), FAD (F6625), MMI, L-tryptophan (T0254), and other substrates were sourced from Sigma-Aldrich (St. Louis, MO). DETAPAC (AC114322500) and sodium phosphate buffer (S374-500) were obtained from Fisher (Waltham, MA).

4.6.18 Serotonin Immobilization Assay

The serotonin immobilization assay was performed as previously described by Ranganathan et al[381]. Briefly, 20-30 worms were washed off of standard NGM plates at day 1 of adulthood and rinsed twice with M9 to remove any residual bacteria. Animals were then placed in 200 µL of 30 M serotonin solution (serotonin creatine sulfate salt in M9 buffer). Videos were recorded for 20 minutes after worms were placed in the serotonin solution, and an experimenter blinded to the condition in each video scored the number of mobile and immobile worms at 1, 2, 4, 5, 7.5, 10, 12.5, 15, 17.5, and 20 minutes. Worms were considered immobile if they did not swim for 5 seconds. Data were plotted by R version 4.3.1 and Adobe Illustrator 2022.

4.6.19 Lifespan Measurements

Lifespan assays were performed as previously described[48]. In short, 10-15 gravid adults were transferred to NGM for a three-hour timed egg lay and then removed. Once their progeny reached day 1 of adulthood, 60-80 worms were transferred to NGM plates with 33 µL of 150 mM fluorodeoxyuridine (FUdR) and 100 µL of 50 mg/mL Ampicillin per 100 mL NGM. The FUdR prevents development of progeny and the Ampicillin prevents bacterial growth. NGM + FUdR + AMP plates were seeded with concentrated bacteria (5x for OP50 fed lifespans), and at least two plates per strain per condition were used for each lifespan replicate. Animals were removed from the experiment and counted as dead when they did not move in response to a gentle touch from a platinum wire pick under a dissection microscope. Lifespans were scored at least 3 times per week until all animals were dead. A ‘fence’ of 75 µL of 100 mM palmitic acid (Sigma-Aldrich) dissolved in 100% ethanol was also applied to the edge of each lifespan plate to prevent fleeing. Data were plotted by R version 4.3.1 and Adobe Illustrator 2022.

4.6.20 RNAi Lifespans

RNAi lifespan assays were performed like other lifespans with the exception of the initial timed egg-lay (TEL) and the food concentrations. To ensure maximum knockdown on RNAi, a first generation of worms was TEL'ed on RNAi for 3-4 hours. The progeny from this TEL were left on RNAi plates to develop into gravid adults and were then used for a second TEL on the same RNAi conditions. Progeny from the second-generation TEL were then used for the lifespan assay. RNAi bacteria (HT115) is AMP resistant and can grow slowly on AMP lifespan plates during the assay. To maintain equivalent amounts of bacterial availability over the course of the lifespan, RNAi lifespan plates are seeded with 2x concentrated bacteria, from a starting optical density (OD_{600}) of 3.0.

4.6.21 Fluorescent Slide Microscopy

Fluorescent images in this study were taken using a Leica M165F fluorescent microscope running Leica Application Suite X (LASX) software. At least 15 worms per condition were imaged at ≥ 70x magnification. For representative images displayed in the figures, worms were paralyzed in 0.5 M sodium azide (NaN_3) and imaged once residual liquid evaporated and the worms clumped together. Paralyzed worms were then gently rearranged so the heads and tails faced the same orientation. For quantification of these images, individual worms were gently pushed apart until they were no longer touching one another. For each worm, an experimenter blinded to the condition traced and measured the mean fluorescence of the worm's head and the cell body of each individual serotonergic neuron in ImageJ bundled with 64-bit Java 1.8.0. The mean fluorescent intensity of the background was subtracted from the mean fluorescence measurements. Data were plotted by R version 4.3.1 and Adobe Illustrator 2022.

4.6.22 Statistical Analysis

The height of all bar plots represents the mean of the condition, and error bars indicate standard error of the mean (SEM). For all comparisons of > 2 conditions, an ANOVA and post-hoc Tukey HSD tests (2-tailed, unpaired) were run to determine interactions between variables and derive statistical comparisons between each condition. p values are *$p < 0.05$, **$p < 0.01$, ***$p< 0.001$, and ****$p<0.0001$. For lifespan assays, the statistical groupwise and pairwise comparisons across survivorship curves were performed using the survfit survival analysis package in R. *P* values comparing two survival curves were acquired using the log-rank analysis. *P* values indicating an interaction between multiple experimental variables and across >2 survival curves were performed using the survivalMPL package in R to perform a Cox regression analysis between covariates of interest. Tests done with data from multiple biological variables were adjusted with a Bonferroni p value correction. p values are *$p < 0.05$, **$p < 0.01$, ***$p< 0.001$, and ****$p<0.0001$. Exact *N*s for each experiment are included in the source data files and minimum *N*s for each plot are included in the figure legends.

RNAi	Figure	Library
fmo-2	S2	Vidal
aat-1	2	Vidal
aat-2	2	Vidal
aat-3	2	Vidal
sams-1	S3	Vidal
tph-1	S4	Vidal
pah-1	S4	Vidal
tdo-2	4	Vidal
afmd-1	4	Vidal
kynu-1	4	Vidal
haao-1	4	Vidal
nkat-1	S5	Vidal
nkat-3	S5	Vidal
tatn-1	S5	Vidal
got-2.1	S5	Vidal
got-2.2	S5	Vidal
kmo-1	S5	Vidal
umps-1	S5	Vidal

acsd-1	S5	Vidal
vhl-1	5	Vidal

Table 4.1 RNAi used in this work.

Strain Description	Strain	Source	Identifier	Outcross
WT	wild-type	CGC	N2	≥4
fmo-2 knockout	*fmo-2(ok2147)*	CGC	VC1668	≥4
fmo-2 overexpressor (ubiquitous)	*seaSi39 [(pCFJ448) (eft-3p::fmo-2 + H2B::GFP) + Cbr-unc-119(+)] I.*	CGC	KAE9	≥4
fmo-2 overexpressor (intestinal)	*[elt-2p::fmo-2 + H2B::GFP]*	this paper	SCL46	≥4
fmo-2 overexpressor (neuronal)	*[rab-3p::fmo-2 + H2B::GFP]*	this paper	SCL48	≥4
intestine-specific *fmo-2* rescue	*fmo-2(ok2147); [elt-2p::fmo-2 + H2B::GFP]*	this paper		≥4
neuronal-specific *fmo-2* rescue	*fmo-2(ok2147); [rab-3p::fmo-2 + H2B::GFP]*	this paper		≥4
neuronal-only RNAi uptake	*sid-1(qt9); sqIs71 [rgef-1p::GFP + rgef-1p::sid-1]*	CGC	MAH677	≥4
intestinal-only RNAi uptake	*sid-1(qt9); alxIs9 [vha-6p::sid-1::SL2::GFP]*	CGC	MGH171	≥4
fmo-1 knockout	*fmo-1(ok405)*	CGC		≥4
fmo-1 overexpressor	*[eft-1p::fmo-1]*	this paper		≥4
fmo-4 knockout	*fmo-4(ok294)*	CGC		≥4
fmo-4 overexpressor	*[eft-3p::fmo-4]*	Tuckowski *et al,* 2024		≥4
mod-5 knockout	*mod-5(n3314)*	CGC	MT9772	≥4
tph-1 transcriptional reporter	*zdIs13 [tph-1p::GFP] IV.*	CGC	SK4013	≥4
fmo-2 KO; *tph-1* transcriptional reporter	*zdIs13 [tph-1p::GFP] IV.; fmo-2(ok2147)*	this paper		≥4
fmo-2 OE; *tph-1* transcriptional reporter	*zdIs13 [tph-1p::GFP] IV.; seaSi39 [(pCFJ448) (eft-3p::fmo-2 + H2B::GFP) + Cbr-unc-119(+)] I.*	this paper		≥4
tph-1 knockout	*tph-1(mg280)*	CGC	MT15434	≥4

pah-1 knockout	*pah-1(syb3601)*	CGC	PHX3601	≥4
pah-1; tph-1	*tph-1(mg280); pah-1(syb3601)*	CGC	PHX3596	≥4
pah-1; fmo-2 knockout	*pah-1(syb3601); fmo-2(ok2147)*	this paper		≥4
tph-1; fmo-2 knockout	*tph-1(mg280); fmo-2(ok2147)*	this paper		≥4
fmo-2 KO; *pah-1; tph-1*	*tph-1(mg280); pah-1(syb3601); fmo-2(ok2147)*	this paper		≥4
afmd-1 knockout	*afmd-1(tm4547)*	CGC	OW477	≥4
kynu-1 knockout	*kynu-1(tm4924)*	CGC	OW454	≥4
haao-1 knockout	*haao-1(tm4627)*	CGC	OW479	≥4
afmd-1 knockout*; fmo-2* OE	*afmd-1(tm4547); seaSi39 [(pCFJ448) (eft-3p::fmo-2 + H2B::GFP) + Cbr-unc-119(+)] I.*	this paper		≥4
kynu-1 knockout*; fmo-2 OE*	*kynu-1(tm4924); seaSi39 [(pCFJ448) (eft-3p::fmo-2 + H2B::GFP) + Cbr-unc-119(+)] I.*	this paper		≥4
haao-1 knockout*; fmo-2 OE*	*haao-1(tm4627); seaSi39 [(pCFJ448) (eft-3p::fmo-2 + H2B::GFP) + Cbr-unc-119(+)] I.*	this paper		≥4
nmr-1; nmr-2 knockout	*nmr-1(ak4); nmr-2(ok3324)*	this paper		≥4
nmr-1; nmr-2 knockout*; fmo-2* OE	*nmr-1(ak4); nmr-2(ok3324); seaSi39 [(pCFJ448) (eft-3p::fmo-2 + H2B::GFP) + Cbr-unc-119(+)] I.*	this paper		≥4
umps-1 knockout	*umps-1(zu456)*	CGC	GH636	≥4
umps-1 knockout*; fmo-2 OE*	*umps-1(zu456); seaSi39 [(pCFJ448) (eft-3p::fmo-2 + H2B::GFP) + Cbr-unc-119(+)] I.*	this paper		≥4
nkat-1 knockout	*nkat-1(ok585)*	CGC	RB795	≥4
nkat-1 knockout*; fmo-2 OE*	*nkat-1(ok585); seaSi39 [(pCFJ448) (eft-3p::fmo-2 + H2B::GFP) + Cbr-unc-119(+)] I.*	this paper		≥4

Table 4.2 *C. elegans* strains used in this work.

Chapter 5 Methods for Metabolic Inactivation of *E. coli* and for Automated Image Quantification in *C. elegans* Research.

5.1 Foreword

In addition to working on research questions related to cell nonautonomous signaling, *fmo-2*, and longevity, I have also spent time optimizing methods for *C. elegans* research in the lab. The first *C. elegans* method presented here is a technique to metabolically inactive *C. elegans*' food source, OP50 *E. coli*, while maintaining its nutritive value to the worm. This method was designed and optimized by Dr. Safa Beydoun and originally published as a methods paper in Communications Biology[411]. However, when Dr. Beydoun was asked to make a more detailed, video-based protocol for the Journal of Visualized Experiments (JoVE)[5], I contributed to the writing and illustrating of a new version of the manuscript that focuses on a detailed protocol for this method. I also contributed to writing and editing the script used for a video documenting this method, and was part of the filming process on the day the video was recorded.

The second *C. elegans* method included in this chapter is a method for automated quantification of fluorescent images. While working on the role of olfaction in DR-mediated *fmo-2* induction during my first year in the lab, I performed many fluorescent imaging experiments to measure *fmo-2* induction in response to various conditions. The method the lab was using to quantify these images at the time was to open a brightfield image of a group of worms in ImageJ and manually trace each individual worm and measure mean pixel intensity.

[5] Published in *Journal of Visual Experiments* (2023 Jul; doi: 10.3791/200464-v) with authors listed as **Kitto, E.S.**, Beydoun, S., Wang, E., Huang, S., and Leiser, S.F.

Then, a recording of the regions traced and measured in the brightfield image was rerun on the corresponding fluorescent image to quantify fluorescence of each worm. This process was slow, subject to user error, and a limiting factor in the size possible for a single fluorescent imaging experiment. To improve this process, I implemented some small changes to the process of taking fluorescent images and wrote the package findWormz in R to automate fluorescent image intensity measurements in single worms. This R code was written in collaboration with Dr. John Dean. The new automated quantification method has been widely used by others in the lab and allowed me to conduct large imaging screens in the work presented in Chapters 2-3. A paper explaining this image quantification method is published at microPublication Biology[6].

5.2 Method to metabolically inactivate bacteria for *Caenorhabditis elegans* research

5.2.1 Abstract

Caenorhabditis elegans is a common model organism for research in genetics, development, aging, metabolism, and behavior. Because *C. elegans* consume a diet of live bacteria, the metabolic activity of their food source can confound experiments looking for direct effects of various interventions on the worm. To avoid the confounding effects of bacterial metabolism, *C. elegans* researchers have used multiple methods to metabolically inactivate bacteria, including ultraviolet (UV)-irradiation, heat-killing, and antibiotics. UV treatment is relatively low-throughput and cannot be used in liquid culture because each plate must be examined for successful bacterial killing. A second treatment method, heat-killing, negatively affects the texture and nutritional quality of the bacteria, leading to the developmental arrest of *C. elegans*. Finally, antibiotic treatment can directly alter *C. elegans* physiology in addition to

[6] Published in *micropublication Biology* (2025 Apr; doi: 10.17912/micropub.biology.001562) with authors listed as **Kitto, E.S.**, Dean, J.C., and Leiser, S.F.

preventing bacterial growth. This manuscript describes an alternative method to metabolically inactivate bacteria using paraformaldehyde (PFA). PFA treatment cross-links proteins within bacterial cells to prevent metabolic activity while preserving cellular structure and nutritional content. This method is high-throughput and can be used in liquid culture or solid plates, as testing one plate of PFA-treated bacteria for growth validates the whole batch. Metabolic inactivation through PFA treatment can be used to eliminate the confounding effects of bacterial metabolism on studies of drug or metabolite supplementation, stress resistance, metabolomics, and behavior in *C. elegans.*

5.2.2 Introduction

Caenorhabditis elegans was originally proposed as a model organism in 1965[412] and has since been widely adopted in studies of genetics, development, behavior, aging, and metabolism[413]. Due to their large brood size and transparent cuticle, *C. elegans* is particularly well-suited for high-throughput screening with fluorescent reporters[414]. Their short life cycle, hermaphroditic reproduction, and genetic homology with humans also make *C. elegans* a valuable model system for studies on development[415] and aging biology[416]. Moreover, *C. elegans* are relatively easy to maintain. Worms can be grown in liquid culture or on solid agar plates and consume a diet of live *Escherichia Coli* OP50 bacteria[415].

However, the live food source of *C. elegans* can confound studies of metabolism, drug supplementation, and behavior. Because live bacteria have their own metabolism, experimental conditions that affect the bacteria also alter the nutrients and metabolites available to the worms. For example, differences in bacterial iron, amino acid, and folate concentrations have diverse effects on *C. elegans* development, physiology, and lifespan[417]. Many common lab practices can elicit such changes in the nutrient composition of, and metabolites produced by OP50.

Specifically, exposure to 5-fluoro-2'-deoxyuridine (FUdR), a compound commonly used to prevent reproduction in *C. elegans*, elicits broad changes in OP50 gene expression, including amino acid biosynthesis pathways[418]. Live bacteria can also confound studies in which *C. elegans* are supplemented with small molecules because bacteria can partially or completely metabolize the active compounds. Moreover, the effects of these small molecules on the bacteria can, in turn, alter *C. elegans* physiology, as was reported with the lifespan-extending drug metformin[419]. Finally, live bacteria can change the worm's environment in ways that alter behavior, such as secreting attractive odorants[420], producing exogenous neuromodulators[421], and creating oxygen gradients in a dense lawn[422].

To mitigate the confounding effects of bacterial metabolism on *C. elegans* research, multiple methods for killing bacteria have been developed (**Table 5.1**). Three common strategies for killing OP50 are UV-irradiation, heat-killing, and antibiotic treatment. While straightforward and relatively low-cost, each of these methods can have undesirable effects on both bacteria and *C. elegans.* UV-killing via a UV crosslinker[423] is low-throughput and the rate is limited by the number of plates that can fit in the UV crosslinker. Moreover, the efficacy of UV-killing can vary from plate to plate within a batch, and testing for growth on all plates can become difficult in large experiments. Heat-killing OP50 by exposing culture to temperatures of >60 °C comes with a separate set of challenges. High heat can damage nutrients essential for the worm and destroy the cellular structure of bacteria, creating a softer texture that decreases the amount of time worms spend on the food[424]. This method also cannot be used throughout the life cycle of *C. elegans* because worm fed heat-killed bacteria from egg can arrest early in development[424]. Antibiotic treatment is a third common method for suppressing bacterial metabolism[425], but antibiotics can also alter worm growth and metabolism[426].

One solution to eliminate the metabolic effects of live bacteria while preserving bacterial structure and essential nutrients is to kill OP50 with paraformaldehyde (PFA)[411]. PFA is a polymer of formaldehyde that can crosslink proteins within cells[427] to prevent bacterial replication without destroying internal cell structures like the inner plasma membrane[428]. Due to this preservation of internal cellular structure, PFA-treated bacteria exhibit no growth or metabolic activity but remain an edible and nutrient-rich food source for *C. elegans*[411].

<table>
<tr><th>Method</th><th>Required Materials</th><th>Scalable?</th><th>Nutritional?</th><th>Effects on Worm?</th></tr>
<tr><td rowspan="4">UV</td><td rowspan="4">Crosslinker</td><td><u>Limited by:</u></td><td rowspan="4">Yes</td><td>Variable effects on lifespan on NGM[423,429,430]</td></tr>
<tr><td>Plates that fit in crosslinker</td><td>Variable effects on lifespan on FUdR[430-432]</td></tr>
<tr><td>Irradiation time per plate</td><td rowspan="2">Decreased food preference[433]</td></tr>
<tr><td>Ability to check every plate for growth[8]</td></tr>
<tr><td rowspan="3">Heat</td><td rowspan="3">>60 °C incubator</td><td rowspan="3">Yes</td><td rowspan="3"><u>No:</u> destroys cell wall, decreased nutritional value</td><td>Developmental arrest[424]</td></tr>
<tr><td>Decreased food preference[424]</td></tr>
<tr><td>Extends lifespan on NGM[258]</td></tr>
</table>

Antibiotics	Antibiotics (kanamycin, carbenicillin, etc)	Yes	Yes	Delays growth and development[426]
				Extends lifespan in liquid media[434]
				Extends lifespan on NGM[426]
PFA	0.5% Paraformaldehyde	Yes	Yes	Small brood size decrease[433]
				Small development time increase[433]
				Decreased food preference[433]

Table 5.1 Comparisons of methods to kill OP50. UV-killing, heat-killing, antibiotic-treatment, and PFA-treatment have varied effects on the nutritional status of the bacteria and the health of worms fed treated bacteria. These methods for replicatively inactivating *E. coli* also differ in their required materials and scalability.

5.2.3 Protocol

1. Bacteria inoculation

    1.1. Prepare Luria Broth (LB) by dissolving 10 g tryptone, 5 g yeast extract, and 10 g sodium chloride (NaCl) in 950 mL of distilled water.

    1.2. Adjust the pH of the LB to 7.0 by adding 5M sodium hydroxide (NaOH). This should only require about 0.2 mL of NaOH.

    1.3. Autoclave the pH-adjusted LB media on a liquid cycle for 45 min at 15 psi. Allow the solution to cool and store at room temperature.

    1.4. Inoculate a single colony of bacteria in 100 mL of LB in a 500 mL Erlenmeyer flask. Culture the bacteria overnight in a 37 °C shaker incubator.

1.5. Depending on the health of the bacterial colony, the size of the flask and the speed that the shaker is set to, the time that it takes for the bacteria to grow may vary. After ~14 h, check the optical density (OD) of the bacteria at 600 nm.

1.6. Remove the bacteria from the shaker when the OD_{600} is 3.0 (1 x 10^9 Colony Forming Units (CFU)/mL). If the OD_{600} is less than 3.0, return the flask to the shaker incubator until the desired OD is reached.

1.7. Aliquot the bacteria in 50 mL conical tubes and store at 4 °C or proceed to the next step.

2. Working with paraformaldehyde

NOTE: The concentration of paraformaldehyde (PFA) used, and the duration of exposure may vary somewhat depending on climate, location, and type of bacteria being treated. A good starting point for OP50 is exposure to 0.5% PFA for 1 h, whereas 0.25% PFA for 1 h may be sufficient for HT115.

2.1. Prepare 32% PFA stock for use. Use proper personal protective equipment (PPE) when working with PFA. Wear gloves and eye protection.

2.2. Add PFA inside a chemical fume hood with proper ventilation. Dispose PFA containing washes and tips in biohazard containers in the fume hood.

3. Bacterial treatment with paraformaldehyde

3.1. Once the bacteria reach an OD_{600} of 3.0, use a serological pipette to transfer 50 mL into a new 250 mL Erlenmeyer flask. Save the rest for a live control, a mock-treated control (see step 4), or to treat as well with PFA as needed.

3.2. Avoid pouring from one flask to another and be cautious not to splash the sides of the new flask with bacteria. Colonies on the side of the flask may receive a lower dose of PFA.

3.3. In the chemical hood, add 781 µL of 32% PFA to 50 mL bacteria to bring the final concentration to 0.5%. Dispose of the tip used in a solid waste chemical hazard container.

3.4. Cover the flask with foil and return to the 37 °C shaker incubator for 1 h. After 1 h, remove the flask from the incubator and proceed to step 5.

4. Mock-treated control

4.1. Once the bacteria reach an OD_{600} of 3.0, use a serological pipette to transfer 50 mL of the bacteria to a 50 mL conical tube.

4.2. Proceed to step 5.3 to complete the washing steps similar to the PFA-treated group.

5. Washing the bacteria to remove residual PFA

5.1. In the chemical hood, use a serological pipette to transfer the treated bacteria from the Erlenmeyer flask to a 50 mL conical tube. Using a serological pipette instead of pouring the bacteria will prevent contamination from any bacterial colonies on the edge of the flask that may have avoided direct treatment with PFA.

5.2. Centrifuge treated bacteria at approximately 3000 x *g* for 20 min. Remove the supernatant by disposing of it in a liquid waste chemical hazard container in the chemical hood.

5.3. Add 25 mL of LB and vortex to resuspend the bacterial pellet. (Filling the tube fully makes it harder to resuspend the pellet.) Repeat centrifugation and pellet resuspension 4x.

5.4. Resuspend the pellet in volumes optimal for different assays. For lifespan assays, seed 60 mm plates with 200 µL of bacteria resuspended in 10 mL of LB. Resuspending the bacteria in 10 mL of LB results in a 5x concentration from the original 50 mL culture.

5.5. Store the bacteria at 4 °C.

6. Quality check of bacterial growth

6.1. After the final wash and resuspension, streak an LB plate (using a sterile pipette tip) with the prepared bacteria. It is good practice to streak the LB used for washing and resuspending on a separate plate as well to make sure that the LB used was not contaminated.

6.2. Place the plates in a 37 °C incubator overnight. Check for any growth. The bacteria are considered replicatively dead when colonies do not grow on the LB plate.

7. Quality check for bacterial metabolism using a respirometer

7.1. After the final wash and resuspension from step 5.4, confirm that the bacteria are metabolically dead using available tools such as respirometers[434,435] and measuring the basal oxygen consumption rate (OCR).

7.2. Prepare M9 solution: Dissolve 3 g potassium phosphate monobasic (KH_2PO_4), 6 g sodium phosphate dibasic (Na_2HPO_4), and 5 g sodium chloride (NaCl) in 950 mL of distilled water. Autoclave on a liquid cycle for 45 min at 15 psi, then allow the solution to cool to room temperature. Add 1 mL of 1 M magnesium sulfate ($MgSO_4$) and store at room temperature.

7.3. Hydrate the respirometer cartridge: Add 200 µL of calibrant to all wells of a 96-well plate. Place the cartridge in the 96-well plate and incubate overnight in a 37 °C incubator.

7.4. Assay calibration: On the following day, place the hydrated cartridge in the machine and begin calibration.

7.5. Assay test plate setup: Using a new 96-well plate, add 160 µL of M9 and 40 µL of the prepped bacteria (1 x 10^9 CFU/mL) to test wells. Add 200 µL of M9 to the 4 corner wells to use as blank wells. Add 160 µL of M9 and 40 µL of LB used for washing and resuspending to use as negative controls. Add 200 µL of M9 to the rest of the wells that will not be used.

7.6. Run the assay: Once the cartridge calibration is complete, insert the assay plate from step 7.5 into the machine for analysis. The settings include steps to mix, wait, measure and loop. The results will be shown as oxygen consumption rate (OCR). The bacteria are metabolically dead and ready to use when the OCR is zero.

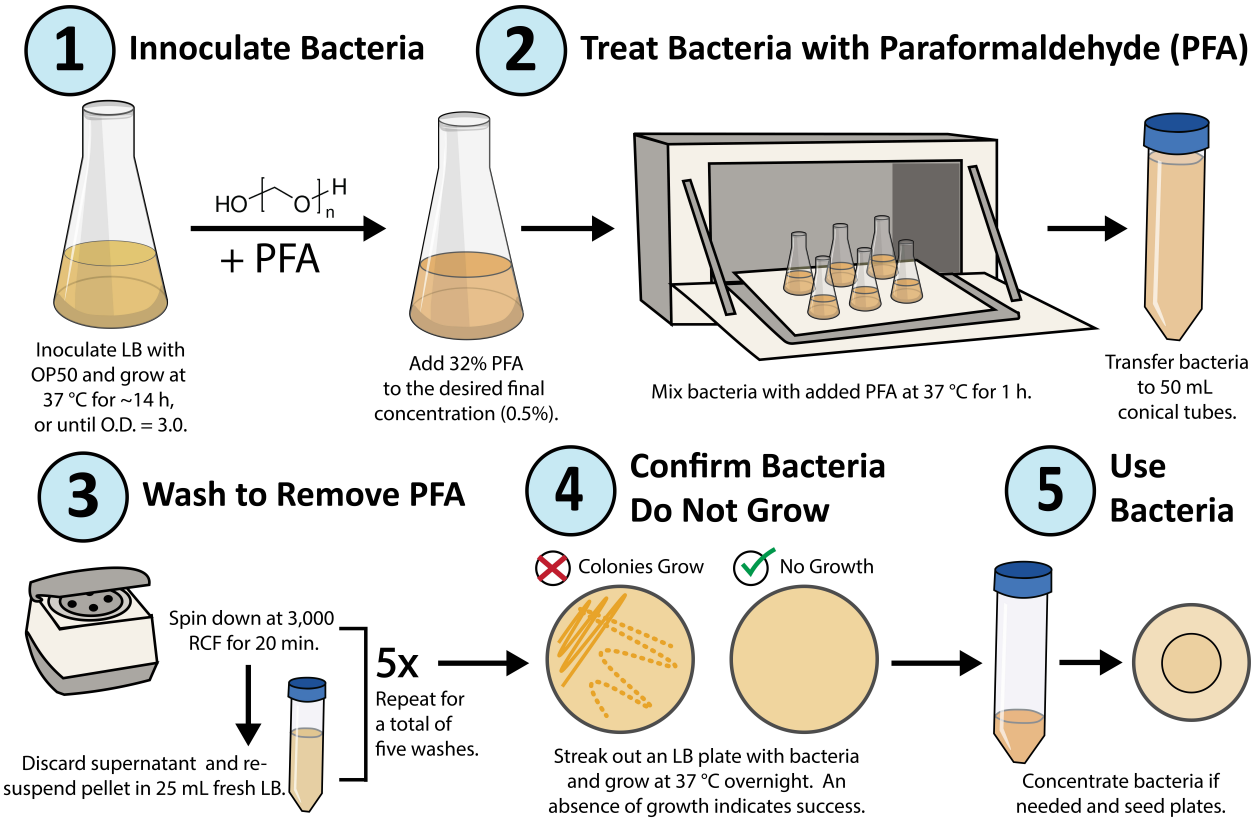


Figure 5.1 Workflow for paraformaldehyde treatment. A single colony of *E. coli* OP50 bacteria is grown overnight. PFA is added to a final concentration of 0.5%, and the PFA-treated culture is shaken for one hour at 37 °C. Finally, the PFA is removed by washing the culture with fresh LB five times. To confirm the treated bacteria are replicateively inactive, streak out an LB plate of the treated bacteria and grow overnight.

5.2.4 Representative Results

A detailed workflow of the protocol is shown in **Figure 5.1**. A high-throughput method was developed and optimized to consistently inactivate bacterial replication (**Figure 5.2A**) and metabolism (**Figure 5.2B**) for metabolic and drug studies in *C. elegans* research using paraformaldehyde[411]. The goal was to determine the lowest concentration of PFA needed and the shortest amount of time required to consistently kill the bacteria without impacting various measures of health in the worms. These values may vary from one location to another depending on lab environment, and from one bacterial strain to another. For example, exposure of HB101 bacteria to 0.25% for 1 h is sufficient to render it metabolically inactive (**Figure 5.2C**), while *Enterococcus faecalis* (EF) requires a 1.0% PFA concentration (**Figure 5.2D**) for a consistent

effect. An approach for optimizing these concentrations for individual lab conditions was previously established[411] and is detailed in this current work.

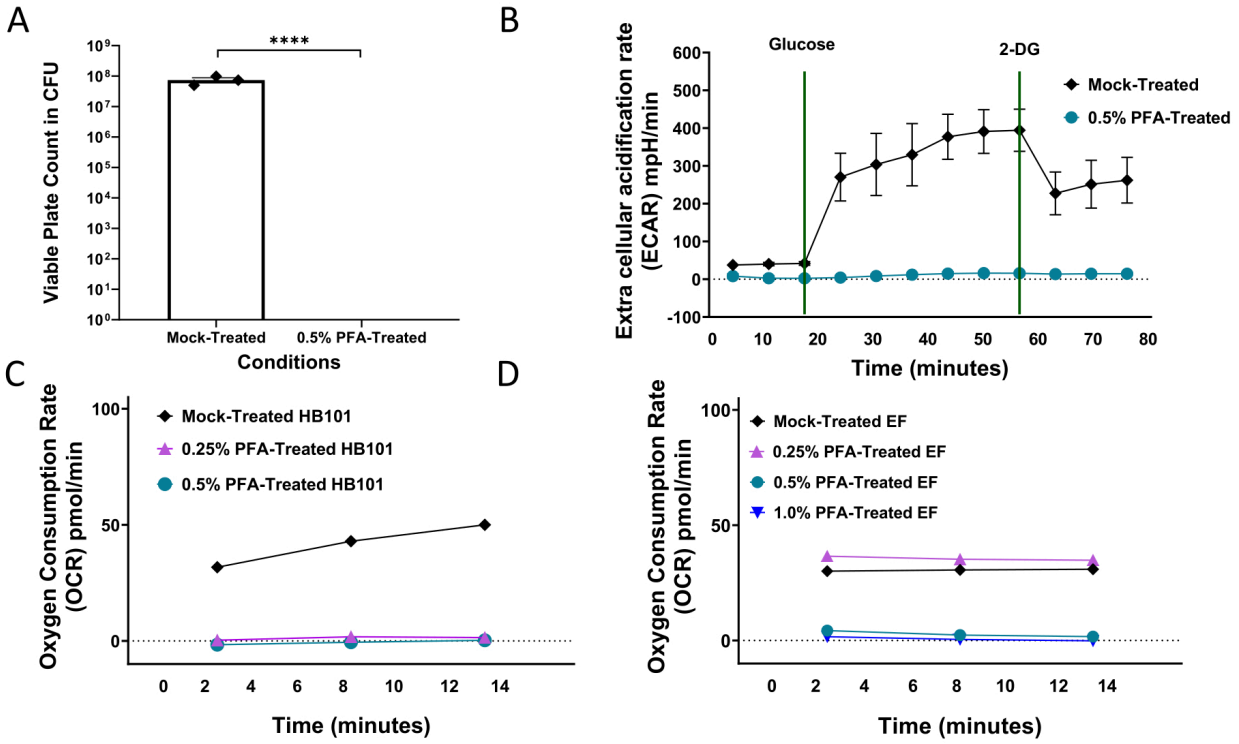


Figure 5.2 Treatment of bacteria with PFA inhibits proliferation and metabolism. (**A**) Bacteria growth in colony forming units (CFU) of mock-treated and 0.5% PFA-treated OP50. (**B**) Extracellular acidification rate (ECAR) in mpH/min of mock-treated and 0.5% PFA-treated OP50. (**C**) Basal oxygen consumption rate (OCR) in pmol/min of mock-treated, 0.25% PFA-treated, and 0.5% PFA-treated HB101. (**D**) Basal oxygen consumption rate (OCR) in pmol/min of mock-treated, 0.25% PFA-treated, 0.5% PFA-treated, and 1.0% PFA-treated *enterococcus faecalis* (EF). All error bars shown in figures represent the standard error of the mean (SEM); A two-tailed t-test was used to derive p-values. **** denotes p-value < 0.0001. This figure has been modified from Beydoun *et al.*[411].

5.2.4.1 Food attraction and consumption

As bacteria grow and replicate, they release various metabolites and pheromones that are attractive to the worms. To determine whether the worms remain attracted to the PFA-treated OP50, plates were seeded with PFA-treated or mock-treated OP50 and the percentage of worms present on the food lawn as compared to off the lawn was tabulated. Data show that worms are attracted to the PFA-treated OP50, since most of the worms remain on the bacterial lawn after 1 h (**Figure 5.3A**), similar to what is observed with the mock-treated control (**Figure 5.3B**).

However, as expected, a sensitive pairwise assay[436] shows that *C. elegans* have a stronger preference for the mock-treated live control (**Figure 5.3C**) when seeded with the PFA-treated on the same plate. Having established that worms are attracted to PFA-killed bacteria, albeit less than live bacteria, it was imperative to establish that they eat the PFA-killed food. To determine whether the worms consume the PFA-treated OP50, the pumping rate of the worms on different food types was measured. As shown in **Figure 5.3D**, worms on PFA-treated OP50 have a higher pumping rate (+25%) than worms on the mock-treated control. This indicates that worms are not purposefully slowing their rate of eating on PFA-killed food and could either indicate a higher rate of eating or a compensatory response to a change in the ease of pumping the treated food.

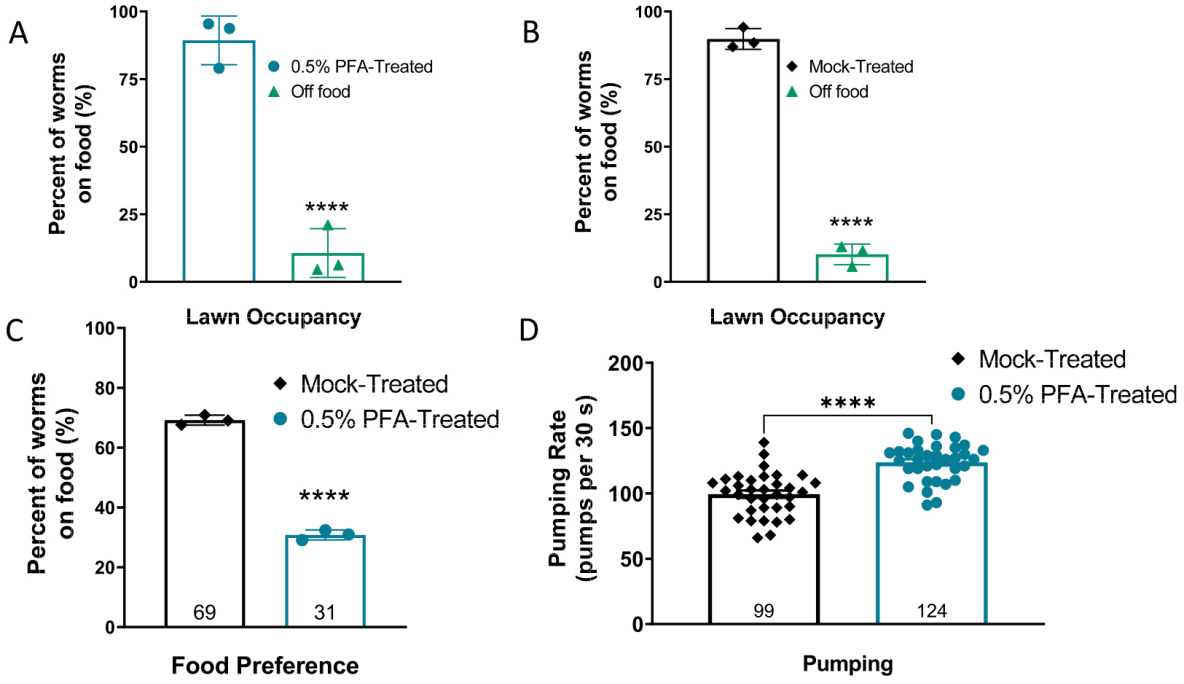


Figure 5.3 Worms attracted to PFA-treated OP50. Percent of worms attracted to (**A**) PFA-treated or (**B**) mock-treated OP50 bacterial lawn. (**C**) Pairwise sensitized assay testing worm preference for mock-treated and PFA-treated OP50. (**D**) Pumping rate (pumps per 30 s) of worms on PFA-treated or mock-treated OP50. A two-tailed t-test analysis was used to derive p-values for all comparisons. All error bars shown in figures represent the standard error of the mean (SEM); **** denotes p-value < 0.0001. Panels A-C have been modified from Beydoun *et al.*[411].

5.2.4.2 Fecundity, development, and lifespan

Changes in food conditions can have physiological effects on worms[424,437]. To test for broad effects, changes in the rate of development, fecundity, and lifespan were measured. PFA-treated OP50 slightly delays development time (~4 h) of wildtype N2 worms as shown in **Figure 5.4A**. Monitoring the egg-laying capacity of worms grown on the different bacterial conditions shows a slight but significant decrease in fecundity (-21%) in the worms fed PFA-treated OP50 (**Figure 5.4B**). For labs interested in *C. elegans* aging, the effect of PFA-treated OP50 on longevity was then determined. Interestingly, the lifespan of wildtype worms fed PFA-treated OP50 was not significantly different from the worms fed mock-treated OP50 on standard Nematode Growth Media (NGM) plates (**Figure 5.4C**), however, PFA-treated OP50 increases wildtype lifespan (+23%) when FUdR is present (**Figure 5.4D**). Feeding PFA-treated OP50 to a long-lived *fmo-2* overexpressing (OE) strain[20] does not alter its longevity compared to wildtype worms (**Figure 5.4E**). UV-, heat-, and antibiotic-killed OP50 have also been shown to alter *C. elegans* lifespan. Specifically, UV-treated bacteria have been reported to extend lifespan on NGM[423,438] and on FudR[430]. However, there is conflicting data on the interaction of FudR and UV-killed bacteria[431,439] that may be due to varied methods of UV-killing and validation of metabolic inactivity in the bacteria. Additionally, heat-killed bacteria extend lifespan on NGM[432], and antibiotics extend lifespan on NGM[426] and in liquid culture[440].

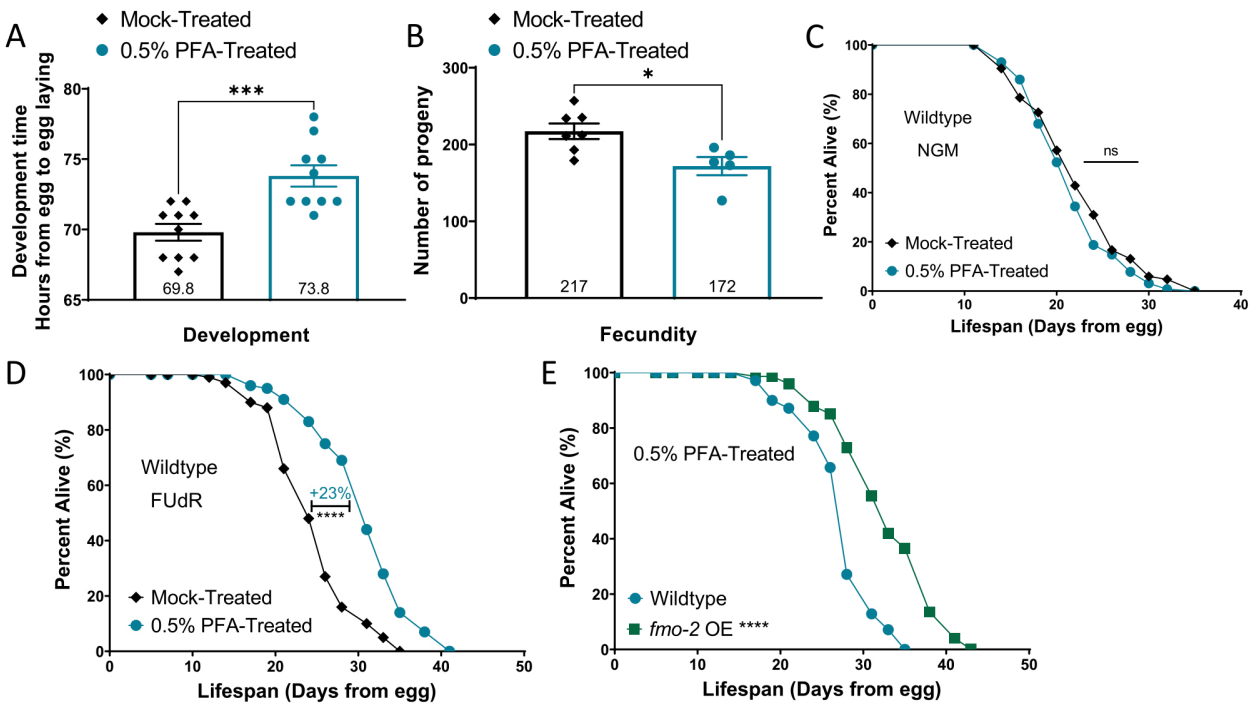


Figure 5.4 Worms grow and develop on PFA-treated OP50. (**A**) Development time (hours) of worms from egg-to-egg-laying adults on mock-treated and PFA-treated OP50. (**B**) Average progeny (number of worms) of worms fed mock-treated or PFA-treated OP50. (**C, D**) Percent alive of worms fed mock-treated or PFA-treated OP50 on (C) NGM and (D) FUdR lifespan plates. (**E**) Percent alive of wildtype and *fmo-2* OE worms fed PFA-treated OP50. A two-tailed t-test analysis was used to derive p-values for development and fecundity comparisons. The log-rank test was used to derive p-values for lifespan comparisons. All error bars shown in figures represent the standard error of the mean (SEM); * denotes p-value < 0.05, *** denotes p-value <0.001, and **** denotes p-value < 0.0001. Panels A, B, and D have been modified from Beydoun, et al.[411].

5.2.5 Discussion

5.2.5.1 Benefits of PFA-killing relative to other bacterial-killing methods

PFA-treatment is a high-throughput method to prevent bacterial metabolism while maintaining a nutritious food source for *C. elegans*. Killing bacteria via PFA-treatment has multiple advantages over other methods. Unlike UV-treatment, where every plate must be tested for successful killing, a single plate from a batch of PFA-treated bacteria can be tested to validate the batch[411]. PFA-treatment is also very effective at eliminating bacterial metabolism (**Figure 5.2B**), and PFA-treated bacteria exhibit decreased metabolic activity relative to antibiotic-treated bacteria[434]. Another benefit of PFA-treatment is that the bacteria maintain their cellular structure

and nutritional profile. Consequently, worms can develop on PFA-treated bacteria, whereas feeding heat-killed bacteria from egg results in developmental arrest[411,424].

5.2.5.2 Critical steps and troubleshooting

While PFA-treating bacteria is a relatively straightforward protocol, it is important to validate that each batch of bacteria is replicatively and metabolically dead (steps 6 and 7) and to ensure the washing steps after PFA-treatment are done thoroughly (step 5). If colonies do grow in step 6, indicating the bacteria is not completely dead, it is possible to troubleshoot the concentration of PFA and duration of PFA-treatment in step 3. When optimizing the PFA-treatment protocol, a 0.5% concentration of PFA was ideal for successful killing OP50 with minimal side effects. 0.25% PFA was not sufficient to metabolically kill all strains of bacteria (**Figure 5.2C-D**) and increasing the concentration to 0.5% PFA did not alter developmental time, lifespan, or food preference of worms on OP50 relative to 0.25% PFA. Also, 1 h of inoculation with PFA was the shortest time sufficient to prevent all bacterial growth. If bacteria are not completely killed by a 1 h inoculation with 0.5% PFA, the inoculation time and/or PFA concentration can be increased to troubleshoot killing efficiency. A second key step in the protocol is washing the bacteria after PFA-treatment (step 5). It is very important to complete all five washes and to completely remove the supernatant with each wash to ensure no formaldehyde remains in the bacteria. If worms are not growing well or not pumping on the PFA-treated bacteria, additional washes can be performed.

5.2.5.3 Limitations of the method

While PFA-killed bacteria are ideal for eliminating the confounding effects of bacterial metabolism (**Figure 5.2B**) from *C. elegans* studies, there are limitations to this method. Specifically, *C. elegans* have slightly slower development on PFA-treated bacteria relative to

live bacteria (**Figure 5.4A**)[411]. PFA-treatment also extends worm lifespan if FUdR is present (**Figure 5.4D**), but not on NGM (**Figure 5.4C**) plates[411]. However, other methods also present these challenges; UV-killed bacteria also alter *C. elegans* lifespan. The majority of reports suggest UV-treated bacteria extend worm lifespan on NGM[423,438] and on FudR[430], with other studies indicating UV-treatment does not affect lifespan[430] and that there is an interaction between UV-treatment and FudR on *C. elegans* lifespan[431,439]. In addition to the lifespan effects of PFA-treated bacteria, worms prefer to spend time on live bacteria relative to PFA-treated bacteria (**Figure 5.3C**)[411] but have a higher pumping rate on the PFA-treated food (**Figure 5.3D**). This suggests that they may consume a similar amount of food or that PFA-treated bacteria are easier or harder to eat. Many of these effects are also observed with other methods of killing bacteria[423-425], suggesting that metabolically active bacteria decrease development time, shorten lifespan, and are more attractive to *C. elegans*.

5.2.5.4 Potential applications of PFA-treated bacteria

Overall, the ability to quickly and reliably kill large batches of bacteria has great potential for eliminating the confounding effects of bacterial metabolism in *C. elegans* studies. This ability is particularly useful for drug screens, supplementation experiments, toxicity assays, metabolomics studies, and examining the effects of microbial metabolism on host behavior. More information on the use of PFA-treated bacteria in each of these applications is below.

Drug, supplementation, and toxicity experiments: Because only one plate per batch of PFA-treated bacteria needs to be tested for killing success, PFA-killed bacteria can be added to liquid culture for high-throughput drug screening. PFA-treated bacteria can also be seeded onto solid plates with small molecules or nutrients incorporated into the agar media. Solid plates seeded with PFA-treated bacteria could also be useful for toxicity or stress-response assays.

Unpublished data suggests PFA-treated bacteria can help distinguish between the role of bacterial stress-response pathways and worm stress-resistance pathways in paraquat and tunicamycin resistance. Using PFA-killed bacteria in these drug supplementation and toxicity studies prevent bacteria from metabolizing the molecule of interest and will ensure that any phenotypes observed results from a compound acting directly on *C. elegans.* Using metabolically dead bacteria for drug and supplementation experiments also minimizes variability in dosing, as live bacteria can metabolize different amounts of the compound of interest from experiment to experiment.

Metabolomics studies: *C. elegans* metabolomics studies can also be confounded by bacterial metabolism: observing changes in worm metabolism requires the absence of bacterial metabolic activity[441]. Even small changes to the bacterial food source can alter the worm metabolome. For example, the metabolome of worms fed live washed bacteria differs from the metabolome of worms fed live unwashed bacteria[411]. Consuming PFA-treated bacteria also changes the worm metabolome relative to consuming live food[411] but allows for comparisons between the effects of experimental conditions on *C. elegans* metabolism in isolation from bacterial metabolism.

Host-microbe behavioral studies: Finally, PFA-treated bacteria could be used to identify interactions between the bacterial metabolism and host behavior. Metabolites secreted by both pathogenic and non-pathogenic bacteria can be attractive or repellent to worms to affect their foraging and feeding behavior[275,421,422]. Moreover, bacteria can produce neuromodulators that drive changes in locomotion[275]. Additionally, growing *C. elegans* on different strains of bacteria results in altered brood size, development time, and physiology[258,442]. Treating these bacteria

with PFA can help determine whether the effects of a given bacteria on *C. elegans* require active bacterial metabolism.

5.2.6 Acknowledgements:

This work was funded by NIH R21AG059117 and the Paul F. Glenn Laboratories for Biology of Aging Research at the University of Michigan. SB was funded by T32AG000114. ESK was funded by NSF DGE 1841052.

5.3 findWormz is a user-friendly automated fluorescence quantification method for *C. elegans* research.

5.3.1 Abstract

The nematode *Caenorhabditis elegans* is a powerful model organism for fluorescent imaging studies due to its simplicity, transparency, well-characterized anatomy, and ease of genetic manipulation. However, the scale and statistical power of *C. elegans* imaging experiments can be limited by the time and effort required to manually quantify fluorescence intensity in individual worms. Recent advances in automated image analysis have used artificial intelligence models and user-supplied training data sets to automate biological image quantification. While these tools have the potential to significantly expedite a variety of research applications in *C. elegans* and other model organisms, they can be difficult to implement and troubleshoot, particularly for researchers with little or no computational training. Here, we introduce a simple method to automate *C. elegans* fluorescence quantification that is accessible to users able to install the free program R and edit a single line of code described here.

5.3.2 Description

Fluorescent imaging in *C. elegans* has been widely used to study processes such as neurobiology, development, aging, and stress responses[443,444]. Increasingly sophisticated image analysis techniques have significantly improved the ability to quantify and interpret fluorescent data in *C. elegans*. Open-source software like ImageJ/Fiji[445] and specialized software such as the WormToolbox component of CellProfiler[446] offer tools for segmenting worm shapes and detecting fluorescence in specific regions of interest. Machine learning algorithms and deep learning-based frameworks are also being developed to automate the analysis of complex imaging applications, such as identifying cellular structures or tracking fluorescence changes over time[447-449]. However, these tools can be difficult to implement and troubleshoot, particularly for researchers with little or no computational training[450,451]. An ideal user-friendly automated image analysis tool should 1) run on freely available and robust software, 2) not require training of an artificial intelligence model, 3) require users to edit as little code as possible, and 4) have a small number of adjustable parameters that can be manipulated to suit a wide variety of inputs. We developed the R-based findWormz method to meet these requirements and provide a simple and effective automated fluorescence quantification system.

Many *C. elegans* researchers quantify fluorescent images manually using open-source platforms like ImageJ/FIJI[93,105,248,452,453]. This process typically involves tracing the outlines of individual worms in a brightfield image, applying the trace pattern to corresponding fluorescent images, and measuring the mean fluorescence intensity of each worm. A user-selected portion of the image background is also traced and the corresponding region measured in the fluorescent channel to subtract the images' fluorescent background. The resulting data are then manually formatted and transferred into data analysis software for analysis (**Fig. 5.5A**). This method, while

functional and simple, requires researchers to manually draw around each individual worm in their sample, limiting maximum potential sample size, statistical power, and experimental scope. By contrast, the findWormz fluorescence quantification method requires slightly more upfront time when taking fluorescent images of *C. elegans* but saves time by automatically identifying and quantifying the fluorescence of each worm in each image of the experiment (**Fig. 5.5B**).

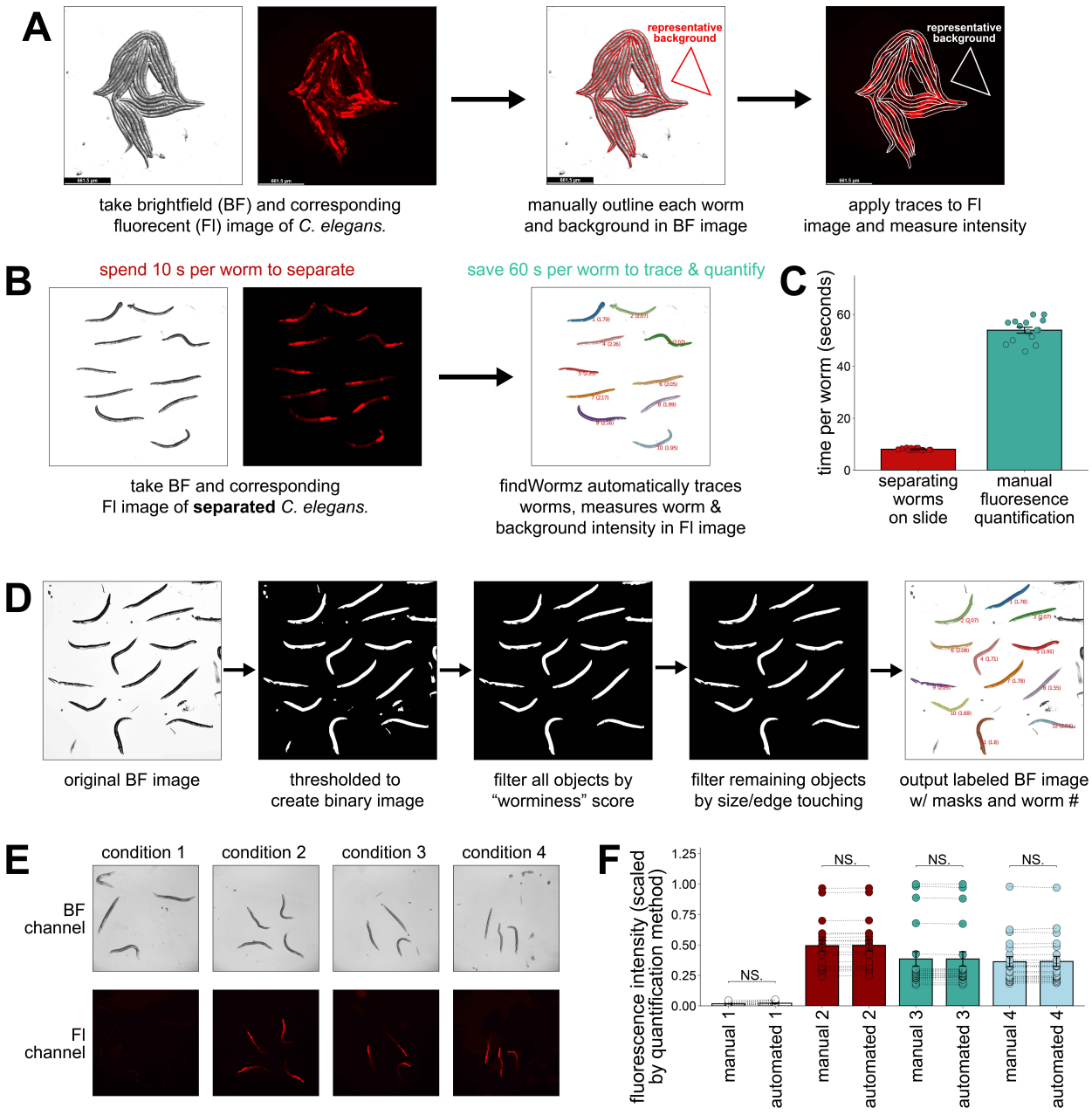


Figure 5.5 The findWormz method automatically identifies and quantifies the fluorescence intensity of individual *C. elegans*. (**A**) Schematic of a traditional workflow for manually tracing and quantifying the fluorescence of individual *C. elegans*. (**B**) Schematic of the findWormz workflow for automated quantification of *C. elegans* fluorescent microscopy images. (**C**) Average time in seconds/worm required for a *C. elegans* researcher to separate each worm in a clump of 20 worms and to trace the outline of each worm in an image of 20 clumped worms. (**D**) A diagram showing the steps findWormz implements to separate pixels containing worms from the image background. (**E**) Representative brightfield (BF) and fluorescent (Fl) channel images of *fmo-2p::mCherry* worms on four conditions with varying fluorescence. (**F**) Quantification of images of *fmo-2p::mCherry* worms on four conditions with varying fluorescence. The same images were quantified manually (method described in panel **A**) or using the findWormz method (described in panel **B**), and the arbitrary units from the same image analyzed by each quantification method were scaled from 0 to 1. Dashed lines show the same individual worm quantified with

each method. Two-way ANOVA with Tukey Post-Hoc pairwise analysis was used to derive p-values. All error bars shown in the figures represent the standard error of the mean (SEM). NS. indicates not significant.

While the transparency of nematodes is beneficial for the ease of imaging fluorescent markers, this transparency does make it difficult for image analysis software to distinguish between multiple worms that are touching. Specifically, their transparency and the backlit background of a standard brightfield microscope create very light and very dark patches within the same worm, depending on what tissues the brightfield light passes through. Consequently, worms do not appear as uniform grey shapes with a dark or light outline, making clumps of touching worms difficult to accurately segment. This challenge can be overcome, but the currently available software that can distinguish between multiple worms touching one another requires training an AI deep learning model for each use case[446,454]. Consequently, the findWormz method requires that users take images of worms that have been pushed apart and are not touching in the input image. While this requires more time on the front-end to separate a clump of worms, these extra 10 seconds/worm are generally worth the 60 seconds/worm saved from eliminating the manual worm tracing step (**Fig. 5.5C**). After taking images of separated worms in the brightfield and fluorescent channels, users can place these images in a folder with a key matching file names to experimental conditions.

In order to run findWormz on these images, users will need to download and install the free program R. Detailed instructions and links to downloading R can be found in the full protocol in the extended data. After installing R, the user can open the worm_batch.R file, and edit one line of code to tell the program the location of the images and program files on their computer. This edit involves copying the file path to where their experiment is located on their computer, and pasting this file path into line 13 of the worm_batch.R file to replace the placeholder text labeled "filepath".

After the file path to the *C. elegans* images is specified, the findWormz pipeline begins by opening the brightfield image, enhancing the contrast, correcting for non-uniform background lighting, and blurring the image slightly to increase color uniformity within each worm. Then, findWormz thresholds this corrected brightfield image into a binary image and fills small holes within larger regions of black or white to reduce noise (**Fig. 5.5D**, steps 1-2). Next, each object within the binary image is scored for its "worminess", or the perimeter of the object divided by the 4 times the square root of the object's area. This resulting worminess score is a scale invariant measure reflecting how spindly or round an object is. The lowest possible worminess score, 0.89, would represent a circle. Given their consistently long and thin shape, *C. elegans* have a default worminess score between 1.5-2.1, but the upper and lower bounds of acceptable worminess can be adjusted by the user to account for morphological differences in *C. elegans* mutants. Objects that fall outside of this worminess range are removed from the analysis (**Fig. 5.5D**, step 3)**.**

Finally, the remaining objects are filtered by size. Users can adjust the minimum acceptable size range for a worm, depending on the magnification of the image (**Fig. 5.5D**, step 4). After this step, the pixel masks of remaining objects are applied to the corresponding fluorescent image and measures of mean fluorescence, standard deviation of fluorescence, worm area, and worm perimeter are recorded. A fluorescent background is also calculated for the image by taking an average intensity measurement of the pixels not identified as worm or debris after initial thresholding (step 2). A colored representation of each identified worm is also plotted onto the original brightfield image, along with a worm number corresponding to each measurement recorded in the analysis spreadsheet (**Fig. 5.5D,** step 5). This color-coded image is saved for users to manually run quality control and ensure all recorded objects are, in fact,

worms. Details about image quantification and analysis using the findWormz method, as well as the adjustable parameters can be found in the detailed protocol included in the extended data files. All annotated code files can also be found in the extended data files and on Github at https://github.com/eskitto/findWormz.git.

When the findWormz method was tested against the lab "gold-standard" technique of manually tracing worms from the same image, the results were consistent across four different images varying in fluorescence intensity (**Fig. 5.5E-F**). In addition to the above tests for accuracy, the findWormz method has been used successfully in-house for over four years by students and scientists with varying levels of computational training. Together, these results indicate that findWormz is an accurate, user-friendly, and efficient method for quantifying fluorescent images in *C. elegans*. However, the findWormz workflow does still require some technical knowledge. The requirement of installing and editing R code makes findWormz less accessible than completely code-free workflows, such as Image J plug-ins. Nevertheless, running findWormz directly on R allows the program to access 3 GB of working memory rather than the maximum of 1.8 GB in Image J. As a result, the direct use of R prevents the program from running out of memory when analyzing large image sets, and increases analysis speed. Future work in this area could re-write the findWormz analysis process in Java to allow for findWormz to run as an Image J plugin, while keeping in mind that this may restrict analysis capacity.

Together, our results indicate that the findWormz method has the potential to save *C. elegans* researchers about 15 minutes of worm-tracing time per fluorescent image with a standard sample size of 20 worms. Additionally, findWormz measures a more accurate background fluorescence reading than manual methods by including all pixels in the image that are not covered by worms, eggs, larva, or artifacts on the slide. Finally, this method can be run on the free coding platform

R and only requires users to modify one line of code under standard imaging conditions. Overall, the findWormz method presents an efficient, user-friendly alternative to manual quantification of *C. elegans* fluorescence images.

5.3.3 Methods

Strains and growth conditions

Standard *Caenorhabditis elegans* cultivation procedures were used as previously described (Kaeberlein et al., 2006; Smith et al., 2008). Briefly, *fmo-2p::mCherry* fluorescent reporter (LZR01) worms were maintained on solid nematode growth media (NGM) seeded with 200 µL live *E. coli* OP50 (OD_{600} 3.0) throughout life and housed in a 20°C Percival incubator. All experiments were conducted at 20°C unless stated otherwise.

Slide Microscopy

Fluorescent images in this study were taken using Leica Application Suite X (LASX version 3.7.5.24914)software and a Leica scope with >15 worms per treatment at ≥35x magnification. For representative images displayed in the figures, worms were paralyzed in 0.5 M sodium azide (NaN_3) and imaged once residual liquid evaporated and the worms clumped together. For quantification of these images and for imaging screens, the same method was used but after the residual sodium azide had evaporated, individual worms were gently pushed apart until they were no longer touching one another. Fluorescent mean comparisons were then quantified using the findWormz method in R (see extended data for protocol and code) to identify individual worms and measure fluorescent intensity. The mean fluorescent intensity of the background (all non-worm pixels) was subtracted from the mean fluorescence of each worm. All outputs from this R code were visually inspected and any non-worm objects that were misidentified by the

program were removed. Data were plotted by R version 4.3.3 and Adobe Illustrator 2022. The brightness of representative fluorescent images in each figure panel was increased to an equal degree across all images within the panel in ImageJ bundled with 64-bit Java 1.8.0.

Statistics and reproducibility

Two-way ANOVA with Tukey Post-Hoc analysis was used to derive p-values for fluorescence comparisons. All error bars shown in the figure represent the standard error of the mean (SEM).

Software Version Information

All R code was tested on R version 4.4.3.tar.gz, and R Studio version 2024.12.1+563. Details about image quantification and analysis using the findWormz method, as well as the adjustable parameters can be found in the Protocol section below. The annotated code files for worm_batch.R, findWormz.R, and analyzeWormz.R can be found in **Appendices A-C**, respectively.

5.3.4 findWormz Detailed Protocol

1. **Prepare your slides:** Microwave a solution of 3% agarose in ddH_20 until it boils. Remove from the microwave, mix the solution a bit until bubbles dissolve, return to microwave and bring to boiling a second time. Take a 1,000 µL pipette tip and remove the bottom third of the tip with scissors or a razor blade. This will allow you to pipette the viscous agarose gel solution. Set your pipette to ~500 µL, and dispense the melted agar onto a glass slide. Take a second glass slide with two layers of tape wrapped around each end, and gently press this taped slide over the slide with the hot agarose. Push on any large bubbles that appear in the agar to pop them and hold until the agar becomes cool.

Remove the slide with the tape. If you are imaging many conditions, you can prepare multiple slides and keep them on ice until imaging.

2. **Put worms on the slide:** fill a 10 µL pipette with ~5 µL of sodium azide solution. Make sure to wear gloves while handling sodium azide. Apply a drop of sodium azide to the location on the agar pad you plan to place your worms. If you are adding multiple conditions to one slide, make sure you leave room to spread multiple clumps of worms out, leaving enough room to take separate images of each condition. This takes at least twice as much space as traditional imaging. Using a worm pick, grab worms from your plate without grabbing any bacteria. Place worms in the sodium azide droplet. Continue until you have achieved your desired sample size.
3. **Separate your worms:** The ideal time to separate your worms is after most, but not all of the sodium azide droplet has evaporated. You want enough liquid for worms to glide across the agar, but not too much that they do not stay in place when you remove your pick. If needed, apply a small amount (~1-2 µL) of additional sodium azide to reach this level of liquid. Using a traditional worm pick or an eyelash pick, gently pull the worms apart into groups of ~10-20 worms that are not touching but are still relatively close together (see example images, **Figure 5.6**). I find it easiest to align the long edge of a pick with the worm so you do not apply too much pressure to the head or tail and damage the worm. Some eggs and larva are OK if they get on the slide in the background, they will be excluded from analysis. However, any eggs or larva that touch the adult worm will be included in the quantification of that worm. Do not add a coverslip to your slide—this will create a bubble around each worm making it impossible for the algorithm to trace. The absence of a coverslip will not affect your fluorescence quantification but does

cause the worms to dry out faster. Make sure you image worms within ~20 minutes of separating them on the slide.



Figure 5.6 Example brightfield input image for findWormz quantification.

4. **Image your worms:** Once you have filled your slide, you are ready to image the worms. For the channel in which you take the brightfield image, set the scope parameters to enhance the contrast between the worm and the background. (i.e. darker worm and white background is much better than gray worm and gray background). I typically set the aperture to ~70% and the intensity to ~40% (see example image above). Set the magnification to a level where you can see all the worms in your largest cluster. Changing magnification between conditions can affect your measurement of fluorescent intensity per pixel. Take images of all conditions. Note that worms touching the edge of the image will be excluded from your analysis.
5. **Naming your images:** The naming scheme is critical to correctly assigning experimental condition values to your final dataset. Each condition should receive a number, and each image taken of worms from that condition will receive a second number. A "key" to decode each condition will be given to the findWormz program to label your data. For example, if I am imaging two conditions (fed and DR), my "C1", or condition1 would be the fed worms. C2 would be DR worms. If I take two images of fed worms, I would label

them “C1_1” and “C1_2”. It is important that the letter C is before the condition number and an underscore separates the condition number from the image number. If you only take one image of a certain condition, you still need to include “_1” in the label.

6. **Exporting your images:** Once you have taken and named all of your images, export them all as TIF images. Do not overlay channels, export the brightfield and fluorescent images separately.
7. **Setup directories to run findWormz:** Create a main folder in which you will have three subfolders. The name of the subfolder can be anything you want. Add three folders within the main folder: “R code”, “input”, and “output”. Place the three R code files (analyzeWormz, findWormz, and worm_batch) within the R code folder. Place all fluorescent images you exported (TIFF files from brightfield and fluorescent channels) in the input folder. Create a csv file in which you label the information you want included with each condition. The first column of this csv file must be called condition_code, but you can add as many additional columns as you like with info about that condition. An example from one of my experiments is below. Name this file “conditions_map.csv” and put it in the inputs folder. Leave the output folder empty.

condition_code	RNAi	condition 1	condition 2	genotype
C1	EV	fed	none	fmo2p::MC; MAH677
C2	EV	fed	OP50	fmo2p::MC; MAH677

C3	EV	DR	none	fmo2p::MC; MAH677
C4	EV	DR	OP50	fmo2p::MC; MAH677

Table 5.2 Example input for the conditions_map file.

8. **Run the code:** First, install R and Rstudio if you do not already have these programs on your computer. Links to download both are below:

- R: https://cloud.r-project.org/
- RStudio: https://rstudio.com/products/rstudio/download/

Then, open the worm_batch.R file in your R code folder. If it is your first time running the program, highlight lines 1-10 and click control/command+enter to install the packages you will need. These lines only need to be run once.

Then, edit line 13 of the code to specify your "working directory", or the main folder that contains the three subfolders specified above. This filepath must be in quotations.

Next, check the names of you brightfield and fluorescent images. Most microscope software will export brightfield images with "_ch00" in the filename, and fluorescent images with "_ch0x" in the filename, with x depending on the number of fluorescent channels. The default designator for brightfield images in findWormz is "_ch00" and the default designator for the fluorescent image is "_ch01". However, if this is different in your files, change the text in quotes in line 16 to include characters that are only in the brightfield image name and not in the fluorescent image name. Do the same but select fluorescent image-specific text in line 17. This will tell findWormz which image to use for finding worms, and which image to analyze.

This is the only code you will normally need to change. After doing so, select all the code in lines 20-44 (from “setwd” to the end of the program), and run them. Worms_batch will then populate your output folder with images of identified worms, a csv file with your quantification, and a csv file with the parameters used on this run. Both csv files will be timestamped with the date you ran the code.

Example output image: the first number is the assigned worm number. The number in parentheses is the “worminess score”. This score is included to help troubleshoot false negatives or false positives. If a non-worm object is identified, you can find the row from that file name and worm number in the analysis output spreadsheet and manually delete it.

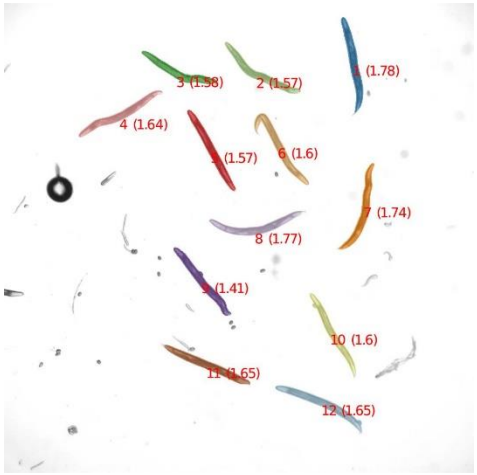


Figure 5.7 Example output image from findWormz quantification.

9. **Advanced options and troubleshooting:** Within the worm_batch code, you can change the inputs to line 13 (analyzeWormz) to troubleshoot or customize your output. These optional changes are explained below. If a parameter is not listed below, I highly recommend you do not change it.
    - **troubleshootMode;** if you change this from “FALSE” to “TRUE”, the code will output four images with the changes made at each step of the code’s analysis pipeline.

This is helpful if you want to decide which other parameters to change in order improve accuracy of worm identification.

- **Worminess_min_thr and worminess_max_thr:** these can be helpful to change if the code is mistakenly identifying non-worm objects. Look through your output files and find these objects. The second number in parentheses next to them is the worminess, which is a measure of how spindly or round an object is. Typically, non-worm objects will have a low worminess score below 1.35 or above 2.05. Changing the min and max worminess threshold will adjust what objects are excluded by changing that range. This can be helpful if you are imaging *C. elegans* strains with morphological phenotypes (ie *dpy*).
- **backgroundCorrect:** the background correction steps enhance image contrast and correct for non-uniform lighting in the brightfield image background. If you do not want these corrections to be made, set backgroundCorrect to FALSE.
- **showPlots:** if you want to see the series of images the code produces as it is running in Rstudio, set showPlots to TRUE. Note that this will slow down the runtime some and will use a lot of memory.

Chapter 6 Conclusions and Future Directions

Demographic shifts towards an increasingly aging population accentuate the need to delay or prevent age-related diseases[2,4]. In response, the field of biogerontology has identified a range of environmental, genetic, and pharmaceutical interventions aimed at promoting longevity. Many of these interventions involve exposure to mild environmental stressors that activate stress-response pathways, which in turn can increase lifespan. As a result, there is growing interest within both the scientific community and the public regarding how these stress-response pathways might be targeted in humans to extend healthspan and lifespan. However, several challenges remain in developing safe and effective anti-aging treatments. This dissertation addresses three such challenges: 1) the impact of complex environmental signals on the efficacy of longevity treatments; 2) the identification of highly specific targets for longevity interventions; and 3) the effects of longevity interventions on behavior and mental state. The key findings of this research are summarized below, along with recommendations for future studies that could build upon the work presented in this dissertation.

6.1 Summary of Conclusions

In Chapter 1 of this dissertation, we reviewed the motivation for studying the biology of aging, previous work on the role of cell nonautonomous signaling in aging, and obstacles facing the implementation of environmental, genetic, and pharmaceutical anti-aging treatments. In Chapter 2, we examined the effects of environmental food cues on one of the best-studied longevity interventions, dietary restriction. In multicellular organisms, sensory perception

influences a wide range of behaviors and physiological processes. For instance, the detection of environmental stressors, such as nutrient scarcity, often triggers adaptive physiological changes that support survival and help slow aging. However, recent research indicates that the detection of food tastes or odors can negate some of the health benefits of dietary restriction across several model organisms[105,112,206,455]. While it is understood that sensory perception by the nervous system can impact health and lifespan across multiple tissues, our knowledge of the specific sensory signals and the underlying molecular pathways involved in this regulation remains incomplete. In Chapter 2, we explored how the sense of touch interacts with nutritional conditions to influence lifespan in *C. elegans*. We found that worms subjected to dietary restriction are shorter-lived when exposed to tactile cues that resemble bacterial food or protective soil. This touch-based modulation of dietary restriction relies on primary mechanoreceptors, the neurotransmitters dopamine and tyramine/adrenaline, and the neuropeptides insulin and GnRH. Ultimately, this touch-mediated pathway regulates multiple peripheral longevity factors, including DAF-2/IGF1R and FMO-2/FMO5. These results demonstrate how neural sensory perception pathways may be linked to growth, aging, and reproduction. Additionally, the observation that touch can influence longevity suggests that physical comfort may play a significant role in health and aging.

After examining the neural circuits driving dietary restriction-mediated longevity in Chapter 2, Chapter 3 investigates the role of cell nonautonomous signaling in a second environmental longevity intervention. Hypoxia, or exposure to reduced oxygen levels, promotes both healthspan and lifespan in *C. elegans*[106,456]. Interestingly, genetic manipulation that mimics hypoxia—such as the suppression of the E3 ubiquitin ligase von Hippel-Lindau 1 (VHL-1) or the stabilization of hypoxia-inducible factor (HIF)—is also capable of extending lifespan in

nematodes[27,48,334]. However, translating these findings to mammalian systems is challenging due to the negative consequences of activating the conserved hypoxic response, including increased likelihood of cancer and cardiovascular disease[338-341]. One way to mitigate these risks could be to identify downstream targets within the hypoxic pathway that regulate aging without triggering harmful components of the hypoxic response. The work presented in Chapter 3 builds on earlier research to identify molecular mechanisms behind hypoxia-induced longevity in *C. elegans*, with the aim of uncovering potential therapeutic targets for aging.

This investigation demonstrated that serotonin signaling in the ADF serotonergic neurons is both necessary and sufficient to extend lifespan under hypoxic conditions. Furthermore, serotonin signaling through the SER-7 receptor in RIS interneurons plays an essential role in this process. Our results also highlight the involvement of additional neurosignaling molecules, such as tyramine, GABA, and NLP-17, in mediating the observed longevity effects. Finally, we reveal that oxygen- and carbon-dioxide-sensing neurons are required for HIF-1 stabilization in ADF neurons to extend lifespan. These findings provide valuable insights into the hypoxia-mediated longevity pathway and present potential targets for neural aging interventions in mammals. For example, inducing hypoxic signaling in neurons could extend lifespan while minimizing undesirable effects due to the post-mitotic status of neurons.

Together, Chapters 2-3 of this dissertation exemplify the ability of stress perception and neuronal signaling to regulate stress-response pathways in peripheral tissues and coordinate an integrated aging response across the organism. However, the nervous system also drives changes in behavior to promote survival in response to acute and chronic stressors. In Chapter 4, we ask whether the behavioral and longevity effects of stress-response pathways act through distinct mechanisms, and whether changes in peripheral metabolism can feedback to modify neural

signaling. To explore these questions, we analyzed the behavior of *C. elegans* mutants with altered expression of the longevity-modifying gene flavin-containing monooxygenase 2 (*fmo-2*).

Our findings in Chapter 4 revealed that either knocking out or overexpressing *fmo-2* changes worms' sensory perception and decision-making behavior when compared to wild-type (WT) controls. Both the knockout and overexpression of *fmo-2* resulted in reduced exploration of novel environments through alterations in tryptophan metabolism. Interestingly, blocking the synthesis of the tryptophan-derived neurotransmitter serotonin was able to restore exploratory behavior in the *fmo-2* knockout, while blocking the production of quinolinic acid, another tryptophan metabolite, reversed the decreased exploration in *fmo-2* overexpressing animals. These interventions that restored exploration also partially rescued other phenotypic traits—such as behavioral, reproductive, and longevity-related outcomes—in both the *fmo-2* knockout and overexpressor, though not all effects of altered *fmo-2* expression were reversed. These findings highlight a novel role for FMO-2 in regulating behavior and underscore the importance of considering pleiotropic effects when evaluating potential longevity interventions.

While Chapters 2-4 make progress in understanding cell nonautonomous modification of longevity and addressing the challenges facing implementation of longevity interventions, there is still much work to be done. *C. elegans* are a valuable model system for studying aging, cell nonautonomous signaling, and behavioral circuits: they have short lifespans, relatively simple and homogeneous neural wiring, their transparency allows for easy fluorescent imaging, and there are abundant tools available for genetic manipulations. Nevertheless, no model system is perfect. Studies of metabolism and pharmaceutical interventions in worms can be complicated by the fact that *C. elegans* consume a diet of live OP50 *E. coli* bacteria. Consequently, the effects of bacterial metabolism can be hard to distinguish from changes in worm metabolism. Additionally,

while fluorescent imaging studies are relatively simple in *C. elegans* due to their transparent cuticle and ease of genetic modification, the scope of these studies can be limited by the time it takes to manually quantify fluorescent images. In Chapter 5, we addressed these methodological challenges in *C. elegans* research through the development of a metabolically inactive bacterial food source and an automated system to quantify fluorescent images of *C. elegans.*

Together, this dissertation demonstrates how sensory perception and neural signaling pathways can regulate aging-related processes across an organism. Through the examination of dietary restriction, hypoxia, and *fmo-2* expression, we reveal the complex interactions between environmental cues, behavioral responses, and longevity outcomes. These findings highlight the importance of considering the integrated roles of neural circuits and peripheral tissues in aging. Additionally, this work underscores the need for further exploration of how these pathways can be harnessed to develop effective anti-aging interventions.

6.2 Recommendations for Future Work

6.2.1 How do multiple forms of food perception interact to modify lifespan?

Work from multiple invertebrate labs shows that the efficacy of DR in lifespan extension is attenuated by the presence of food smells[105,112]. In Chapter 2 of this work, we find that food-like touch can also blunt DR-mediated longevity. However, smell and touch are not the only means through which *C. elegans* and other organisms perceive food cues. For example, gustatory perception (taste) and enteric perception (the detection of food inside the gastrointestinal tract) are also critical indicators of nutrient availability[457-459]. To follow up on this work exploring food perception in dietary restriction and aging, the field should explore two key questions: 1) do gustatory and enteric food cues regulate aging rate, and 2) does information about different food cues like smell and touch modify DR through parallel or converging neural circuits?

6.2.1.1 Do gustatory and enteric food cues regulate aging rate?

Work from multiple research groups clearly shows that olfactory food perception attenuates the longevity benefits of dietary restriction in invertebrates[105,112]. While no lifespan studies have been conducted to examine the effects of food smell on dietary restriction-mediated longevity in mammals, there is some evidence that this phenomenon may be conserved. For example, work by the Dillin lab discovered that ablating the olfactory neurons of adult mice led to fat loss in animals on a standard chow and on a high-fat diet. Markers of metabolic health, such as circulating insulin and performance on a glucose tolerance test also improved in the hyposmic mice on the high fat diet[455]. Importantly, in both the control and high fat diet groups, the olfactory ablation did not decrease food consumption but did increase energy expenditure. Interestingly, these effects required beta adrenergic receptors that respond to adrenaline and noradrenine[455]. Given that the *C. elegans* food touch circuit described in Chapter 2 also requires tyramine/adrenaline signaling for food perception to modify health, this could be a shared mechanism of integrating environmental food cues to produce a metabolic response.

Similar to food smells, Chapter 2 of this work demonstrates that mechanosensory perception of a food-like texture also decreases DR-mediated longevity in *C. elegans*. While food touch may be more difficult to study in higher model systems, multiple groups have shown that touch and pain circuits do play a role in aging rate. In worms, a repetitive and stressful touch stimulus that persists over the lifespan (tapping the petri dish housing *C. elegans*) decreases their lifespan under fed conditions in a tyramine-dependent manner[58]. In mice, ablation of the TRPV-1 painful touch receptor extends lifespan by modifying release of the neuropeptide CGRP, which in turn improves insulin sensitivity[51]. Together, this work indicates touch and pain perception could play an essential role in metabolic health and longevity.

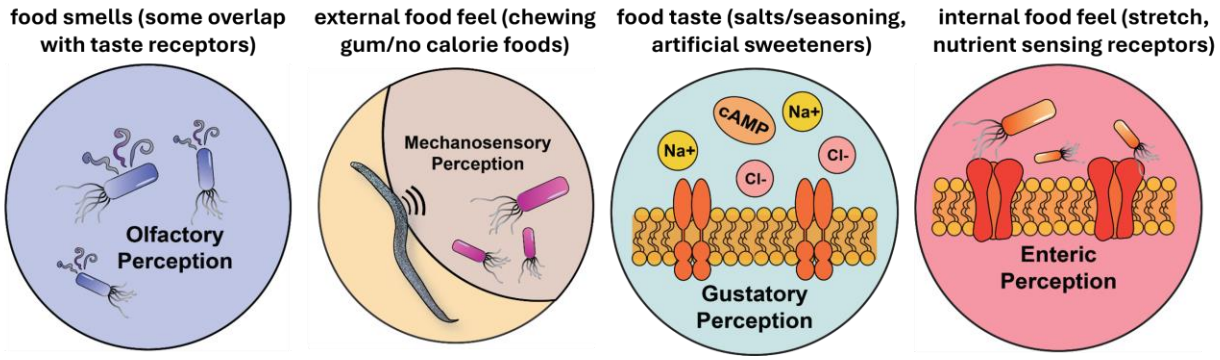


Figure 6.1 Olfaction, mechanosensation, gustation, and enteric perception contribute to food sensing across taxa.

In addition to smell and touch, other sensory systems like gustation (taste) and enteric perception (detection of food entering the body) are essential to perceiving nutrient availability across taxa[460] (**Figure 6.1**)**.** However, it is unclear whether the absence of these sensory food cues is as important to DR-mediated longevity as the absence of food smell and touch. While exploring the role of food perception in aging, I collected some preliminary data suggesting that enteric and gustatory perception may also modify health and lifespan, but future work is needed to confirm and follow up on these results.

With respect to enteric perception, there is relatively little known about how *C. elegans* detect the presence of food in their grinder, pharynx, or intestine. However, work by the Flavell lab did identify two acid-sensing ion channels (ASICs) that are expressed on a projection from the serotonergic NSM neuron right next to where food enters the grinder of the worm. These channels, DEL-3 and DEL-7, activate the food-sensing NSM neuron when the worm starts eating, and are required for the worm to slow their speed upon entering a bacterial lawn[298]. Consequently, these channels may act like enteric food sensors, detecting when food first enters the worm. Interestingly, food smell does not attenuate DR-mediated longevity in *del-3; del-7* knockout worms[105], and *del-7* is also required for food touch to blunt DR longevity (Chapter 2). Moreover, *del-3; del-7* knockouts are long-lived relative to fed worms, but are not further

extended by dietary restriction (**Figure 6.2**). This suggests that enteric food perception through activation of ASICs could contribute to DR-mediated longevity, much like olfactory and mechanosensory food perception. While these data show the absence of enteric food cues can extend lifespan, future work in this area should also confirm whether the perception of enteric food cues (e.g., non-nutritive digestible materials or high-volume, low-calorie foods) are sufficient to blunt DR-mediated longevity in WT animals. Similarly, the interactions between other mechanisms of enteric food perception and aging should be explored both in invertebrates and in mammalian models systems.

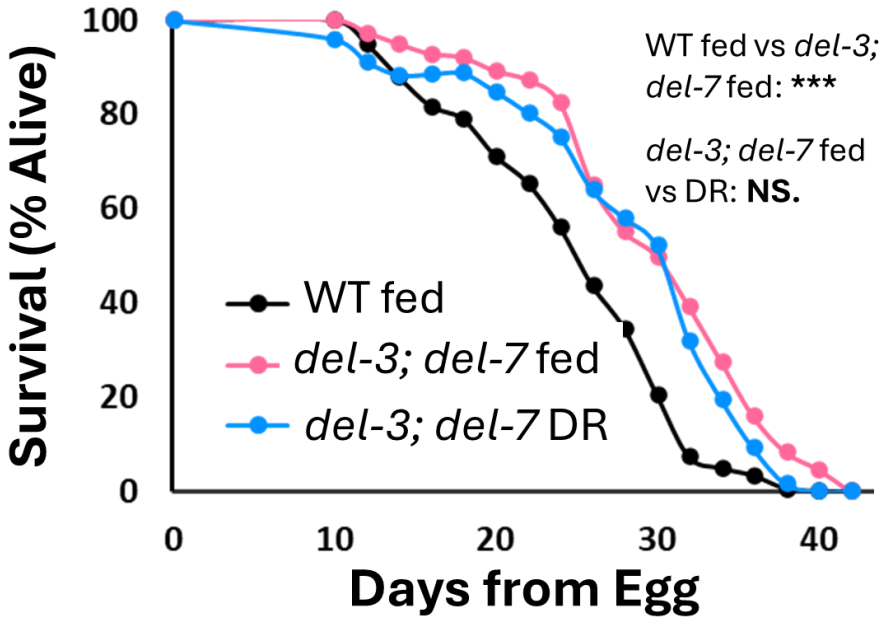


Figure 6.2 *del-3; del-7* knockout extends lifespan non-additively with dietary restriction. Survival curve of WT, and *del-3(ok2613); del-7(ok1187)* worms on fed or DR conditions. $N \geq 65$ worms per condition. NS. = $p > 0.05$, and *** = $p < 0.001$ from a log-rank test comparing median survival.

In addition to olfaction, mechanosensation, and enteric food perception, I was also curious whether taste cues could influence dietary restriction and aging. To test the role of gustatory perception in DR, I screened for *fmo-2* induction on fed and DR conditions with and without 17 water-soluble 'tastes' found in the nematode's natural environment (summarized in

Table 6.1). In this screen, we used DR-mediated *fmo-2* induction as a short-term proxy for DR-mediated longevity because *fmo-2* is required for DR-mediated longevity, and because overexpressing *fmo-2* extends lifespan non-additively with DR[48,105,326]**.** The taste compounds used in this screen fall into three main categories of tastes detected by *C. elegans*: salts, small molecules, and amino acids. Within each of these categories, we included compounds that are attractive, neutral, or repellent to the worm[461,462]. Because attractive smells and touches blunt DR-mediated *fmo-2* induction in *C. elegans*, we hypothesized that many of the attractive taste compounds would similarly blunt DR. By contrast, we expected the neutral compounds to have minimal effects on *fmo-2* induction and the repellent compounds to potentially induce *fmo-2* by mimicking pathogen exposure or other environmental stressors.

Category	Valence of Compound	Taste Compound(s)
salts	attractive	NaOAc, NH_4Cl, NaCl
	neutral	NH_4OAc, Ni(II)OAc
	repellent	Cu(II)OAc, Cd(II)OAc, high [NaCl]
small molecules	attractive	cAMP, biotin
	neutral	low [glycerol]
	repellent	quinine
amino acids	attractive	lysine, histidine
	neutral	glycine
	repellent	NA
other	repellent	high [glycerol]

Table 6.1 Water-soluble taste compounds screened for effects on *fmo-2* induction under fed and DR conditions.

Under fed conditions, we found that the addition of many water-soluble compounds across all valence categories induced *fmo-2*. The average effect of attractive, neutral, and repellent compounds was a 21%, 14%, and 52% increase in *fmo-2* induction, respectively (**Figure 6.3A**). Under DR conditions (24 hours of fasting with or without the compound), attractive and neutral compounds decreased DR-mediated *fmo-2* induction by 20% and 19%, respectively, while repellents increased DR-mediated *fmo-2* induction by 14% (**Figure 6.3B**). Looking at the effect of each compound separately, we found that two of the seven attractive compounds (low concentration sodium chloride and biotin), none of the four neutral compounds, and three of the five repellent compounds (cadmium chloride, quinine, and copper sulfate) induced *fmo-2* induction under fed conditions (**Figure 6.3C**). Under DR conditions, four of the seven attractive tastes (sodium acetate, sodium chloride, histidine, and cAMP), two of the four neutral compounds (ammonium acetate and glycerol), and none of the repellent compounds decreased *fmo-2* induction (**Figure 6.3D**). Interestingly, the compound with the strongest DR-blunting effect was the neutral salt ammonium acetate (**Figure 6.3D**).

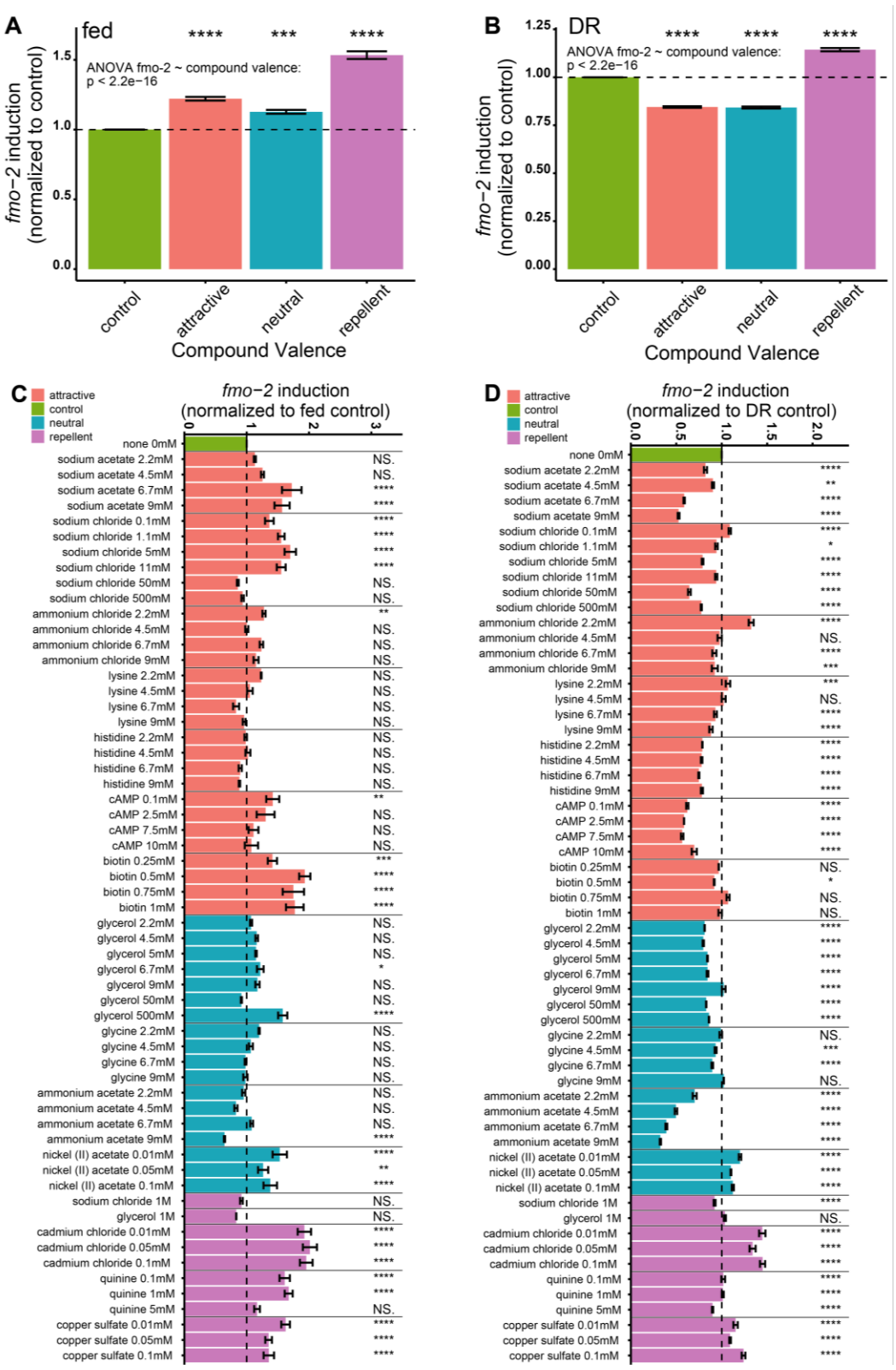

A
fed
ANOVA fmo-2 ~ compound valence:
p < 2.2e−16
fmo−2 induction
(normalized to control)
control
attractive
neutral
repellent
Compound Valence
B
DR
ANOVA fmo-2 ~ compound valence:
p < 2.2e−16
fmo−2 induction
(normalized to control)
Compound Valence
C
attractive
control
neutral
repellent
fmo−2 induction
(normalized to fed control)
D
fmo−2 induction
(normalized to DR control)

Figure 6.3 Many water-soluble taste compounds affect *fmo-2* induction under fed and DR conditions in *C. elegans*. (A-B) Quantification of *fmo-2p::mCherry* on fed (**A**) or DR (**B**) +/- attractive, neutral, or repellent taste compounds. N ≥ 300 worms per condition. Significance is from a one-way ANOVA (*fmo-2* induction ~ valence) and post-hoc Tukey HSD test (unpaired, two-tailed) with a Bonferroni p-adjustment. **(C-D)** Quantification of *fmo-2p::mCherry* on fed (**C**) or DR **(D**) +/- each concentration of each taste compound screened. *N* ≥ 75 worms per condition. Significance is from a two-way ANOVA (*fmo-2* induction ~ compound*concentration) and post-hoc Tukey HSD test (unpaired, two-tailed) with a Bonferroni p-adjustment. In all panels, the bar height indicates mean fluorescence normalized to the no taste control, and the error bars represent the standard error of the mean. NS. = p > 0.05, * = p < 0.05, ** = p < 0.01, *** = p < 0.001, **** = p < 0.0001.

While these results suggest that taste-like compounds could influence aging and metabolism through *fmo-2* induction, there are many potential confounding factors. First and foremost, the *fmo-2* inducing effects of many attractive and neutral compounds on fed conditions suggests that the worms may either be responding to changes in the osmolarity of the media, and/or could be inducing *fmo-2* as part of a response to detoxify xenobiotic metabolites[372,405,463]. Some of the aversive water-soluble compounds can also induce heavy-metal stress and toxicity at high enough concentrations, affecting stress response circuits independent of nutrient sensing[464]. This interpretation is supported by the ability of repellent compounds to induce *fmo-2* in the DR condition, indicating at least some of the repellent *fmo-2* induction effect is acting through a mechanism separable from DR. Secondly, because these water-soluble compounds are dissolved in the agar of the plate *C. elegans* are grown on, it is challenging to untangle whether these effects on *fmo-2* induction are the result of gustatory perception or the result of metabolic changes from consumption of salts and/or other nutritive small molecules and amino acids.

With these limitations in mind, we only followed up on the top hits from the taste imaging screen with one replicate of a lifespan. In this experiment, we measured survival of WT worms under fed and DR conditions with and without the compound with the largest decrease in DR-mediated *fmo-2* induction (ammonium acetate), and a compound that had no effect on fed or DR-mediated *fmo-2* induction (glycerol). We found that 3mM and 10mM ammonium acetate had no effect on fed lifespan, but both concentrations blunted DR-mediated longevity (**Figure 6.4A**).

Similarly, 3mM glycerol did not alter fed lifespan but partially attenuated DR lifespan. However, 10mM glycerol led to a small decrease in fed lifespan but did not alter DR lifespan in this experiment (**Figure 6.4B**). Together, these data suggest that water-soluble 'taste' compounds could phenocopy food smells or food touch to blunt DR. However, more replicates of this lifespan are needed, and additional experiments will be important to disentangle the effects of altered molarity and taste perception on lifespan.

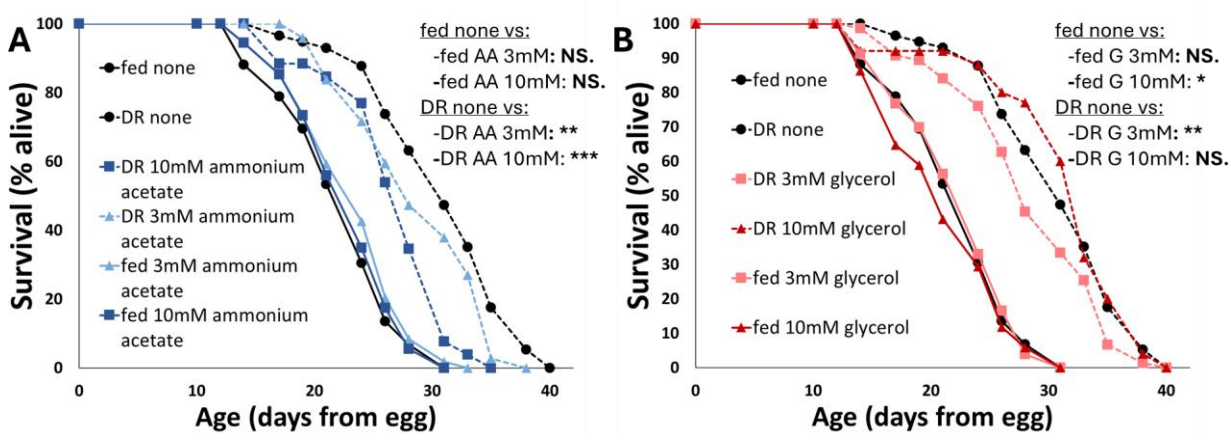


Figure 6.4 Ammonium acetate and glycerol can modify lifespan under fed and dietary restriction conditions. Survival curve of WT worms on fed or DR conditions with or without ammonium acetate (**A**) or glycerol (**B**). $N \geq$ 65 worms per condition. NS. = $p > 0.05$, * = $p < 0.05$, ** = $p < 0.01$, and *** = $p < 0.001$ from a log-rank test comparing median survival.

6.2.1.2 Can multiple forms of food perception combine to fully replicate the fed state, or is internal detection of metabolic state also an essential component in dietary restriction?

Based on our findings that food-like smell and touch blunt DR-mediated longevity and our results indicating enteric and gustatory perception in aging, it appears that many distinct forms of food perception can modify aging. Together, these data lead to several interesting questions. Do different nutrient cues modify aging through an integrated circuit, or through distinct mechanisms? Can the detection of multiple food cues block the benefits of DR to a greater extent than the detection of a single food cue? And, if so, is it possible to completely

replicate the 'fed state' by combining many food-like cues, or does internal metabolic state also contribute to a coordinated aging response?

Because we have partially mapped the food smell and the food touch cell nonautonomous circuits, we can begin to examine some of these questions. For example, we know that the food smell and food touch pathways do not completely overlap: serotonin production is required for smell but not for touch to attenuate DR-mediated longevity[105,326]. However, both circuits do require dopamine signaling, and the CEP dopaminergic neuron may play a central role in each pathway. Consequently, it is possible that multiple nutrient signals (i.e. smell and touch) are integrated within the nervous system before a common signal is sent to modify intestinal *fmo-2* induction. To more directly answer the question of whether the smell and touch circuits modify *fmo-2* induction additively, we measured *fmo-2* induction in worms on fed and DR conditions with just food smell, just food touch, or smell and touch. We found that the combination of smell and touch suppressed DR-mediated *fmo-2* induction to a greater extent than either touch or smell alone (**Figure 6.5A**). Conversely, when we performed a lifespan experiment under the same conditions, we found that the combination of smell and touch did not attenuate DR-mediated longevity more than either smell or touch alone (**Figure 6.5B**). These results could indicate that beyond a certain threshold, further decreases in DR-mediated *fmo-2* induction do not result in further decreases in longevity. However, only one replicate of this lifespan was performed and additional experiments will be required to draw firm conclusions.

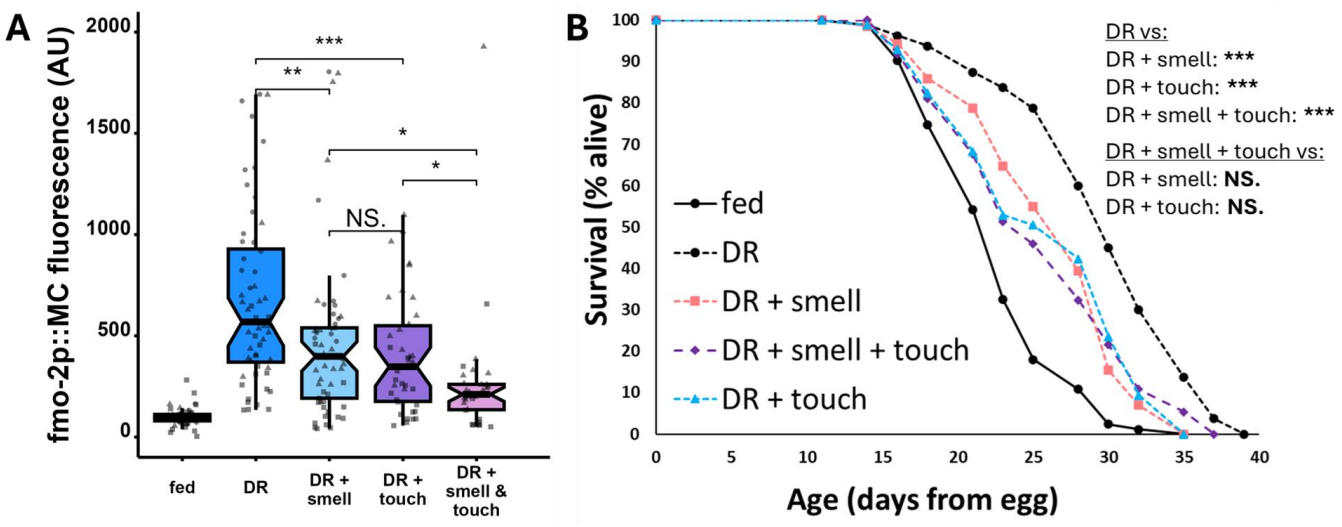


Figure 6.5 Food-like smell and touch additively suppress DR-mediated *fmo-2* induction but not lifespan. (A) Quantification of *fmo-2p::mCherry* on fed or DR +/- smell, touch, or both. $N \geq 34$ worms per condition. Significance is from a one-way ANOVA and post-hoc Tukey HSD test (unpaired, two-tailed). **(B)** Survival curve of WT worms on fed or DR +/- smell, touch, or both. $N \geq 65$ worms per condition. NS. = $p > 0.05$, * = $p < 0.05$, ** = $p < 0.01$, and *** = $p < 0.001$ from a log-rank test comparing median survival.

Together, these preliminary data suggest a potential role for enteric and/or gustatory perception in dietary restriction and aging. Additionally, there may be overlap between different food-sensing circuits, highlighting the possibility of a neural integrator of environmental food cues. Future work in this area should investigate a variety of forms of food perception across different model organisms, as well as examine combinatorial effects of these nutritional signals.

6.2.2 Can we use our knowledge of these neural circuits to identify a central regulator of aging, and/or new longevity interventions?

The complex interplay between sensory perception, cell nonautonomous signaling, and aging rate suggests a central set of neural cells and/or pathways could integrate diverse environmental cues to modulate aging rate. Many stress-response pathways that extend lifespan can be triggered by sensory perception of environmental stressors[48,52,105,128], and similarly, the nervous system plays a critical role in regulating lifespan by modulating longevity genes in peripheral tissues[77,78,80,81] (discussed in Chapter 1). As the nervous system receives sensory

information about both the internal and external environment and is involved in modifying key downstream metabolic signals, it is possible that specific neural circuits act as central regulators of aging. For example, previous work in *Drosophila* found that the serotonin 2A receptor plays a role in modifying lifespan downstream of a variety of environmental signals[52,142,143], while the mammalian hypothalamus is a potential central aging hub[50,165,465-467]. Discovering neural circuits involved in coordinating multiple longevity-modifying pathways in peripheral tissues could uncover powerful new targets for longevity interventions.

6.2.2.1 Tyramine/adrenaline signaling in multiple C. elegans longevity pathways

A promising approach to identifying central regulators of aging is to continue mapping cell nonautonomous longevity pathways in invertebrate models, where neural circuits are well-defined and easily manipulated. The most promising discoveries made in these systems should then be tested in mammals to evaluate translatability. Based on this type of circuit-mapping work in the literature and in this dissertation, one signal that may integrate multiple longevity pathways in *C. elegans* is the neurotransmitter tyramine (**Table 6.2**). Tyramine is an invertebrate-specific neurotransmitter but is thought to play a role analogous to adrenaline in mammals[304]. In the context of hormesis and longevity, tyramine acts as a signal from the nervous system to the intestine that modifies insulin signaling in response to heat and oxidative stress[327]. Additionally, *xbp-1s* mediated longevity requires changes in neuronal tyramine signaling to activate the ER-UPR in the intestine[81]. In the work presented in this dissertation, we also found that tyramine signaling is involved in the dietary restriction (DR) and hypoxia longevity circuits (Chapters 2-3).

Upstream Longevity Intervention(s)	Tyraminergic Signaling Component(s)	Downstream/ Peripheral Longevity Pathway(s)	Reference
heat stress, oxidative stress	tyramine	insulin signaling	Veuthey *et al.*, 2024
xbp-1s overexpression	tyramine, RIML neuron	ER-UPR	Özbey *et al.*, 2020
DR/food touch perception	tyramine, uv1 neuroendocrine cells	*fmo-2*, insulin signaling	Chapter 2
hypoxia/*vhl-1* knockdown	tyramine, RIML neuron, TYRA-3 receptor	*fmo-2*	Chapter 3

Table 6.2 Tyramine signaling contributes to multiple cell nonautonomous longevity circuits. A summary of published longevity pathways that act through tyramine signaling in *C. elegans*.

In Chapter 2, we demonstrated that tyramine acts within the touch perception/DR pathway to modulate lifespan. Specifically, exogenous tyramine induces the longevity effector *fmo-2*, a necessary gene in DR-mediated longevity[48]. Tyramine production is also required for touch to blunt DR-mediated longevity, and restoring tyramine signaling from the uv1 neuroendocrine cells—but not from the RIML neuron—rescues a wild-type-like response. Notably, these tyraminergic uv1 cells also produce another key signal in the DR-mediated longevity pathway, NLP-2/GnRH. Interestingly, knocking down either *nlp-2* or the NLP-2 receptor, *gnrr-3* blunted DR-mediated *fmo-2* induction and longevity (**Figure 6.6A-C**),

suggesting this could be a downstream mechanism through which tyramine modifies lifespan.

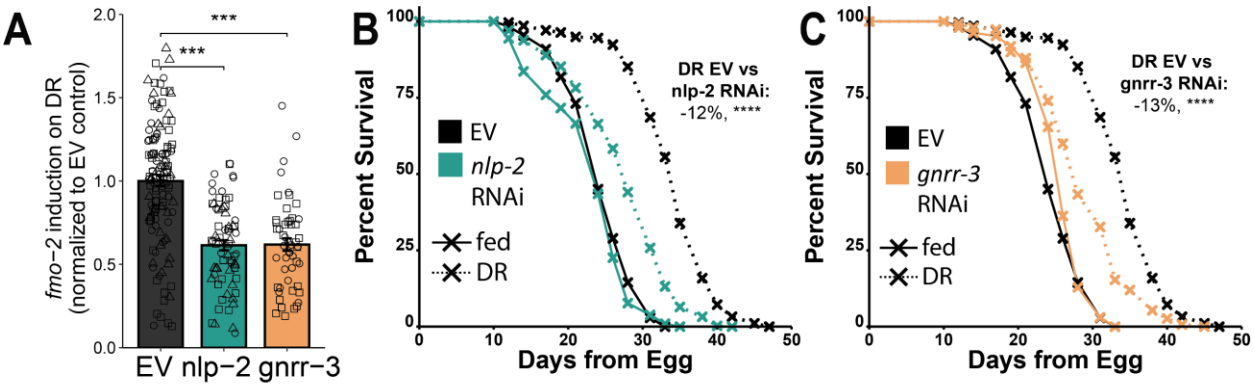


Figure 6.6 NLP-2/GnRH is required for DR-mediated *fmo-2* induction and longevity in *C. elegans.* (**A**) DR-mediated *fmo-2* induction in *fmo-2p::mCherry* worms on empty vector (EV) or *nlp-2* or *gnrr-3* RNAi. The top of the bar represents the mean of the population and error bars indicate standard error of the mean (SEM). Significance is from a one-way ANOVA and post-hoc Tukey HSD test (unpaired, two-tailed). (**B-C**) Survival curves of TU3311 (*unc-119p::sid-1*) worms on fed and sDR conditions after 2 generations on empty vector (EV) or *nlp-2* (**B**) or *gnrr-3* (**C**) RNAi. Significance is from a log-rank test comparing median survival. Percent represents the percent decrease in mean lifespan from DR EV to DR *nlp-2* or *gnrr-3* RNAi. In all panels, NS. = $p > 0.05$, and **** = $p < 0.0001$.. In all panels, three replicates were plotted together, and all statistics include a Bonferroni correction for multiple comparisons.

In Chapter 3, we also discovered that tyramine and its receptor, *tyra-3*, are required for the hypoxia memetic *vhl-1* to extend lifespan. Here, the RIML neuron was integral to this pathway rather than the uv1 cells, suggesting a more complex network of tyraminergic signaling in lifespan regulation. Interestingly, both cell-specific tyraminergic rescue strains, which restored tyramine synthesis in either the uv1 or the RIML cell(s), were significantly long-lived under fed, normoxic conditions (**Figure 6.7**). These results indicate that multiple modifications to tyramine production can modify lifespan.

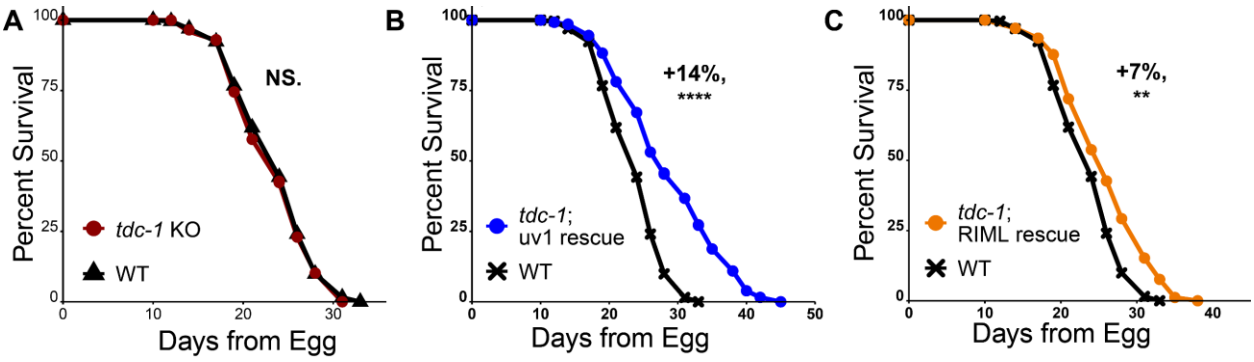


Figure 6.7 Restoring tyramine synthesis in the uv1 and the RIML neurons extends lifespan in *C. elegans.* (**A-C**) Survival curves of WT and *tdc-1(n3419)* (**A**), uv1 *tdc-1* rescue (*tdc-1 (n3419);* Ex[*gcy-13p::tdc-1]*) (**B**), and RIML rescue (*tdc-1 (n3419);* Ex[*ocr-4p::tdc-1]*) worms. Significance is from a log-rank test comparing median survival. Percent represents the percent change in mean lifespan from WT to the *tdc-1* mutant strains. In all panels, NS. = $p > 0.05$, ** = $p < 0.01$, and **** = $p < 0.0001$. In all panels, three replicates were plotted together, and all statistics include a Bonferroni correction for multiple comparisons.

However, it remains unclear whether tyramine acts as a pro- or anti-aging signal, or alternatively if the effects of tyramine are context and location dependent. Given that tyramine deficient *tdc-1* knockout worms are not long-lived (**Figure 6.8A**), the presence of high levels of tyramine could act as a pro-longevity signal. However, the long-lived cell-specific tyramine rescue strains do not help us answer this question, as blocking tyramine production in a cell where it is endogenously produced may reduce overall tyramine synthesis. Conversely, rescuing tyramine signaling under a non-endogenous promoter within a multi-copy extrachromosomal array could potentially increase overall tyramine levels. Moreover, tyramine can be converted into octopamine by cells expressing *tbh-1*, adding another layer of complexity. Future work should measure the net levels of tyramine and octopamine in these long-lived strains, develop more precise tyramine signaling mutants, and determine whether tyraminergic receptors in the nervous system or peripheral tissues are necessary for the lifespan extension observed in these rescue strains. Additionally, some FDA-approved pharmaceuticals that modify adrenaline and noradrenaline signaling in mammals—such as beta blockers, bupropion[468], and mianserin[469]—may offer potential candidates for testing as longevity interventions. In fact, mianserin extends

lifespan in *C. elegans* and *D. melanogaster*[104,105], although it is unclear whether its effects are tyramine dependent.

6.2.2.2 RIS interneuron signaling in multiple C. elegans longevity pathways

Another potential integrator of multiple longevity pathways in *C. elegans* is the RIS interneuron (**Table 6.3**). Previous studies show that altering RIS activity affects sleep behavior, stress resistance, and lifespan, making it a candidate for modulating aging[347,366-368]. Previous work also implicates the RIS neuron in the DR-mediated *fmo-2* induction pathway examined in Chapter 2. While RIS may not play a role in touch effects on DR lifespan, we found that expression of the serotonin receptor SER-4 on a GABAergic interneuron is required for food smell to blunt DR[105]. Although the RIS neuron was not directly tested in this work, it is one of the neurons with the highest expression of SER-4 and is also a GABAergic neuron[295], thereby making RIS a likely candidate in the DR-smell circuit. Additionally, in Chapter 3, we explored the role of RIS neurons in hypoxia-mediated longevity, where we found that serotonin signaling via the SER-7 receptor in RIS neurons is necessary for *vhl-1*-mediated lifespan extension. Together, these findings suggest that RIS neurons are key recipients of serotonergic signals that could integrate multiple longevity circuits.

Upstream Intervention(s)	RIS involvement	Peripheral Longevity Pathway(s)	Reference
starvation/ wound healing response	RIS activity required for survival	insulin/FOXO signaling	Wu *et al.*, 2019; Koutsoumparis *et al.* 2022
NA	chronic RIS activation extends lifespan	ER-UPR	Busack and Bringmann, 2023
DR/food smell perception	GABAergic neuron with highest *ser-4* expression	*fmo-2*	Chapter 2
hypoxia/*vhl-1* knockdown	RIS ablation blocks *vhl-1* longevity	*fmo-2*	Chapter 3

Table 6.3 RIS signaling may contribute to multiple cell nonautonomous longevity circuits. A summary of longevity and stress-response pathways that act through RIS signaling in *C. elegans.*

Because the RIS neuron acts downstream of both the DR and hypoxia pathways, both of which act in peripheral tissues through the longevity effector protein FMO-2, it is possible that RIS activity modifies *fmo-2* induction to extend lifespan. However, it remains unclear whether RIS modifies longevity exclusively through intestinal FMO-2 activity or whether other signaling pathways are involved. Future work should confirm the necessity of RIS signaling for DR-mediated longevity and explore whether RIS activity impacts other longevity circuits, including those that rely on different peripheral longevity effectors. Additionally, understanding which signaling molecules produced by RIS are critical for lifespan modulation will be crucial for elucidating its role as a possible central regulator of aging.

6.2.3 Do other genetic and pharmaceutical longevity interventions affect behavior and could altered behavior be used as a screening tool for pro-longevity genes?

Our finding in Chapter 4 that *fmo-2* expression has profound behavioral effects raises another significant question: Do other longevity effectors, including environmental stressors or

genetic manipulations, also influence behavior? Furthermore, could behavioral changes be used as a tool for identifying novel longevity interventions? Answers to these questions might suggest new avenues for research aimed at better understanding the link between longevity and behavior.

To begin exploring these questions, we conducted a small screen to assess the exploratory behavior of several other long-lived *C. elegans* strains and WT worms on conditions that extend lifespan. Preliminary data from this screen reveals that many of these longevity interventions exhibit modified exploratory behavior, although there is no clear correlation between exploratory behavior and lifespan (**Figure 6.8**). For example, the long-lived serotonin producing enzyme mutant *tph-1* strain and treatment with the lifespan-extending drug, mianserin, display increased exploration relative to wild-type (WT) controls. In contrast, other long-lived strains, such as mutations in the tryptophan pathway enzymes *kynu-1* and *haao-1*, did not show any significant changes in exploration, while the long-lived *vhl-1* knockout and *xbp-1s* overexpressing worms showed decreased exploration, similarly to *fmo-2* overexpressing animals. Dietary restriction also decreased exploration, as might be expected by a condition that induces *fmo-2* expression.

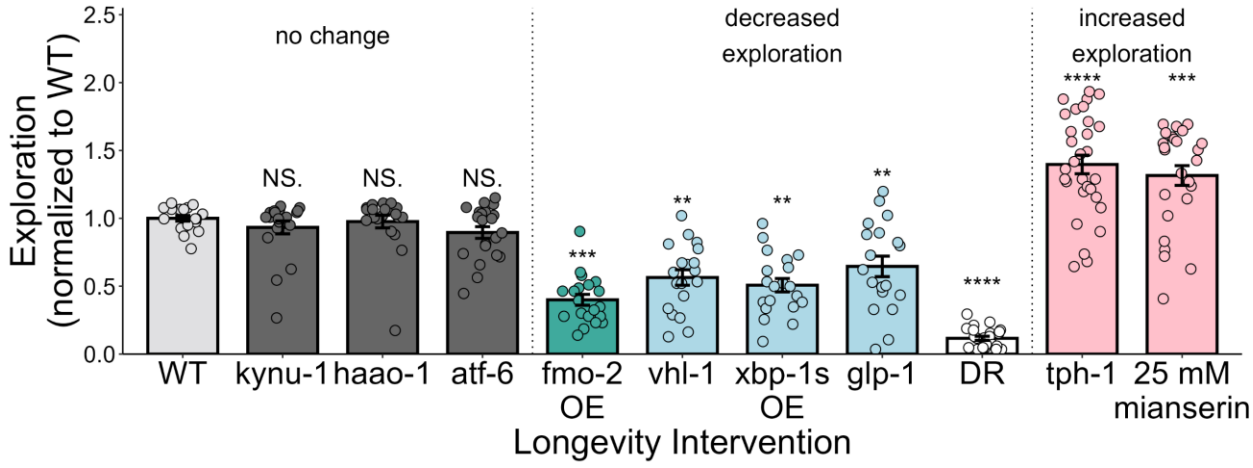


Figure 6.8 Multiple longevity interventions alter exploratory behavior in *C. elegans*. Exploration of WT, *kynu-1(tm4924)*, *haao-1(tm4627)*, *atf-6(ok551)*, *fmo-2* overexpressor (*vha-6p::fmo-2), vhl-1(ok161), xbp-1s* overexpressor (*rab-3p::xbp-1s*), *glp-1(e2141)* worms, dietary restricted WT worms, *tph-1(mg280)* worms, and WT worms treated with 25mM mianserin. The top of the bar represents the mean of the population and error bars indicate standard error of the mean (SEM). Significance is from a one-way ANOVA and post-hoc Tukey HSD test (unpaired, two-tailed). NS. = $p > 0.05$, ** = $p < 0.01$, *** = $p < 0.001$, and **** = $p < 0.0001$.

These findings suggest that many longevity interventions, both genetic and pharmaceutical, can modify behavior, but the relationship between behavioral changes and lifespan extension is complex. Notably, while a substantial proportion of the lifespan-extending treatments we tested had significant effects on exploration, no clear predictive correlation between exploration and lifespan was observed in this preliminary screen. This highlights the importance of further exploring how longevity interventions affect behavior, and it emphasizes the need to investigate whether behavioral changes can reflect broader physiological shifts. For example, we can ask whether behavioral changes are a result of feedback from peripheral metabolic changes, like those seen with *fmo-2*, or if they are linked to neuroendocrine signals produced by peripheral tissues, such as the intestine, and received by the nervous system.

There is also emerging evidence that retrograde signals from peripheral tissues to the nervous system can play a critical role in lifespan extension. For instance, work by the Wang lab has shown that changes to lysosome metabolism in peripheral tissues can trigger the release of lipids that act as cell nonautonomous signals to the nervous system. This lipid-mediated retrograde signaling then promotes longevity through the activity of neuronal NLP-11 neuropeptide signaling[470]. These findings suggest that it is important to not only assess how behavioral changes reflect underlying metabolic shifts but also consider retrograde cell nonautonomous signaling as a key component of longevity. Therefore, future studies should examine whether behavioral changes induced by longevity interventions are linked to peripheral signals that influence the nervous system.

While *C. elegans* have a short lifespan that facilitates experiments using lifespan as an output, the scale of these experiments is still limited by the 30-60 days required to conduct a lifespan in worms. In contrast, many behavioral assays can be conducted in 1-2 days, especially

those with a phenotype present in young adulthood. Consequently, it is worth exploring whether behavioral changes early in life could be used as short-term indicators of lifespan. Although the preliminary data included here indicate that many longevity interventions can modify exploratory behavior, they also suggest that exploratory behavior alone may not be an ideal predictor of lifespan. Future research should examine additional behavioral metrics such as chemotaxis responses, pathogen fleeing behavior, and lawn-slowing behaviors in these and other long-lived strains. These assays may provide a more comprehensive understanding of how longevity pathways affect behavior and whether behavior could ultimately serve as an effective screening tool for pro-longevity genes and interventions.

6.2.4 Can we identify commonalities between extensively mapped behavioral circuits and newly discovered cell nonautonomous longevity pathways?

In addition to our preliminary data that multiple longevity therapies affect behavior in *C. elegans* (**Fig. 6.8**), there is also some overlap in circuits through which longevity-promoting environmental stressors affect aging and behavior. For example, hypoxia and dietary restriction both induce behavioral changes that require activity of cells and signals that also play a role in the longevity response to these stressors[281,298,363,375,471]. Many of these behavioral stress-response pathways downstream of DR and hypoxia are extensively mapped, allowing for comparison between the circuits governing behavior and longevity.

Studies of behavioral adaptations to hypoxia in *C. elegans* have shown that the transcription factor HIF-1 is required for food-dependent hyperoxia avoidance, a phenotype in which wild-type animals avoid high-oxygen environments unless food is present[363]. This behavior requires *hif-1* expression in both neurons and the tyraminergic uv1 neuroendocrine cells and also depends on serotonin signaling from the ADF neuron[363,471]. Although this behavioral

circuit shares features with the hypoxic response longevity pathway explored in Chapter 3, the two diverge at several points. In hyperoxia avoidance, the uv1 cells are key, while lifespan extension relies more on the RIM tyraminergic neurons. Additionally, the neuropeptide receptor NPR-1, known to regulate oxygen-driven behavior[363,472], was not required for hypoxic response mediated *fmo-2* induction (Chapter 3). These distinctions suggest that activation of the hypoxic response may modify behavior and aging through some common mechanisms, the overlap between circuits is only partial. Further research is needed to pinpoint where these pathways intersect and where they operate independently.

Much like the hypoxic response, dietary restriction drives behavioral changes through circuits that overlap some with the mechanisms of DR-mediated longevity. The neuromodulators serotonin[105,112,281,298,375,473,474], dopamine[105,281,301,326,475-477], and tyramine/adrenaline[304,326,327,350,352,363] all contribute to both behavioral and longevity responses to changes in nutrient availability. In addition to acting in smell attenuation of DR-mediated longevity[105], serotonin signaling from the NSM neuron facilitates a behavioral slowing response when *C. elegans* encounter a food source[298]. Serotonin signaling from multiple neuron types also signals food availability across taxa, leading to decreased foraging activity[375,478-480]. Dopamine signaling, on the other hand, allows for reward-based learning behavior by indicating that an outcome or environment either falls short of or exceeds expectations[476,481-483]. In the context of DR, this signaling can facilitate behavioral changes when encountering a food source[281], or when choosing between complex environmental cues[476]. Unlike serotonin, dopamine does not contribute to hypoxia-mediated longevity in worms (Chapter 3), but dopamine signaling is required for both food smell and food touch to attenuate DR-mediated longevity[326,484]. Tyramine/adrenaline also mediates behavioral responses to nutrient perception in invertebrates,

such as head movements near a food source[304,350-352,485], as well as contributing to touch attenuation of DR-mediated longevity[326].

Together, the extensive work in behavioral circuit mapping offers a wealth of information to analyze for possible points of overlap and divergence between behavioral and longevity pathways. Future work in this area should include a more in-depth comparison between behavioral and longevity circuits downstream of environmental stressors. Additionally, it remains unclear whether *fmo-2* overexpression alters *C. elegans* behavior through the same mechanisms as the *fmo-2*-inducing conditions dietary restriction and hypoxia. To answer this question, some of the genetic interventions that rescue the exploratory behavior of the *fmo-2* overexpressor, such as *haao-1* knockout (Chapter 4), should be examined for their ability to prevent DR- and hypoxia-mediated behavioral change.

6.2.5 Are the effects of Fmos on longevity and behavior conserved from worms to mammals?

Chapters 2 through 4 of this dissertation explore cell nonautonomous signaling pathways that converge on the *C. elegans* enzyme FMO-2. A growing body of work suggests that the functions of *C. elegans* FMO-2 are likely to be at least partially analogous to the functions of Fmos play in mammals. FMOs are structurally conserved from worms to humans, upregulated in multiple long-lived mouse models[109,110,372], and overexpressing multiple FMOs improves stress resistance in human cells[373]. Several potential anti-aging pharmaceuticals induce *fmo-2* and promote healthspan in *C. elegans* and mammalian cell culture[105,230]. Both the longevity and behavioral effects of *C. elegans* FMO-2 are thought to be linked to its role in the oxygenation of tryptophan into N-formyl-kynurenine and, importantly, tryptophan is also a substrate of the mammalian FMO most homologous to *C. elegans* FMOs—mFmo5[282]. Like *fmo-2* in *C. elegans*, mFmo5 is expressed in tissues such as the nervous system and intestine[404,486]. Since tryptophan

metabolism is highly conserved across species[487], this strengthens the potential for these findings to extend from worms to humans.

The ultimate goal of this research on *C. elegans* FMO-2 is to leverage the findings to improve human health. While there is compelling evidence regarding the conservation of FMO functions, substrates, and tissue specificity between *C. elegans* and mammals, truly determining whether these functions are conserved requires direct investigation in mammalian systems. Previous studies on flavin-containing monooxygenases in mammalian models have primarily focused on their role in xenobiotic metabolism[372,405,463,488], the immune response[390,391] and endogenous metabolism[372,373,392,393]. However, future work should directly test whether the effects of Fmos on lifespan and behavior are conserved. While studying lifespan in mice can be resource-intensive, the preliminary data from *C. elegans* provide a strong rationale for investigating mFmo5 knockout mice under both ad libitum and caloric restriction conditions to assess the necessity of mFmo5 in dietary restriction-mediated longevity. Additionally, mFmo5 overexpression in mice should be tested to determine its potential to extend lifespan in both males and females. Finally, behavioral assays, such as the open field test[489,490], elevated plus maze[491,492], tail suspension test[493,494], and forced swim test[495,496], should be performed on mFmo5 knockout and overexpressing mice to evaluate whether FMOs influence behavior in mammals.

In summary, the research presented in this dissertation suggests that neural signals such as dopamine, tyramine and RIS interneuron activity could play central roles in integrating environmental cues to modulate aging and longevity. These findings highlight the potential of targeting specific neural pathways to influence lifespan, emphasizing the need for further investigation into the context-dependent effects of various neuromodulators on aging. Additionally, while many longevity interventions modify *C. elegans* behavior even in young

adulthood, the complexity of this relationship necessitates further exploration to determine whether altered behavior can serve as a reliable screening tool for longevity interventions. Finally, the conservation of longevity-related mechanisms between *C. elegans* and mammals, particularly through the modulation of Fmos, offers a promising avenue for future research aimed at translating these findings into human health applications. Ultimately, these studies underscore the potential for neural and metabolic interventions to enhance healthspan and lifespan across species.

6.2.6 Methods

The following methods were employed in the data collected in Chapter 6:

6.2.6.1 Strains and Growth Conditions

C. elegans were cultivated using standard, previously described methods[48]. Briefly, all worms were maintained at 20 °C on solid nematode growth media (NGM). Worms were fed *E. coli* OP50 throughout life, except in experiments using double stranded (ds) RNAi (*E. coli* HT115). Worm transfers were conducted using a platinum wire unless otherwise specified. All genotypes were confirmed using PCR and all RNAi imaging hits were sequence-validated and qPCR-validated before use.

6.2.6.2 Exploration Assays

Exploration assays were performed as previously described by Flavell et al[375]. Individual worms from a timed egg lay were transferred at young adulthood to a 35 mm NGM agar plate completely covered with *E. coli* OP50 (350 µL). Images were taken of each plate using an iPad attached to a brightfield microscope. A custom ImageJ java script was used to enhance the contrast of each image to an equal degree to improve visibility of worm tracks through the bacteria and to overlay a grid of uniform-size across the image. The number of squares entered

by the worm tracks were counted for each worm, with the maximum number of squares possible being 109. 20-30 worms were assayed for each condition. Worms that fled the plate during the assay were excluded from analysis. Data were plotted by R version 4.3.1 and Adobe Illustrator 2022.

6.2.6.3 Fake Lawn Preparation

G-200 Sephadex beads (Sigma G5050) were suspended S-basal buffer at a concentration of 30mg/ml and autoclaved for 45 minutes. For fed + touch plates, OP50 bacteria was grown overnight to an optical density (OD_{600}) of 3.0, then pelleted at 3000 *rcf* for 20 minutes. The supernatant was discarded and replaced with the Sephadex in S-basal, then the mixture was vortexed until the pellet was dissolved. 200 µL was seeded onto the center of a 60mm diameter NGM plate. For DR + touch conditions, autoclaved Sephadex in S-basal was added directly to the center of the NGM plate (overnight imaging experiments) or the autoclaved Sephadex in S-basal was used to resuspend a pellet from a diluted concentration of bacteria (DR lifespan experiments). For fed controls and DR lifespan controls, the bacterial pellet was resuspended in S-basal instead of S-basal + Sephadex. For DR imaging controls, 200µl autoclaved S-basal was added directly to the plate.

6.2.6.4 Food Smell Preparation

E. coli OP50 was grown from a single colony in Luria broth for 16 hours at 37 °C. 200 µL of the fresh bacteria was seeded onto the center of a ~30 mm diameter agar bad on the lid of a standard 60 mm diameter petri dish plate. The smell lid was allowed to dry before use.

6.2.6.5 Lifespan Measurements

Lifespan assays were conducted as previously described [320] with the exception of the fake lawn conditions (see fake lawn preparation). In short, 10-15 gravid adults were left on NGM plates for

a 3-4 hour timed egg lay and then removed. Once the progeny of these adults reached late L4/early adult stage of development, they were transferred to NGM plates with 33µL of 150mM fluorodeoxyuridine (FUdR) and 100µL of 50mg/mL Ampicillin per 100mL NGM. The FUdR prevents development of progeny and the Ampicillin prevents bacterial growth. 60-80 worms were placed on each NGM + FUdR + AMP plate seeded with concentrated bacteria (5x for OP50 fed lifespans, 0.5x OP50 (10^9 CFU/mL) for DR lifespans), and at least two plates per strain per condition were used for each lifespan replicate. In all DR lifespans, OP50 in the fed and DR conditions was resuspended in S-media to prevent bacterial growth. In the DR and DR + touch conditions, worms were kept on 5x fed bacteria until day 2 of adulthood, when they were transferred to fresh DR or DR + touch plates every other day for four transfers. This form of DR is referred to as solid DR (sDR)[321]. Worms on fed and fed + touch conditions were transferred to fresh fed plates at the same time as each DR transfer. Fresh smell lids were changed out with every transfer of the lifespan, and then twice per week after transfers were completed. Animals were removed from the experiment and counted as dead when they did not move in response to a gentle touch from a platinum wire pick under a dissection microscope. Lifespans were scored at least 3 times per week until all animals were dead. A 'fence' of 75µL of 100mM palmitic acid (Sigma-Aldrich) dissolved in 100% ethanol was also applied to the edge of each lifespan plate to prevent fleeing. While FUdR can extend lifespan, FUdR was used in all lifespan plates to prevent matricide under DR conditions[322]. NGM lifespans without FUdR were attempted to test the necessity of FUdR for the attractive touch phenotype, but were not successful due to excessive matricide and fleeing under the DR conditions. Data were plotted by R version 4.3.1 and Adobe Illustrator 2022.

6.2.6.6 Slide Microscopy

Fluorescent images in this study were taken using Leica Application Suite X (LASX) software and a Leica scope with >15 worms per treatment at ≥35x magnification. For representative images displayed in the figures, worms were paralyzed in 0.5 M sodium azide (NaN_3) and imaged once residual liquid evaporated and the worms clumped together. For quantification of these images and for imaging screens, the same method was used but after the residual sodium azide had evaporated, individual worms were gently pushed apart until they were no longer touching one another. Fluorescent mean comparisons were then quantified using custom R code to identify individual worms and measure fluorescent intensity. The mean fluorescent intensity of the background (all non-worm pixels) was subtracted from the mean fluorescence of each worm. All outputs from this R code were manually quality controlled to eliminate any non-worm objects that were misidentified. This code will be provided upon request to the corresponding author. In the taste compound imaging screen, all taste compounds were incorporated into the agar media of the plates before they were poured. Data were plotted by R version 4.3.1 and Adobe Illustrator 2022. The brightness of fluorescent images of clumped worms was increased to an equal degree across all images compared to one another in ImageJ bundled with 64-bit Java 1.8.0.

Appendices

Appendix A: Annotated worm_batch.R Code

```
##set your filepath, change the text within the quotes
setwd("C:/Users/elizb/University of Michigan Dropbox")

##load paths of the three folders within your working directory
rcode_folder <- file.path(".", "R code")
image_folder <- file.path(".", "input")  # all the tifs are here
output_folder <- file.path(".", "output")   # relative to wd
conditions_map_filename <- file.path(image_folder,
"conditions_map.csv")

##load the findWormz and analyzeWormz packages
source(file.path(rcode_folder, "findWormz.R"))
source(file.path(rcode_folder, "analyzeWormz.R"))

#change any adjustable parameters and run the code
analyzeWormz(image_folder, output_folder,
conditions_map_filename,
```

```
troubleshootMode = FALSE, # set to TRUE for add
#intermediate images (good for troubleshooting)
lightBackground = TRUE,
threshold = "auto",
thresholdAdjust = 1.18,
fillNumPix = 0,
cleanNumPix = 0,
keepNumPix = 2000,
worminess_min_thr = 1.5,
worminess_max_thr = 2.1,
blurSigma = 2,
backgroundCorrect = TRUE,
showPlots = FALSE)
```

Appendix B: Annotated findWormz.R Code

```
# Simple approach to image segmentation for worms when
#background is much lighter than worm tone
# in the visible light image, and no reflections or vignetting
#in the image.
# return value is a list with three objects:
#      * final.worms is a list of masks of the pixels, one for
#each worm candidate
#      * worm_imgs a list of worm images taken along the way
#(5 total)
#      * stats = dataframe of statistics with one row for each
#final.worm in the image

findWormz <- function(
  filename,
  lightBackground = TRUE,  # dark worms on light background is
                                #default
  threshold       = "auto",
  thresholdAdjust = 1,
  fillNumPix      = 0, # would use 1-5 here if needed
```

```
  cleanNumPix     = 0, # would use 1-5 here if needed
  keepNumPix      = 700,   # throw away small objects
  worminess_min_thr   = 1.35,  # threshold for perimeter to
                            #area ratio where 1 = square worm
  worminess_max_thr   = 2.05,
  blurSigma       = 2.0,  # used by isoblur
  backgroundCorrect = TRUE,
  showPlots = TRUE
) {

  library(imager)
  library(imagerExtra)
  library(tibble)
  library(RColorBrewer)
  library(colorspace)
  library(tools)
  library(tiff)

  extn <- str_to_lower(file_ext(filename))
  if (extn == "tif") {
    im <- as.cimg(readTIFF(filename))
  } else if (extn == "jpg") {
    im <- load.image(filename) # handled natively by imager
                               # library
```

```
  } else {
    cat("\nWarning: ", extn, "is an unknown file type,
skipping findWormz", filename, "\n\n")
    return(NULL)
  }

  if (dim(im)[4] > 1) im  <- grayscale(im) # dim 4 stores
          #color channels, only convert to grayscale if needed

  im.final <- im  # will be plotted at the end (possibly with
                      #colored worms)
  final.worms <- NULL # list of worm pixsets if any worms
                      #found

  # small "background" correction (can create artifacts if too
   #large lambda)
  if (backgroundCorrect) {
    im <- im %>% SPE(0.0001)
    if (showPlots) im %>% plot()
  }

  # blur image then compute thresholded pixset
  px <- im %>%
    isoblur(
```

```
    sigma = blurSigma
  ) %>%
  threshold(
    thr = threshold,
    adjust = thresholdAdjust
  ) %>%
  as.pixset()

if (lightBackground) px <- !px

# fill then clean to fill in some holes inside worms,
#eliminate some specks
if (fillNumPix > 0 || cleanNumPix > 0) {
  px <- px %>% fill(fillNumPix) %>% clean(cleanNumPix)
}

if (showPlots) plot(px)
# compute connected components, then discard those with too
#few pixels
candidates <- split_connected(px) %>%
  purrr::discard(~ sum(.) < keepNumPix)

# discard any components touching the 4 image edges
```

```
  # note: need to be careful about coordinates since image
format in imager library is 4 dimensional
  touchesEdge <- function(im) {
    return(any(im[1,,1,1], im[dim(im)[1],,1,1], im[,1,1,1],
im[,dim(im)[2],1,1]))
  }

  if (length(candidates) > 0) {
    if (showPlots) candidates %>% parany %>% plot()   # this
                                                #plots them all
    obj.stats <- tibble(
      numPix = unlist(lapply(candidates, sum)),
      bndryLen = unlist(lapply(candidates, function(x)
sum(imager::boundary(x)))),
      touchesEdge = unlist(lapply(candidates, touchesEdge)),
      worminess = bndryLen / 4 / sqrt(numPix),  # worminess is
                                      #1 for a square worm :)
      include = (worminess > worminess_min_thr & worminess <
worminess_max_thr) & !touchesEdge
    )

    final.worms <- candidates[obj.stats$include]
    final.stats <- obj.stats %>% filter(include)
```

```
    print(obj.stats)

    if (!is.null(final.worms) && length(final.worms) > 0) {

      if (showPlots) final.worms %>% parany %>% plot()
      N <- length(final.worms)
      cat("Number of final worm candidates:",N,"\n")
      colors <- col2rgb(brewer.pal(min(12, max(N,3)),
"Paired")) / 256.0 # color scheme - only has 12

      # superimpose the colored final worm candidates one by
        #one
      for (i in 1:N) {
        df <- final.worms[[i]]
        df <- imager::where(df)
        #df <- which(final.worms[[i]])
        xbar <- round(median(df$x))
        ybar <- df %>% filter(abs(df$x - xbar) <= 1) %>%
pull(y) %>% median

        im.final <- im.final %>%
          colorise(final.worms[[i]], colors[,  1 + (i %%
ncol(colors))], alpha = 0.6) %>%
```

```
          draw_text(xbar, ybar, paste0(i, " (",
round(final.stats[i, "worminess"], 2), ")"), col="red",
fsize=35)
      }
      if (showPlots) plot(im.final)
      # im below includes any background processing
#adjustments
      # px includes blur/threshold/clean/fill
      worm_imgs <- list(im_corrected = im, px_all_objects =
px, px_all_candidates = parany(candidates), px_all_final =
parany(final.worms), im.final = im.final)

      return(list(final.worms = final.worms, worm_imgs =
worm_imgs, stats = obj.stats[obj.stats$include,]))
    }
  }
  cat("\nWarning:  no worms found, returning NULL for ",
filename, "\n\n")
  return(NULL)
}
```

Appendix C: Annotated findWormz.R Code

```
analyzeWormz <- function(imageFolder, outputFolder,
                     conditionsMapFile,
                          troubleshootMode = FALSE,  # if true
#additional intermediate images are saved to troubleshoot
                          lightBackground = TRUE,
                          #findWormz() parameters...
                          threshold = "auto",
                          thresholdAdjust = 1.18,
                          fillNumPix = 0,
                          cleanNumPix = 0,
                          keepNumPix = 2000,
                          worminess_min_thr = 1.35,
                          worminess_max_thr = 2.05,
                          blurSigma = 2,
                          backgroundCorrect = TRUE,
                          showPlots = FALSE) {

  library(imager)
  library(tibble)
```

```
  library(imagerExtra)
  library(tools)
  library(tiff)
  library(stringr)
  library(jpeg)
  library(dplyr)

# write the set of parameters in the function call for the
#record
params_df <- data.frame(lapply(as.list(match.call())[-1], eval))
  timestamp <- format(Sys.time(),"%Y%m%dT%H%M%S")
write.csv(t(params_df), file = file.path(outputFolder,
paste0("run_", timestamp, "_params.csv")))

  # worm names will look like cx...x_y...y_ch0z.tif
  # where x...x, y...y, and z are digits
  # x...x represents the condition
  # y...y is the image number
  # z is the channel (visible light = 0, fluorescent = 1)

filenames <- Sys.glob(file.path(imageFolder, "*.tif"))
filenames <- filenames[str_which(filenames, "ch00")]  # grab
#just the ch00 channels
```

```
#create a dataframe with analysis output
names_analysis_output<- c("filename",
            "worm_number","condition_code",
            "fluo_worm",
            "fluo_background",
            "fluo_adjusted",
            "flu_sd",
            "worm_size",
            "worm_perimeter",
            "worminess")
analysis_output <- data.frame(matrix(ncol =
length(names_analysis_output), nrow = 0))
colnames(analysis_output) <- names_analysis_output


  #loop through each ch00 file
  for (fname in filenames) {
    cat("\nAnalyzing", fname, "\n")
    results <- findWormz(fname,
                         lightBackground,
                         threshold,
                         thresholdAdjust,
                         fillNumPix,
                         cleanNumPix,
```

```
                        keepNumPix,
                        worminess_min_thr,
                        worminess_max_thr,
                        blurSigma,
                        backgroundCorrect,
                        showPlots)

    # results list from findWormz:
    #       * final.worms is a list of masks of the pixels, one
                #for each worm candidate
    #       * worm_imgs a list of worm images taken along the way
                #(5 total)
    #       * stats = dataframe of statistics with one row for
                #each final.worm in the image

    # only do stuff if worms are found in this image.  Note that
     #findWormz will issue a warning message if none found
if (!is.null(results) && !is.null(results$final.worms) &&
length(results$final.worms) > 0) {
      # this stuff is used to create various output filenames
      fname_dir      <- dirname(fname)
      fname_basename <- basename(fname)
      fname_root     <- file_path_sans_ext(fname_basename)
      fname_extn     <- file_ext(fname_basename)
```

```
      # construct filename of fluorescent image data
fname_data_image <- paste0(str_sub(fname_root, start = 1, end =
-3), "01.", fname_extn) # extract all but last two characters
(which should be "00"), replace with "01"
worm_data <- readTIFF(file.path(imageFolder, fname_data_image))
condition <- str_match(fname_root, "(C\\d+)_")[,2]  # condition
                          #looks like _C1234_ in filename

all_objects <- results$worm_imgs$px_all_objects  # includes all
          #worm candidates (including touching edge), dust, etc
background <- !all_objects
 background_mean <- mean(worm_data[background])
#loop through the individual worms from this image, and add a
#new row to analysis_output for each worm
      for (i in 1:length(results$final.worms)) {
        worm <- results$final.worms[[i]]
        #create a new row to add to the analysis_output
          #dataframe
        new_worm_data <- data.frame(matrix(ncol =
        length(names_analysis_output), nrow = 0))
        colnames(new_worm_data) <- names_analysis_output
        new_worm_data[1,] <- c(fname_data_image,
```

```
                        i,
                        condition,
                        mean(worm_data[worm]),
                        background_mean, # background non-worm
                                         #mask,
                        mean(worm_data[worm]) -
                                 background_mean,
                        sd(worm_data[worm]),
                        results$stats$numPix[i],
                        results$stats$bndryLen[i],
                        results$stats$worminess[i])
        analysis_output <- rbind(analysis_output, new_worm_data)
      }

# save some of the images for documentation and troubleshooting
      ims <- results$worm_imgs
# save the worm images to output (just final bw (4) and
#brightfield with color tracing (5))
      if (troubleshootMode) {
        start_index = 1
      } else {
        start_index = 4
      }
      for (i in start_index:5) {
```

```
        # we save the output files as jpg, not tifs, since they
        #are much smaller
        imager::save.image(as.cimg(ims[[i]]),
        file.path(outputFolder, paste0(fname_root, "_", i, ".",
        "jpg") ) )
      }
    }
  }
  # link condition map file (effectively add 3 columns)
  conditions_map <- read.csv(conditionsMapFile)
  names(conditions_map)[1]<-"condition_code"
  analysis_output <- left_join(analysis_output, conditions_map)

#save the analysis output file as a csv in your output directory
write.csv(analysis_output, file = file.path(outputFolder,
paste0("run_", timestamp, "_analyzed_data.csv")), row.names =
FALSE)
  cat("\nDone.\n\n")
}
```

Bibliography

1. Population Division, U.N. World Population Prospects.
2. Crimmins, E.M. (2015). Lifespan and Healthspan: Past, Present, and Promise. The Gerontologist *55*, 901-911. 10.1093/geront/gnv130.
3. IGME), U.N.I.-a.G.f.C.M.E.U. (2023). Levels and trends in child mortality. UNICEF.
4. Kaeberlein, M. (2013). Longevity and aging. F1000Prime Reports *5*. 10.12703/P5-5.
5. James, L.S., Abate, D., Abate, H.K., Abay, M.S., Abbafati, C., Abbasi, N., Abbastabar, H., Abd-Allah, F., Abdela, J., Abdelalim, A., et al. (2018). Global, regional, and national incidence, prevalence, and years lived with disability for 354 diseases and injuries for 195 countries and territories, 1990–2017: a systematic analysis for the Global Burden of Disease Study 2017. The Lancet *392*, 1789-1858. 10.1016/S0140-6736(18)32279-7.
6. Goldman, P.D., Cutler, D., Rowe, W.J., Michaud, P.-C., Sullivan, J., Peneva, D., and Olshansky, J.S. (2013). Substantial Health And Economic Returns From Delayed Aging May Warrant A New Focus For Medical Research. Health Affairs *32*, 1698-1705. https://doi.org/10.1377/hlthaff.2013.0052.
7. Barnett, K., Mercer, S.W., Norbury, M., Watt, G., Wyke, S., and Guthrie, B. (2012). Epidemiology of multimorbidity and implications for health care, research, and medical education: a cross-sectional study. Lancet *380*, 37-43. 10.1016/S0140-6736(12)60240-2.
8. McCay, C.M., Crowell, M.F., and Maynard, L.A. (1935). The Effect of Retarded Growth Upon the Length of Life Span and Upon the Ultimate Body Size: One Figure. The Journal of Nutrition *10*, 63-79. 10.1093/jn/10.1.63.
9. Partridge, L., Piper, M.D., and Mair, W. (2005). Dietary restriction in Drosophila. Mech Ageing Dev *126*, 938-950. 10.1016/j.mad.2005.03.023.
10. Houthoofd, K., Johnson, T.E., and Vanfleteren, J.R. (2005). Dietary restriction in the nematode Caenorhabditis elegans. J Gerontol A Biol Sci Med Sci *60*, 1125-1131. 10.1093/gerona/60.9.1125.
11. Kemnitz, J.W., Weindruch, R., Roecker, E.B., Crawford, K., Kaufman, P.L., and Ershler, W.B. (1993). Dietary Restriction of Adult Male Rhesus Monkeys: Design, Methodology, and Preliminary Findings From the First Year of Study. Journal of Gerontology *48*, B17-B26.
12. Weindruch, R., Walford, R.L., Fligiel, S., and Guthrie, D. (1986). The retardation of aging in mice by dietary restriction: longevity, cancer, immunity and lifetime energy intake. J Nutr *116*, 641-654. 10.1093/jn/116.4.641.
13. Stewart, T.M., Bhapkar, M., Das, S., Galan, K., Martin, C.K., McAdams, L., Pieper, C., Redman, L., Roberts, S., Stein, R.I., et al. (2013). Comprehensive Assessment of Long-term Effects of Reducing Intake of Energy Phase 2 (CALERIE Phase 2) screening and recruitment: methods and results. Contemp Clin Trials *34*, 10-20. 10.1016/j.cct.2012.08.011.

14. Rochon, J., Bales, C.W., Ravussin, E., Redman, L.M., Holloszy, J.O., Racette, S.B., Roberts, S.B., Das, S.K., Romashkan, S., Galan, K.M., et al. (2011). Design and conduct of the CALERIE study: comprehensive assessment of the long-term effects of reducing intake of energy. J Gerontol A Biol Sci Med Sci *66*, 97-108. 10.1093/gerona/glq168.
15. Heilbronn, L.K., de Jonge, L., Frisard, M.I., DeLany, J.P., Larson-Meyer, D.E., Rood, J., Nguyen, T., Martin, C.K., Volaufova, J., Most, M.M., et al. (2006). Effect of 6-month calorie restriction on biomarkers of longevity, metabolic adaptation, and oxidative stress in overweight individuals: a randomized controlled trial. JAMA *295*, 1539-1548. 10.1001/jama.295.13.1539.
16. Campisi, J., Kapahi, P., Lithgow, G.J., Melov, S., Newman, J.C., and Verdin, E. (2019). From discoveries in ageing research to therapeutics for healthy ageing. Nature *571*, 183-192. 10.1038/s41586-019-1365-2.
17. Klass, M. (1983). A method for the isolation of longevity mutants in the nematode Caenorhabditis elegans and initial results. Mech Ageing Dev *22*, 279.
18. Klass, M., Nguyen, P.N., and Dechavigny, A. (1983). Age-correlated changes in the DNA template in the nematode Caenorhabditis elegans. Mech Ageing Dev *22*, 253-263.
19. Friedman, D.B., and Johnson, T.E. (1988). A Mutation in the age-1 Gene in Caenorhabditis elegans Lengthens Life and Reduces Hermaphrodite Fertility. Genetics *118*, 75-86.
20. Kenyon, C., Chang, J., Gensch, E., Rudner, A., and Tabtiang, R. (1993). A *C. elegans* mutant that lives twice as long as wild type. Nature *366*, 461 - 464.
21. Kimura, K.D., Tissenbaum, H.A., Liu, Y., and Ruvkun, G. (1997). daf-2, an insulin receptor-like gene that regulates longevity and diapause in Caenorhabditis elegans. Science *277*, 942-946. 10.1126/science.277.5328.942.
22. Fontana, L., Partridge, L., and Longo, V.D. (2010). Extending healthy life span--from yeast to humans. Science *328*, 321-326. 10.1126/science.1172539.
23. Vakkayil, K.L., and Hoppe, T. (2022). Temperature-Dependent Regulation of Proteostasis and Longevity. Front Aging *3*, 853588. 10.3389/fragi.2022.853588.
24. Chen, Y.C., Chen, H.J., Tseng, W.C., Hsu, J.M., Huang, T.T., Chen, C.H., and Pan, C.L. (2016). A *C. elegans* Thermosensory Circuit Regulates Longevity through crh-1/CREB-Dependent flp-6 Neuropeptide Signaling. Dev Cell *39*, 209-223. 10.1016/j.devcel.2016.08.021.
25. Hwangbo, D.S., Gershman, B., Gersham, B., Tu, M.P., Palmer, M., and Tatar, M. (2004). Drosophila dFOXO controls lifespan and regulates insulin signalling in brain and fat body. Nature *429*, 562-566. 10.1038/nature02549.
26. Flurkey, K., Papaconstantinou, J., Miller, R.A., and Harrison, D.E. (2001). Lifespan extension and delayed immune and collagen aging in mutant mice with defects in growth hormone production. Proc Natl Acad Sci U S A *98*, 6736-6741. 10.1073/pnas.111158898.
27. Zhang, Y., Shao, Z., Zhai, Z., Shen, C., and Powell-Coffman, J.A. (2009). The HIF-1 hypoxia-inducible factor modulates lifespan in *C. elegans*. PLoS One *4*, e6348. 10.1371/journal.pone.0006348.
28. Rascón, B., and Harrison, J.F. (2010). Lifespan and oxidative stress show a non-linear response to atmospheric oxygen in Drosophila. J Exp Biol *213*, 3441-3448. 10.1242/jeb.044867.

29. Calabrese, E.J., Dhawan, G., Kapoor, R., Iavicoli, I., and Calabrese, V. (2015). What is hormesis and its relevance to healthy aging and longevity? Biogerontology *16*, 693-707. 10.1007/s10522-015-9601-0.
30. Rattan, I.S.S. (2008). Hormesis in aging. Ageing Research Reviews *7*, 63-78. 10.1016/j.arr.2007.03.002.
31. Miller, H.A., Dean, E.S., Pletcher, S.D., and Leiser, S.F. (2020). Cell non-autonomous regulation of health and longevity. Elife *9*. 10.7554/eLife.62659.
32. Gems, D., and Partridge, L. (2008). Stress-Response Hormesis and Aging: "That which Does Not Kill Us Makes Us Stronger". Cell Metabolism *7*, 200-203. 10.1016/j.cmet.2008.01.001.
33. Martin, K.C., Höchsmann, C., Dorling, L.J., Bhapkar, M., Pieper, F.C., Racette, B.S., Das, K.S., Redman, M.L., Kraus, E.W., and Ravussin, E. (2022). Challenges in defining successful adherence to calorie restriction goals in humans: Results from CALERIE™ 2. Experimental Gerontology *162*, 111757. 10.1016/j.exger.2022.111757.
34. Redman, L.M., and Ravussin, E. (2011). Caloric Restriction in Humans: Impact on Physiological, Psychological, and Behavioral Outcomes. Antioxidants & Redox Signaling *14*, 275-287. 10.1089/ars.2010.3253.
35. Cherif, A., Roelands, B., Meeusen, R., and Chamari, K. (2016). Effects of Intermittent Fasting, Caloric Restriction, and Ramadan Intermittent Fasting on Cognitive Performance at Rest and During Exercise in Adults. Sports Medicine *46*, 35-47. 10.1007/s40279-015-0408-6.
36. Veronese, N., and Reginster, J.-Y. (2019). The effects of calorie restriction, intermittent fasting and vegetarian diets on bone health. Aging Clinical and Experimental Research *31*, 753-758. 10.1007/s40520-019-01174-x.
37. Fontana, L., and Partridge, L. (2015). Promoting health and longevity through diet: from model organisms to humans. Cell *161*, 106-118. 10.1016/j.cell.2015.02.020.
38. Kenyon, C., Chang, J., Gensch, E., Rudner, A., and Tabtiang, R. (1993). A *C. elegans* mutant that lives twice as long as wild type. Nature *366*, 461-464. 10.1038/366461a0.
39. Clancy, D.J., Gems, D., Harshman, L.G., Oldham, S., Stocker, H., Hafen, E., Leevers, S.J., and Partridge, L. (2001). Extension of life-span by loss of CHICO, a Drosophila insulin receptor substrate protein. Science *292*, 104-106. 10.1126/science.1057991.
40. Flurkey, K., Papaconstantinou, J., and Harrison, D.E. (2002). The Snell dwarf mutation Pit1(dw) can increase life span in mice. Mech Ageing Dev *123*, 121-130. 10.1016/s0047-6374(01)00339-6.
41. Harrison, D.E., Strong, R., Sharp, Z.D., Nelson, J.F., Astle, C.M., Flurkey, K., Nadon, N.L., Wilkinson, J.E., Frenkel, K., Carter, C.S., et al. (2009). Rapamycin fed late in life extends lifespan in genetically heterogeneous mice. Nature *460*, 392-395. 10.1038/nature08221.
42. Vaiserman, A., and Lushchak, O. (2017). Implementation of longevity-promoting supplements and medications in public health practice: achievements, challenges and future perspectives. Journal of Translational Medicine *15*. 10.1186/s12967-017-1259-8.
43. Maehle, A.H. (2004). "Receptive substances": John Newport Langley (1852-1925) and his path to a receptor theory of drug action. Med Hist *48*, 153-174. 10.1017/s0025727300000090.
44. Cohen, S. (1965). The stimulation of epidermal proliferation by a specific protein (EGF). Dev Biol *12*, 394-407. 10.1016/0012-1606(65)90005-9.

45. Paton, W.D., and Rang, H.P. (1965). THE UPTAKE OF ATROPINE AND RELATED DRUGS BY INTESTINAL SMOOTH MUSCLE OF THE GUINEA-PIG IN RELATION TO ACETYLCHOLINE RECEPTORS. Proc R Soc Lond B Biol Sci *163*, 1-44. 10.1098/rspb.1965.0058.
46. Nusse, R. (2003). Wnts and Hedgehogs: lipid-modified proteins and similarities in signaling mechanisms at the cell surface. Development *130*, 5297-5305. 10.1242/dev.00821.
47. Schinzel, R., and Dillin, A. (2015). Endocrine aspects of organelle stress—cell non-autonomous signaling of mitochondria and the ER. Curr Opin Cell Biol *33*, 102-110. 10.1016/j.ceb.2015.01.006.
48. Leiser, S.F., Miller, H., Rossner, R., Fletcher, M., Leonard, A., Primitivo, M., Rintala, N., Ramos, F.J., Miller, D.L., and Kaeberlein, M. (2015). Cell nonautonomous activation of flavin-containing monooxygenase promotes longevity and health span. Science. 10.1126/science.aac9257.
49. Zhang, Y., Lanjuin, A., Chowdhury, S.R., Mistry, M., Silva-García, C.G., Weir, H.J., Lee, C.L., Escoubas, C.C., Tabakovic, E., and Mair, W.B. (2019). Neuronal TORC1 modulates longevity via AMPK and cell nonautonomous regulation of mitochondrial dynamics in. Elife *8*. 10.7554/eLife.49158.
50. Zhang, G., Li, J., Purkayastha, S., Tang, Y., Zhang, H., Yin, Y., Li, B., Liu, G., and Cai, D. (2013). Hypothalamic programming of systemic ageing involving IKK-β, NF-κB and GnRH. Nature *497*, 211-216. 10.1038/nature12143.
51. Riera, C.E., Huising, M.O., Follett, P., Leblanc, M., Halloran, J., Van Andel, R., de Magalhaes Filho, C.D., Merkwirth, C., and Dillin, A. (2014). TRPV1 pain receptors regulate longevity and metabolism by neuropeptide signaling. Cell *157*, 1023-1036. 10.1016/j.cell.2014.03.051.
52. Ro, J., Pak, G., Malec, P.A., Lyu, Y., Allison, D.B., Kennedy, R.T., and Pletcher, S.D. (2016). Serotonin signaling mediates protein valuation and aging. Elife *5*. 10.7554/eLife.16843.
53. Apfeld, J., and Kenyon, C. (1998). Cell nonautonomy of *C. elegans* daf-2 function in the regulation of diapause and life span. Cell *95*, 199-210.
54. Gottlieb, S., and Ruvkun, G. (1994). daf-2, daf-16 and daf-23: genetically interacting genes controlling Dauer formation in Caenorhabditis elegans. Genetics *137*, 107-120.
55. Libina, N., Berman, J.R., and Kenyon, C. (2003). Tissue-specific activities of *C. elegans* DAF-16 in the regulation of lifespan. Cell *115*, 489-502.
56. Kaletsky, R., Lakhina, V., Arey, R., Williams, A., Landis, J., Ashraf, J., and Murphy, C.T. (2016). The *C. elegans* adult neuronal IIS/FOXO transcriptome reveals adult phenotype regulators. Nature *529*, 92-96. 10.1038/nature16483.
57. Silva, M.C., Amaral, M.D., and Morimoto, R.I. (2013). Neuronal reprograming of protein homeostasis by calcium-dependent regulation of the heat shock response. PLoS Genet *9*, e1003711. 10.1371/journal.pgen.1003711.
58. De Rosa, M.J., Veuthey, T., Florman, J., Grant, J., Blanco, M.G., Andersen, N., Donnelly, J., Rayes, D., and Alkema, M.J. (2019). The flight response impairs cytoprotective mechanisms by activating the insulin pathway. Nature *573*, 135-138. 10.1038/s41586-019-1524-5.
59. Apfeld, J., and Kenyon, C. (1999). Regulation of lifespan by sensory perception in Caenorhabditis elegans. Nature *402*, 804-809. 10.1038/45544.

60. Alcedo, J., and Kenyon, C. (2004). Regulation of *C. elegans* longevity by specific gustatory and olfactory neurons. Neuron *41*, 45-55.
61. McCormick, M., Chen, K., Ramaswamy, P., and Kenyon, C. (2012). New genes that extend Caenorhabditis elegans' lifespan in response to reproductive signals. Aging Cell *11*, 192-202. 10.1111/j.1474-9726.2011.00768.x.
62. Hsin, H., and Kenyon, C. (1999). Signals from the reproductive system regulate the lifespan of *C. elegans*. Nature *399*, 362-366. 10.1038/20694.
63. Yamawaki, T.M., Berman, J.R., Suchanek-Kavipurapu, M., McCormick, M., Gaglia, M.M., Lee, S.J., and Kenyon, C. (2010). The somatic reproductive tissues of *C. elegans* promote longevity through steroid hormone signaling. PLoS Biol *8*. 10.1371/journal.pbio.1000468.
64. Reinhart, B.J., Slack, F.J., Basson, M., Pasquinelli, A.E., Bettinger, J.C., Rougvie, A.E., Horvitz, H.R., and Ruvkun, G. (2000). The 21-nucleotide let-7 RNA regulates developmental timing in Caenorhabditis elegans. Nature *403*, 901-906. 10.1038/35002607.
65. Boulias, K., and Horvitz, H.R. (2012). The *C. elegans* microRNA mir-71 acts in neurons to promote germline-mediated longevity through regulation of DAF-16/FOXO. Cell Metab *15*, 439-450. 10.1016/j.cmet.2012.02.014.
66. Steinbaugh, M.J., Narasimhan, S.D., Robida-Stubbs, S., Moronetti Mazzeo, L.E., Dreyfuss, J.M., Hourihan, J.M., Raghavan, P., Operaña, T.N., Esmaillie, R., and Blackwell, T.K. (2015). Lipid-mediated regulation of SKN-1/Nrf in response to germ cell absence. Elife *4*. 10.7554/eLife.07836.
67. Ratnappan, R., Amrit, F.R., Chen, S.W., Gill, H., Holden, K., Ward, J., Yamamoto, K.R., Olsen, C.P., and Ghazi, A. (2014). Germline signals deploy NHR-49 to modulate fatty-acid β-oxidation and desaturation in somatic tissues of *C. elegans*. PLoS Genet *10*, e1004829. 10.1371/journal.pgen.1004829.
68. Apfeld, J., O'Connor, G., McDonagh, T., DiStefano, P.S., and Curtis, R. (2004). The AMP-activated protein kinase AAK-2 links energy levels and insulin-like signals to lifespan in *C. elegans*. Genes Dev *18*, 3004-3009. 10.1101/gad.1255404.
69. Mair, W., Morantte, I., Rodrigues, A.P., Manning, G., Montminy, M., Shaw, R.J., and Dillin, A. (2011). Lifespan extension induced by AMPK and calcineurin is mediated by CRTC-1 and CREB. Nature *470*, 404-408. 10.1038/nature09706.
70. Burkewitz, K., Morantte, I., Weir, H.J., Yeo, R., Zhang, Y., Huynh, F.K., Ilkayeva, O.R., Hirschey, M.D., Grant, A.R., and Mair, W.B. (2015). Neuronal CRTC-1 governs systemic mitochondrial metabolism and lifespan via a catecholamine signal. Cell *160*, 842-855. 10.1016/j.cell.2015.02.004.
71. Moreno-Arriola, E., El Hafidi, M., Ortega-Cuéllar, D., and Carvajal, K. (2016). AMP-Activated Protein Kinase Regulates Oxidative Metabolism in Caenorhabditis elegans through the NHR-49 and MDT-15 Transcriptional Regulators. PLoS One *11*, e0148089. 10.1371/journal.pone.0148089.
72. Schreiber, M.A., Pierce-Shimomura, J.T., Chan, S., Parry, D., and McIntire, S.L. (2010). Manipulation of behavioral decline in Caenorhabditis elegans with the Rag GTPase raga-1. PLoS Genet *6*, e1000972. 10.1371/journal.pgen.1000972.
73. Durieux, J., Wolff, S., and Dillin, A. (2011). The cell-non-autonomous nature of electron transport chain-mediated longevity. Cell *144*, 79-91. 10.1016/j.cell.2010.12.016.

74. Zhang, Q., Wu, X., Chen, P., Liu, L., Xin, N., Tian, Y., and Dillin, A. (2018). The Mitochondrial Unfolded Protein Response Is Mediated Cell-Non-autonomously by Retromer-Dependent Wnt Signaling. Cell *174*, 870-883.e817. 10.1016/j.cell.2018.06.029.
75. Prasad, B.C., and Clark, S.G. (2006). Wnt signaling establishes anteroposterior neuronal polarity and requires retromer in *C. elegans*. Development *133*, 1757-1766. 10.1242/dev.02357.
76. Taylor, R.C., and Dillin, A. (2013). XBP-1 is a cell-nonautonomous regulator of stress resistance and longevity. Cell *153*, 1435-1447. 10.1016/j.cell.2013.05.042.
77. Imanikia, S., Özbey, N.P., Krueger, C., Casanueva, M.O., and Taylor, R.C. (2019). Neuronal XBP-1 Activates Intestinal Lysosomes to Improve Proteostasis in *C. elegans*. Curr Biol *29*, 2322-2338.e2327. 10.1016/j.cub.2019.06.031.
78. Frakes, A.E., Metcalf, M.G., Tronnes, S.U., Bar-Ziv, R., Durieux, J., Gildea, H.K., Kandahari, N., Monshietehadi, S., and Dillin, A. (2020). Four glial cells regulate ER stress resistance and longevity via neuropeptide signaling in. Science *367*, 436-440. 10.1126/science.aaz6896.
79. Daniele, J.R., Higuchi-Sanabria, R., Durieux, J., Monshietehadi, S., Ramachandran, V., Tronnes, S.U., Kelet, N., Sanchez, M., Metcalf, M.G., Garcia, G., et al. (2020). UPR. Sci Adv *6*, eaaz1441. 10.1126/sciadv.aaz1441.
80. Imanikia, S., Sheng, M., Castro, C., Griffin, J.L., and Taylor, R.C. (2019). XBP-1 Remodels Lipid Metabolism to Extend Longevity. Cell Rep *28*, 581-589.e584. 10.1016/j.celrep.2019.06.057.
81. Özbey, N.P., Imanikia, S., Krueger, C., Hardege, I., Morud, J., Sheng, M., Schafer, W.R., Casanueva, M.O., and Taylor, R.C. (2020). Tyramine Acts Downstream of Neuronal XBP-1s to Coordinate Inter-tissue UPR. Dev Cell *55*, 754-770.e756. 10.1016/j.devcel.2020.10.024.
82. Li, C., Kim, K., and Nelson, L.S. (1999). FMRFamide-related neuropeptide gene family in Caenorhabditis elegans. Brain Res *848*, 26-34. 10.1016/s0006-8993(99)01972-1.
83. Li, C., Nelson, L.S., Kim, K., Nathoo, A., and Hart, A.C. (1999). Neuropeptide gene families in the nematode Caenorhabditis elegans. Ann N Y Acad Sci *897*, 239-252. 10.1111/j.1749-6632.1999.tb07895.x.
84. Lamb, M.J. (1968). Temperature and lifespan in Drosophila. Nature *220*, 808-809.
85. Miller, H., Fletcher, M., Primitivo, M., Leonard, A., Sutphin, G.L., Rintala, N., Kaeberlein, M., and Leiser, S.F. (2017). Genetic interaction with temperature is an important determinant of nematode longevity. Aging Cell. 10.1111/acel.12658.
86. Walther, D.M., Kasturi, P., Zheng, M., Pinkert, S., Vecchi, G., Ciryam, P., Morimoto, R.I., Dobson, C.M., Vendruscolo, M., Mann, M., and Hartl, F.U. (2015). Widespread Proteome Remodeling and Aggregation in Aging *C. elegans*. Cell *161*, 919-932. 10.1016/j.cell.2015.03.032.
87. Labbadia, J., and Morimoto, R.I. (2015). Repression of the Heat Shock Response Is a Programmed Event at the Onset of Reproduction. Mol Cell *59*, 639-650. 10.1016/j.molcel.2015.06.027.
88. Santra, M., Dill, K.A., and de Graff, A.M.R. (2019). Proteostasis collapse is a driver of cell aging and death. Proc Natl Acad Sci U S A *116*, 22173-22178. 10.1073/pnas.1906592116.

89. Prahlad, V., Cornelius, T., and Morimoto, R.I. (2008). Regulation of the cellular heat shock response in Caenorhabditis elegans by thermosensory neurons. Science *320*, 811-814. 10.1126/science.1156093.
90. Tatum, M.C., Ooi, F.K., Chikka, M.R., Chauve, L., Martinez-Velazquez, L.A., Steinbusch, H.W., Morimoto, R.I., and Prahlad, V. (2015). Neuronal serotonin release triggers the heat shock response in *C. elegans* in the absence of temperature increase. Curr Biol *25*, 163-174. 10.1016/j.cub.2014.11.040.
91. Lee, S.J., and Kenyon, C. (2009). Regulation of the longevity response to temperature by thermosensory neurons in Caenorhabditis elegans. Curr Biol *19*, 715-722. 10.1016/j.cub.2009.03.041.
92. Douglas, P.M., Baird, N.A., Simic, M.S., Uhlein, S., McCormick, M.A., Wolff, S.C., Kennedy, B.K., and Dillin, A. (2015). Heterotypic Signals from Neural HSF-1 Separate Thermotolerance from Longevity. Cell Rep *12*, 1196-1204. 10.1016/j.celrep.2015.07.026.
93. Kumsta, C., Ching, T.T., Nishimura, M., Davis, A.E., Gelino, S., Catan, H.H., Yu, X., Chu, C.C., Ong, B., Panowski, S.H., et al. (2014). Integrin-linked kinase modulates longevity and thermotolerance in *C. elegans* through neuronal control of HSF-1. Aging Cell *13*, 419-430. 10.1111/acel.12189.
94. Zhang, B., Gong, J., Zhang, W., Xiao, R., Liu, J., and Xu, X.Z.S. (2018). Brain-gut communications via distinct neuroendocrine signals bidirectionally regulate longevity in. Genes Dev *32*, 258-270. 10.1101/gad.309625.117.
95. Artan, M., Jeong, D.E., Lee, D., Kim, Y.I., Son, H.G., Husain, Z., Kim, J., Altintas, O., Kim, K., Alcedo, J., and Lee, S.J. (2016). Food-derived sensory cues modulate longevity via distinct neuroendocrine insulin-like peptides. Genes Dev *30*, 1047-1057. 10.1101/gad.279448.116.
96. Xiao, R., Zhang, B., Dong, Y., Gong, J., Xu, T., Liu, J., and Xu, X.Z. (2013). A genetic program promotes *C. elegans* longevity at cold temperatures via a thermosensitive TRP channel. Cell *152*, 806-817. 10.1016/j.cell.2013.01.020.
97. McCay, C., Crowell, M., and Maynard, L. (1935). The effect of retarded growth upon the length of life span and upon the ultimate body size. J Nutr. *10*, 63-79.
98. Bishop, N.A., and Guarente, L. (2007). Two neurons mediate diet-restriction-induced longevity in *C. elegans*. Nature *447*, 545-549. 10.1038/nature05904.
99. You, Y.J., Kim, J., Raizen, D.M., and Avery, L. (2008). Insulin, cGMP, and TGF-beta signals regulate food intake and quiescence in *C. elegans*: a model for satiety. Cell Metab *7*, 249-257. 10.1016/j.cmet.2008.01.005.
100. McCloskey, R.J., Fouad, A.D., Churgin, M.A., and Fang-Yen, C. (2017). Food responsiveness regulates episodic behavioral states in. J Neurophysiol *117*, 1911-1934. 10.1152/jn.00555.2016.
101. Waggoner, L.E., Zhou, G.T., Schafer, R.W., and Schafer, W.R. (1998). Control of alternative behavioral states by serotonin in Caenorhabditis elegans. Neuron *21*, 203-214. 10.1016/s0896-6273(00)80527-9.
102. Srinivasan, S., Sadegh, L., Elle, I.C., Christensen, A.G., Faergeman, N.J., and Ashrafi, K. (2008). Serotonin regulates *C. elegans* fat and feeding through independent molecular mechanisms. Cell Metab *7*, 533-544. 10.1016/j.cmet.2008.04.012.
103. Zheng, S., Chiu, H., Boudreau, J., Papanicolaou, T., Bendena, W., and Chin-Sang, I. (2018). A functional study of all 40. J Biol Chem *293*, 16912-16922. 10.1074/jbc.RA118.004542.

104. Petrascheck, M., Ye, X., and Buck, L.B. (2009). A high-throughput screen for chemicals that increase the lifespan of Caenorhabditis elegans. Ann N Y Acad Sci *1170*, 698-701. 10.1111/j.1749-6632.2009.04377.x.
105. Miller, H.A., Huang, S., Dean, E.S., Schaller, M.L., Tuckowski, A.M., Munneke, A.S., Beydoun, S., Pletcher, S.D., and Leiser, S.F. (2022). Serotonin and dopamine modulate aging in response to food odor and availability. Nat Commun *13*, 3271. 10.1038/s41467-022-30869-5.
106. Mehta, R., Steinkraus, K.A., Sutphin, G.L., Ramos, F.J., Shamieh, L.S., Huh, A., Davis, C., Chandler-Brown, D., and Kaeberlein, M. (2009). Proteasomal regulation of the hypoxic response modulates aging in *C. elegans*. Science *324*, 1196-1198. 1173507 [pii] 10.1126/science.1173507.
107. Leiser, S.F., Fletcher, M., Begun, A., and Kaeberlein, M. (2013). Life-span extension from hypoxia in Caenorhabditis elegans requires both HIF-1 and DAF-16 and is antagonized by SKN-1. J Gerontol A Biol Sci Med Sci *68*, 1135-1144. 10.1093/gerona/glt016.
108. Swindell, W.R. (2009). Genes and gene expression modules associated with caloric restriction and aging in the laboratory mouse. BMC Genomics *10*, 585. 10.1186/1471-2164-10-585.
109. Steinbaugh, M.J., Sun, L.Y., Bartke, A., and Miller, R.A. (2012). Activation of genes involved in xenobiotic metabolism is a shared signature of mouse models with extended lifespan. Am J Physiol Endocrinol Metab *303*, E488-495. 10.1152/ajpendo.00110.2012.
110. Bhat, A., Carranza, R.F., Tuckowski, M.A., and Leiser, F.S. (2024). Flavin-containing monooxygenase (FMO): Beyond xenobiotics. BioEssays *46*. 10.1002/bies.202400029.
111. Fitch, D.H.A. (2005). Introduction to nematode evolution and ecology. Wormbook.
112. Libert, S., Zwiener, J., Chu, X., Vanvoorhies, W., Roman, G., and Pletcher, S.D. (2007). Regulation of Drosophila life span by olfaction and food-derived odors. Science *315*, 1133-1137. 10.1126/science.1136610.
113. Kannan, K., and Fridell, Y.W. (2013). Functional implications of Drosophila insulin-like peptides in metabolism, aging, and dietary restriction. Front Physiol *4*, 288. 10.3389/fphys.2013.00288.
114. Tatar, M., Kopelman, A., Epstein, D., Tu, M.P., Yin, C.M., and Garofalo, R.S. (2001). A mutant Drosophila insulin receptor homolog that extends life-span and impairs neuroendocrine function. Science *292*, 107-110. 10.1126/science.1057987.
115. Giannakou, M.E., Goss, M., Junger, M.A., Hafen, E., Leevers, S.J., and Partridge, L. (2004). Long-lived Drosophila with overexpressed dFOXO in adult fat body. Science *305*, 361. 10.1126/science.1098219.
116. Hwangbo, D.S., Gershman, B., Tu, M.P., Palmer, M., and Tatar, M. (2004). Drosophila dFOXO controls lifespan and regulates insulin signalling in brain and fat body. Nature *429*, 562-566. 10.1038/nature02549.
117. Brogiolo, W., Stocker, H., Ikeya, T., Rintelen, F., Fernandez, R., and Hafen, E. (2001). An evolutionarily conserved function of the Drosophila insulin receptor and insulin-like peptides in growth control. Curr Biol *11*, 213-221. 10.1016/s0960-9822(01)00068-9.
118. Colombani, J., Andersen, D.S., and Leopold, P. (2012). Secreted peptide Dilp8 coordinates Drosophila tissue growth with developmental timing. Science *336*, 582-585. 10.1126/science.1216689.

119. Gronke, S., Clarke, D.F., Broughton, S., Andrews, T.D., and Partridge, L. (2010). Molecular evolution and functional characterization of Drosophila insulin-like peptides. PLoS Genet *6*, e1000857. 10.1371/journal.pgen.1000857.
120. Bai, H., Kang, P., and Tatar, M. (2012). Drosophila insulin-like peptide-6 (dilp6) expression from fat body extends lifespan and represses secretion of Drosophila insulin-like peptide-2 from the brain. Aging Cell *11*, 978-985. 10.1111/acel.12000.
121. Broughton, S.J., Slack, C., Alic, N., Metaxakis, A., Bass, T.M., Driege, Y., and Partridge, L. (2010). DILP-producing median neurosecretory cells in the Drosophila brain mediate the response of lifespan to nutrition. Aging Cell *9*, 336-346. 10.1111/j.1474-9726.2010.00558.x.
122. Broughton, S.J., Piper, M.D., Ikeya, T., Bass, T.M., Jacobson, J., Driege, Y., Martinez, P., Hafen, E., Withers, D.J., Leevers, S.J., and Partridge, L. (2005). Longer lifespan, altered metabolism, and stress resistance in Drosophila from ablation of cells making insulin-like ligands. Proc Natl Acad Sci U S A *102*, 3105-3110. 10.1073/pnas.0405775102.
123. Haselton, A., Sharmin, E., Schrader, J., Sah, M., Poon, P., and Fridell, Y.W. (2010). Partial ablation of adult Drosophila insulin-producing neurons modulates glucose homeostasis and extends life span without insulin resistance. Cell Cycle *9*, 3063-3071. 10.4161/cc.9.15.12458.
124. Enell, L.E., Kapan, N., Söderberg, J.A., Kahsai, L., and Nässel, D.R. (2010). Insulin signaling, lifespan and stress resistance are modulated by metabotropic GABA receptors on insulin producing cells in the brain of Drosophila. PLoS One *5*, e15780. 10.1371/journal.pone.0015780.
125. Wang, M.C., Bohmann, D., and Jasper, H. (2005). JNK extends life span and limits growth by antagonizing cellular and organism-wide responses to insulin signaling. Cell *121*, 115-125. 10.1016/j.cell.2005.02.030.
126. Post, S., Liao, S., Yamamoto, R., Veenstra, J.A., Nassel, D.R., and Tatar, M. (2019). Drosophila insulin-like peptide dilp1 increases lifespan and glucagon-like Akh expression epistatic to dilp2. Aging Cell *18*, e12863. 10.1111/acel.12863.
127. Bednarova, A., Kodrik, D., and Krishnan, N. (2013). Unique roles of glucagon and glucagon-like peptides: Parallels in understanding the functions of adipokinetic hormones in stress responses in insects. Comp Biochem Physiol A Mol Integr Physiol *164*, 91-100. 10.1016/j.cbpa.2012.10.012.
128. Waterson, M.J., Chung, B.Y., Harvanek, Z.M., Ostojic, I., Alcedo, J., and Pletcher, S.D. (2014). Water sensor ppk28 modulates Drosophila lifespan and physiology through AKH signaling. Proc Natl Acad Sci U S A *111*, 8137-8142. 10.1073/pnas.1315461111.
129. Waterson, M.J., Chan, T.P., and Pletcher, S.D. (2015). Adaptive Physiological Response to Perceived Scarcity as a Mechanism of Sensory Modulation of Life Span. The Journals of Gerontology: Series A *70*, 1088-1091. 10.1093/gerona/glv039.
130. Giannakou, M.E., Goss, M., and Partridge, L. (2008). Role of dFOXO in lifespan extension by dietary restriction in Drosophila melanogaster: not required, but its activity modulates the response. Aging Cell *7*, 187-198. 10.1111/j.1474-9726.2007.00362.x.
131. Yamamoto, R., and Tatar, M. (2011). Insulin receptor substrate chico acts with the transcription factor FOXO to extend Drosophila lifespan. Aging Cell *10*, 729-732. 10.1111/j.1474-9726.2011.00716.x.

132. Ulgherait, M., Rana, A., Rera, M., Graniel, J., and Walker, D.W. (2014). AMPK modulates tissue and organismal aging in a non-cell-autonomous manner. Cell Rep *8*, 1767-1780. 10.1016/j.celrep.2014.08.006.
133. Copeland, J.M., Cho, J., Lo, T., Hur, J.H., Bahadorani, S., Arabyan, T., Rabie, J., Soh, J., and Walker, D.W. (2009). Extension of Drosophila life span by RNAi of the mitochondrial respiratory chain. Curr Biol *19*, 1591-1598. 10.1016/j.cub.2009.08.016.
134. Owusu-Ansah, E., Song, W., and Perrimon, N. (2013). Muscle mitohormesis promotes longevity via systemic repression of insulin signaling. Cell *155*, 699-712. 10.1016/j.cell.2013.09.021.
135. Feng, J., Bussière, F., and Hekimi, S. (2001). Mitochondrial electron transport is a key determinant of life span in Caenorhabditis elegans. Dev Cell *1*, 633-644. 10.1016/s1534-5807(01)00071-5.
136. Fridell, Y.W., Sánchez-Blanco, A., Silvia, B.A., and Helfand, S.L. (2005). Targeted expression of the human uncoupling protein 2 (hUCP2) to adult neurons extends life span in the fly. Cell Metab *1*, 145-152. 10.1016/j.cmet.2005.01.005.
137. Humphrey, D.M., Toivonen, J.M., Giannakou, M., Partridge, L., and Brand, M.D. (2009). Expression of human uncoupling protein-3 in Drosophila insulin-producing cells increases insulin-like peptide (DILP) levels and shortens lifespan. Exp Gerontol *44*, 316-327. 10.1016/j.exger.2009.02.001.
138. Demontis, F., and Perrimon, N. (2010). FOXO/4E-BP signaling in Drosophila muscles regulates organism-wide proteostasis during aging. Cell *143*, 813-825. 10.1016/j.cell.2010.10.007.
139. Rallis, A., Navarro, J.A., Rass, M., Hu, A., Birman, S., Schneuwly, S., and Thérond, P.P. (2020). Hedgehog Signaling Modulates Glial Proteostasis and Lifespan. Cell Rep *30*, 2627-2643.e2625. 10.1016/j.celrep.2020.02.006.
140. Linford, N.J., Ro, J., Chung, B.Y., and Pletcher, S.D. (2015). Gustatory and metabolic perception of nutrient stress in Drosophila. Proc Natl Acad Sci U S A *112*, 2587-2592. 10.1073/pnas.1401501112.
141. Weaver, K.J., Holt, R.A., Henry, E., Lyu, Y., and Pletcher, S.D. (2023). Effects of hunger on neuronal histone modifications slow aging in. Science *380*, 625-632. 10.1126/science.ade1662.
142. Lyu, Y., Weaver, K.J., Shaukat, H.A., Plumoff, M.L., Tjilos, M., Promislow, D.E., and Pletcher, S.D. (2021). serotonin 2A receptor signaling coordinates central metabolic processes to modulate aging in response to nutrient choice. Elife *10*. 10.7554/eLife.59399.
143. Chakraborty, T.S., Gendron, C.M., Lyu, Y., Munneke, A.S., DeMarco, M.N., Hoisington, Z.W., and Pletcher, S.D. (2019). Sensory perception of dead conspecifics induces aversive cues and modulates lifespan through serotonin in Drosophila. Nat Commun *10*, 2365. 10.1038/s41467-019-10285-y.
144. Harvanek, Z.M., Lyu, Y., Gendron, C.M., Johnson, J.C., Kondo, S., Promislow, D.E.L., and Pletcher, S.D. (2017). Perceptive costs of reproduction drive ageing and physiology in male Drosophila. Nat Ecol Evol *1*, 152. 10.1038/s41559-017-0152.
145. Munneke, A.S., Chakraborty, T.S., Porter, S.S., Gendron, C.M., and Pletcher, S.D. (2022). The serotonin receptor 5-HT2A modulates lifespan and protein feeding in. Front Aging *3*, 1068455. 10.3389/fragi.2022.1068455.

146. Waterson, M.J., Chung, B.Y., Harvanek, Z.M., Ostojic, I., Alcedo, J., and Pletcher, S.D. (2014). Water sensor ppk28 modulates Drosophila lifespan and physiology through AKH signaling. Proceedings of the National Academy of Sciences of the United States of America *111*, 8137-8142. 10.1073/pnas.1315461111.
147. Ostojic, I., Boll, W., Waterson, M.J., Chan, T., Chandra, R., Pletcher, S.D., and Alcedo, J. (2014). Positive and negative gustatory inputs affect Drosophila lifespan partly in parallel to dFOXO signaling. Proc Natl Acad Sci U S A *111*, 8143-8148. 10.1073/pnas.1315466111.
148. Solon-Biet, S.M., McMahon, A.C., Ballard, J.W., Ruohonen, K., Wu, L.E., Cogger, V.C., Warren, A., Huang, X., Pichaud, N., Melvin, R.G., et al. (2014). The ratio of macronutrients, not caloric intake, dictates cardiometabolic health, aging, and longevity in ad libitum-fed mice. Cell Metab *19*, 418-430. 10.1016/j.cmet.2014.02.009.
149. Mair, W., Piper, M.D., and Partridge, L. (2005). Calories do not explain extension of life span by dietary restriction in Drosophila. PLoS Biol *3*, e223. 10.1371/journal.pbio.0030223.
150. Skorupa, D.A., Dervisefendic, A., Zwiener, J., and Pletcher, S.D. (2008). Dietary composition specifies consumption, obesity and lifespan in Drosophila melanogaster. Aging Cell.
151. Simpson, S.J., and Raubenheimer, D. (2007). Caloric restriction and aging revisited: the need for a geometric analysis of the nutritional bases of aging. J Gerontol A Biol Sci Med Sci *62*, 707-713.
152. Steck, K., Walker, S.J., Itskov, P.M., Baltazar, C., Moreira, J.M., and Ribeiro, C. (2018). Internal amino acid state modulates yeast taste neurons to support protein homeostasis in Drosophila. Elife *7*. 10.7554/eLife.31625.
153. Liu, Q., Tabuchi, M., Liu, S., Kodama, L., Horiuchi, W., Daniels, J., Chiu, L., Baldoni, D., and Wu, M.N. (2017). Branch-specific plasticity of a bifunctional dopamine circuit encodes protein hunger. Science *356*, 534-539. 10.1126/science.aal3245.
154. Gendron, C.M., Kuo, T.H., Harvanek, Z.M., Chung, B.Y., Yew, J.Y., Dierick, H.A., and Pletcher, S.D. (2014). Drosophila life span and physiology are modulated by sexual perception and reward. Science *343*, 544-548. 10.1126/science.1243339.
155. Suh, G.S., Ben-Tabou de Leon, S., Tanimoto, H., Fiala, A., Benzer, S., and Anderson, D.J. (2007). Light activation of an innate olfactory avoidance response in Drosophila. Curr Biol *17*, 905-908. 10.1016/j.cub.2007.04.046.
156. Poon, P.C., Kuo, T.H., Linford, N.J., Roman, G., and Pletcher, S.D. (2010). Carbon dioxide sensing modulates lifespan and physiology in Drosophila. PLoS Biol *8*, e1000356. 10.1371/journal.pbio.1000356.
157. Brown-Borg, H.M., Borg, K.E., Meliska, C.J., and Bartke, A. (1996). Dwarf mice and the ageing process. Nature *384*, 33. 10.1038/384033a0.
158. Coschigano, K.T., Holland, A.N., Riders, M.E., List, E.O., Flyvbjerg, A., and Kopchick, J.J. (2003). Deletion, but not antagonism, of the mouse growth hormone receptor results in severely decreased body weights, insulin, and insulin-like growth factor I levels and increased life span. Endocrinology *144*, 3799-3810.
159. Holzenberger, M., Dupont, J., Ducos, B., Leneuve, P., Géloën, A., Even, P.C., Cervera, P., and Le Bouc, Y. (2003). IGF-1 receptor regulates lifespan and resistance to oxidative stress in mice. Nature *421*, 182-187. 10.1038/nature01298.

160. Kappeler, L., De Magalhaes Filho, C., Dupont, J., Leneuve, P., Cervera, P., Périn, L., Loudes, C., Blaise, A., Klein, R., Epelbaum, J., et al. (2008). Brain IGF-1 receptors control mammalian growth and lifespan through a neuroendocrine mechanism. PLoS Biol *6*, e254. 10.1371/journal.pbio.0060254.
161. Zullo, J.M., Drake, D., Aron, L., O'Hern, P., Dhamne, S.C., Davidsohn, N., Mao, C.A., Klein, W.H., Rotenberg, A., Bennett, D.A., et al. (2019). Regulation of lifespan by neural excitation and REST. Nature *574*, 359-364. 10.1038/s41586-019-1647-8.
162. De Luca, M., Rose, G., Bonafè, M., Garasto, S., Greco, V., Weir, B.S., Franceschi, C., and De Benedictis, G. (2001). Sex-specific longevity associations defined by Tyrosine Hydroxylase-Insulin-Insulin Growth Factor 2 haplotypes on the 11p15.5 chromosomal region. Exp Gerontol *36*, 1663-1671. 10.1016/s0531-5565(01)00146-2.
163. Nagatsu, T. (1995). Tyrosine hydroxylase: human isoforms, structure and regulation in physiology and pathology. Essays Biochem *30*, 15-35.
164. Grady, D.L., Thanos, P.K., Corrada, M.M., Barnett, J.C., Ciobanu, V., Shustarovich, D., Napoli, A., Moyzis, A.G., Grandy, D., Rubinstein, M., et al. (2013). DRD4 genotype predicts longevity in mouse and human. J Neurosci *33*, 286-291. 10.1523/JNEUROSCI.3515-12.2013.
165. Taguchi, A., Wartschow, L.M., and White, M.F. (2007). Brain IRS2 signaling coordinates life span and nutrient homeostasis. Science *317*, 369-372. 10.1126/science.1142179.
166. de Cabo, R., Carmona-Gutierrez, D., Bernier, M., Hall, M.N., and Madeo, F. (2014). The search for antiaging interventions: from elixirs to fasting regimens. Cell *157*, 1515-1526. 10.1016/j.cell.2014.05.031.
167. Bitto, A., Ito, T.K., Pineda, V.V., LeTexier, N.J., Huang, H.Z., Sutlief, E., Tung, H., Vizzini, N., Chen, B., Smith, K., et al. (2016). Transient rapamycin treatment can increase lifespan and healthspan in middle-aged mice. Elife *5*. 10.7554/eLife.16351.
168. Bobkova, N.V., Evgen'ev, M., Garbuz, D.G., Kulikov, A.M., Morozov, A., Samokhin, A., Velmeshev, D., Medvinskaya, N., Nesterova, I., Pollock, A., and Nudler, E. (2015). Exogenous Hsp70 delays senescence and improves cognitive function in aging mice. Proc Natl Acad Sci U S A *112*, 16006-16011. 10.1073/pnas.1516131112.
169. Barbosa, D.A.N., de Oliveira-Souza, R., Monte Santo, F., de Oliveira Faria, A.C., Gorgulho, A.A., and De Salles, A.A.F. (2017). The hypothalamus at the crossroads of psychopathology and neurosurgery. Neurosurg Focus *43*, E15. 10.3171/2017.6.FOCUS17256.
170. Conti, B., Sanchez-Alavez, M., Winsky-Sommerer, R., Morale, M.C., Lucero, J., Brownell, S., Fabre, V., Huitron-Resendiz, S., Henriksen, S., Zorrilla, E.P., et al. (2006). Transgenic mice with a reduced core body temperature have an increased life span. Science *314*, 825-828. 10.1126/science.1132191.
171. Taniguchi, K., and Karin, M. (2018). NF-κB, inflammation, immunity and cancer: coming of age. Nature Reviews Immunology *18*, 309-324. 10.1038/nri.2017.142.
172. Widjaja, A.A., Lim, W.-W., Viswanathan, S., Chothani, S., Corden, B., Dasan, M.C., Goh, T.W.J., Lim, R., Singh, K.B., Tan, J., et al. (2024). Inhibition of IL-11 signalling extends mammalian healthspan and lifespan. Nature *632*, 157-165. doi.org/10.1038/s41586-024-07701-9.
173. Satoh, A., Brace, C.S., Rensing, N., Cliften, P., Wozniak, D.F., Herzog, E.D., Yamada, K.A., and Imai, S. (2013). Sirt1 extends life span and delays aging in mice through the

regulation of Nk2 homeobox 1 in the DMH and LH. Cell Metab *18*, 416-430. 10.1016/j.cmet.2013.07.013.
174. Rea, J.N., Carvalho, A., McNerlan, S.E., Alexander, H.D., and Rea, I.M. (2015). Genes and life-style factors in BELFAST nonagenarians: Nature, Nurture and Narrative. Biogerontology *16*, 587-597. 10.1007/s10522-015-9567-y.
175. Spadafora, F.L., Curti, A., Teti, R., Belmonte, M., Castagna, A., Mercurio, M., Infusino, P., Tavernese, G., Iannazzo, P.S., Iorio, C., and Mattace, R. (1996). Aspects of sleep in centenarians. Arch Gerontol Geriatr *22 Suppl 1*, 419-422. 10.1016/0167-4943(96)86975-5.
176. Simonsick, E.M., Meier, H.C.S., Shaffer, N.C., Studenski, S.A., and Ferrucci, L. (2016). Basal body temperature as a biomarker of healthy aging. Age (Dordr) *38*, 445-454. 10.1007/s11357-016-9952-8.
177. Carmeliet, P., Kieckens, L., Schoonjans, L., Ream, B., van Nuffelen, A., Prendergast, G., Cole, M., Bronson, R., Collen, D., and Mulligan, R.C. (1993). Plasminogen activator inhibitor-1 gene-deficient mice. I. Generation by homologous recombination and characterization. J Clin Invest *92*, 2746-2755. 10.1172/JCI116892.
178. Eren, M., Painter, C.A., Atkinson, J.B., Declerck, P.J., and Vaughan, D.E. (2002). Age-dependent spontaneous coronary arterial thrombosis in transgenic mice that express a stable form of human plasminogen activator inhibitor-1. Circulation *106*, 491-496. 10.1161/01.cir.0000023186.60090.fb.
179. Eren, M., Boe, A.E., Murphy, S.B., Place, A.T., Nagpal, V., Morales-Nebreda, L., Urich, D., Quaggin, S.E., Budinger, G.R., Mutlu, G.M., et al. (2014). PAI-1-regulated extracellular proteolysis governs senescence and survival in Klotho mice. Proc Natl Acad Sci U S A *111*, 7090-7095. 10.1073/pnas.1321942111.
180. Yamamoto, K., Takeshita, K., Kojima, T., Takamatsu, J., and Saito, H. (2005). Aging and plasminogen activator inhibitor-1 (PAI-1) regulation: implication in the pathogenesis of thrombotic disorders in the elderly. Cardiovasc Res *66*, 276-285. 10.1016/j.cardiores.2004.11.013.
181. Campisi, J., and Robert, L. (2014). Cell senescence: role in aging and age-related diseases. Interdiscip Top Gerontol *39*, 45-61. 10.1159/000358899.
182. Demaria, M., Ohtani, N., Youssef, S.A., Rodier, F., Toussaint, W., Mitchell, J.R., Laberge, R.M., Vijg, J., Van Steeg, H., Dollé, M.E., et al. (2014). An essential role for senescent cells in optimal wound healing through secretion of PDGF-AA. Dev Cell *31*, 722-733. 10.1016/j.devcel.2014.11.012.
183. Campisi, J. (2013). Aging, cellular senescence, and cancer. Annu Rev Physiol *75*, 685-705. 10.1146/annurev-physiol-030212-183653.
184. Kulkarni, A.S., Gubbi, S., and Barzilai, N. (2020). Benefits of Metformin in Attenuating the Hallmarks of Aging. Cell Metab *32*, 15-30. 10.1016/j.cmet.2020.04.001.
185. Gonzales, M.M., Garbarino, V.R., Zilli, M.E., Petersen, R.C., Kirkland, J.L., Tchkonia, T., Musi, N., Seshadri, S., Craft, S., and Orr, M.E. (2021). Senolytic Therapy to Modulate the Progression of Alzheimer's Disease (SToMP-AD): A Pilot Clinical Trial. The Journal of Prevention of Alzheimer's Disease, 1-8. 10.14283/jpad.2021.62.
186. Conboy, I.M., Conboy, M.J., Wagers, A.J., Girma, E.R., Weissman, I.L., and Rando, T.A. (2005). Rejuvenation of aged progenitor cells by exposure to a young systemic environment. Nature *433*, 760-764. 10.1038/nature03260.

187. Loffredo, F.S., Steinhauser, M.L., Jay, S.M., Gannon, J., Pancoast, J.R., Yalamanchi, P., Sinha, M., Dall'Osso, C., Khong, D., Shadrach, J.L., et al. (2013). Growth differentiation factor 11 is a circulating factor that reverses age-related cardiac hypertrophy. Cell *153*, 828-839. 10.1016/j.cell.2013.04.015.
188. Katsimpardi, L., Litterman, N.K., Schein, P.A., Miller, C.M., Loffredo, F.S., Wojtkiewicz, G.R., Chen, J.W., Lee, R.T., Wagers, A.J., and Rubin, L.L. (2014). Vascular and neurogenic rejuvenation of the aging mouse brain by young systemic factors. Science *344*, 630-634. 10.1126/science.1251141.
189. Rebo, J., Mehdipour, M., Gathwala, R., Causey, K., Liu, Y., Conboy, M.J., and Conboy, I.M. (2016). A single heterochronic blood exchange reveals rapid inhibition of multiple tissues by old blood. Nat Commun *7*, 13363. 10.1038/ncomms13363.
190. Yousefzadeh, M.J., Wilkinson, J.E., Hughes, B., Gadela, N., Ladiges, W.C., Vo, N., Niedernhofer, L.J., Huffman, D.M., and Robbins, P.D. (2020). Heterochronic parabiosis regulates the extent of cellular senescence in multiple tissues. Geroscience *42*, 951-961. 10.1007/s11357-020-00185-1.
191. Sinha, M., Jang, Y.C., Oh, J., Khong, D., Wu, E.Y., Manohar, R., Miller, C., Regalado, S.G., Loffredo, F.S., Pancoast, J.R., et al. (2014). Restoring systemic GDF11 levels reverses age-related dysfunction in mouse skeletal muscle. Science *344*, 649-652. 10.1126/science.1251152.
192. Shytikov, D., Balva, O., Debonneuil, E., Glukhovskiy, P., and Pishel, I. (2014). Aged mice repeatedly injected with plasma from young mice: a survival study. BioResearch open access *3*, 226-232. 10.1089/biores.2014.0043.
193. Minniti, A.N., Arriagada, H., Zúñiga, S., Bravo-Zehnder, M., Alfaro, I.E., and Aldunate, R. (2019). Temporal pattern of neuronal insulin release during Caenorhabditis elegans aging: Role of redox homeostasis. Aging Cell *18*, e12855. 10.1111/acel.12855.
194. Bouagnon, A.D., Lin, L., Srivastava, S., Liu, C.C., Panda, O., Schroeder, F.C., Srinivasan, S., and Ashrafi, K. (2019). Intestinal peroxisomal fatty acid β-oxidation regulates neural serotonin signaling through a feedback mechanism. PLoS Biol *17*, e3000242. 10.1371/journal.pbio.3000242.
195. Ulgherait, M., Rana, A., Rera, M., Graniel, J., and Walker, D.W. (2014). AMPK modulates tissue and organismal aging in a non-cell-autonomous manner. Cell Rep *8*, 1767-1780. 10.1016/j.celrep.2014.08.006.
196. Crimmins, M.E. (2020). Social hallmarks of aging: Suggestions for geroscience research. Ageing Research Reviews *63*, 101136. https://doi.org/10.1016/j.arr.2020.101136.
197. Whipple, O.M., Schorr, N.E., Talley, M.C.K., Lindquist, R., Bronas, G.U., and Treat-Jacobson, D. (2018). Variability in Individual Response to Aerobic Exercise Interventions Among Older Adults. Journal of Aging and Physical Activity *26*, 655-670. 10.1123/japa.2017-0054 , 10.1161/CIRCULATIONAHA.116.018093, https://doi.org/10.1111/sms.13650.
198. Baer, B.S., Dorn, D.A., and Osborne, M.D. (2024). Sex differences in response to obesity and caloric restriction on cognition and hippocampal measures of autophagic-lysosomal transcripts and signaling pathways. BMC Neuroscience *25*. https://doi.org/10.1186/s12868-023-00840-1.
199. Mitnitski, A., Howlett, E.S., and Rockwood, K. (2016). Heterogeneity of Human Aging and Its Assessment. The Journals of Gerontology Series A: Biological Sciences and Medical Sciences, glw089. 10.1093/gerona/glw089.

200. Mobbs, D., Hagan, C.C., Dalgleish, T., Silston, B., and Prã©Vost, C. (2015). The ecology of human fear: survival optimization and the nervous system. Frontiers in Neuroscience *9*. https://doi.org/10.3389/fnins.2015.00055.
201. Bellisari, A. (2008). Evolutionary origins of obesity. Obesity Reviews *9*, 165-180. https://doi.org/10.1111/j.1467-789X.2007.00392.x.
202. Crescent B. Martin, M.P.H., M.A., Kirsten A. Herrick, Ph.D., M.Sc., Neda Sarafrazi, Ph.D., and Cynthia L. Ogden, Ph.D., M.R.P. (2018). Attempts to Lose Weight Among Adults in the United States, 2013–2016. In N.C.f.H. Statistics, ed.
203. Wing, R.R., and Hill, O.J. (2001). Successful Weightloss Maintenance. Annual Review of Nutrition *21*, 323-341. 10.1146/annurev.nutr.21.1.323.
204. Rothblum, D.E. (2018). Slim chance for permanent weight loss. Archives of Scientific Psychology *6*, 63-69. https://doi.org/10.1037/arc0000043.
205. Gjestvang, C., Abrahamsen, F., Stensrud, T., and Haakstad, H.A.L. (2021). What Makes Individuals Stick to Their Exercise Regime? A One-Year Follow-Up Study Among Novice Exercisers in a Fitness Club Setting. Frontiers in Psychology *12*. 10.3389/fpsyg.2021.638928.
206. Smith, E.D., Kaeberlein, T.L., Lydum, B.T., Sager, J., Welton, K.L., Kennedy, B.K., and Kaeberlein, M. (2008). Age- and calorie-independent life span extension from dietary restriction by bacterial deprivation in Caenorhabditis elegans. BMC Dev Biol *8*, 49. 1471-213X-8-49 [pii] 10.1186/1471-213X-8-49.
207. Taillie, L.S., Ng, S.W., Xue, Y., Busey, E., and Harding, M. (2017). No Fat, No Sugar, No Salt . . . No Problem? Prevalence of "Low-Content" Nutrient Claims and Their Associations with the Nutritional Profile of Food and Beverage Purchases in the United States. Journal of the Academy of Nutrition and Dietetics 1*17,* 1366-1374.e1366. 10.1016/j.jand.2017.01.011.
208. Sylvetsky, A.C., and Rother, K.I. (2016). Trends in the Consumption of Low-Calorie Sweeteners. Physiology & behavior 1*64,* 446-450. 10.1016/j.physbeh.2016.03.030.
209. Snell, T.W., Johnston, R.K., Srinivasan, B., Zhou, H., Gao, M., and Skolnick, J. (2016). Repurposing FDA-approved drugs for anti-aging therapies. Biogerontology 1*7,* 907-920. 10.1007/s10522-016-9660-x.
210. de Cabo, R., Carmona-Gutierrez, D., Bernier, M., Hall, M.N., and Madeo, F. (2014). The search for anti-aging interventions: From elixirs to fasting regimens. Cell 1*57,* 1515-1526. 10.1016/j.cell.2014.05.031.
211. Harrison, D.E., Strong, R., Alavez, S., Astle, C.M., DiGiovanni, J., Fernandez, E., Flurkey, K., Garratt, M., Gelfond, J.A.L., Javors, M.A., et al. (2019). Acarbose improves health and lifespan in aging HET3 mice. Aging Cell 1*8,* e12898. 10.1111/acel.12898.
212. Miller, R.A., Harrison, D.E., Astle, C.M., Baur, J.A., Boyd, A.R., de Cabo, R., Fernandez, E., Flurkey, K., Javors, M.A., Nelson, J.F., et al. (2011). Rapamycin, but not resveratrol or simvastatin, extends life span of genetically heterogeneous mice. J Gerontol A Biol Sci Med Sci 6*6,* 191-201. 10.1093/gerona/glq178.
213. Harrison, D.E., Strong, R., Allison, D.B., Ames, B.N., Astle, C.M., Atamna, H., Fernandez, E., Flurkey, K., Javors, M.A., Nadon, N.L., et al. (2014). Acarbose, 17-α-estradiol, and nordihydroguaiaretic acid extend mouse lifespan preferentially in males. Aging Cell 1*3,* 273-282. 10.1111/acel.12170.
214. Mann, N.S., Hadad, N., Holte, N.M., Rothman, R.A., Sathiaseelan, R., Mondal, A.S., Agbaga, M.-P., Unnikrishnan, A., Subramaniam, M., Hawse, J., et al. (2020). Health

benefits attributed to 17α-estradiol, a lifespan-extending compound, are mediated through estrogen receptor α. eLife 9. https://doi.org/10.7554/eLife.59616.
215. Anisimov, N.V., Berstein, M.L., Popovich, G.I., Zabezhinski, A.M., Egormin, A.P., Piskunova, S.T., Semenchenko, V.A., Tyndyk, L.M., Yurova, N.M., Kovalenko, G.I., and Poroshina, E.T. (2011). If started early in life, metformin treatment increases life span and postpones tumors in female SHR mice. Aging 3*,* 148-157. 10.18632/aging.100273.
216. Martin-Montalvo, A., Mercken, E.M., Mitchell, S.J., Palacios, H.H., Mote, P.L., Scheibye-Knudsen, M., Gomes, A.P., Ward, T.M., Minor, R.K., Blouin, M.J., et al. (2013). Metformin improves healthspan and lifespan in mice. Nat Commun 4*,* 2192. 10.1038/ncomms3192.
217. Strong, R., Miller, A.R., Antebi, A., Astle, M.C., Bogue, M., Denzel, S.M., Fernandez, E., Flurkey, K., Hamilton, L.K., Lamming, W.D., et al. (2016). Longer lifespan in male mice treated with a weakly estrogenic agonist, an antioxidant, an α-glucosidase inhibitor or a Nrf2-inducer. Aging Cell 1*5,* 872-884. doi: 10.1111/acel.12496.
218. Admasu, T.D., Chaithanya Batchu, K., Barardo, D., Ng, L.F., Lam, V.Y.M., Xiao, L., Cazenave-Gassiot, A., Wenk, M.R., Tolwinski, N.S., and Gruber, J. (2018). Drug Synergy Slows Aging and Improves Healthspan through IGF and SREBP Lipid Signaling. Dev Cell 4*7,* 67-79.e65. 10.1016/j.devcel.2018.09.001.
219. Castillo-Quan, J.I., Tain, L.S., Kinghorn, K.J., Li, L., Grönke, S., Hinze, Y., Blackwell, T.K., Bjedov, I., and Partridge, L. (2019). A triple drug combination targeting components of the nutrient-sensing network maximizes longevity. Proc Natl Acad Sci U S A 1*16,* 20817-20819. 10.1073/pnas.1913212116.
220. Rasool, F.M., Rehman, U.A., Khan, I., Latif, M., Ahmad, I., Shakeel, S., Sadiq, M., Hayat, K., Shah, S., Ashraf, W., et al. (2023). Assessment of risk factors associated with potential drug-drug interactions among patients suffering from chronic disorders. PLOS ONE 1*8,* e0276277. 10.1371/journal.pone.0276277.
221. Dumbreck, S., Flynn, A., Nairn, M., Wilson, M., Treweek, S., Mercer, W.S., Alderson, P., Thompson, A., Payne, K., and Guthrie, B. (2015). Drug-disease and drug-drug interactions: systematic examination of recommendations in 12 UK national clinical guidelines. BMJ 3*50,* h949-h949. 10.1136/bmj.h949.
222. Lin, S.Y., Thummel, E.K., Thompson, D.B., Totah, A.R., and Cho, W.C. (2021). Sources of Interindividual Variability. Methods in Molecular Biology.
223. Sweeney, G.D. (1983). Variability in the human drug response. Thrombosis Research 2*9,* 3-15. 10.1016/0049-3848(83)90353-5.
224. Jiang, Y., Gaur, U., Cao, Z., Hou, S.T., and Zheng, W. (2022). Dopamine D1- and D2-like receptors oppositely regulate lifespan via a dietary restriction mechanism in Caenorhabditis elegans. BMC Biol 2*0,* 71. 10.1186/s12915-022-01272-9.
225. Bar-Ziv, R., Dutta, N., Hruby, A., Sukarto, E., Averbukh, M., Alcala, A., Henderson, H.R., Durieux, J., Tronnes, S.U., Ahmad, Q., et al. (2023). Glial-derived mitochondrial signals affect neuronal proteostasis and aging. Sci Adv 9*,* eadi1411. 10.1126/sciadv.adi1411.
226. Berendzen, K.M., Durieux, J., Shao, L.W., Tian, Y., Kim, H.E., Wolff, S., Liu, Y., and Dillin, A. (2016). Neuroendocrine Coordination of Mitochondrial Stress Signaling and Proteostasis. Cell 1*66,* 1553-1563.e1510. 10.1016/j.cell.2016.08.042.

227. Alic, N., Tullet, J.M., Niccoli, T., Broughton, S., Hoddinott, M.P., Slack, C., Gems, D., and Partridge, L. (2014). Cell-nonautonomous effects of dFOXO/DAF-16 in aging. Cell Rep 6*,* 608-616. 10.1016/j.celrep.2014.01.015.
228. Williams, K.W., Liu, T., Kong, X., Fukuda, M., Deng, Y., Berglund, E.D., Deng, Z., Gao, Y., Sohn, J.W., Jia, L., et al. (2014). Xbp1s in Pomc neurons connects ER stress with energy balance and glucose homeostasis. Cell Metab 2*0,* 471-482. 10.1016/j.cmet.2014.06.002.
229. Bazopoulou, D., Chaudhury, A.R., Pantazis, A., and Chronis, N. (2017). An automated compound screening for anti-aging effects on the function of *C. elegans* sensory neurons. Sci Rep 7*,* 9403. 10.1038/s41598-017-09651-x.
230. Huang, S., Cox, R.L., Tuckowski, A., Beydoun, S., Bhat, A., Howington, M.B., Sarker, M., Miller, H., Ruwe, E., Wang, E., et al. (2024). Fmo induction as a tool to screen for pro-longevity drugs. Geroscience 4*6,* 4689-4706. 10.1007/s11357-024-01207-y.
231. Yuan, R., Hascup, E., Hascup, K., and Bartke, A. (2023). Relationships among Development, Growth, Body Size, Reproduction, Aging, and Longevity - Trade-Offs and Pace-Of-Life. Biochemistry (Mosc) 8*8,* 1692-1703. 10.1134/S0006297923110020.
232. Mautz, B.S., Lind, M.I., and Maklakov, A.A. (2020). Dietary Restriction Improves Fitness of Aging Parents But Reduces Fitness of Their Offspring in Nematodes. J Gerontol A Biol Sci Med Sci 7*5,* 843-848. 10.1093/gerona/glz276.
233. Ganeshan, K., Nikkanen, J., Man, K., Leong, A.Y., Sogawa, Y., Maschek, A.J., Ry, V.T., Chagwedera, N.D., Cox, E.J., and Chawla, A. (2019). Energetic Trade-Offs and Hypometabolic States Promote Disease Tolerance. Cell 1*77,* 399-413.e312. 10.1016/j.cell.2019.01.050.
234. Libert, S., Chao, Y., Chu, X., and Pletcher, S.D. (2006). Trade-offs between longevity and pathogen resistance in Drosophila melanogaster are mediated by NFkappaB signaling. Aging Cell 5*,* 533-543. 10.1111/j.1474-9726.2006.00251.x.
235. Wani, A.K., Goswamy, D., and Irazoqui, E.J. (2019). A Nutrition-Longevity Tradeoff Enforced by Innate Immunity. Molecular Cell 7*4,* 864-865. 10.1016/j.molcel.2019.05.012.
236. Duric, V., Clayton, S., Leong, L.M., and Yuan, L.-L. (2016). Comorbidity Factors and Brain Mechanisms Linking Chronic Stress and Systemic Illness. Neural Plasticity 2*016,* 1-16. https://doi.org/10.1155/2016/5460732.
237. Mariotti, A. (2015). The Effects of Chronic Stress On Health: New Insights Into the Molecular Mechanisms of Brain–Body Communication. Future Science OA 1. https://doi.org/10.4155/fso.15.21.
238. Polivy, J. (1996). Psychological consequences of food restriction. J Am Diet Assoc 9*6,* 589-592; quiz 593-584. 10.1016/S0002-8223(96)00161-7.
239. Rony, M.K.K., and Alamgir, H.M. (2023). High temperatures on mental health: Recognizing the association and the need for proactive strategies-A perspective. Health Sci Rep 6*,* e1729. 10.1002/hsr2.1729.
240. Salim, S. (2014). Oxidative Stress and Psychological Disorders. Current Neuropharmacology 1*2,* 140-147. https://doi.org/10.2174/1570159X11666131120230309.
241. Hansen, M., Flatt, T., and Aguilaniu, H. (2013). Reproduction, Fat Metabolism, and Life Span: What Is the Connection? Cell Metabolism 1*7,* 10-19. 10.1016/j.cmet.2012.12.003.

242. Liu, Y., Masternak, M.M., Schneider, A., and Zhi, X. (2022). Dwarf mice as models for reproductive ageing research. Reproductive BioMedicine Online 4*4,* 5-13. 10.1016/j.rbmo.2021.09.016.
243. Vergara, M., Smith-Wheelock, M., Harper, M.J., Sigler, R., and Miller, A.R. (2004). Hormone-Treated Snell Dwarf Mice Regain Fertility But Remain Long Lived and Disease Resistant. The Journals of Gerontology Series A: Biological Sciences and Medical Sciences 5*9,* 1244-1250. 10.1093/gerona/59.12.1244.
244. Qin, X., Du, D., Chen, Q., Wu, M., Wu, T., Wen, J., Jin, Y., Zhang, J., and Wang, S. (2019). Metformin prevents murine ovarian aging. Aging 1*1,* 3785-3794. 10.18632/aging.102016.
245. Zhang, X.-M., Li, L., Xu, J.-J., Wang, N., Liu, W.-J., Lin, X.-H., Fu, Y.-C., and Luo, L.-L. (2013). Rapamycin preserves the follicle pool reserve and prolongs the ovarian lifespan of female rats via modulating mTOR activation and sirtuin expression. Gene 5*23,* 82-87. 10.1016/j.gene.2013.03.039.
246. Zhou, K.I., Pincus, Z., and Slack, F.J. (2011). Longevity and stress in Caenorhabditis elegans. Aging (Albany NY) 3*,* 733-753. 10.18632/aging.100367.
247. Amrit, G.R.F., Naim, N., Ratnappan, R., Loose, J., Mason, C., Steenberge, L., Mcclendon, T.B., Wang, G., Driscoll, M., Yanowitz, L.J., and Ghazi, A. (2019). The longevity-promoting factor, TCER-1, widely represses stress resistance and innate immunity. Nature Communications 1*0.* https://doi.org/10.1038/s41467-019-10759-z.
248. Wu, Z., Isik, M., Moroz, N., Steinbaugh, M.J., Zhang, P., and Blackwell, T.K. (2021). Dietary Restriction Extends Lifespan through Metabolic Regulation of Innate Immunity. Cell Metab 3*3,* 2090. 10.1016/j.cmet.2021.08.016.
249. Lee, J.E., Rayyan, M., Liao, A., Edery, I., and Pletcher, S.D. (2017). Acute Dietary Restriction Acts via TOR, PP2A, and Myc Signaling to Boost Innate Immunity in Drosophila. Cell Rep 2*0,* 479-490. 10.1016/j.celrep.2017.06.052.
250. Ayres, S.J., and Schneider, S.D. (2009). The Role of Anorexia in Resistance and Tolerance to Infections in Drosophila. PLoS Biology 7*,* e1000150. https://doi.org/10.1371/journal.pbio.1000150.
251. Janssen, H., Kahles, F., Liu, D., Downey, J., Koekkoek, L.L., Roudko, V., D'Souza, D., Mcalpine, S.C., Halle, L., Poller, C.W., et al. (2023). Monocytes re-enter the bone marrow during fasting and alter the host response to infection. Immunity 5*6,* 783-796.e787. 10.1016/j.immuni.2023.01.024.
252. Domínguez-Andrés, J., Reinecke, H., and Sohrabi, Y. (2023). The immune hunger games: the effects of fasting on monocytes. Cellular & Molecular Immunology 2*0,* 1098-1100. https://doi.org/10.1038/s41423-023-01033-w.
253. Lacey, A.K., Pickrum, M.A., Gonzalez, S., Bartnicki, E., Castellaw, H.A., Rodrick, C.T., Jones, R.D., Khanna, M.K., and Torres, J.V. (2024). Dietary and water restriction leads to increased susceptibility to antimicrobial resistant pathogens. Science Advances 1*0.* 10.1126/sciadv.adi7438.
254. Saunders, N.R., Metcalfe, S.M., and Nicholson, L.M. (2001). Rapamycin in transplantation: A review of the evidence. Kidney International 5*9,* 3-16. 10.1046/j.1523-1755.2001.00460.x.
255. Mannick, B.J., Giudice, D.G., Lattanzi, M., Valiante, M.N., Praestgaard, J., Huang, B., Lonetto, A.M., Maecker, T.H., Kovarik, J., Carson, S., et al. (2014). mTOR inhibition

improves immune function in the elderly. Science Translational Medicine 6*,* 268ra179-268ra261. 10.1126/scitranslmed.3009892.
256. Phillips, J.E., and Simons, P.J.M. (2023). Rapamycin not dietary restriction improves resilience against pathogens: a meta-analysis. GeroScience 45*,* 1263-1270. https://doi.org/10.1007/s11357-022-00691-4.
257. Drummond, J.M., Fry, S.C., Glynn, L.E., Dreyer, C.H., Dhanani, S., Timmerman, L.K., Volpi, E., and Rasmussen, B.B. (2009). Rapamycin administration in humans blocks the contraction-induced increase in skeletal muscle protein synthesis. The Journal of Physiology 587*,* 1535-1546. 10.1113/jphysiol.2008.163816.
258. Stuhr, N.L., and Curran, S.P. (2020). Bacterial diets differentially alter lifespan and healthspan trajectories in *C. elegans*. Communications Biology 3. 10.1038/s42003-020-01379-1.
259. Houtkooper, R.H., Pirinen, E., and Auwerx, J. (2012). Sirtuins as regulators of metabolism and healthspan. Nat Rev Mol Cell Biol 13*,* 225-238. 10.1038/nrm3293.
260. Sutphin, G.L., Bishop, E., Yanos, M.E., Moller, R.M., and Kaeberlein, M. (2012). Caffeine extends life span, improves healthspan, and delays age-associated pathology in Caenorhabditis elegans. Longev Healthspan 1*,* 9. 10.1186/2046-2395-1-9.
261. Kirkland, J.L., and Peterson, C. (2009). Healthspan, translation, and new outcomes for animal studies of aging. J Gerontol A Biol Sci Med Sci 64*,* 209-212. 10.1093/gerona/gln063.
262. Hahm, J.H., Kim, S., DiLoreto, R., Shi, C., Lee, S.J., Murphy, C.T., and Nam, H.G. (2015). *C. elegans* maximum speed correlates with healthspan and is maintained in worms with an insulin receptor mutation. Nat Commun 6*,* 8919. 10.1038/ncomms9919.
263. Stein, G.M., and Murphy, C.T. (2012). The Intersection of Aging, Longevity Pathways, and Learning and Memory in *C. elegans*. Front Genet 3*,* 259. 10.3389/fgene.2012.00259.
264. Kauffman, L.A., Ashraf, M.J., Corces-Zimmerman, R.M., Landis, N.J., and Murphy, T.C. (2010). Insulin Signaling and Dietary Restriction Differentially Influence the Decline of Learning and Memory with Age. PLoS Biology 8*,* e1000372. 10.1371/journal.pbio.1000372.
265. Zhang, Y.P., Zhang, W.H., Zhang, P., Li, Q., Sun, Y., Wang, J.W., Zhang, S.O., Cai, T., Zhan, C., and Dong, M.Q. (2022). Intestine-specific removal of DAF-2 nearly doubles lifespan in Caenorhabditis elegans with little fitness cost. Nat Commun 13*,* 6339. 10.1038/s41467-022-33850-4.
266. Lee, Y., Hwang, W., Jung, J., Park, S., Cabatbat, T.J.J., Kim, P.-J., and Lee, V.S.-J. (2016). Inverse correlation between longevity and developmental rate among wild *C. elegans* strains. Aging 8*,* 986-994. 10.18632/aging.100960.
267. Bross, T.G., Rogina, B., and Helfand, S.L. (2005). Behavioral, physical, and demographic changes in Drosophila populations through dietary restriction. Aging Cell 4*,* 309-317. 10.1111/j.1474-9726.2005.00181.x.
268. Lee, P.K., Simpson, J.S., Clissold, J.F., Brooks, R., Ballard, O.W.J., Taylor, W.P., Soran, N., and Raubenheimer, D. (2008). Lifespan and reproduction in D*rosophila:* New insights from nutritional geometry. Proceedings of the National Academy of Sciences 105*,* 2498-2503. 10.1073/pnas.0710787105.
269. Watts, M.E., Pocock, R., and Claudianos, C. (2018). Brain Energy and Oxygen Metabolism: Emerging Role in Normal Function and Disease. Front Mol Neurosci 11*,* 216. 10.3389/fnmol.2018.00216.

270. Kim, Y., Lee, S.J., and Joo, H.Y. (2020). Rapamycin increases the incidence of neuropsychiatric illness in kidney transplant patients through the suppression of neural stem cells. Translational Psychiatry 1*0.* https://doi.org/10.1038/s41398-020-0838-2.
271. Rena, G., Hardie, G.D., and Pearson, R.E. (2017). The mechanisms of action of metformin. Diabetologia 6*0,* 1577-1585. https://doi.org/10.1007/s00125-017-4342-z.
272. Meira, D.A.I., Romão, T.T., Prado, D.P.J.H., Krüger, T.L., Pires, P.E.M., and Conceição, D.O.P. (2019). Ketogenic Diet and Epilepsy: What We Know So Far. Frontiers in Neuroscience 1*3.* 10.3389/fnins.2019.00005.
273. Chourpiliadis, C., Zeng, Y., Lovik, A., Wei, D., Valdimarsdóttir, U., Song, H., Hammar, N., and Fang, F. (2024). Metabolic Profile and Long-Term Risk of Depression, Anxiety, and Stress-Related Disorders. JAMA Network Open 7*,* e244525. 10.1001/jamanetworkopen.2024.4525.
274. Sasso, M.J., Ammar, M.R., Tenchov, R., Lemmel, S., Kelber, O., Grieswelle, M., and Zhou, A.Q. (2023). Gut Microbiome–Brain Alliance: A Landscape View into Mental and Gastrointestinal Health and Disorders. ACS Chemical Neuroscience 1*4,* 1717-1763. 10.1021/acschemneuro.3c00127.
275. O'Donnell, M.P., Fox, B.W., Chao, P.H., Schroeder, F.C., and Sengupta, P. (2020). A neurotransmitter produced by gut bacteria modulates host sensory behaviour. Nature 5*83,* 415-420. 10.1038/s41586-020-2395-5.
276. Sarkar, A., Lehto, S.M., Harty, S., Dinan, T.G., Cryan, J.F., and Burnet, P.W.J. (2016). Psychobiotics and the Manipulation of Bacteria-Gut-Brain Signals. Trends Neurosci 3*9,* 763-781. 10.1016/j.tins.2016.09.002.
277. O'Mahony, S.M., Clarke, G., Borre, Y.E., Dinan, T.G., and Cryan, J.F. (2015). Serotonin, tryptophan metabolism and the brain-gut-microbiome axis. Behav Brain Res 2*77,* 32-48. 10.1016/j.bbr.2014.07.027.
278. Conti, B. (2008). Considerations on temperature, longevity and aging. Cell Mol Life Sci 6*5,* 1626-1630. 10.1007/s00018-008-7536-1.
279. Libert, S., Zwiener, J., Chu, X., Vanvoorhies, W., Roman, G., and Pletcher, S.D. (2007). Regulation of Drosophila life span by olfaction and food-derived odors. Science (New York, N.Y.) 3*15,* 1133-1137. 10.1126/science.1136610.
280. Elmi, M., Pawar, V.M., Shaw, M., Wong, D., Zhan, H., and Srinivasan, M.A. (2017). Determining the biomechanics of touch sensation in *C. elegans*. Sci Rep 7*,* 12329. 10.1038/s41598-017-12190-0.
281. Sawin, E.R., Ranganathan, R., and Horvitz, H.R. (2000). *C. elegans* locomotory rate is modulated by the environment through a dopaminergic pathway and by experience through a serotonergic pathway. Neuron 2*6,* 619-631. 10.1016/s0896-6273(00)81199-x.
282. Choi, H.S., Bhat, A., Howington, M.B., Schaller, M.L., Cox, R.L., Huang, S., Beydoun, S., Miller, H.A., Tuckowski, A.M., Mecano, J., et al. (2023). FMO rewires metabolism to promote longevity through tryptophan and one carbon metabolism in *C. elegans*. Nat Commun 1*4,* 562. 10.1038/s41467-023-36181-0.
283. Rossner, R., Kaeberlein, M., and Leiser, S.F. (2017). Flavin-containing monooxygenases in aging and disease: Emerging roles for ancient enzymes. Journal of Biological Chemistry 2*92,* 11138-11146. 10.1074/jbc.R117.779678.
284. Kapahi, P., Kaeberlein, M., and Hansen, M. (2017). Dietary restriction and lifespan: Lessons from invertebrate models. Ageing Res Rev 3*9,* 3-14. 10.1016/j.arr.2016.12.005.

285. Green, C.L., Lamming, D.W., and Fontana, L. (2022). Molecular mechanisms of dietary restriction promoting health and longevity. Nat Rev Mol Cell Biol 2*3,* 56-73. 10.1038/s41580-021-00411-4.
286. Goodman, M.B. (2006). Mechanosensation. WormBook, 1-14. 10.1895/wormbook.1.62.1.
287. Schafer, W.R. (2015). Mechanosensory molecules and circuits in *C. elegans*. Pflugers Arch 4*67,* 39-48. 10.1007/s00424-014-1574-3.
288. Goodman, M.B., and Schwarz, E.M. (2003). Transducing touch in Caenorhabditis elegans. Annu Rev Physiol 6*5,* 429-452. 10.1146/annurev.physiol.65.092101.142659.
289. García-Añoveros, J., García, J.A., Liu, J.D., and Corey, D.P. (1998). The nematode degenerin UNC-105 forms ion channels that are activated by degeneration- or hypercontraction-causing mutations. Neuron 2*0,* 1231-1241. 10.1016/s0896-6273(00)80503-6.
290. Goodman, M.B., Ernstrom, G.G., Chelur, D.S., O'Hagan, R., Yao, C.A., and Chalfie, M. (2002). MEC-2 regulates *C. elegans* DEG/ENaC channels needed for mechanosensation. Nature 4*15,* 1039-1042. 10.1038/4151039a.
291. Kaulich, E., McCubbin, P.T.N., Schafer, W.R., and Walker, D.S. (2023). Physiological insight into the conserved properties of Caenorhabditis elegans acid-sensing degenerin/epithelial sodium channels. J Physiol 6*01,* 1625-1653. 10.1113/JP283238.
292. Colbert, H.A., Smith, T.L., and Bargmann, C.I. (1997). OSM-9, a novel protein with structural similarity to channels, is required for olfaction, mechanosensation, and olfactory adaptation in Caenorhabditis elegans. J Neurosci 1*7,* 8259-8269. 10.1523/JNEUROSCI.17-21-08259.1997.
293. Zhang, B., Xiao, R., Ronan, E.A., He, Y., Hsu, A.L., Liu, J., and Xu, X.Z. (2015). Environmental Temperature Differentially Modulates *C. elegans* Longevity through a Thermosensitive TRP Channel. Cell Rep 1*1,* 1414-1424. 10.1016/j.celrep.2015.04.066.
294. Petrus, M., Peier, A.M., Bandell, M., Hwang, S.W., Huynh, T., Olney, N., Jegla, T., and Patapoutian, A. (2007). A role of TRPA1 in mechanical hyperalgesia is revealed by pharmacological inhibition. Mol Pain 3*,* 40. 10.1186/1744-8069-3-40.
295. Taylor, S.R., Santpere, G., Weinreb, A., Barrett, A., Reilly, M.B., Xu, C., Varol, E., Oikonomou, P., Glenwinkel, L., McWhirter, R., et al. (2021). Molecular topography of an entire nervous system. Cell 1*84,* 4329-4347.e4323. 10.1016/j.cell.2021.06.023.
296. Lee, H., Choi, M.-K., Lee, D., Kim, H.-S., Hwang, H., Kim, H., Park, S., Paik, Y.-K., and Lee, J. (2012). Nictation, a dispersal behavior of the nematode Caenorhabditis elegans, is regulated by IL2 neurons. Nature Neuroscience 1*5,* 107-112. 10.1038/nn.2975.
297. Kaplan, M.J., and Horvitz, R.H. (1993). A dual mechanosensory and chemosensory neuron in Caenorhabditis elegans. Proceedings of the National Academy of Sciences 9*0,* 2227-2231. 10.1073/pnas.90.6.2227.
298. Rhoades, J.L., Nelson, J.C., Nwabudike, I., Yu, S.K., McLachlan, I.G., Madan, G.K., Abebe, E., Powers, J.R., Colón-Ramos, D.A., and Flavell, S.W. (2019). ASICs Mediate Food Responses in an Enteric Serotonergic Neuron that Controls Foraging Behaviors. Cell 1*76,* 85-97.e14. 10.1016/j.cell.2018.11.023.
299. Way, C.J., and Chalfie, M. (1989). The mec-3 gene of Caenorhabditis elegans requires its own product for maintained expression and is expressed in three neuronal cell types. Genes & Development 3*,* 1823-1833. 10.1101/gad.3.12a.1823.

300. Hobert, O. (2013). The neuronal genome of Caenorhabditis elegans. WormBook, 1-106. 10.1895/wormbook.1.161.1.
301. Hills, T., Brockie, P.J., and Maricq, A.V. (2004). Dopamine and glutamate control area-restricted search behavior in Caenorhabditis elegans. J Neurosci 2*4,* 1217-1225. 10.1523/JNEUROSCI.1569-03.2004.
302. Rex, E., Molitor, S.C., Hapiak, V., Xiao, H., Henderson, M., and Komuniecki, R. (2004). Tyramine receptor (SER-2) isoforms are involved in the regulation of pharyngeal pumping and foraging behavior in Caenorhabditis elegans. Journal of Neurochemistry 9*1,* 1104-1115. 10.1111/j.1471-4159.2004.02787.x.
303. Ghosh, D.D., Sanders, T., Hong, S., McCurdy, L.Y., Chase, D.L., Cohen, N., Koelle, M.R., and Nitabach, M.N. (2016). Neural Architecture of Hunger-Dependent Multisensory Decision Making in *C. elegans*. Neuron 9*2,* 1049-1062. 10.1016/j.neuron.2016.10.030.
304. Alkema, M.J., Hunter-Ensor, M., Ringstad, N., and Horvitz, H.R. (2005). Tyramine Functions independently of octopamine in the Caenorhabditis elegans nervous system. Neuron 4*6,* 247-260. 10.1016/j.neuron.2005.02.024.
305. Chase, D.L., and Koelle, M.R. (2007). Biogenic amine neurotransmitters in *C. elegans*. WormBook, 1-15. 10.1895/wormbook.1.132.1.
306. Ortiz, C.O., Etchberger, J.F., Posy, S.L., Frøkjaer-Jensen, C., Lockery, S., Honig, B., and Hobert, O. (2006). Searching for neuronal left/right asymmetry: genomewide analysis of nematode receptor-type guanylyl cyclases. Genetics 1*73,* 131-149. 10.1534/genetics.106.055749.
307. Upadhyay, A., Pisupati, A., Jegla, T., Crook, M., Mickolajczyk, K.J., Shorey, M., Rohan, L.E., Billings, K.A., Rolls, M.M., Hancock, W.O., and Hanna-Rose, W. (2016). Nicotinamide is an endogenous agonist for a *C. elegans* TRPV OSM-9 and OCR-4 channel. Nat Commun 7*,* 13135. 10.1038/ncomms13135.
308. Cook, S.J., Jarrell, T.A., Brittin, C.A., Wang, Y., Bloniarz, A.E., Yakovlev, M.A., Nguyen, K.C.Q., Tang, L.T., Bayer, E.A., Duerr, J.S., et al. (2019). Whole-animal connectomes of both Caenorhabditis elegans sexes. Nature 5*71,* 63-71. 10.1038/s41586-019-1352-7.
309. Li, C. (2008). Neuropeptides. WormBook, 1-36. 10.1895/wormbook.1.142.1.
310. Speese, S., Petrie, M., Schuske, K., Ailion, M., Ann, K., Iwasaki, K., Jorgensen, E.M., and Martin, T.F.J. (2007). UNC-31 (CAPS) Is Required for Dense-Core Vesicle But Not Synaptic Vesicle Exocytosis in Caenorhabditis elegans. Journal of Neuroscience 2*7,* 6150-6162. 10.1523/JNEUROSCI.1466-07.2007.
311. Harris, T.W., Arnaboldi, V., Cain, S., Chan, J., Chen, W.J., Cho, J., Davis, P., Gao, S., Grove, C.A., Kishore, R., et al. (2020). WormBase: a modern Model Organism Information Resource. Nucleic Acids Research 4*8,* D762-D767. 10.1093/nar/gkz920.
312. Lee, K., and Mylonakis, E. (2017). An Intestine-Derived Neuropeptide Controls Avoidance Behavior in Caenorhabditis elegans. Cell Rep 2*0,* 2501-2512. 10.1016/j.celrep.2017.08.053.
313. Bliss, S.P., Navratil, A.M., Xie, J., and Roberson, M.S. (2010). GnRH signaling, the gonadotrope and endocrine control of fertility. Front Neuroendocrinol 3*1,* 322-340. 10.1016/j.yfrne.2010.04.002.
314. Maklakov, A.A., and Chapman, T. (2019). Evolution of ageing as a tangle of trade-offs: energy versus function. Proc Biol Sci 2*86,* 20191604. 10.1098/rspb.2019.1604.

315. Fok, A., Brissette, B., Hallacy, T., Ahamed, H., Ho, E., Ramanathan, S., and Ringstad, N. (2023). High-fidelity encoding of mechanostimuli by tactile food-sensing neurons requires an ensemble of ion channels. Cell Reports 4*2,* 112452. https://doi.org/10.1016/j.celrep.2023.112452.
316. Tanimoto, Y., Zheng, G.Y., Fei, X., Fujie, Y., Hashimoto, K., and Kimura, D.K. (2016). In actio optophysiological analyses reveal functional diversification of dopaminergic neurons in the nematode *C. elegans*. Scientific Reports 6*,* 26297. https://doi.org/10.1038/srep26297.
317. Fitch, D. (2005). Introduction to nematode evolution and ecology. Wormbook.
318. Pang, S., and Curran, S.P. (2014). Adaptive capacity to bacterial diet modulates aging in *C. elegans*. Cell Metab 1*9,* 221-231. 10.1016/j.cmet.2013.12.005.
319. Maier, W., Adilov, B., Regenass, M., and Alcedo, J. (2010). A neuromedin U receptor acts with the sensory system to modulate food type-dependent effects on *C. elegans* lifespan. PLoS Biol 8*,* e1000376. 10.1371/journal.pbio.1000376.
320. Sutphin, G.L., and Kaeberlein, M. (2009). Measuring Caenorhabditis elegans life span on solid media. J Vis Exp. 1152 [pii]10.3791/1152.
321. Greer, E.L., and Brunet, A. (2009). Different dietary restriction regimens extend lifespan by both independent and overlapping genetic pathways in *C. elegans*. Aging Cell 8, 113-127. 10.1111/j.1474-9726.2009.00459.x.
322. Anderson, E.N., Corkins, M.E., Li, J.C., Singh, K., Parsons, S., Tucey, T.M., Sorkaç, A., Huang, H., Dimitriadi, M., Sinclair, D.A., and Hart, A.C. (2016). *C. elegans* lifespan extension by osmotic stress requires FUdR, base excision repair, FOXO, and sirtuins. Mech Ageing Dev 15*4,* 30-42. 10.1016/j.mad.2016.01.004.
323. Kitto, E., Dean, J., and Leiser, S. (2025). findWormz is a user-friendly automated fluorescence quantification method for *C. elegans* research. microPublication Biology.
324. Burch, J.B., Augustine, A.D., Frieden, L.A., Hadley, E., Howcroft, T.K., Johnson, R., Khalsa, P.S., Kohanski, R.A., Li, X.L., Macchiarini, F., et al. (2014). Advances in geroscience: impact on healthspan and chronic disease. J Gerontol A Biol Sci Med Sci 69 *Suppl 1,* S1-3. 10.1093/gerona/glu041.
325. Guo, J., Huang, X., Dou, L., Yan, M., Shen, T., Tang, W., and Li, J. (2022). Aging and aging-related diseases: from molecular mechanisms to interventions and treatments. Signal Transduction and Targeted Therapy 7. https://doi.org/10.1038/s41392-022-01251-0.
326. Kitto, E.S., Beydoun, S., and Leiser, S.F. (2024). Food touch limits lifespan through bioamine and neuroendocrine signaling. bioRxiv, 2024.2004.2019.590228. 10.1101/2024.04.19.590228.
327. Veuthey, T., Giunti, S., Rosa, D.J.M., Alkema, M., and Rayes, D. (2024). The neurohormone tyramine stimulates the secretion of an Insulin-Like Peptide from the intestine to modulate the systemic stress response in *C. elegans*.
328. Wolkow, C.A., Kimura, K.D., Lee, M.S., and Ruvkun, G. (2000). Regulation of *C. elegans* life-span by insulinlike signaling in the nervous system. Science 29*0,* 147-150.
329. Boylston, W.H., DeFord, J.H., and Papaconstantinou, J. (2006). Identification of longevity-associated genes in long-lived Snell and Ames dwarf mice. Age (Dordr) 28*,* 125-144. 10.1007/s11357-006-9008-6.
330. Blüher, M., Kahn, B.B., and Kahn, C.R. (2003). Extended longevity in mice lacking the insulin receptor in adipose tissue. Science 29*9,* 572-574. 10.1126/science.1078223.

331. Shen, C., Nettleton, D., Jiang, M., Kim, S.K., and Powell-Coffman, J.A. (2005). Roles of the HIF-1 hypoxia-inducible factor during hypoxia response in Caenorhabditis elegans. J Biol Chem 28*0,* 20580-20588. 10.1074/jbc.M501894200.
332. Epstein, A.C.R., Gleadle, J.M., McNeill, L.A., Hewitson, K.S., O'Rourke, J., Mole, D.R., Mukherji, M., Metzen, E., Wilson, M.I., Dhanda, A., et al. (2001). *C. elegans* EGL-9 and Mammalian Homologs Define a Family of Dioxygenases that Regulate HIF by Prolyl Hydroxylation. Cell 10*7,* 43-54.
333. Kaeberlein, M., and Kapahi, P. (2009). The hypoxic response and aging. Cell Cycle 8, 2324. 9126 [pii].
334. Muller, R.U., Fabretti, F., Zank, S., Burst, V., Benzing, T., and Schermer, B. (2009). The von Hippel Lindau Tumor Suppressor Limits Longevity. J Am Soc Nephrol 20*,* 2513-2517. ASN.2009050497 [pii] 10.1681/ASN.2009050497.
335. Rogers, S.R., Wang, H., Durham, J.T., Stefely, A.J., Owiti, A.N., Markhard, L.A., Sandler, L., To, T.-L., and Mootha, K.V. (2023). Hypoxia extends lifespan and neurological function in a mouse model of aging. PLOS Biology 21*,* e3002117. 10.1371/journal.pbio.3002117.
336. Li, Y., Wang, M.-S., Otecko, O.N., Wang, W., Shi, P., Wu, D.-D., and Zhang, Y.-P. (2017). Hypoxia potentially promotes Tibetan longevity. Cell Research 27*,* 302-305. https://doi.org/10.1038/cr.2016.105.
337. Burtscher, M. (2014). Effects of Living at Higher Altitudes on Mortality: A Narrative Review. Aging and Disease. 10.14336/AD.2014.0500274.
338. Ohh, M., Taber, C.C., Ferens, F.G., and Tarade, D. (2022). Hypoxia-inducible factor underlies von Hippel-Lindau disease stigmata. Elife 11. 10.7554/eLife.80774.
339. Wind, J.J., and Lonser, R.R. (2011). Management of von Hippel-Lindau disease-associated CNS lesions. Expert Rev Neurother 11*,* 1433-1441. 10.1586/ern.11.124.
340. Lonser, R.R., Glenn, G.M., Walther, M., Chew, E.Y., Libutti, S.K., Linehan, W.M., and Oldfield, E.H. (2003). von Hippel-Lindau disease. Lancet 36*1,* 2059-2067. 10.1016/S0140-6736(03)13643-4.
341. Kaelin, W.G. (2002). Molecular basis of the VHL hereditary cancer syndrome. Nat Rev Cancer 2, 673-682.
342. Pocock, R., and Hobert, O. (2008). Oxygen levels affect axon guidance and neuronal migration in Caenorhabditis elegans. Nat Neurosci 11*,* 894-900. 10.1038/nn.2152.
343. Sze, J.Y., Victor, M., Loer, C., Shi, Y., and Ruvkun, G. (2000). Food and metabolic signalling defects in a Caenorhabditis elegans serotonin-synthesis mutant. Nature 40*3,* 560-564. 10.1038/35000609.
344. Flavell, S.W., Pokala, N., Macosko, E.Z., Albrecht, D.R., Larsch, J., and Bargmann, C.I. (2013). Serotonin and the neuropeptide PDF initiate and extend opposing behavioral states in *C. elegans*. Cell 15*4,* 1023-1035. 10.1016/j.cell.2013.08.001.
345. Hobson, R.J., Hapiak, V.M., Xiao, H., Buehrer, K.L., Komuniecki, P.R., and Komuniecki, R.W. (2006). SER-7, a Caenorhabditis elegans 5-HT7-like receptor, is essential for the 5-HT stimulation of pharyngeal pumping and egg laying. Genetics 17*2,* 159-169. 10.1534/genetics.105.044495.
346. Carre-Pierrat, M., Baillie, D., Johnsen, R., Hyde, R., Hart, A., Granger, L., and Ségalat, L. (2006). Characterization of the Caenorhabditis elegans G protein-coupled serotonin receptors. Invert Neurosci 6, 189-205. 10.1007/s10158-006-0033-z.

347. Turek, M., Besseling, J., Spies, J.-P., König, S., and Bringmann, H. (2016). Sleep-active neuron specification and sleep induction require FLP-11 neuropeptides to systemically induce sleep. eLife 5. https://doi.org/10.7554/eLife.12499.
348. Banerjee, N., Bhattacharya, R., Gorczyca, M., Collins, M.K., and Francis, M.M. (2017). Local neuropeptide signaling modulates serotonergic transmission to shape the temporal organization of *C. elegans* egg-laying behavior. PLOS Genetics 13*,* e1006697. 10.1371/journal.pgen.1006697.
349. Bauknecht, P., and Jékely, G. (2017). Ancient coexistence of norepinephrine, tyramine, and octopamine signaling in bilaterians. BMC Biology 15*.* 10.1186/s12915-016-0341-7.
350. Rex, E., Molitor, S.C., Hapiak, V., Xiao, H., Henderson, M., and Komuniecki, R. (2004). Tyramine receptor (SER-2) isoforms are involved in the regulation of pharyngeal pumping and foraging behavior in Caenorhabditis elegans. J Neurochem 91*,* 1104-1115. 10.1111/j.1471-4159.2004.02787.x.
351. Pirri, J.K., McPherson, A.D., Donnelly, J.L., Francis, M.M., and Alkema, M.J. (2009). A tyramine-gated chloride channel coordinates distinct motor programs of a Caenorhabditis elegans escape response. Neuron 62*,* 526-538. 10.1016/j.neuron.2009.04.013.
352. Wragg, R.T., Hapiak, V., Miller, S.B., Harris, G.P., Gray, J., Komuniecki, P.R., and Komuniecki, R.W. (2007). Tyramine and octopamine independently inhibit serotonin-stimulated aversive behaviors in Caenorhabditis elegans through two novel amine receptors. J Neurosci 27*,* 13402-13412. 10.1523/JNEUROSCI.3495-07.2007.
353. Rex, E., Hapiak, V., Hobson, R., Smith, K., Xiao, H., and Komuniecki, R. (2005). TYRA-2 (F01E11.5): a Caenorhabditis elegans</i> tyramine receptor expressed in the MC and NSM pharyngeal neurons. Journal of Neurochemistry 94*,* 181-191. 10.1111/j.1471-4159.2005.03180.x.
354. Zimmer, M., Gray, J.M., Pokala, N., Chang, A.J., Karow, D.S., Marletta, M.A., Hudson, M.L., Morton, D.B., Chronis, N., and Bargmann, C.I. (2009). Neurons detect increases and decreases in oxygen levels using distinct guanylate cyclases. Neuron 61*,* 865-879. 10.1016/j.neuron.2009.02.013.
355. Bretscher, J.A., Kodama-Namba, E., Busch, E.K., Murphy, J.R., Soltesz, Z., Laurent, P., and Bono, D.M. (2011). Temperature, Oxygen, and Salt-Sensing Neurons in *C. elegans* Are Carbon Dioxide Sensors that Control Avoidance Behavior. Neuron 69*,* 1099-1113. 10.1016/j.neuron.2011.02.023.
356. Hallem, A.E., and Sternberg, W.P. (2008). Acute carbon dioxide avoidance in Caenorhabditis elegans. Proceedings of the National Academy of Sciences 10*5,* 8038 8043. https://doi.org/10.1073/pnas.0707469105.
357. Z.F, A., and D.H, H. Handbook of *C. elegans* Anatomy. WormAtlas.
358. Noble, T., Stieglitz, J., and Srinivasan, S. (2013). An integrated serotonin and octopamine neuronal circuit directs the release of an endocrine signal to control *C. elegans* body fat. Cell Metab 18*,* 672-684. 10.1016/j.cmet.2013.09.007.
359. Speese, S., Petrie, M., Schuske, K., Ailion, M., Ann, K., Iwasaki, K., Jorgensen, E.M., and Martin, T.F. (2007). UNC-31 (CAPS) is required for dense-core vesicle but not synaptic vesicle exocytosis in Caenorhabditis elegans. J Neurosci 27*,* 6150-6162. 10.1523/JNEUROSCI.1466-07.2007.
360. Palamiuc, L., Noble, T., Witham, E., Ratanpal, H., Vaughan, M., and Srinivasan, S. (2017). A tachykinin-like neuroendocrine signalling axis couples central serotonin action

and nutrient sensing with peripheral lipid metabolism. Nature Communications 8, 14237. https://doi.org/10.1038/ncomms14237.
361. Jacob, C.T., and Kaplan, M.J. (2003). The EGL-21 Carboxypeptidase E Facilitates Acetylcholine Release at Caenorhabditis elegans</i>Neuromuscular Junctions. The Journal of Neuroscience 23*,* 2122-2130. https://doi.org/10.1523/JNEUROSCI.23-06-02122.2003.
362. Thacker, C., and Rose, M.A. (2000). A look at the Caenorhabditis elegans Kex2/Subtilisin-like proprotein convertase family. BioEssays 22*,* 545-553. 10.1002/(SICI)1521-1878(200006)22:6<545::AID-BIES7>3.0.CO;2-F.
363. Chang, J.A., and Bargmann, I.C. (2008). Hypoxia and the HIF-1 transcriptional pathway reorganize a neuronal circuit for oxygen-dependent behavior in Caenorhabditis elegans. Proceedings of the National Academy of Sciences 10*5,* 7321-7326. https://doi.org/10.1073/pnas.0802164105.
364. Powell-Coffman, J.A., and Coffman, C.R. (2010). Apoptosis: Lack of oxygen aids cell survival. Nature 46*5,* 554-555. 10.1038/465554a.
365. Kruempel, J.C.P., Miller, H.A., Schaller, M.L., Fretz, A., Howington, M., Sarker, M., Huang, S., and Leiser, S.F. (2020). Hypoxic response regulators RHY-1 and EGL-9/PHD promote longevity through a VHL-1-independent transcriptional response. Geroscience 42*,* 1621-1633. 10.1007/s11357-020-00194-0.
366. Costa, S.W., Auwera, D.V.P., Glock, C., Liewald, F.J., Bach, M., Schüler, C., Wabnig, S., Oranth, A., Masurat, F., Bringmann, H., et al. (2019). A GABAergic and peptidergic sleep neuron as a locomotion stop neuron with compartmentalized Ca2+ dynamics. Nature Communications 10*.* 10.1038/s41467-019-12098-5.
367. Wu, Y., Masurat, F., Preis, J., and Bringmann, H. (2018). Sleep Counteracts Aging Phenotypes to Survive Starvation-Induced Developmental Arrest in *C. elegans*. Curr Biol 28*,* 3610-3624.e3618. 10.1016/j.cub.2018.10.009.
368. Busack, I., and Bringmann, H. (2023). A sleep-active neuron can promote survival while sleep behavior is disturbed. PLOS Genetics 19*,* e1010665. 10.1371/journal.pgen.1010665.
369. Berkowitz, L.A., Knight, A.L., Caldwell, G.A., and Caldwell, K.A. (2008). Generation of stable transgenic *C. elegans* using microinjection. J Vis Exp. 10.3791/833.
370. Kaeberlein, M. (2013). Longevity and aging. F1000Prime Rep 5, 5. 10.12703/P5-5.
371. McCay, C.M., Crowell, M.F., and Maynard, L.A. (1989). The effect of retarded growth upon the length of life span and upon the ultimate body size. 1935. Nutrition (Burbank, Los Angeles County, Calif.) 5, 155-171; discussion 172.
372. Rossner, R., Kaeberlein, M., and Leiser, S.F. (2017). Flavin-containing monooxygenases in aging and disease: Emerging roles for ancient enzymes. J Biol Chem 29*2,* 11138-11146. 10.1074/jbc.R117.779678.
373. Huang, S., Howington, M.B., Dobry, C.J., Evans, C.R., and Leiser, S.F. (2021). Flavin-Containing Monooxygenases Are Conserved Regulators of Stress Resistance and Metabolism. Front Cell Dev Biol 9, 630188. 10.3389/fcell.2021.630188.
374. Singh, J., and Aballay, A. (2020). Bacterial Lawn Avoidance and Bacterial Two Choice Preference Assays in. Bio Protoc 10*,* e3623. 10.21769/BioProtoc.3623.
375. Flavell, S.W., Pokala, N., Macosko, E.Z., Albrecht, D.R., Larsch, J., and Bargmann, C.I. (2013). Serotonin and the neuropeptide PDF initiate and extend opposing behavioral states in *C. elegans*. Cell 15*4,* 1023-1035. 10.1016/j.cell.2013.08.001.

376. Flavell, S.W., Raizen, D.M., and You, Y.J. (2020). Behavioral States. Genetics 21*6,* 315-332. 10.1534/genetics.120.303539.
377. Veljkovic, E., Stasiuk, S., Skelly, J.P., Shoemaker, B.C., and Verrey, F. (2004). Functional Characterization of Caenorhabditis elegans Heteromeric Amino Acid Transporters. Journal of Biological Chemistry 27*9,* 7655-7662. 10.1074/jbc.M309528200.
378. Lin, L., Lemieux, A.G., Enogieru, J.O., Giacomini, M.K., and Ashrafi, K. (2020). Neural production of kynurenic acid in Caenorhabditis elegans</i> requires the AAT-1 transporter. Genes & Development 34*,* 1033-1038. 10.1101/gad.339119.120.
379. Ishita, Y., Chihara, T., and Okumura, M. (2020). Serotonergic modulation of feeding behavior in Caenorhabditis elegans and other related nematodes. Neuroscience Research 15*4,* 9-19. https://doi.org/10.1016/j.neures.2019.04.006.
380. Churgin, M.A., McCloskey, R.J., Peters, E., and Fang-Yen, C. (2017). Antagonistic Serotonergic and Octopaminergic Neural Circuits Mediate Food-Dependent Locomotory Behavior in Caenorhabditis elegans. J Neurosci 37*,* 7811-7823. 10.1523/JNEUROSCI.2636-16.2017.
381. Ranganathan, R., Sawin, E.R., Trent, C., and Horvitz, H.R. (2001). Mutations in the Caenorhabditis elegans serotonin reuptake transporter MOD-5 reveal serotonin-dependent and -independent activities of fluoxetine. J Neurosci 21*,* 5871-5884. 10.1523/JNEUROSCI.21-16-05871.2001.
382. Yu, J., Vogt, M.C., Fox, B.W., Wrobel, C.J.J., Fajardo Palomino, D., Curtis, B.J., Zhang, B., Le, H.H., Tauffenberger, A., Hobert, O., and Schroeder, F.C. (2023). Parallel pathways for serotonin biosynthesis and metabolism in *C. elegans*. Nat Chem Biol 19*,* 141-150. 10.1038/s41589-022-01148-7.
383. Tissenbaum, H.A., and Guarente, L. (2001). Increased dosage of a sir-2 gene extends lifespan in Caenorhabditis elegans. Nature 41*0,* 227-230. 35065638 [pii] 10.1038/35065638.
384. Lin, S.J., Defossez, P.A., and Guarente, L. (2000). Requirement of NAD and SIR2 for life-span extension by calorie restriction in Saccharomyces cerevisiae. Science 289*,* *2*126-2128.
385. Lemieux, G.A., Cunningham, K.A., Lin, L., Mayer, F., Werb, Z., and Ashrafi, K. (2015). Kynurenic acid is a nutritional cue that enables behavioral plasticity. Cell 160*, 1*19-131. 10.1016/j.cell.2014.12.028.
386. Vohra, M., Lemieux, G.A., Lin, L., and Ashrafi, K. (2018). Kynurenic acid accumulation underlies learning and memory impairment associated with aging. Genes Dev 32, *1*4-19. 10.1101/gad.307918.117.
387. Kano, T., Brockie, P.J., Sassa, T., Fujimoto, H., Kawahara, Y., Iino, Y., Mellem, J.E., Madsen, D.M., Hosono, R., and Maricq, A.V. (2008). Memory in Caenorhabditis elegans is mediated by NMDA-type ionotropic glutamate receptors. Curr Biol 18, *1*010-1015. 10.1016/j.cub.2008.05.051.
388. Brockie, P.J., Mellem, J.E., Hills, T., Madsen, D.M., and Maricq, A.V. (2001). The *C. elegans* glutamate receptor subunit NMR-1 is required for slow NMDA-activated currents that regulate reversal frequency during locomotion. Neuron 31, *6*17-630. 10.1016/s0896-6273(01)00394-4.
389. Dang, H., Castro-Portuguez, R., Espejo, L., Backer, G., Freitas, S., Spence, E., Meyers, J., Shuck, K., Gardea, E.A., Chang, L.M., et al. (2023). On the benefits of the tryptophan

metabolite 3-hydroxyanthranilic acid in Caenorhabditis elegans and mouse aging. Nat Commun 14, *8*338. 10.1038/s41467-023-43527-1.
390. Megan, L.S., Madeline, L.S., Joy, M., Sumeet, S., Wesley, H., Ryan, J.R., Safa, B., Emily, W., Amara, B.-L., Yatrik, M.S., and Scott, F.L. (2024). Fmo5 plays a sex-specific role in goblet cell maturation and mucus barrier formation. bioRxiv, 2024.2004.2005.588360. 10.1101/2024.04.05.588360.
391. Wani, K.A., Goswamy, D., Taubert, S., Ratnappan, R., Ghazi, A., and Irazoqui, J.E. (2021). NHR-49/PPAR-α and HLH-30/TFEB cooperate for. Elife 10. *1*0.7554/eLife.62775.
392. Phillips, I.R., Veeravalli, S., Khadayate, S., and Shephard, E.A. (2023). Metabolomic and transcriptomic analyses of Fmo5-/- mice reveal roles for flavin-containing monooxygenase 5 (FMO5) in NRF2-mediated oxidative stress response, unfolded protein response, lipid homeostasis, and carbohydrate and one-carbon metabolism. PLoS One 18, *e*0286692. 10.1371/journal.pone.0286692.
393. Phillips, I.R., and Shephard, E.A. (2017). Drug metabolism by flavin-containing monooxygenases of human and mouse. Expert Opin Drug Metab Toxicol 13, *1*67-181. 10.1080/17425255.2017.1239718.
394. Tuckowski, A., Safa, B., Profile, K.E.V.O., Ajay, B., Marshall, H., Aditya, S., Mira, B., K, C., and Francis, L.S. (2024). fmo-*4 pro*motes longevity and stress resistance via ER to mitochondria calcium regulation in C. *elegans.*
*3*95. Jee, C., Batsaikhan, E., and Salim, C. (2022). Neurobiological Basis of Aversion-Resistant Ethanol Seeking in. Metabolites 13. *1*0.3390/metabo13010062.
396. Pocock, R., and Hobert, O. Hypoxia activates a latent circuit for processing gustatory information in *C. elegans*. Nat Neurosci 13, *6*10-614.
397. Suryawinata, N., Yokosawa, R., Tan, C.H.K., Lai, L.A., Sone, R., Mori, I., and Noma, K. (2024). Dietary *E. coli* promotes age-dependent chemotaxis decline in *C. elegans*. Scientific Reports 14. *1*0.1038/s41598-024-52272-4.
398. Li, B., and An, Z. (2023). Flavin-containing Monooxygenases in the Brain and their Involvement in Neurodegeneration and Aging. Journal of Exploratory Research in Pharmacology 000*, 0*00-000. 10.14218/JERP.2022.00067.
399. Hunt-Newbury, R., Viveiros, R., Johnsen, R., Mah, A., Anastas, D., Fang, L., Halfnight, E., Lee, D., Lin, J., Lorch, A., et al. (2007). High-throughput in vivo analysis of gene expression in Caenorhabditis elegans. PLoS Biol 5, *e*237. 10.1371/journal.pbio.0050237.
400. Miura, H., Ozaki, N., Sawada, M., Isobe, K., Ohta, T., and Nagatsu, T. (2008). A link between stress and depression: Shifts in the balance between the kynurenine and serotonin pathways of tryptophan metabolism and the etiology and pathophysiology of depression. Stress 11, *1*98-209. 10.1080/10253890701754068.
401. Hestad, K., Alexander, J., Rootwelt, H., and Aaseth, J.O. (2022). The Role of Tryptophan Dysmetabolism and Quinolinic Acid in Depressive and Neurodegenerative Diseases. Biomolecules 12. *1*0.3390/biom12070998.
402. Badawy, A.A. (2017). Kynurenine Pathway of Tryptophan Metabolism: Regulatory and Functional Aspects. Int J Tryptophan Res 10, *1*178646917691938. 10.1177/1178646917691938.
403. Schwarcz, R., and Stone, W.T. (2017). The kynurenine pathway and the brain: Challenges, controversies and promises. Neuropharmacology 112*, 2*37-247. 10.1016/j.neuropharm.2016.08.003.

404. Li, B., Yuan, Y., Zhang, W., He, W., Hu, J., and Chen, N. (2014). Flavin-containing monooxygenase, a new clue of pathological proteins in the rotenone model of parkinsonism. Neurosci Lett 566*, 1*1-16. 10.1016/j.neulet.2013.11.036.
405. Phillips, I.R., and Shephard, E.A. (2019). Endogenous Roles of Mammalian Flavin-Containing Monooxygenases. Catalysts 9, *1*001. https://doi.org/10.3390/catal9121001.
406. Medkour, Y., Svistkova, V., and Titorenko, V.I. (2016). Cell-Nonautonomous Mechanisms Underlying Cellular and Organismal Aging. Int Rev Cell Mol Biol 321*, 2*59-297. 10.1016/bs.ircmb.2015.09.003.
407. McCracken, A.W., Adams, G., Hartshorne, L., Tatar, M., and Simons, M.J.P. (2020). The hidden costs of dietary restriction: Implications for its evolutionary and mechanistic origins. Sci Adv 6, *e*aay3047. 10.1126/sciadv.aay3047.
408. Nussbaum-Krammer, C.I., Neto, M.F., Brielmann, R.M., Pedersen, J.S., and Morimoto, R.I. (2015). Investigating the spreading and toxicity of prion-like proteins using the metazoan model organism *C. elegans*. J Vis Exp, 52321. 10.3791/52321.
409. Chalfie, M., Hart, A.C., Rankin, C.H., and Goodman, M.B. (2014). Assaying mechanosensation. WormBook. 10.1895/wormbook.1.172.1.
410. Motika, M.S., Zhang, J., Zheng, X., Riedler, K., and Cashman, J.R. (2009). Novel variants of the human flavin-containing monooxygenase 3 (FMO3) gene associated with trimethylaminuria. Mol Genet Metab 97, *1*28-135. 10.1016/j.ymgme.2009.02.006.
411. Beydoun, S., Choi, H.S., Dela-Cruz, G., Kruempel, J., Huang, S., Bazopoulou, D., Miller, H.A., Schaller, M.L., Evans, C.R., and Leiser, S.F. (2021). An alternative food source for metabolism and longevity studies in Caenorhabditis elegans. Commun Biol 4, *2*58. 10.1038/s42003-021-01764-4.
412. Riddle, D.L., Blumenthal, T., Meyer, B.J., and Priess, J.R. (1997). Introduction to *C. elegans*. In *C. elegans* II, D.L. Riddle, T. Blumenthal, B.J. Meyer, and J.R. Priess, eds.
413. Corsi, A.K., Wightman, B., and Chalfie, M. (2015). A Transparent window into biology: A primer on Caenorhabditis elegans. WormBook, 1-31. 10.1895/wormbook.1.177.1.
414. Kaletta, T., and Hengartner, M.O. (2006). Finding function in novel targets: *C. elegans* as a model organism. Nat Rev Drug Discov 5, *3*87-398. 10.1038/nrd2031.
415. Meneely, P.M., Dahlberg, C.L., and Rose, J.K. (2019). Working with Worms: Caenorhabditis elegans as a Model Organism. Current Protocols Essential Laboratory Techniques 19. *1*0.1002/cpet.35.
416. Zhang, S., Li, F., Zhou, T., Wang, G., and Li, Z. (2020). Caenorhabditis elegans as a Useful Model for Studying Aging Mutations. Front Endocrinol (Lausanne) 11, *5*54994. 10.3389/fendo.2020.554994.
417. Feng, M., Gao, B., Garcia, L.R., and Sun, Q. (2023). Microbiota-derived metabolites in regulating the development and physiology of Caenorhabditis elegans. Front Microbiol 14, *1*035582. 10.3389/fmicb.2023.1035582.
418. McIntyre, G., Wright, J., Wong, H.T., Lamendella, R., and Chan, J. (2021). Effects of FUdR on gene expression in the *C. elegans* bacterial diet OP50. BMC Res Notes 14, *2*07. 10.1186/s13104-021-05624-6.
419. Cabreiro, F., Au, C., Leung, K.Y., Vergara-Irigaray, N., Cocheme, H.M., Noori, T., Weinkove, D., Schuster, E., Greene, N.D., and Gems, D. (2013). Metformin retards aging in *C. elegans* by altering microbial folate and methionine metabolism. Cell 153*, 2*28-239. 10.1016/j.cell.2013.02.035.

420. Worthy, S.E., Haynes, L., Chambers, M., Bethune, D., Kan, E., Chung, K., Ota, R., Taylor, C.J., and Glater, E.E. (2018). Identification of attractive odorants released by preferred bacterial food found in the natural habitats of *C. elegans*. PLoS One 13, *e*0201158. 10.1371/journal.pone.0201158.
421. Chen, Y.C., Seyedsayamdost, M.R., and Ringstad, N. (2020). A microbial metabolite synergizes with endogenous serotonin to trigger *C. elegans* reproductive behavior. Proc Natl Acad Sci U S A 117*, 3*0589-30598. 10.1073/pnas.2017918117.
422. Kim, D.H., and Flavell, S.W. (2020). Host-microbe interactions and the behavior of Caenorhabditis elegans. J Neurogenet 34, *5*00-509. 10.1080/01677063.2020.1802724.
423. Gems, D., and Riddle, D.L. (2000). Genetic, behavioral and environmental determinants of male longevity in Caenorhabditis elegans. Genetics 154*, 1*597-1610. 10.1093/genetics/154.4.1597.
424. Qi, B., Kniazeva, M., and Han, M. (2017). A vitamin-B2-sensing mechanism that regulates gut protease activity to impact animal's food behavior and growth. Elife 6. *1*0.7554/eLife.26243.
425. Garigan, D., Hsu, A.L., Fraser, A.G., Kamath, R.S., Ahringer, J., and Kenyon, C. (2002). Genetic analysis of tissue aging in Caenorhabditis elegans: a role for heat-shock factor and bacterial proliferation. Genetics 161*, 1*101-1112. 10.1093/genetics/161.3.1101.
426. Virk, B., Jia, J., Maynard, C.A., Raimundo, A., Lefebvre, J., Richards, S.A., Chetina, N., Liang, Y., Helliwell, N., Cipinska, M., and Weinkove, D. (2016). Folate Acts in *E. coli* to Accelerate *C. elegans* Aging Independently of Bacterial Biosynthesis. Cell Rep 14, *1*611-1620. 10.1016/j.celrep.2016.01.051.
427. Thavarajah, R., Mudimbaimannar, V.K., Elizabeth, J., Rao, U.K., and Ranganathan, K. (2012). Chemical and physical basics of routine formaldehyde fixation. J Oral Maxillofac Pathol 16, *4*00-405. 10.4103/0973-029X.102496.
428. Felix, H. (1988). Permeabilized and immobilized cells. Methods Enzymol 137*, 6*37-641. 10.1016/0076-6879(88)37060-6.
429. Kumar, S., Egan, B.M., Kocsisova, Z., Schneider, D.L., Murphy, J.T., Diwan, A., and Kornfeld, K. (2019). Lifespan Extension in *C. elegans* Caused by Bacterial Colonization of the Intestine and Subsequent Activation of an Innate Immune Response. Dev Cell 49, *1*00-117.e106. 10.1016/j.devcel.2019.03.010.
430. Nakagawa, H., Shiozaki, T., Kobatake, E., Hosoya, T., Moriya, T., Sakai, F., Taru, H., and Miyazaki, T. (2016). Effects and mechanisms of prolongevity induced by Lactobacillus gasseri SBT2055 in Caenorhabditis elegans. Aging Cell 15, *2*27-236. 10.1111/acel.12431.
431. Beaudoin-Chabot, C., Wang, L., Celik, C., Abdul Khalid, A.T., Thalappilly, S., Xu, S., Koh, J.H., Lim, V.W.X., Low, A.D., and Thibault, G. (2022). The unfolded protein response reverses the effects of glucose on lifespan in chemically-sterilized *C. elegans*. Nat Commun 13, *5*889. 10.1038/s41467-022-33630-0.
432. Komura, T., Takemoto, A., Kosaka, H., Suzuki, T., and Nishikawa, Y. (2022). Prolonged Lifespan, Improved Perception, and Enhanced Host Defense of Caenorhabditis elegans by Lactococcus cremoris subsp. cremoris. Microbiol Spectr 10, *e*0045421. 10.1128/spectrum.00454-21.
433. Beydoun, S., Choi, H.S., Dela-Cruz, G., Kruempel, J., Huang, S., Bazopoulou, D., Miller, H.A., Schaller, M.L., Evans, C.R., and Leiser, S.F. (2021). An alternative food source for

metabolism and longevity studies in C. *elegans. C*ommunications Biology In *Press. 1*0.1038/s42003-021-01764-4.
434. Lobritz, M.A., Belenky, P., Porter, C.B., Gutierrez, A., Yang, J.H., Schwarz, E.G., Dwyer, D.J., Khalil, A.S., and Collins, J.J. (2015). Antibiotic efficacy is linked to bacterial cellular respiration. Proc Natl Acad Sci U S A 112*, 8*173-8180. 10.1073/pnas.1509743112.
435. Nadanaciva, S., Rana, P., Beeson, G.C., Chen, D., Ferrick, D.A., Beeson, C.C., and Will, Y. (2012). Assessment of drug-induced mitochondrial dysfunction via altered cellular respiration and acidification measured in a 96-well platform. J Bioenerg Biomembr 44, *4*21-437. 10.1007/s10863-012-9446-z.
436. Shtonda, B.B., and Avery, L. (2006). Dietary choice behavior in Caenorhabditis elegans. J Exp Biol 209*, 8*9-102. 10.1242/jeb.01955.
437. MacNeil, L.T., Watson, E., Arda, H.E., Zhu, L.J., and Walhout, A.J. (2013). Diet-induced developmental acceleration independent of TOR and insulin in *C. elegans*. Cell 153*, 2*40-252. 10.1016/j.cell.2013.02.049.
438. Kumar, S., Egan, B.M., Kocsisova, Z., Schneider, D.L., Murphy, J.T., Diwan, A., and Kornfeld, K. (2019). Lifespan Extension in *C. elegans* Caused by Bacterial Colonization of the Intestine and Subsequent Activation of an Innate Immune Response. Dev Cell 49, *1*00-117 e106. 10.1016/j.devcel.2019.03.010.
439. Kaeberlein, T.L., Smith, E.D., Tsuchiya, M., Welton, K.L., Thomas, J.H., Fields, S., Kennedy, B.K., and Kaeberlein, M. (2006). Lifespan extension in Caenorhabditis elegans by complete removal of food. Aging Cell 5, *4*87-494. 10.1111/j.1474-9726.2006.00238.x.
440. Ye, X., Linton, J.M., Schork, N.J., Buck, L.B., and Petrascheck, M. (2014). A pharmacological network for lifespan extension in Caenorhabditis elegans. Aging Cell 13, *2*06-215. 10.1111/acel.12163.
441. Hastings, J., Mains, A., Artal-Sanz, M., Bergmann, S., Braeckman, B.P., Bundy, J., Cabreiro, F., Dobson, P., Ebert, P., Hattwell, J., et al. (2017). WormJam: A consensus *C. elegans*</i>Metabolic Reconstruction and Metabolomics Community and Workshop Series. Worm 6, *e*1373939. 10.1080/21624054.2017.1373939.
442. Dirksen, P., Assie, A., Zimmermann, J., Zhang, F., Tietje, A.M., Marsh, S.A., Felix, M.A., Shapira, M., Kaleta, C., Schulenburg, H., and Samuel, B.S. (2020). CeMbio - The Caenorhabditis elegans Microbiome Resource. G3 (Bethesda) 10, *3*025-3039. 10.1534/g3.120.401309.
443. Corsi, A.K., Wightman, B., and Chalfie, M. (2015). A Transparent Window into Biology: A Primer on Caenorhabditis elegans. Genetics 200*, 3*87-407. 10.1534/genetics.115.176099.
444. Hutter, H. (2006). Fluorescent reporter methods. Methods Mol Biol 351*, 1*55-173. 10.1385/1-59745-151-7:155.
445. Schneider, C.A., Rasband, W.S., and Eliceiri, K.W. (2012). NIH Image to ImageJ: 25 years of image analysis. Nat Methods 9, *6*71-675.
446. Wählby, C., Kamentsky, L., Liu, H.Z., Riklin-Raviv, T., Conery, L.A., O'Rourke, J.E., Sokolnicki, L.K., Visvikis, O., Ljosa, V., Irazoqui, E.J., et al. (2012). An image analysis toolbox for high-throughput *C. elegans* assays. Nature Methods 9, *7*14-716. 10.1038/nmeth.1984.
447. Bonnard, E., Liu, J., Zjacic, N., Alvarez, L., and Scholz, M. (2022). Automatically tracking feeding behavior in populations of foraging. Elife 11. *1*0.7554/eLife.77252.

448. Jung, S.-K. (2021). AniLength: GUI-based automatic worm length measurement software using image processing and deep neural network. SoftwareX 15, *1*00795. https://doi.org/10.1016/j.softx.2021.100795.
449. Pan, P., Zhang, P., Premachandran, S., Peng, R., Wang, S., Fan, Q., Sun, Y., Calarco, A.J., and Liu, X. (2024). High-Resolution Imaging and Morphological Phenotyping of*C. elegans* through Stable Robotic Sample Rotation and Artificial Intelligence-Based 3-Dimensional Reconstruction. Research 7. *1*0.34133/research.0513.
450. Carpenter, E.A., and Singh, S. (2024). Bringing computation to biology by bridging the last mile. Nature Cell Biology 26, *5*-7. 10.1038/s41556-023-01286-7.
451. Mangul, S., Mosqueiro, T., Abdill, J.R., Duong, D., Mitchell, K., Sarwal, V., Hill, B., Brito, J., Littman, J.R., Statz, B., et al. (2019). Challenges and recommendations to improve the installability and archival stability of omics computational tools. PLOS Biology 17, *e*3000333. 10.1371/journal.pbio.3000333.
452. Bennett, F.C., Wende, V.H., Simko, M., Klum, S., Barfield, S., Choi, H., Pineda, V.V., and Kaeberlein, M. (2014). Activation of the mitochondrial unfolded protein response does not predict longevity in Caenorhabditis elegans. Nature Communications 5. *1*0.1038/ncomms4483.
453. Schindelin, J., Arganda-Carreras, I., Frise, E., Kaynig, V., Longair, M., Pietzsch, T., Preibisch, S., Rueden, C., Saalfeld, S., Schmid, B., et al. (2012). Fiji: an open-source platform for biological-image analysis. Nature Methods 9, *6*76-682. https://doi.org/10.1038/nmeth.2019.
454. Wählby, C., Conery, A.L., Bray, M.A., Kamentsky, L., Larkins-Ford, J., Sokolnicki, K.L., Veneskey, M., Michaels, K., Carpenter, A.E., and O'Rourke, E.J. (2014). High- and low-throughput scoring of fat mass and body fat distribution in *C. elegans*. Methods 68, *4*92-499. 10.1016/j.ymeth.2014.04.017.
455. Riera, C.E., Tsaousidou, E., Halloran, J., Follett, P., Hahn, O., Pereira, M.M.A., Ruud, L.E., Alber, J., Tharp, K., Anderson, C.M., et al. (2017). The Sense of Smell Impacts Metabolic Health and Obesity. Cell Metab 26, *1*98-211.e195. 10.1016/j.cmet.2017.06.015.
456. Honda, S., Ishii, N., Suzuki, K., and Matsuo, M. (1993). Oxygen-dependent perturbation of life span and aging rate in the nematode. J Gerontol 48, *B*57-61.
457. Chen, Y., Liu, Y., and Feng, X. (2023). Food Perception: Taste, Smell and Flavour. Foods 12, *3*628. 10.3390/foods12193628.
458. Lal, K.M., Sharma, E., Tiwari, K.R., Devi, R., Mishra, N.U., Thakur, R., Gupta, R., Dey, A., Lal, P., Kumar, A., et al. (2022). Nutrient-Mediated Perception and Signalling in Human Metabolism: A Perspective of Nutrigenomics. International Journal of Molecular Sciences 23, *1*1305. 10.3390/ijms231911305.
459. Sharkey, A.K., and Mawe, M.G. (2023). The enteric nervous system. Physiological Reviews 103*, 1*487-1564. 10.1152/physrev.00018.2022.
460. Gendron, C.M., Chakraborty, T.S., Chung, B.Y., Harvanek, Z.M., Holme, K.J., Johnson, J.C., Lyu, Y., Munneke, A.S., and Pletcher, S.D. (2020). Neuronal Mechanisms that Drive Organismal Aging Through the Lens of Perception. Annu Rev Physiol 82, *2*27-249. 10.1146/annurev-physiol-021119-034440.
461. Queirós, L., Marques, C., Pereira, J.L., Gonçalves, F.J.M., Aschner, M., and Pereira, P. (2021). Overview of Chemotaxis Behavior Assays in Caenorhabditis elegans. Curr Protoc 1, *e*120. 10.1002/cpz1.120.

462. CI, B. (2006). Chemosensation in *C. elegans*. In WormBook: The Online Review of *C. elegans* Biology [Internet]. (WormBook; 2005-2018.).
463. Ziegler, D.M. (2002). An overview of the mechanism, substrate specificities, and structure of FMOs. Drug Metab Rev 34, *5*03-511. 10.1081/DMR-120005650.
464. Barsyte, D., Lovejoy, D.A., and Lithgow, G.J. (2001). Longevity and heavy metal resistance in daf-2 and age-1 long-lived mutants of Caenorhabditis elegans. FASEB J 15, *6*27-634. 10.1096/fj.99-0966com.
465. Ramadori, G., and Coppari, R. (2011). Does hypothalamic SIRT1 regulate aging? Aging (Albany NY) 3, *3*25-328. 10.18632/aging.100311.
466. Liu, T., Xu, Y., Yi, C.-X., Tong, Q., and Cai, D. (2022). The hypothalamus for whole-body physiology: from metabolism to aging. Protein & Cell 13, *3*94-421. https://doi.org/10.1007/s13238-021-00834-x.
467. Kim, K., and Choe, K.H. (2019). Role of hypothalamus in aging and its underlying cellular mechanisms. Mechanisms of Ageing and Development 177*, 7*4-79. 10.1016/j.mad.2018.04.008.
468. Stahl, M.S., Pradko, J., Haight, R.B., Modell, G.J., Rockett, B.C., and Learned-Coughlin, S. (2004). A Review of the Neuropharmacology of Bupropion, a Dual Norepinephrine and Dopamine Reuptake Inhibitor. The Primary Care Companion For CNS Disorders 6, *1*59-166. 10.4088/pcc.v06n0403.
469. Charney, S.D., Heninger, R.G., and Sternberg, E.D. (1984). The Effect of Mianserin on Alpha-2 Adrenergic Receptor Function in Depressed Patients. British Journal of Psychiatry 144*, 4*07-416. 10.1192/bjp.144.4.407.
470. Savini, M., Folick, A., Lee, Y.T., Jin, F., Cuevas, A., Tillman, M.C., Duffy, J.D., Zhao, Q., Neve, I.A., Hu, P.W., et al. (2022). Lysosome lipid signalling from the periphery to neurons regulates longevity. Nat Cell Biol 24, *9*06-916. 10.1038/s41556-022-00926-8.
471. Chang, A.J., Chronis, N., Karow, D.S., Marletta, M.A., and Bargmann, C.I. (2006). A distributed chemosensory circuit for oxygen preference in *C. elegans*. PLoS Biol 4, *e*274. 10.1371/journal.pbio.0040274.
472. Pocock, R., and Hobert, O. (2010). Hypoxia activates a latent circuit for processing gustatory information in *C. elegans*. Nat Neurosci 13, *6*10-614. 10.1038/nn.2537.
473. Lee, K.S., Iwanir, S., Kopito, R.B., Scholz, M., Calarco, J.A., Biron, D., and Levine, E. (2017). Serotonin-dependent kinetics of feeding bursts underlie a graded response to food availability in *C. elegans*. Nat Commun 8, *1*4221. 10.1038/ncomms14221.
474. Iwanir, S., Brown, A.S., Nagy, S., Najjar, D., Kazakov, A., Lee, K.S., Zaslaver, A., Levine, E., and Biron, D. (2016). Serotonin promotes exploitation in complex environments by accelerating decision-making. BMC Biol 14, *9*. 10.1186/s12915-016-0232-y.
475. Ezcurra, M., Tanizawa, Y., Swoboda, P., and Schafer, R.W. (2011). Food sensitizes *C. elegans* avoidance behaviours through acute dopamine signalling. The EMBO Journal 30, *1*110-1122. https://doi.org/10.1038/emboj.2011.22.
476. Wang, D., Yu, Y., Li, Y., and Wang, Y. (2014). Dopamine receptors antagonistically regulate behavioral choice between conflicting alternatives in *C. elegans*. PLoS One 9, *e*115985. 10.1371/journal.pone.0115985.
477. Oranth, A., Schultheis, C., Tolstenkov, O., Miller, D., Beets, I., and Gottschalk, A. Food Sensation Modulates Locomotion by Dopamine and Neuropeptide Signaling in a Distributed Neuronal Network. 44.

478. Avery, L.Y.-J.Y. (2012). *C. elegans* Feeding. WormBook. 10.1895.
479. Bacqué-Cazenave, J., Bharatiya, R., Barrière, G., Delbecque, J.-P., Bouguiyoud, N., Giovanni, D.G., Cattaert, D., and Deurwaerdère, D.P. (2020). Serotonin in Animal Cognition and Behavior. International Journal of Molecular Sciences 21, *1*649. 10.3390/ijms21051649.
480. Voigt, J.-P., and Fink, H. (2015). Serotonin controlling feeding and satiety. Behavioural Brain Research 277*,* *1*4-31. 10.1016/j.bbr.2014.08.065.
481. Baidya, M., Genovez, M., Torres, M., and Chao, M.Y. (2014). Dopamine modulation of avoidance behavior in Caenorhabditis elegans requires the NMDA receptor NMR-1. PLoS One 9, *e*102958. 10.1371/journal.pone.0102958.
482. Vidal-Gadea, A.G., and Pierce-Shimomura, J.T. (2012). Conserved role of dopamine in the modulation of behavior. Communicative & Integrative Biology 5, *4*40-447. 10.4161/cib.20978.
483. Arias-Carrión, O., Stamelou, M., Murillo-Rodríguez, E., Menéndez-González, M., and Pöppel, E. (2010). Dopaminergic reward system: a short integrative review. Int Arch Med 3, *2*4. 10.1186/1755-7682-3-24.
484. Miller, H.A., Huang, S., Schaller, M.L., Dean, E.S., Tuckowski, A.M., Munneke, A.S., Beydoun, S., Pletcher, S.D., and Leiser, S.F. (2021). Serotonin and dopamine modulate aging in response to food perception and availability. 2021/03/23. https://www.biorxiv.org/content/10.1101/2021.03.23.436516v1.
485. Sinakevitch, I.T., Daskalova, S.M., and Smith, B.H. (2017). The Biogenic Amine Tyramine and its Receptor (AmTyr1) in Olfactory Neuropils in the Honey Bee (Apis mellifera) Brain. Frontiers in Systems Neuroscience 11.
*4*86. Phillips, I.R., and A., S.E. (2019). Endogenous Roles of Mammalian Flavin-Containing Monooxygenases.
487. van der Goot, A.T., and Nollen, E.A. (2013). Tryptophan metabolism: entering the field of aging and age-related pathologies. Trends Mol Med 19, *3*36-344. 10.1016/j.molmed.2013.02.007.
488. Veeravalli, S., Omar, B.A., Houseman, L., Hancock, M., Gonzalez Malagon, S.G., Scott, F., Janmohamed, A., Phillips, I.R., and Shephard, E.A. (2014). The phenotype of a flavin-containing monooyxgenase knockout mouse implicates the drug-metabolizing enzyme FMO1 as a novel regulator of energy balance. Biochem Pharmacol 90, *8*8-95. 10.1016/j.bcp.2014.04.007.
489. Seibenhener, L.M., and Wooten, C.M. (2015). Use of the Open Field Maze to Measure Locomotor and Anxiety-like Behavior in Mice. Journal of Visualized Experiments. 10.3791/52434.
490. Hall, S.C. (1934). Emotional behavior in the rat. I. Defecation and urination as measures of individual differences in emotionality. Journal of Comparative Psychology 18, *3*85-403. https://doi.org/10.1037/h0071444.
491. Walf, A.A., and Frye, A.C. (2007). The use of the elevated plus maze as an assay of anxiety-related behavior in rodents. Nature Protocols 2, *3*22-328. https://doi.org/10.1038/nprot.2007.44.
492. Pellow, S., Chopin, P., File, E.S., and Briley, M. (1985). Validation of open : closed arm entries in an elevated plus-maze as a measure of anxiety in the rat. Journal of Neuroscience Methods 14, *1*49-167. https://doi.org/10.1016/0165-0270(85)90031-7.

493. Steru, L., Chermat, R., Thierry, B., and Simon, P. (1985). The tail suspension test: A new method for screening antidepressants in mice. Psychopharmacology 85, *3*67-370. 10.1007/BF00428203.
494. Can, A., Dao, T.D., Terrillion, E.C., Piantadosi, C.S., Bhat, S., and Gould, D.T. (2011). The Tail Suspension Test. Journal of Visualized Experiments. 10.3791/3769.
495. Can, A., Dao, T.D., Arad, M., Terrillion, E.C., Piantadosi, C.S., and Gould, D.T. (2011). The Mouse Forced Swim Test. Journal of Visualized Experiments. 10.3791/3638.
496. Porsolt, R.D., Bertin, A., and Jalfre, M. (1977). Behavioral despair in mice: a primary screening test for antidepressants. Archives internationales de pharmacodynamie et de therapie 229*, 3*27-336.